TECHNISCHE UNIVERSITÄT MÜNCHEN
Fakultät für Medizin

Characterization of Igfr-L1 and Igfr-L2 as two novel regulators of the Ins/Igf system

Sarah Homberg

Vollständiger Abdruck der von der Fakultät für Medizin der Technischen Universität München zur Erlangung des akademischen Grades eines

Doktors der Naturwissenschaften
(Dr. rer. nat.)

genehmigten Dissertation.

Vorsitzender: Prof. Dr. Dieter Saur

Prüfer der Dissertation:

1. Prof. Dr. Heiko Lickert

2. Priv.-Doz. Dr. Karl Kramer

Die Dissertation wurde am 18.02.2020 bei der Technischen Universität München eingereicht und durch die Fakultät für Medizin am 14.07.2020 angenommen.

1. Content

1.1 Figures

1.2 Tables

1.3 Abbreviations

5330417C22Rik	KIAA1324, EIG121, Igfr-L1
9330182L06Rik	KIAA1324L, EIG121L, Igfr-L2
aa	amino acid(s)
ACTH	adrenal corticotropic hormone
ADP	adenosine diphosphate
Akt	serine-threonine kinase Akt
AMPK	AMP-activated protein kinase
Amy	amylase
ANOVA	analysis of variants
Ap2	adaptor protein 2
APS	ammonium persulfate
ATP	adenosine triphosphate
AUC	area under the curve
Bad	Bcl2-associated agonist of cell death
BFP	blue fluorescent protein
Bl6	C57Bl/6J
BMI	body mass index
BMP	bone morphogenetic protein
BO	beads only
bp	base pair(s)
BW	body weight
Cas9	CRISPR-associated protein 9
CCP	clathrin-coated pit
ChrA	chromogranin A
CI-M6PR	cation-independent mannose-6-phosphate receptor, Igf2r

CKO	conditional *knock-out*
CME	clathrin-mediated endocytosis
COP I/II	coatamer complex I/II, CM1
CRD	cysteine-rich domain
CRISPR	clustered regularly interspaced short palindromic repeats
ctrl	control
DAPI	4',6-diamidin-2-phenylindol
DBS	donkey blocking solution
DM	diabetes mellitus
DMSO	dimethyl sulfoxide
DNA	deoxyribonucleic acid
DTT	dithiothreitol
E + no.	embryonic stage
ECad	E-Cadherin
EdU	5'-ethynyl-2'-deoxyuridine
Eea1	early endosome antigen 1
EGFR	epidermal growth factor receptor
EIG121	estrogen-induced gene 121, Igfr-L1
EIG121L	estrogen-induced gene 121-like, Igfr-L2
ELISA	enzyme-linked immunosorbent assay
EMP	endomembrane protein
ER	endoplasmic reticulum
Ergic	ER-golgi intermediate compartment
ER(α/β)	estrogen receptor (α/β)
ESRD	end-stage renal disease
EUCOMM	European Conditional Mouse Mutagenesis Program
FACS	fluorescence-activated cell sorting
FCS	fetal calf serum
FD	flox-deleted
Foxa1/2/3	forkhead-box protein A1/2/3
FP	$FVFPBF^{DHom}$
FVF	Foxa2-Venus-fusion
$FVFPBF^{DHom}$	Foxa2-Venus-fusion, Pdx1-BFP-fusion double homozygous
Gh	growth hormone
Gcg	glucagon
Gcgr	glucagon receptor
Glp1/2	glucagon-like peptide 1/2
Glut2	glucose transporter type 2
GM130	golgi matrix protein 130
Gnrh	gonadotropin-releasing hormone
Golgb1	golgi autoantigen, giantin
Grb2/10	growth factor receptor bound protein 2/10
GRP78	glucose-regulated protein 78 kDa, Bip
GSIS	glucose-stimulated insulin secretion
Gsk3	glycogen synthase kinase 3
GTP	guanosine triphosphate
(ip)GTT	(intraperitoneal) glucose tolerance test
GWAS	genome-wide association study
HBSS	HEPES-balanced salt solution
het	heterozygous ($^{+/-}$)
hom	homozygous ($^{-/-}$)

HPG	hypothalamic-pituitary-gonadal (axis)
HPLC	high performance liquid chromatography
HR	hybrid receptor
Hsp90	heat shock protein 90
ICC	Immunocytochemistry
Igf(1/2)	insulin-like growth factor (1/2)
IgG	immunoglobulin G
Igf1r	insulin-like growth factor 1 receptor
Igf2r	insulin-like growth factor 2 receptor
Igfr-L1/Igfr-L2	Igf receptor-like 1/2
IHC	Immunohistochemistry
In	Input/whole cell lysate
Ins	insulin
Insr (-A/B)	insulin receptor A/B
(co-) IP	(co-) immunoprecipitation
Irs	insulin receptor substrate
ITT	insulin tolerance test
KI	knock-in
KIAA1324	5330417C22Rik, EIG121, UPF0577, Igfr-L1
KIAA1324L	9330182L06Rik, EIG121L, Igfr-L2
KO	knock-out ($^{-/-}$)
LacZ	β-galactosidase
Lamp2	lysosomal-associated membrane protein 2
LSM	laser scanning microscopy
M6P(R)	mannose-6-phosphate (receptor)
Mapk	mitogen-activated protein kinase
Mek	Mapk kinase
MODY	Maturity onset of diabetes of the young
MS	mass spectrometry
Mtor	mammalian target of rapamycin
Nedd4	neural precursor cell expressed developmentally downregulated protein 4
NeoR	neomycin resistance
Ngn3	neurogenin 3
o.n.	overnight
OCT	optimal cutting temperature (medium)
P + no.	postnatal day
(RT-) PCR	(real time) polymerase chain reaction
Pdx1	pancreatic and duodenal homeobox 1
PFA	paraformaldehyde
p-HH3	phospho-histone H3
PI3K	phosphoinositide-3 kinase
PLA	proximity ligation assay
PM	plasma membrane
PP	pancreatic polypeptide
Rab7	ras-associated protein 7
RFP	red fluorescent protein
(m)/(sg)RNA	(messenger)/(single guide) ribonucleic acid
RT	room temperature
RTK	receptor tyrosine kinase
SDS	sodium dodecyl sulfate

SEM	standard error of the mean
SN	supernatant (antibody or immunoprecipitation)
SNP	single nucleotide polymorphism
T1D(M)	diabetes (mellitus) type 1
T2D(M)	diabetes (mellitus) type 2
TCA	tri-carboxylic acid (cycle)
TF	transcription factor
TGN	trans-golgi network
TPM	transcripts per million
Ucn3	urocortin 3
UTR	untranslated region
WB	Western Blot
wt	wildtype ($^{+/+}$)
ΔEx	delta exon

2. Abstract

Diabetes mellitus is a chronic metabolic disease and associated with dysregulation of the insulin/insulin-like growth factor (Ins/Igf) system, a major regulator of growth and metabolism. Here, we describe two novel components of the Ins/Igf system, which we named Igf receptor-like 1 and 2 (Igfr-L1 and Igfr-L2) because of their domain structure similarities to Insr, Igf1r (growth factor receptor cysteine-rich domain) and Igf2r (Mannose-6-phosphate receptor binding domain).

Igfr-L1 has been identified in a screen for novel regulators of secondary transition during pancreas development and the protein was found to be highly expressed in the embryonic and adult pancreas. Strikingly, Igfr-L1 full-body knock-out (KO) mice died postpartum without developmental defects but signs of hypoglycemia and hyperinsulinemia. In respect of the pancreas, no alterations in gross morphology or lineage allocation were detected and insulin secretion was unchanged. Therefore, tamoxifen-inducible β-cell-specific KO mice were generated. Upon insulin stimulation, Insr/Igf1r signaling was increased in *ex vivo*-induced isolated islets hinting to Igfr-L1 as a negative regulator of this pathway. Apart from β-cells, Igfr-L1 is expressed in all endocrine subtypes, which is why a Ngn3-Cre-mediated conditional KO (CKO) was generated. CKO mice were viable and showed, despite a potential increase in α-cell number, no alterations in glucose homeostasis or tolerance suggesting that intra-islet paracrine signaling is involved. In MODY males (FVFPBF^{DHom}, FP), expression of Igfr-L1 was found to be upregulated, while its genetic reduction led to decreased blood glucose levels at P25. Insulin and C-peptide levels were increased and β-cells showed signs of maturity and functionality, while insulin sensitivity was not altered. FP females were hyperglycemic at P25 and normoglycemic in adulthood but showed a drastically impaired glucose tolerance independent of the Igfr-L1 allele. Insulin tolerance, however, was improved in FP; Igfr-L1$^{-/-}$ females. During early gestation, lactation and post-weaning, FP; Igfr-L1$^{+/-}$ mice suffered from acerbated glucose homeostasis compared to FP; Igfr-L1$^{+/+}$. The sexual dimorphism hints to estrogen suggesting a further role of Igfr-L1 in the regulation of reproduction via the hypothalamic-pituitary-gonadal (HPG) axis. Endocrine-specific CKO of Igfr-L1 in FP males showed an increased α-cell number, similar to the CKO in C57Bl/6J, and improved islet architecture without regulation of glucose homeostasis at P25. *In vitro* experiments revealed that Igfr-L1 potentially interacts with the adaptor protein Ap2 as well as with Insr and Igf1r and facilitates their clathrin-mediated endocytosis.

Further identification of interaction partners by co-IP with HPLC-MS analysis showed a strong interaction with the paralogue Igfr-L2 depending on the metabolic condition. After generation of specific antibodies, Igfr-L2 was found to be a novel endocrine cell marker, which localized in the ER-Golgi. Full-body KO mice were viable, whereas homozygosity of both parents adversely affected litter size and postnatal survival, potentially via dysregulation of the HPG axis. Adult Igfr-L2$^{-/-}$ animals showed no difference in glucose tolerance or in hormone expression in the islets and the pituitary. However *in vitro,* Igfr-L2$^{-/-}$ in Min6 revealed diminished proliferation and augmented apoptosis potentially due to a reduction of total Igf1r and an increase in total Insr levels. This suggests that Igfr-L2 is not involved in acute Insr/Igf1r signaling but might be important for β-cell proliferation e.g. during compensation.

We further showed that Igfr-L1 and Igfr-L2 were heterogeneously expressed in endocrine cells and able to form homo- and heterodimers. In Min6 double KO cells, Insr/Igf1r-phosphorylation was rather associated with Igf1r. Igfr-L1$^{+/-}$; Igfr-L2$^{+/-}$ or Igfr-L1$^{+/-}$; Igfr-L2$^{-/-}$ animals did so far not show a significant disturbance in glucose homeostasis. Thus, the paralogues might regulate each other as well as Insr and Igf1r, which either results in growth or metabolism.

In conclusion, we identified Igfr-L1 and Igfr-L2 as two novel regulators of the Ins/Igf system, which could be potential targets in diabetes therapy.

3. Introduction

3.1 Diabetes mellitus

Diabetes mellitus (DM) is a complex metabolic disease with increasing prevalence in industrial countries. In 2019, 463 million people suffered from DM worldwide and the number is predicted to increase to 700 million by 2045 according to the International Diabetes Federation. With 10 % of total expenditure spent on adults, DM causes high costs for health care systems and is with 4.2 million deceased a major cause of death (IDF, 2019).
There are four types of DM (Alberti & Zimmet, 1998; American Diabetes, 2009): In type 1 DM, patients suffer from an absolute lack of insulin due to an autoimmune destruction of pancreatic β-cells within the islets of Langerhans. They are dependent on daily external insulin administration, which drastically reduces their life quality (Bonifacio & Ziegler, 2010). In type 2 DM (T2DM), however, peripheral insulin resistance is acquired by environmental factors such as physical inactivity and obesity in combination with genetic predisposition. Although patients do not depend on insulin, they often need medication to lower their blood glucose levels (DeFronzo et al., 2015; Kahn, 1995). Gestational DM can be developed due to the increased demand of insulin during pregnancy but is mostly reverted after birth. However, women and children are at higher risk to develop T2DM (Rieck & Kaestner, 2010). In case of maturity onset of diabetes of the young (MODY), impaired glucose homeostasis occurs already in children or young adults and is due to mutations in genes important for glucose metabolism. Over 10 MODY genes exist including *insulin*, transcription factors such as *pancreatic and duodenal homeobox 1*, *hepatic nuclear factor 1α, 1β* or *4α* and enzymes such as *glucokinase* or *carboxyl-ester lipase*. In general, DM is characterized by chronic hyperglycemia, which can finally result in micro- and macrovascular long-term complications such as cardiovascular disease, retinopathy, stroke and nephropathy.
Insulin has been discovered 100 years ago and still remains a powerful tool in the treatment of DM (Roth et al., 2012; Vecchio, Tornali, Bragazzi, & Martini, 2018). Apart from its side-effects such as body weight gain or risk of hypoglycemia, clinical studies showed that intensive insulin therapy can improve glycemic control and preserve β-cell function (H. S. Chen et al., 2008; Harrison, Adams-Huet, Raskin, & Lingvay, 2012; Kramer, Zinman, & Retnakaran, 2013; Weng et al., 2008). Physiological concentrations of insulin exert anti-apoptotic effects in the islets (Johnson et al., 2006) and counteract the dedifferentiation of β-cells observed in DM, which can also be pharmacologically targeted (Sachs et al., 2020; Z. Wang, York, Nichols, & Remedi, 2014). Hence, agents that mimic insulin action on β-cells to ensure their function, proliferation and overall health would be needed.
Otherwise, loss or dysfunction of pancreatic β-cells (C. Chen, Cohrs, Stertmann, Bozsak, & Speier, 2017; Weir & Bonner-Weir, 2004) can so far be counteracted by bariatric surgery/sleeve gastrectomy (Abu-Gazala et al., 2018; Sarruf, Bonner-Weir, & Schwartz, 2012; Schlager et al., 2011) or islet transplantation (Gala-Lopez et al., 2018; Weir & Bonner-Weir, 1998; Weir, Bonner-Weir, & Leahy, 1990) that are invasive and come along with other risks. Regeneration of the endocrine pancreas by use of stem cell-derived β-cells or via transdifferentiation from α-cells and neogenesis from duct cells is under investigation but has not yet been implemented (Aguayo-Mazzucato & Bonner-Weir, 2018; Bakhti, Bottcher, & Lickert, 2019; Bakhti & Lickert, 2019; Chera et al., 2014; Furuyama et al., 2019; Matsuoka et al., 2017; Roscioni, Migliorini, Gegg, & Lickert, 2016; Thorel et al., 2010; Y. Wang et al., 2018; Q. Zhou & Melton, 2018). In order to provide alternative interventions, research to identify the underlying pathomechanisms of DM and novel therapeutic strategies is needed (C. Chen et al., 2017; Clemmensen, Muller, Finan, Tschop, & DiMarchi, 2016; P. Wang et al., 2015).

3.2 The pancreas

Systemic glucose homeostasis and energy metabolism are tightly regulated by various circulating hormones, which are produced in different organs such as the pituitary, the liver and the gut as well as the pancreas (Clemmensen et al., 2017; Kulkarni & Kahn, 2004; MacDonald, Joseph, & Rorsman, 2005; Roder, Wu, Liu, & Han, 2016; Rorsman, 1997; Shirakawa, De Jesus, & Kulkarni, 2017). The pancreas is a gland divided into an endocrine and an exocrine compartment, i.e. the islets of Langerhans and acinar cells surrounding ductal epithelium, respectively (Figure 3.2.1.1). The main pancreatic duct is connected to the duodenum and branches into interlobular and finally small intralobular ducts with acinar cells forming grape-like clusters at their ends (Bastidas-Ponce, Scheibner, Lickert, & Bakhti, 2017; Edlund, 2002). Acini secrete digestive enzymes such as trypsinogen, lipase or amylase into the duct and thus into the duodenum (Grapin-Botton, 2005). Additionally, ductal cells secret mucin and an aqueous bicarbonate solution for neutralization of gastric acid.

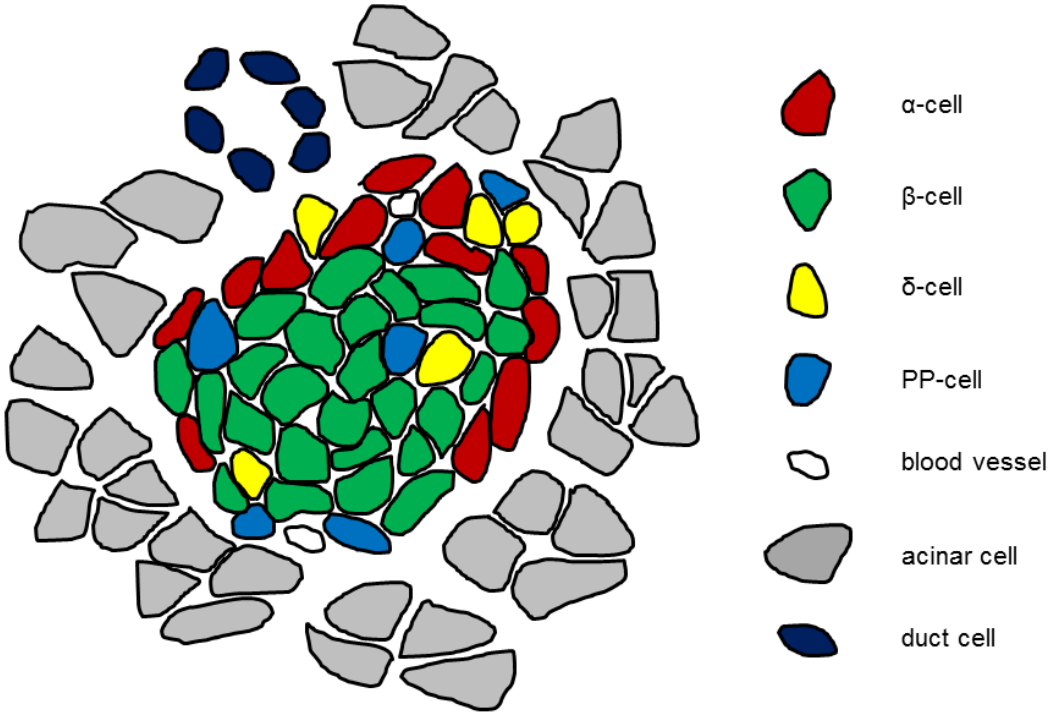

Figure 3.2.1.1 The endocrine and exocrine pancreas
Schematic representation of endocrine cells (α-, β-, δ- and PP cells) forming the islets of Langerhans and surrounding exocrine cells (acini) with indication of duct cells and blood vessels. Modified from Efrat et al., 2012.

The ductal and acinar network is interspersed with the hormone-producing islets of Langerhans, which only represent 1-2 % of the pancreatic volume (Brissova et al., 2005). These clusters are comprised of five different endocrine cell types which are, in the murine pancreas, predominately insulin (Ins)-producing β-cells (65–80 %) in the center and glucagon (Gcg)-producing α-cells (15–20 %), pancreatic polypeptide (PP)-producing γ-cells (3–5 %), somatostatin-producing δ-cells (3-10 %) and ghrelin-producing ε-cells (<1 %) in the periphery. Among innervation with sensory, sympathetic and parasympathetic nerves, islets are highly vascularized so that the secreted hormones rapidly enter the circulation (Cleaver & Dor, 2012). The major regulators of blood glucose levels are insulin and glucagon, which and inhibits insulin and glucagon secretion in a paracrine manner, while this pathway is disturbed in diabetes (Hauge-Evans et al., 2009; Rorsman & Huising, 2018; Weir & Bonner-Weir, 1985). Ghrelin is predominantly a gastric hormone and the endogenous ligand of the growth

hormone secretagogue receptor in the hypothalamus (van der Lely, Tschop, Heiman, & Ghigo, 2004). The orexigenic peptide exerts a plethora of physiological effects by modulating systemic energy homeostasis and glucose metabolism (Heppner, Muller, Tong, & Tschop, 2012; Muller et al., 2015). Therefore, it is studied in the treatment of obesity and diabetes as it is also able to inhibit insulin secretion from β-cells (Collden, Tschop, & Muller, 2017; Poher, Tschop, & Muller, 2018; Tong et al., 2010; Wiedmer, Nogueiras, Broglio, D'Alessio, & Tschop, 2007). PP is acting in the gastrointestinal tract by suppressing exocrine secretion and exerts anorexigenic effects through regulation of energy metabolism (Khandekar, Berning, Sainsbury, & Lin, 2015). Thus, paracrine action of these hormones results in intra-islet communication, which is why disturbances in one of them also affect other endocrine cells (Briant, Salehi, Vergari, Zhang, & Rorsman, 2016; Samols, Bonner-Weir, & Weir, 1986; Weir & Bonner-Weir, 1990).

3.2.1 Insulin and glucagon

Pancreatic β-cells are the source of insulin, where it is synthesized as the prohormone preproinsulin consisting of a signal peptide (21 aa), followed by the B-chain (30 aa), the C-chain (31 aa) and the A-chain (21 aa). In the endoplasmic reticulum (ER), it is further processed to proinsulin by cleavage of the signal peptide and folding via the formation of disulfide bonds. In the Golgi apparatus, membranous proteases cleave proinsulin into C-peptide and the active peptide hormone insulin, which is then stored in granular vesicles. Insulin exocytosis into the circulation is triggered by an increase in blood glucose levels after food intake and nutrient absorption from the gastrointestinal tract. This process is called glucose-stimulated insulin secretion (GSIS) (Rorsman & Ashcroft, 2018; Rorsman et al., 2000; Rorsman & Renstrom, 2003; Straub & Sharp, 2002).

In β-cells, glucose is actively internalized via type 2 glucose transporters (Glut2) that have been recruited to the membrane. It is subsequently oxidized in glycolysis to pyruvate which serves as substrate for the generation of adenosine-triphosphate (ATP) from adenosine diphosphate (ADP) in the tri-carboxylic acid (TCA) cycle. The increased intracellular ATP/ADP ratio results in membrane depolarization after inactivation of ATP-sensitive potassium channels (K_{ATP}) and thus to activation of voltage-gated calcium channels. Elevated intracellular Ca^{2+} levels trigger a biphasic insulin release via the fusion of insulin granules with the plasma membrane. The first phase secretion after 5-10 min is strong but transient, whereas the second phase after 30 min is weaker but more sustained.
Circulating insulin acts on the three metabolic tissues, i.e. liver, adipose tissue and skeletal muscle to ensure glucose uptake via activation of the insulin receptor (Heesom, Harbeck, Kahn, & Denton, 1997; Kahn & Goldfine, 1993; Rui, 2014; Saltiel & Kahn, 2001; Tokarz, MacDonald, & Klip, 2018). On the one hand, glucose is used for ATP synthesis in the TCA cycle after glycolysis, which is multiplied via oxidative phosphorylation in mitochondria and consequently inhibits gluconeogenesis. On the other hand, excessive glucose is stored as glycogen by synchronously enhancing glycogen synthase, i.e. glycogenesis, and inhibiting glycogen synthase kinase 3 (Gsk3) as well as glycogen phosphorylase, i.e. glycogenolysis, through activation of the phosphinositide-3 kinase (PI3K) pathway. Apart from that, lipogenesis is activated resulting in the production of triglycerides, phospholipids and cholesterol from fatty acids that are either stored in lipid droplets or released to the circulation in lipoproteins of different densities. Ultimately, insulin action results in a reduction of systemic blood glucose levels.

Glucagon action has the opposite effect. The glucagon precursor peptide is synthesized in α-cells and consists of 180 aa that are cleaved into glucagon and 7 other peptides among

them the incretins glucagon-like peptide 1 and 2 (Glp1, Glp2). Glucagon is released upon nutrient starvation, e.g. in between meals or during sleep resulting in glycogenolysis and gluconeogenesis to provide glucose for cellular ATP synthesis (Heppner et al., 2010; Kawamori, Welters, & Kulkarni, 2010). Lipolysis is promoted resulting in the production of free fatty acids and glycerol that can be converted into glucose. Apart from that, ketone bodies are synthesized by mitochondrial β-oxidation and ketogenesis from non-esterified fatty acids. In consequence, glucagon action raises systemic blood glucose levels and might serve as a target in diabetes therapy (Habegger et al., 2010; Y. H. Lee, Wang, Yu, & Unger, 2016; Muller, Finan, Clemmensen, DiMarchi, & Tschop, 2017).

3.2.2 Foxa2, Pdx1 and Ngn3

During pancreas development various transcription factors (TF) are expressed that trigger differentiation of progenitor cells (Bastidas-Ponce, Scheibner, et al., 2017; Pan & Wright, 2011). Forkhead homeobox A2 (Foxa2), pancreatic and duodenal homeobox 1 (Pdx1) and neurogenin 3 (Ngn3) are important for lineage decision depending on their expression level and also co-expression.

Foxa2, former hepatocyte nuclear factor 3β (Hnf-3β), is beside Foxa1 and Foxa3 one member of the forkhead homeobox TF family Foxa that have been described in the liver (Kaestner, 2000). In early development, Foxa2 is required for embryonic endoderm formation, which finally gives rise to lung, liver, pancreas and the gastro-intestinal tract. As a winged-helix TF it is able to open up compact chromatin and allow binding of other TF to cis-regulatory elements of the DNA (Zaret & Carroll, 2011). Generation of a Foxa2-Venus fusion (FVF) reporter mouse line allowed visualization and developmental analysis of endoderm-derived organs (Burtscher, Barkey, & Lickert, 2013). It was used for the separation of Foxa2-Venus-positive epithelial cells during secondary transition in order to understand the spatio-temporal regulation of genes during endocrine, exocrine and ductal lineage formation (Willmann et al., 2016). Furthermore, mice with a Foxa2 deletion under the *Foxa3* promoter die within a week due to hypoglycemia caused by hypoglucagonemia. Even though, α-cell progenitors are formed, they fail to differentiate into mature α-cells (C. S. Lee, Sund, Behr, Herrera, & Kaestner, 2005).
However, Foxa2 is not only essential for pancreas development and differentiation but also for proper endocrine function in adult animals. β-cell-specific deletion of Foxa2 leads to hyperinsulinemic hypoglycemia originating from defects in insulin secretion upon glucose and amino acid stimulation (Sund et al., 2001). This phenotype is comparable to familial hyperinsulinism and suggests ATP-sensitive K^+-channels as targets of Foxa2. Analysis of isolated islets from these mice identified further Foxa2 target genes regulating multiple pathways of insulin secretion and causing persistent hyperinsulinemic hypoglycemia of infancy (Lantz et al., 2004). A conditional knock-out (KO) of Foxa2 specifically in the pancreas via *Pdx1* also enhances the first-phase of glucose-induced insulin secretion in mature β-cells by increasing the docking of insulin granules, which is accompanied by changes in signaling of the intracellular second messenger Ca^{2+} (Gao et al., 2007). Double KO of Foxa1 and Foxa2 in mature β-cells leads to more pronounced defects in insulin secretion and also affects genes controlling neural differentiation and function as well as carbohydrate metabolism (Gao et al., 2010). Hence, Foxa TF could be modulated in diabetes to improve β-cell function.

Pdx1, also known as insulin-promoter factor 1, is a TF essential for pancreas development. Targeted mutation within the *Pdx1* gene prevents pancreas formation, which is why mice die within a few days after birth (Jonsson, Carlsson, Edlund, & Edlund, 1994). In adult mice,

Pdx1 is selectively expressed in β-cells where it regulates glucose homeostasis as specific mutations lead to MODY4 (C. S. Lee et al., 2002). $Pdx1^{+/-}$ animals show impaired glucose tolerance and insulin secretion with age accompanied by alterations in islet architecture and increased apoptosis via lack of direct regulation of *Pdx1* by insulin (Johnson et al., 2003; Johnson et al., 2006). In line, Pdx1 haploinsufficiency abrogated compensatory β-cell proliferation in $Insr^{+/-}$; $Irs1^{+/-}$ and liver-specific $Insr^{-/-}$ mice resulting in β-cell apoptosis and death of animals (Kulkarni et al., 2004). Cell death is caused by autophagy during starvation shown by inhibition of this pathway suggesting Pdx1 as a target in diabetes treatment (Fujimoto et al., 2009). Regarding islet plasticity, forced Pdx1 expression in progenitors postnatally transform α- into β-cells (Yang, Thorel, Boyer, Herrera, & Wright, 2011). Transdifferentiation from β- to α-cells in aggregates of human primary cells occurs spontaneously after degranulation shown by Pdx1 and homeobox protein Nkx6.1 co-expression with glucagon (Spijker et al., 2013). Lack of Pdx1 specifically in duct cells does not prevent β-cell formation but their maturation (Guo et al., 2013). In β-cells, reduction of the Pdx1 and MafA TF levels as well as incretin receptors as a consequence of glucotoxicity in diabetes results in downregulation of insulin synthesis and secretion (Kaneto & Matsuoka, 2015). This loss of β-cell identity and conversion to other subtypes could be a novel target for diabetes therapy (Swisa, Glaser, & Dor, 2017).
Foxa2 is a major upstream regulator of *Pdx1* by occupying regulatory domains within the gene (C. S. Lee et al., 2002). β-cell-specific deletion of Foxa2 in adult animals results in reduction of Pdx1 levels. Similarly, ablation of both Foxa1 and Foxa2 in the pancreatic primordium leads to pancreatic hypoplasia accompanied by a lack of Pdx1 expression. Mutant mice die shortly after birth suffering from hyperglycemia showing defects in exocrine and endocrine development (Gao et al., 2008). In cooperation, Pdx1 and Foxa2 are crucial to maintain postnatal β-cell identity and maturation (Bastidas-Ponce, Roscioni, et al., 2017).

Ngn3, a basic helix-loop-helix TF, is expressed during pancreas development in all endocrine progenitors with a peak at E15.5 (Schwitzgebel et al., 2000). $Ngn3^{-/-}$ mice do not have any endocrine cells and die from diabetes showing that Ngn3 is essential for the formation of the different endocrine subtypes (Gradwohl, Dierich, LeMeur, & Guillemot, 2000). Lineage allocation occurs in a dosage-dependent manner, i.e. high levels of Ngn3 are needed for islet cells, whereas progenitors with low levels become acinar or ductal cells (S. Wang et al., 2010). Single-cell RNA sequencing of Ngn3-Venus transgenic cells during secondary transition revealed a detailed roadmap of endocrinogenesis by dissecting low and high expression of Ngn3 as well as Fev- and hormone-positive cells (Bastidas-Ponce et al., 2019). Furthermore, feedback inhibition of generated endocrine cells ensures proper pancreas morphogenesis without overgrowth of the ductal epithelium (Magenheim et al., 2011). Similarly, Ngn3 is expressed in the arcuate and ventromedial hypothalamus of the embryonic brain and involved in neurogenesis and subtype specification (Pelling et al., 2011). In already differentiated islet cells, Ngn3 expression is necessary to sustain their maturation and function (S. Wang et al., 2009). Partial duct ligation induces Ngn3-positive progenitors to differentiate into β-cells and also increases β-cell volume due to higher proliferation of existing β-cells (Van de Casteele et al., 2013). Forced expression of the pancreatic TFs Ngn3, Pdx1 and MafA in exocrine cells results in reprogramming to glucose unresponsive β-like cells, while this mechanism is impaired under hyperglycemia (Cavelti-Weder et al., 2016; Yamada et al., 2015). In coherence, fasting-mimicking diet increases the amount of β-cells due to reprogramming via Ngn3 expression and restores insulin secretion in diabetic animals (Cheng et al., 2017). To summarize, Ngn3 expression is crucial for endocrine lineage decision during pancreas formation which can be taken advantage of for β-cell neogenesis in diabetic patients.

3.3 The Ins/Igf system

Cellular metabolism and proliferation are mainly regulated by the insulin/insulin-like growth factor (Ins/Igf) system, while the dysregulation of its signaling pathways causes diabetes and cancer (Annunziata, Granata, & Ghigo, 2011; Bach & Rechler, 1992; Haeusler, McGraw, & Accili, 2018; Hiden, Glitzner, Hartmann, & Desoye, 2009; Le Roith, 2003; Trajkovic-Arsic, Kalideris, & Siveke, 2013).

3.3.1 Receptors and Ligands

The system is composed of the three ligands insulin, Igf1 and Igf2 and the respective receptors, i.e. insulin receptors (Insr-A and Insr-B), Igf1 receptors (Igf1r), Insr/Igf1r-hybrid receptors (HR) and Igf2 receptors (Igf2r) (Figure 3.3.1.1a) (Annunziata et al., 2011; Le Roith, 2003). Insr and Igf1r co-evolved and first occurred as distinct proteins in vertebrates. Therefore, their sequence identity is high in the receptor tyrosine kinase (RTK) domain but differs in the ligand binding region. They consist of a 130 kDa α- and a 95 kDa β-subunit, which are covalently linked via disulfide bonds of their fibronectin regions after processing of the proreceptor in the ER (Bass, Chiu, Argon, & Steiner, 1998; Gorden, Arakaki, Collier, & Carpentier, 1989). In the α-chain, leucine-rich repeats (large domains L1 and L2) flank a highly conserved cysteine-rich domain (CRD) with a fibronectin type III domain being C-terminal of L2 (Belfiore, Frasca, Pandini, Sciacca, & Vigneri, 2009). The β-chain consists of a C-terminal tail, followed by the catalytic domain, a juxta- and transmembrane regulatory region, the transmembrane helix and N-terminal fibronectin regions. The two splice isoforms of Insr only differ in the transcription of exon 11 making the α-subunit of Insr-B 12 amino acids longer than that of Insr-A. Homo- and heterodimerization of Insr-A, Insr-B and Igf1r results in a α2β2 heterotetramer (Lemmon & Schlessinger, 2010).
Insulin and Igf1 as well as related growth factors bind with different affinities to the receptors, which are further regulated by their homo- and heterodimerization but also depend on expression levels and ligand concentration in different tissues (Belfiore & Malaguarnera, 2011; Clayton, Banerjee, Murray, & Renehan, 2011; LeRoith & Yakar, 2007; Nakae, Kido, & Accili, 2001). Thus, insulin has a higher affinity to Insr-A and Insr-B than to Igf1r or HR, whereas Igf1 preferably binds to Igf1r and with less extent to Igf2r, Insr or HR. Igf2 predominantly binds to Igf2r but can also stimulate Insr, especially Insr-A, and Igf1r (J. Giudice, 2013). Cryo-electron microscopy revealed a conformational change of Insr in a synthetic membrane from a turned U to a T after insulin binding (Gutmann, Kim, Grzybek, Walz, & Coskun, 2018). Additionally, it has been found that the dimeric Insr has four insulin binding sites (Gutmann et al., 2020). While insulin is synthesized in pancreatic β-cells, Igf1 and Igf2 are produced in the liver and bound to Igf-binding proteins in the circulation what prevents their rapid degradation and regulates their bioavailability.
Alterations in the expression of Insr splice isoforms may be related to diabetes and cancer (Belfiore et al., 2009; Belfiore et al., 2017). Insr-B can be mostly found in adult, differentiated tissues such as the liver where it promotes the metabolic effects of insulin. Apart from the brain, Insr-A is predominantly expressed during embryogenesis and in cancer where it displays equal affinities to Igf2 and to insulin, which are also similar to the affinity of Igf2 to Igf1r. Thus, differential activation of downstream signaling after stimulation of Insr-A by insulin or Igf2 induces metabolic or mitogenic effects, respectively (Frasca et al., 1999). In pancreatic β-cells, insulin selectively activates transcription of insulin via activation of Insr-A but the one of glucokinase via Insr-B (B. Leibiger et al., 2001). Controlled dimerization studies in breast cancer cells showed that activation of Insr results exclusively in glucose uptake and the one of Igf1r in survival, whereas stimulation of Igf1r and HR induced both

proliferation and glucose uptake (J. Chen, Nagle, Wang, Boone, & Lee, 2018). In conclusion, Insr isoforms A and B as well as their homo- and heterodimers including Igf1r modulate the affinities to the different ligands. Thus, receptor stimulation results in differential downstream signaling, which may play a pivotal role in physiology and disease.

Other than Insr and Igf1r, the Igf2r or cation-independent mannose-6-phosphate receptor (CI-M6PR) lacks a tyrosine kinase domain and mainly serves as scavenger receptor for Igf2 (Brown, Jones, & Forbes, 2009; Ghosh, Dahms, & Kornfeld, 2003; Kornfeld, 1992; Lau et al., 1994). The single type I transmembrane glycoprotein has a short cytoplasmic tail followed by a transmembrane and a large extracellular region that consists of 15 homologous repeats, the M6P binding domains. Igf2 predominantly binds to domain 11, while a fibronectin type II-like region of domain 13 enhances the binding affinity. Lysosomal enzymes that have been marked with M6P bind to repeats 3, 5 and 9. Igf2r exists as monomer but tends to form dimers at the plasma membrane. It mainly localizes within the trans-Golgi where phospho-mannosyl residues of newly synthesized lysosomal enzymes bind to the M6PR binding domain. Thereby, the enzyme-receptor complex is translocated to endosomes in clathrin-coated vesicles where the low pH initiates its dissociation (Braulke & Bonifacino, 2009).

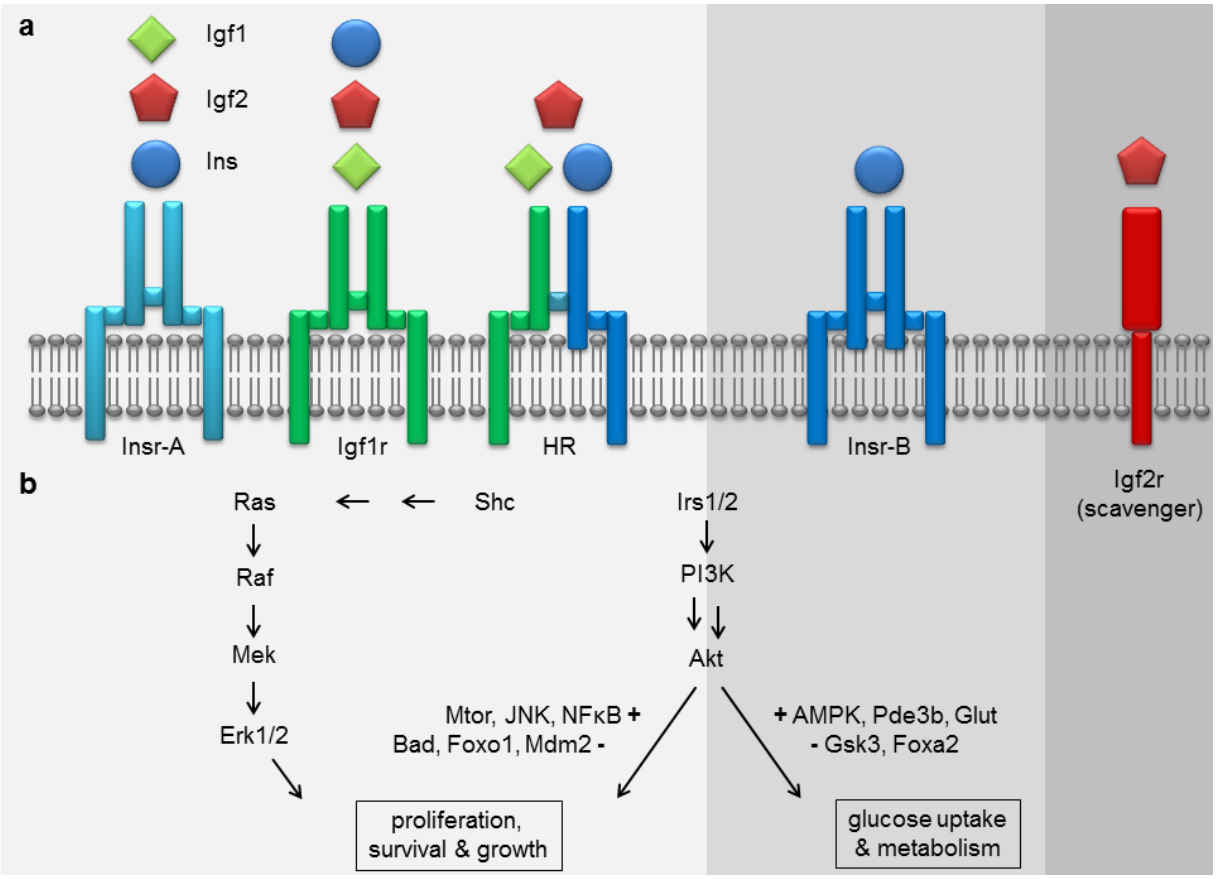

Figure 3.3.1.1 The Ins/Igf system

a, Schematic representation of the receptors of the Ins/Igf system, i.e. Insr-A, Insr-B, Igf1r, Insr/Igf1r-hybrids as well as Igf2r and the three ligands Ins, Igf1 and Igf2 with their affinities.

b, Schematic representation of Insr/Igf1r downstream signaling with indication of the predominant pathway, i.e. Insr-A, Igf1r and hybrids induce proliferation, while Insr-B activates metabolism. Modified from Clayton et al., 2011 and Belfiore et al., 2011.

3.3.2 Downstream signaling of Insr/Igf1r

Ligand stimulation of Insr, Igf1r and HR leads to auto-/transphosphorylation via their RTK domains and initiation of a complex downstream signaling cascade with two major pathways (Figure 3.3.1.1b) (Khan & Pessin, 2002). On the one hand, the phosphatidyl-inositol-4,5-bis-phosphate 3 kinase (PI3K)/serine threonine kinase Akt (Akt) pathway promotes metabolic activity. On the other hand, the mitogen-activated protein kinase (Mapk) pathway triggers proliferation. Despite their common downstream signaling proteins, activation of Insr-B is connected to cellular metabolism, whereas Igf1r and Insr-A activation rather results in cell growth and survival (Belfiore & Malaguarnera, 2011; Taniguchi, Emanuelli, & Kahn, 2006). The distinct signaling activity has been related to ligand binding to their intracellular juxtamembrane region shown by chimeric and site-mutated insulin and Igf1 receptors (Cai et al., 2017). Autophosphorylation leads to a specific dimeric arrangement of Insr and Igf1r enabling recruitment of downstream signaling proteins (Cabail et al., 2015). Pathway selectivity is achieved by phosphorylation of distinct serine and threonine residues of the insulin receptor substrates (Irs) and Shc proteins, which interact with the cytoplasmic domain of the RTKs. Thereby, the activity of Irs can either be inhibited or activated via autoregulatory feedback mechanisms (Rabiee, Kruger, Ardenkjaer-Larsen, Kahn, & Emanuelli, 2018).
PI3K/Akt pathway: Irs itself binds the regulatory subunit of PI3K which phosphorylates phosphatidyl-inositol-4,5-bisphosphate to phosphatidyl-inositol-3,4,5-trisphosphate leading to recruitment of phospho-inositide-dependent kinase 1 that phosphorylates Akt. Akt is a central mediator and upstream of multiple signaling cascades depending on the tissue. For example, Akt activation induces glucose transporter translocation to the membrane in liver and adipose tissue for glucose uptake and glycogenesis by phosphorylating Gsk3. In various cell types, the transcription factor forkhead box O1 is inhibited, which modulates gluconeogenesis and apoptosis. Proliferation and metabolism are further regulated via the phosphorylation of the Rheb GTPase activating complex tuberous sclerosis 1/2, which modulates the activity of mammalian target of rapamycin (Mtor). Apoptosis is regulated via Bcl2-associated agonist of cell death (Bad) and glucose transport via TBC1 domain family member 4.
Mapk pathway: Irs and Shc proteins can also interact with the adaptor protein growth factor receptor bound protein 2 (Grb2) that is recruited to the plasma membrane together with the guanine nucleotide exchange factor Sos. Phosphorylation of the small G-protein Ras and exchange of guanosine diphosphate with guanosine triphosphate (GTP) activates the proto-oncogene c-RAF, the dual specificity kinase Mapk kinase (Mek) and Mapk3/Erk. After translocation of Mek/Erk dimers to the nucleus, mitogens such as c-fos and Ets transcription factor Elk1 are phosphorylated.

3.3.3 Biological function of the Ins/Igf system

It is known that glucagon binds to glucagon receptors on the α-cell surface (X. Ma et al., 2005; Walker et al., 2011). However, whether insulin can act in an autocrine manner on β-cells is controversially discussed (I. B. Leibiger, Leibiger, & Berggren, 2008; Rhodes, White, Leahy, & Kahn, 2013; M. Wang, Li, Lim, & Johnson, 2013). Both, Insr and Igf1r are highly expressed in the islets of Langerhans (Kulkarni, 2004) (www.proteomicsdb.org).
In order to delineate the signaling pathways that are disturbed in diabetes, various full-body and tissue-specific KO mouse models were studied (Kahn, Bruning, Michael, & Kulkarni, 2000; Kulkarni & Okada, 2002; Mauvais-Jarvis & Kahn, 2000). Full-body $Insr^{-/-}$ mice display slight postnatal growth retardation but mainly suffer from hyperinsulinemia and hyperglycemia, which is why they die from diabetic ketoacidosis within 7 days due to β-cell failure (Joshi et al., 1996). In contrast, Igf1r regulates growth during embryonic development

via interaction with Igf1 and Igf2 (Baker, Liu, Robertson, & Efstratiadis, 1993). Surviving $Igf1^{-/-}$ mice display growth retardation and are infertile. $Igf1r^{-/-}$ mice die postnatally from respiratory failure and suffer from severe growth retardation with organ hypoplasia accompanied by ossification delay as well as central nervous system and epidermal abnormalities (J. P. Liu, Baker, Perkins, Robertson, & Efstratiadis, 1993). $Igf1^{-/-}/Igfr1^{-/-}$ as well as $Igf2^{-/-}/Igf1r^{-/-}$ and $Igf1^{-/-}/Igf2^{-/-}$ display a similar phenotype, while the $Igf2^{-/-}$ double mutants suffer from greater growth retardation. The Igf2r is paternally imprinted and genetic disruption either results in no phenotype or in postnatal lethality with fetal overgrowth depending on inheritage by the father or mother, respectively (Lau et al., 1994).

Specific inactivation of Insr in pancreatic β-cells mimicked the alterations in insulin secretion and glucose tolerance seen in T2DM (Kulkarni et al., 1999; Otani et al., 2004). Hence, GSIS is directly linked to Insr signaling in insulin-secreting cells proving an autocrine loop. Similarly, β-cell-specific KO of Igf1r also impairs glucose tolerance and GSIS via reduced levels of Glut2 and glucokinase accompanied by hyperinsulinemia (Kulkarni et al., 2002). Mice lacking both Insr and Igf1r in β-cells suffer from overt diabetes (Ueki et al., 2006). Thus, β-cell-specific KO models not only of Insr and Igf1r themselves but also of their downstream targets, especially insulin receptor substrates Irs1 (E. Araki et al., 1994; Kido et al., 2000; Kulkarni et al., 1999; Tamemoto et al., 1994) and Irs2, as well as their combinations (Assmann, Ueki, Winnay, Kadowaki, & Kulkarni, 2009; Withers et al., 1999) have underlined that Insr/Igf1r signaling is crucial for insulin secretion and β-cell function (Braun, Ramracheya, & Rorsman, 2012; Ullrich, 2013).

Additionally, insulin is known to have anti-apoptotic and pro-mitogenic effects. In β-cells, this process was shown to be concentration-dependent and regulated via Raf1-Kinase (Johnson & Alejandro, 2008) and might also be important for mitochondrial function (S. Liu et al., 2009) or ER stress-induced cell cycle arrest (De Vas & Ferrer, 2016; Szabat et al., 2016), while a compensatory or synergistic regulation of the paralogous proteins should be considered.

3.3.4 Trafficking of Insr and Igf1r

Insr and Igf1r pro-receptors are folded and processed to dimers in the ER by the chaperones calnexin and calreticulin before being transported to the Golgi apparatus where they are further post-translationally modified e.g. glycosylated (Bass et al., 1998). Via the secretory pathway, they are routed from the trans-Golgi to various organelles but especially to the plasma membrane to be available for signal transduction of extracellular ligands. Stimulation of Insr, Igf1r or other RTKs results in their endocytosis followed either by lysosomal degradation or recycling back to the membrane, a process crucial for blunting the signaling of activated receptors (Carpentier, 1994; Carpentier, Fehlmann, Van Obberghen, Gorden, & Orci, 1985; Ceresa, Kao, Santeler, & Pessin, 1998; Goh & Sorkin, 2013; Popova, Deyev, & Petrenko, 2013). The major internalization pathway is clathrin-mediated endocytosis (CME) with ligand-occupied RTKs being present in clathrin-coated pits (CCP) and either rapidly sorted to the lysosomes for degradation or more slowly recycled back to the membrane from endosomes. Clathrin-independent endocytosis occurs especially under high, rather unphysiological ligand concentrations and is more slowly compared to CME. It is associated with caveolin and cholesterol but also with actin (macropinocytosis) and studied in less detail (Boothe et al., 2016).

The clathrin triskelion consists of three light and three heavy chains. The clathrin adaptor protein Ap2 is a heterotetrameric complex consisting of the four subunits α, β2, μ2 and σ2, which directly recognize YxxΘ and dileucine (LL) internalization motifs in the cytoplasmic domain of transmembrane proteins (Braulke & Bonifacino, 2009; Hamer et al., 1997). Ubiquitination of lysine residues by E3 ubiquitin ligases that interact with phosphorylated

tyrosine residues is also characteristic for RTKs and important for their membrane trafficking. Binding of proteins with a ubiquitin binding domain such as epsin results in interaction with clathrin or Ap2 and routes ubiquitinated RTKs to CCPs. A complex of the adaptor protein Grb10 and the ubiquitin ligase Nedd4 has been described to be required for Insr/Igf1r polyubiquitinylation and internalization (Vecchione, Marchese, Henry, Rotin, & Morrione, 2003). Additionally, ubiquilin1 has been found to be important for silencing of Igf1r signaling after ligand stimulation (Kurlawala et al., 2017). Furthermore, internalization mechanisms including the downstream signaling proteins are specific to either propagate growth or metabolism of activated receptors (Choi et al., 2019; Romanelli et al., 2007). These feedback mechanisms are important for maintenance of cellular sensitivity to the ligands but have not yet been completely elucidated.

3.4 The pituitary

The pituitary is an endocrine gland that consists of the posterior (neurohypophysis, ~20 %) and the anterior pituitary (adenohypophysis, ~80 %) and regulates multiple physiological processes including blood pressure, growth, metabolism and reproduction (Dorton, 2000). The posterior pituitary is a hypothalamic extension and contains neuroendocrine cells secreting hormones synthesized by the hypothalamus. These magnocellular neurons release antidiuretic hormone alias vasopressin and oxytocin additionally to the hypothalamus.
In the anterior pituitary, there are five different endocrine cell types transducing hypothalamic signals: 38–50 % somatotropes, around 25 % corticotropes and 4-6 % each thyrotropes, gonadotropes and lactotropes. Somatotropes secrete growth hormone (Gh) alias somatotropin after activation by growth hormone releasing hormone and are inhibited by somatostatin. Corticotropin-releasing hormone induces the release of β-endorphin, adrenocorticotropin (ACTH) and melanocyte-stimulating hormone from corticotropes. Somatostatin also inhibits thyrotropes that are activated by thyrotropin releasing hormone consequently secreting thyroid stimulating hormone. Luteinizing hormone as well as follicle stimulating hormone are released from gonadotropes by gonadotropin releasing-hormone (Gnrh). Prolactin can be released from lactotropes by various factors, which are inhibited by dopamine.
Thus, the pituitary is a central regulator of different organs such as the kidneys, the thyroid gland and the gonads. Stress response is modulated via the hypothalamic pituitary adrenal and thyroid axis, whereas systemic endocrinology is described as the hypothalamic-pituitary-gonadal (HPG) axis. In the gonads, estrogen and testosterone are produced, which inhibit the production of Gnrh in the hypothalamus via a negative feedback mechanism. However, leptin and insulin activate, whereas ghrelin inhibits this production. Dysregulation or insufficiency of one or several hormones of the anterior pituitary leads to various local or systemic adverse effects including reproduction and the immune system.
Regarding the Ins/Igf system, Igf1 is produced predominantly in ACTH-positive cells and might act in a autocrine and paracrine manner and thus be involved in the development of adenomas (Jevdjovic, Bernays, & Eppler, 2007). Apart from Igf1, insulin signaling via Insr in gonadotrophs is connected to female infertility in obese mice (Brothers et al., 2010). Lack of Insr and Igf1r in somatotrophs leads to elevated Gh and Igf1 levels (Gahete et al., 2011). In lean mice, glucose clearance is enhanced, while mice develop hyperglycemia and insulin resistance under caloric excess. Furthermore, men with type 2 diabetes display decreased testosterone levels, while the correlation to adverse cardiovascular and metabolic effects is not yet elucidated (Cheung et al., 2015).

3.5 *5330417C22Rik* and *9330182L06Rik*: state of the art

3.5.1 *5330417C22Rik*

The RIKEN clone *5330417C22Rik* has been identified in a cDNA microarray for sequencing the murine genome (Bono, Kasukawa, Furuno, Hayashizaki, & Okazaki, 2002; Bono, Kasukawa, Hayashizaki, & Okazaki, 2002; Bono et al., 2003; Miki et al., 2001). The human orthologue KIAA1324 belongs to the unknown protein family UPF0577 and has so far been described in the context of cancer in various tissues, especially in female reproductive organs. First, *KIAA1324* is overexpressed in breast and lung cancer cell lines with high metastatic capacity, whereas alternatively spliced proteins are detected in non-metastatic cells (Bauer, Aust, & Schumacher, 2004). *KIAA1324* has also been identified in different types of endometrial cancer and been named estrogen-induced gene 121 (EIG121) due to its upregulation during postmenopausal estrogen replacement therapy (Deng et al., 2005). Expression of *EIG121* is increased in the estrogen-proliferative phase of premenopausal endometrium and in endometrioid carcinoma, while mRNA levels decrease in later disease stages, and only detected in low levels in estrogen-independent tumors. High expression of *estrogen receptor (ER) α* and *EIG121* correlates with shorter overall survival and could be used as prognostic biomarker to predict responsiveness to hormone treatment in women with advanced stage ovarian/primary peritoneal high-grade serous carcinoma after surgery (Schlumbrecht, Xie, Shipley, Urbauer, & Broaddus, 2011). A polymorphic short tandem repeat in the upstream regulatory region of *EIG121* is not responsible for its altered expression and therefore not associated with the risk for breast or endometrioid tumor development (Bolton et al., 2016). Additionally, *KIAA1324* is among nine genes differentially expressed after ovarian failure that could be used for potential prediction of fertility and preventive therapies (Jaillard et al., 2016). Transcriptomic comparison of endometrioid and clear cell carcinoma histotypes with high-grade serous carcinoma revealed a differential expression of *KIAA1324* in these distinct malignant ovarian epithelial cells (Fridley et al., 2018) and proteomic studies identified KIAA1324 as a novel biomarker being associated with favorable prognosis via estrogen and interferon signaling pathways (Dieters-Castator et al., 2019).

In vitro, EIG121 is further described as transmembrane protein in the cell surface and in endosomal-lysosomal compartments. Its overexpression diminishes cellular proliferation and induces autophagy, whereas its knock-down in combination with starvation or cytotoxic conditions results in augmented apoptosis (Deng, Feng, & Broaddus, 2010). Also in endometrial cancer stem cells, EIG121 is involved in autophagy correlating with stemness and could be involved in chemoresistance mechanisms (X. Ran, Zhou, & Zhang, 2017).

In pancreatic neuroendocrine tumors increased mRNA expression of *EIG121* together with *progesterone receptor* and *ERβ* was favorable for the prognostic outcome (Estrella et al., 2014). In gastric cancer, transcriptomic analysis show downregulation of *KIAA1324* via histone deacetylase and association with poor prognosis. Less tumors are formed in a xenograft model by inhibition of proliferation, invasion and drug resistance and increased apoptosis by blocking oncogenic actions of GRP78 (Kang et al., 2015). By *in silico* analysis, *KIAA1324* was furthermore identified as potential biomarker to distinguish between pseudoinvasive colorectal adenoma and invasive adenocarcinoma (Hauptman, Bostjancic, Zlajpah, Rankovic, & Zidar, 2018). Analysis of secretory cell function upon deletion or forced expression of basic helix-loop-helix MIST1 in parietal cells and hepatocytes identified KIAA1324 as a downstream target resulting in similar down- or upregulation, respectively. Thus, KIAA1324 is involved in autophagy and lysosomal trafficking to maintain physiology of mature endo- and exocrine cells (Lo et al., 2017). Additionally, KIAA1324 was discovered in exosomes of human parotid saliva (Gonzalez-Begne et al., 2009).

To summarize, KIAA1324/EIG121 is differentially expressed in tumors of distinct tissues and involved in autophagy. In our lab, gene *5330417C22Rik* was found to be differentially expressed in pancreatic epithelial cells during secondary transition of pancreas development (Willmann et al., 2016). Its role in energy metabolism and molecular function has been initially described in the PhD thesis of Felizitas Gräfin von Hahn.

3.5.2 *9330182L06Rik*

Analogously, gene *9330182L06Rik* has been identified in the RIKEN project(Bono, Kasukawa, Furuno, et al., 2002; Bono, Kasukawa, Hayashizaki, et al., 2002; Bono et al., 2003; Miki et al., 2001). It is the paralogue of gene *5330417C22Rik* and has thus been named EIG121-like (EIG121L) or KIAA1324-like (KIAA1324L). The protein is evolutionary highly conserved as well but has so far not been described in mouse or human. In *Xenopus laevis,* EIG121L is expressed during embryonic development and *knock-down* of EIG121L leads to severe developmental defects (T. Araki, Kusakabe, & Nishida, 2007, 2011). It was shown that lack of EIG121L suppresses bone morphogenetic protein (BMP) receptor signaling necessary for epidermal differentiation as EIG121L physically interacts with BMP receptors. In human dyslipidemia patients, DNA methylation associated with the anti-inflammatory response upon treatment with fenofibrate, a peroxisome-proliferator-activated receptor α inhibitor, was assessed (Yusuf et al., 2017). Significant changes in CpG sites were mapped to KIAA1324L, which also interacts with genes related to inflammation. In human patients with psoriasis, EIG121L was identified as a target gene of microRNA miR-31 whose downregulation in dermal mesenchymal stem cells results in 5 fold upregulation of EIG121L expression and inhibition of proliferation (Q. Wang et al., 2019). Thus, EIG121L seems to be involved in embryonic differentiation via modulation of RTK signaling. The involvement of EIG121L in inflammation and proliferation has not yet been elucidated.

3.6 Aim of the thesis

Diabetes and cancer are caused by a dysregulation of the insulin/insulin-like growth factor (Ins/Igf) system, which is a major regulator of growth and metabolism. In our laboratory, we identified two putative novel components of the Ins/Igf system, which we named Igf receptor-like 1 and 2 (Igfr-L1 and Igfr-L2) due to their domain structure similarities to Insr, Igf1r and Igf2r. Therefore, the overall aim of this thesis was to further delineate the function of the paralogous proteins especially in the endocrine pancreas where Insr/Igf1r signaling regulates cellular proliferation and systemic glucose homeostasis.

For Igfr-L1, several full-body and tissue-specific knock-out mouse models were used: As full-body Igfr-L1$^{-/-}$ animals died postnatally with signs of hypoglycemia and hyperinsulinemia, potential morphological or functional alterations in the pancreas were analyzed. As β-cells are the source of insulin, alterations in Insr/Igf1r signaling were studied after *ex vivo* Cre recombinase induction in isolated islets of tamoxifen-inducible β-cell-specific Igfr-L1$^{-/-}$ (MIP-CreERT) animals. Because Igfr-L1 is highly expressed in all subtypes of pancreatic endocrine cells, constitutive endocrine-specific (Ngn3-Cre) Igfr-L1$^{-/-}$ mice were analyzed in respect of their glucose tolerance. Furthermore, a role of Igfr-L1 in impaired glucose homeostasis was studied regarding expression and genetic reduction of Igfr-L1 levels either in Igfr-L1$^{+/-}$ or endocrine-specific Igfr-L1$^{-/-}$ diabetic animals. Blood glucose homeostasis and β-cell function were investigated at different postnatal and adult stages. To shed light on the underlying mechanism, i.e. how Igfr-L1 might be involved in the Ins/Igf system, Min6 wildtype and Igfr-L1$^{-/-}$ cells were used. Potential interaction partners were identified by co-immunoprecipitation as well as proximity ligation and studied in respect of receptor endocytosis from the surface.
The paralogue Igfr-L2 strongly interacts with Igfr-L1 depending on the metabolic activity of the cells and has so far not been described in mouse or human. Therefore, bioinformatic analyses were performed and Igfr-L2 detected in endocrine cells after generation of specific antibodies. Full-body Igfr-L2$^{-/-}$ animals were studied to delineate a biological role of Igfr-L2 in survival and endocrine function. Mechanistically, Insr/Igf1r signaling was investigated in CRISPR/Cas9-mediated Igfr-L2$^{-/-}$ and Igfr-L1$^{-/-}$+L2$^{-/-}$ Min6 cells. To identify synergistic or compensatory functions of the paralogues *in vivo*, a double knock-out mouse line was generated in addition.
Unravelling the involvement of Igfr-L1 and Igfr-L2 in the regulation of metabolism and proliferation of the endocrine pancreas via the Ins/Igf system will help to understand the pathomechanisms of diabetes and might provide new potential targets in its therapy.

4. Results

4.1 Analysis of Igfr-L1 *in vivo*

Our laboratory previously identified *Igfr-L1* as being differentially regulated during pancreas development and endocrine cell differentiation (Willmann et al., 2016). The similarities to Insr, Ifg1r and Igf2r in the extracellular domain structure suggested a potential role of Igfr-L1 in endocrinogenesis and the Ins/Igf system. To analyze the expression and function of Igfr-L1 in the pancreas and particularly in the islets of Langerhans, different knock-out (KO) mouse models were used, i.e. full-body KO, tamoxifen-inducible β-cell-specific (MIP-CreERT) as well as endocrine-specific (Ngn3-Cre) conditional KO animals.

4.1.1 Targeting strategy for Igfr-L1$^{-/-}$

The Cre-loxP recombination system has become a useful tool to analyze gene function in a time- and tissue-specific manner (Metzger & Chambon, 2001; Sternberg & Hamilton, 1981). Within the scope of the European conditional mouse mutagenesis program (EUCOMM), gene *5330417C22Rik* (wildtype) was targeted, generating a so called gene trap allele with a β-galactosidase (LacZ) reporter cassette and a neomycin resistance (NeoR) as well as loxP and FRT sites for recombination with Cre recombinase or FLPe, respectively (Figure 4.1.1.1a). Thus, there are three possibilities for generating a KO: First, the gene trap allele itself results in a null mutant due to a shortened transcript. Second, deletion of exon 3 by Rosa-Cre leads to a full-body KO (ΔEx3) still having the LacZ reporter cassette for expression analysis (Figure 4.1.1.1b). Third, excision of the LacZ and NeoR cassette by recombination with FLPe generates a floxed allele (fl). Subsequent crossing with Rosa-Cre results in the so called flox-deleted (FD) allele (Figure 4.1.1.1c). Additionally, tissue-specific Cre recombinases (MIP-CreERT, Ngn3-Cre) can be used for the generation of conditional KO animals (Magnuson & Osipovich, 2013).

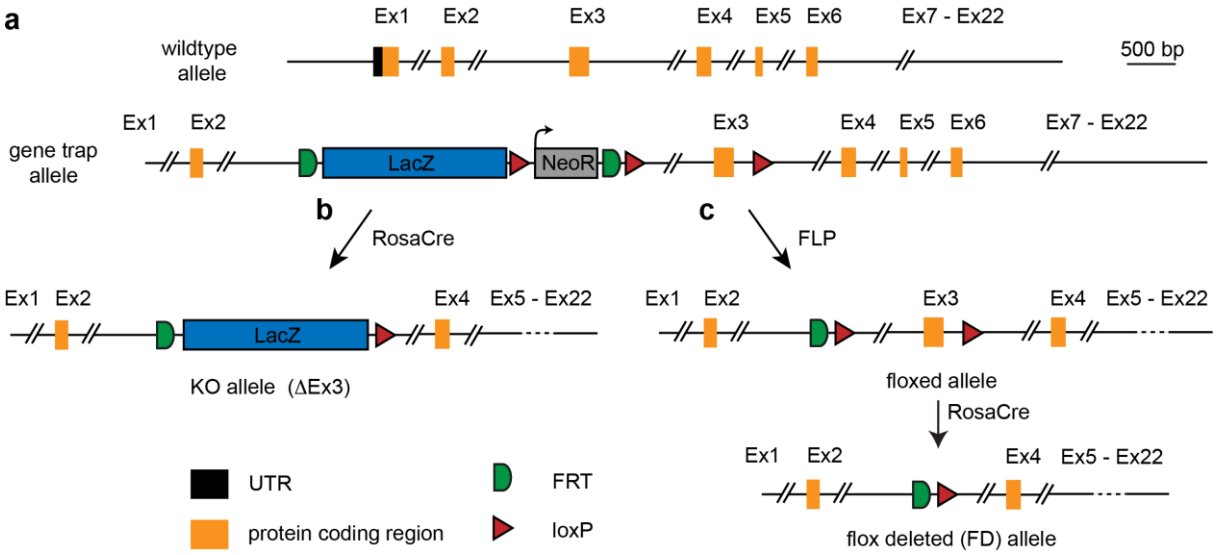

Figure 4.1.1.1 Targeting of gene *5330417C22Rik* to obtain Igfr-L1$^{-/-}$ animals

Schematic representation of the three alleles used for generation of Igfr-L1$^{-/-}$, i.e. gene trap (a), ΔEx3 (b) or flox-deleted (c).

a, Gene trap allele with the LacZ reporter and NeoR cassette as well as loxP and FRT sites for potential recombination in comparison to the wildtype allele.

b, KO allele (ΔEx3) with the LacZ reporter and NeoR cassette after recombination of loxP sites in the gene trap allele with Rosa-Cre.

c, flox-deleted allele (FD) after recombination of loxP sites in the floxed allele with Rosa-Cre recombinase. The floxed allele was obtained by excision of the LacZ reporter and NeoR cassette by recombination of FRT sites in the gene trap allele with FLPe.

4.1.2 Pancreatic expression of Igfr-L1

In order to study the function of Igfr-L1 in the islets of Langerhans, its expression in the endocrine pancreas was confirmed. At embryonic stage E14.5, when *Igfr-L1* has been identified in the screen, mRNA expression was highest within the pancreas as shown by *in silico* hybridization analysis (Figure 4.1.2.1a). Also in adult mice, broad expression of *Igfr-L1* was detectable within the whole pancreas using the ΔEx3 allele and performing a β-galactosidase staining (Figure 4.1.2.1b). Protein expression was confirmed by immunohistochemistry (IHC) on the cellular level where Igfr-L1 was detected in endocrine α- and β-cells as well as exocrine cells in the postnatal pancreas (Figure 4.1.2.1c).

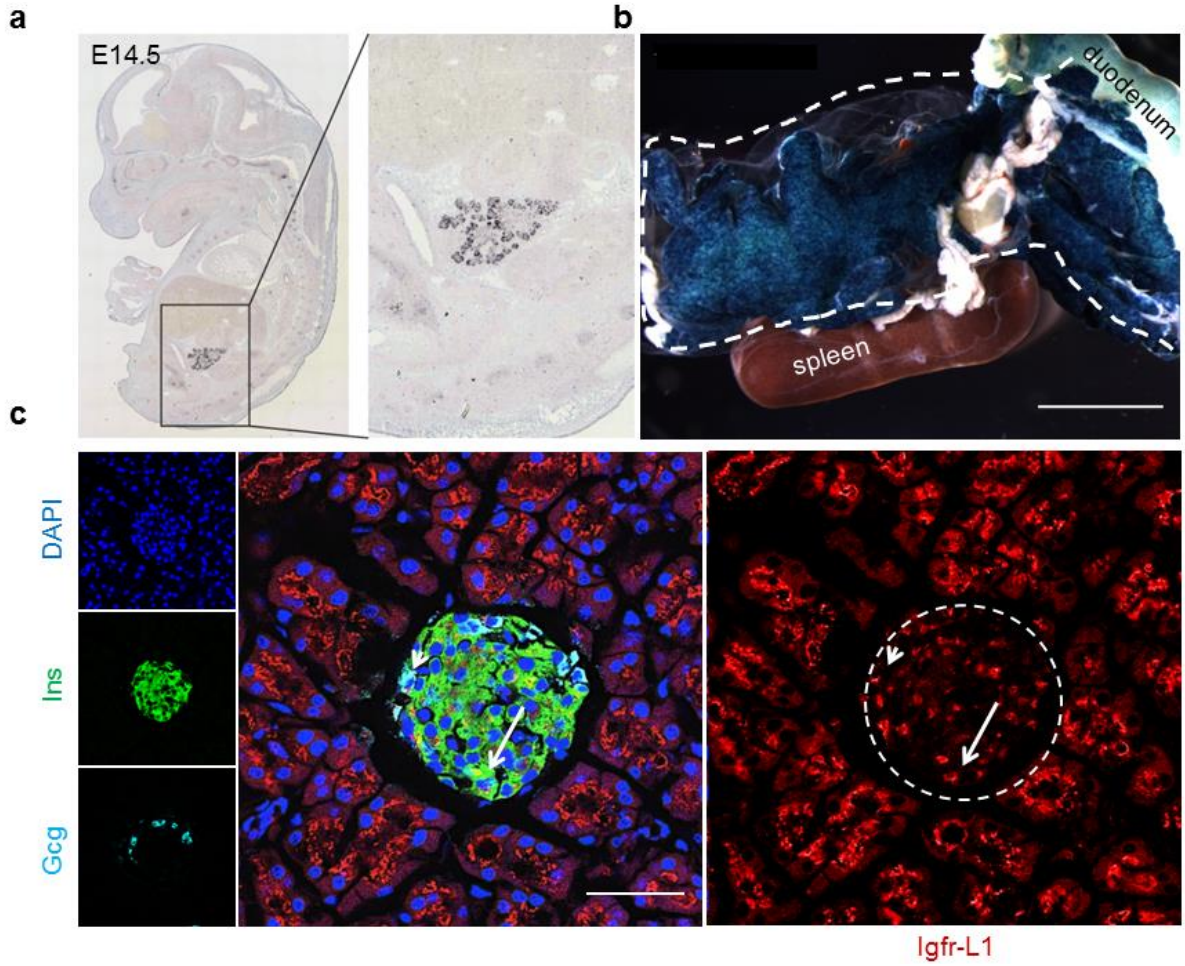

Figure 4.1.2.1 Expression of Igfr-L1 in the pancreas

a, mRNA expression of *Igfr-L1* at E14.5 detected by *in silico* hybridization (genepaint.org).

b, LacZ staining of *Igfr-L1* in the pancreas (dashed line) dissected from an adult Igfr-L1$^{+/-}$ female (8 months). Scale bar, 5 mm.

c, Representative Laser scanning microscopy (LSM) images of the expression of Igfr-L1 (red) in islets (dashed line) marked by insulin (green, arrow) and glucagon (cyan, arrowhead) as well as in surrounding acinar cells in C57Bl/6J at P25. Scale bar, 50 µm.

4.1.3 Analysis of full-body Igfr-L1$^{-/-}$ (ΔEx3)

Full-body KO animals (Igfr-L1$^{-/-}$) were generated to study the biological function of Igfr-L1, especially in respect of the pancreas. Strikingly, Igfr-L1$^{-/-}$ neonates died postnatally within a few hours but were born at the expected Mendelian ratio and without significant differences in body weight compared to Igfr-L1$^{+/+}$ and Igfr-L1$^{+/-}$ (Figure 4.1.3.1a-b). After Caesarian section at E19.5, Igfr-L1$^{-/-}$ neonates did not show any developmental defects but suffered from cyanotic episodes and respiratory distress resulting in blueish discoloration (Figure 4.1.3.1c). Postpartum, Igfr-L1$^{-/-}$ neonates did not have milk in their stomach and physiological analysis (PhD project of Fataneh Fathi Far) suggested that hypoglycemia due to hyperinsulinemia might be a possible cause of death. Furthermore, it was found that lack of Igfr-L1 resulted in increased endocrine proliferation at E16.5 potentially due to overactivation of the Insr/Igf1r signaling pathway.

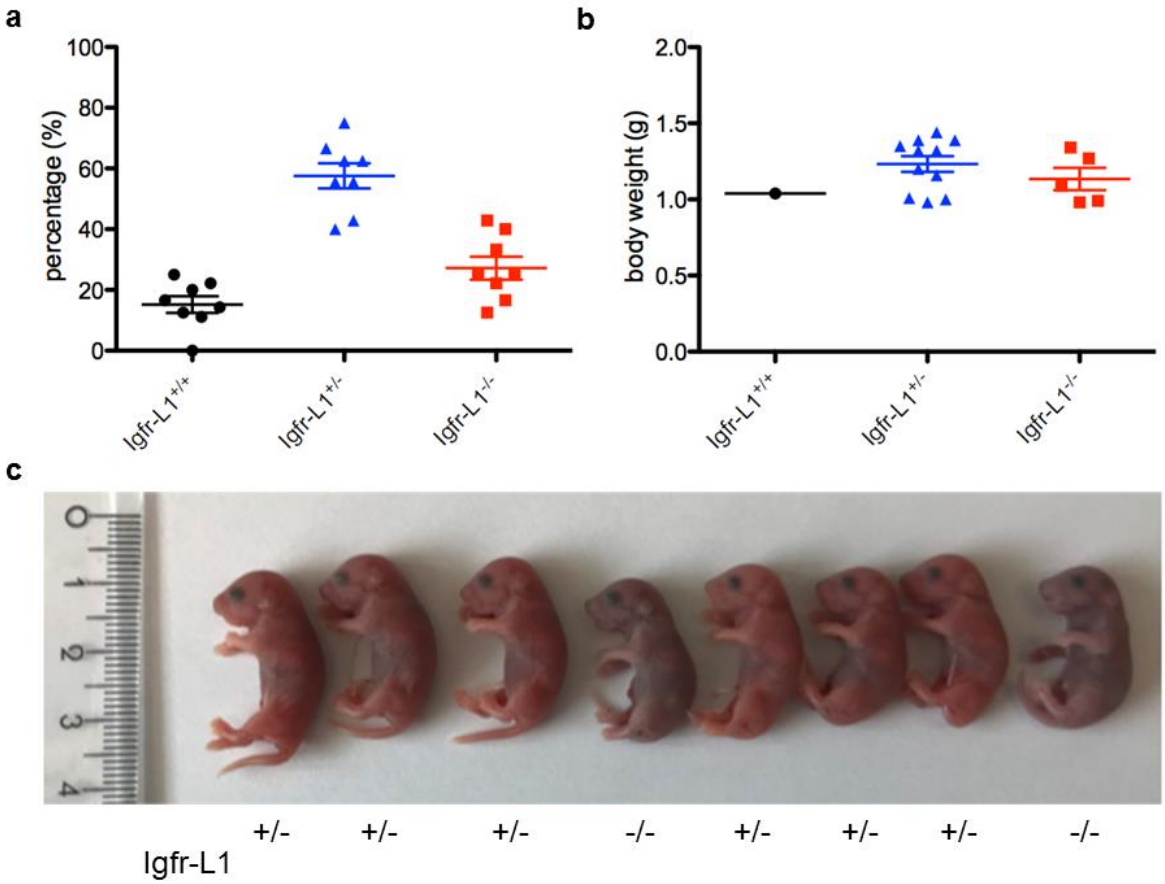

Figure 4.1.3.1 Mendelian ratio, body weight and appearance of Igfr-L1$^{-/-}$ neonates

a, Mendelian ratio of neonates at E19.5 obtained from eight Igfr-L1$^{+/-}$ intercrosses. Igfr-L1$^{+/+}$, n=9; Igfr-L1$^{+/-}$, n=35; Igfr-L1$^{-/-}$, n=14; higher n available outside of this thesis.

b, Body weight of neonates at E19.5 from two Igfr-L1$^{+/-}$ intercrosses. n.s., *P*=0.2987; (Igfr-L1$^{+/+}$, n=1;) Igfr-L1$^{+/-}$, n=11; Igfr-L1$^{-/-}$, n=5.

c, Appearance of neonates at E19.5 obtained from an Igfr-L1$^{+/-}$ intercross with indication of the genotype.

Error bars represent SEM and *, *P*<0.05; **, *P*<0.01; ***, *P*<0.001. *P*-values were analyzed using a two-tailed, unpaired student's t-test.

To analyze the functional role of Igfr-L1 in the pancreas, gross morphological analysis was performed at E19.5, which did not reveal obvious differences between Igfr-L1$^{+/+}$ and Igfr-L1$^{-/-}$ pancreata (Figure 4.1.3.2a). Lack of Igfr-L1 within the pancreas was confirmed by IHC with a

polyclonal rabbit anit-extracellular-IGFR-L1 (1374) and a monoclonal rat anti-cytoplasmic-IGFR-L1 (16F6) antibody (Figure 4.1.3.2b). On the cellular level, all three lineages, i.e. endocrine (chromogranin A, ChrA), ductal (Sox9) and exocrine (amylase, Amy), were formed in Igfr-L1$^{-/-}$ confirming that there were no developmental defects in the pancreas at E19.5 (Figure 4.1.3.2c).

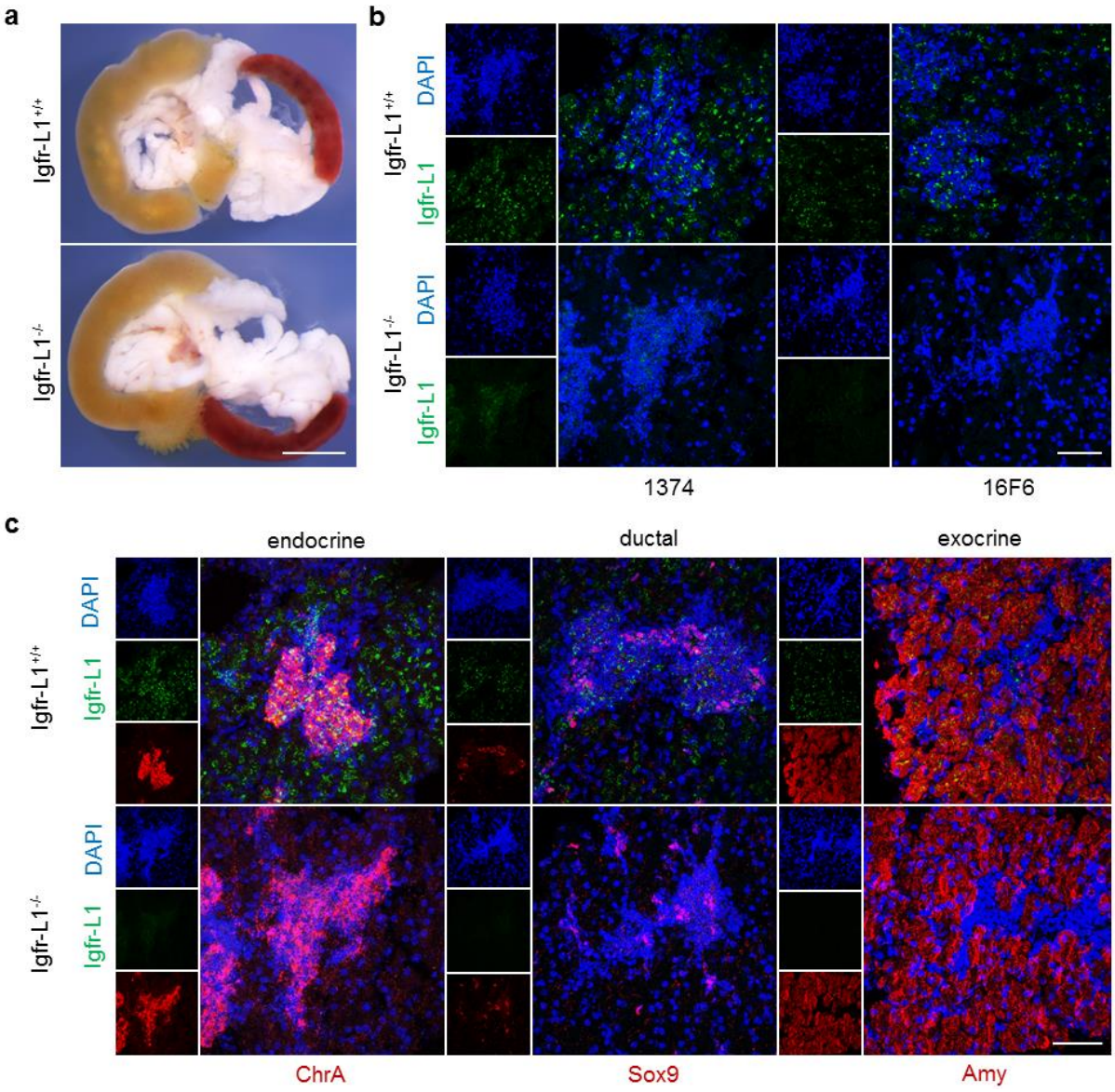

Figure 4.1.3.2 Morphological analysis of Igfr-L1$^{-/-}$ pancreata

a, Gross morphology of pancreata dissected from Igfr-L1$^{+/+}$ and Igfr-L1$^{-/-}$ neonates. White, pancreas; yellow, duodenum; red, spleen. Scale bar, 2 mm.

b, Confirmation of Igfr-L1$^{-/-}$ in pancreata at E19.5 with two different antibodies (1374, 16F6). Images of c without marker. Scale bar, 50 µm.

c, LSM images of the expression of markers for the endocrine, ductal and exocrine lineage (red) in pancreata of Igfr-L1$^{+/+}$ and Igfr-L1$^{-/-}$ at E19.5. Scale bar, 50 µm.

To identify a reason for hyperinsulinemia and any functional endocrine defects, exocytosis of insulin upon amino acid and glucose stimulation was analyzed in whole pancreata in a dynamic perfusion assay together with Dr. Ansarullah. No significant difference in insulin secretion could be observed between Igfr-L1$^{+/+}$ and Igfr-L1$^{-/-}$ pancreata (Figure 4.1.3.3). In conclusion, pancreata of Igfr-L1$^{-/-}$ did not show histological alterations or impaired function.

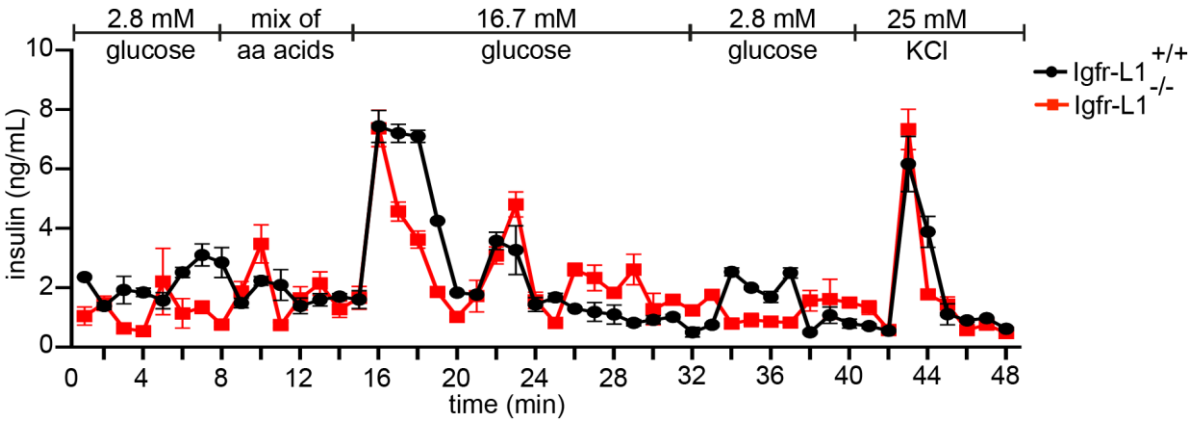

Figure 4.1.3.3 Dynamic insulin secretion in Igfr-L1$^{+/+}$ and Igfr-L1$^{-/-}$ pancreata

Insulin secreted from pancreata of Igfr-L1$^{+/+}$ and Igfr-L1$^{-/-}$ neonates at E19.5 during incubation with glucose, amino acids and KCl. Performed with Dr. Ansarullah.
Igfr-L1$^{+/+}$, n=3; Igfr-L1$^{-/-}$, n=3 mice.

4.1.4 Analysis of β-cell-specific Igfr-L1$^{-/-}$ islets (MIP-CreERT)

Due to the postnatal death of Igfr-L1$^{-/-}$ neonates, an inducible β-cell-specific Igfr-L1$^{-/-}$ line was generated in order to analyze the function of Igfr-L1 in adult β-cell homeostasis. Therefore, the Cre-recombinase was expressed under the insulin promoter (MIP-CreERT (Tamarina, Roe, & Philipson, 2014)) and induced by tamoxifen administration (*in vivo*, PhD project of Fataneh Fathi Far). To study Insr/Igf1r signaling and proliferation, islets were isolated from MIP-CreERT+, Igfr-L1$^{fl/FD}$ (βCKO, tamoxifen) and MIP-CreERT+, Igfr-L1$^{+/fl}$ (control (ctrl), vehicle) and Cre recombinase induced *ex vivo.*

First, *ex vivo* deletion efficiency was analyzed by IHC at different time points after tamoxifen or vehicle treatment including an overnight (o.n.) rest (Figure 4.1.4.1a). For whole islets, antibody penetration to the core was expected to be impaired and thus, islets were dispersed as well after isolation. After 24 h and 48 h, Igfr-L1 could still be detected in β-cells in whole and dispersed islets, whereas expression was reduced compared to ctrl (Figure 4.1.4.1b). The strong expression of Igfr-L1 in α-cells was comparable. Including a 72 h wash period, complete lack of Igfr-L1 in the majority of islet cells was observed and a deletion efficiency of 80 % was quantified by Western Blot (WB) (Figure 4.1.4.1c, Figure 4.1.4.2b-c). Hence, genetic recombination and protein loss is not fully accomplished after 48 h.

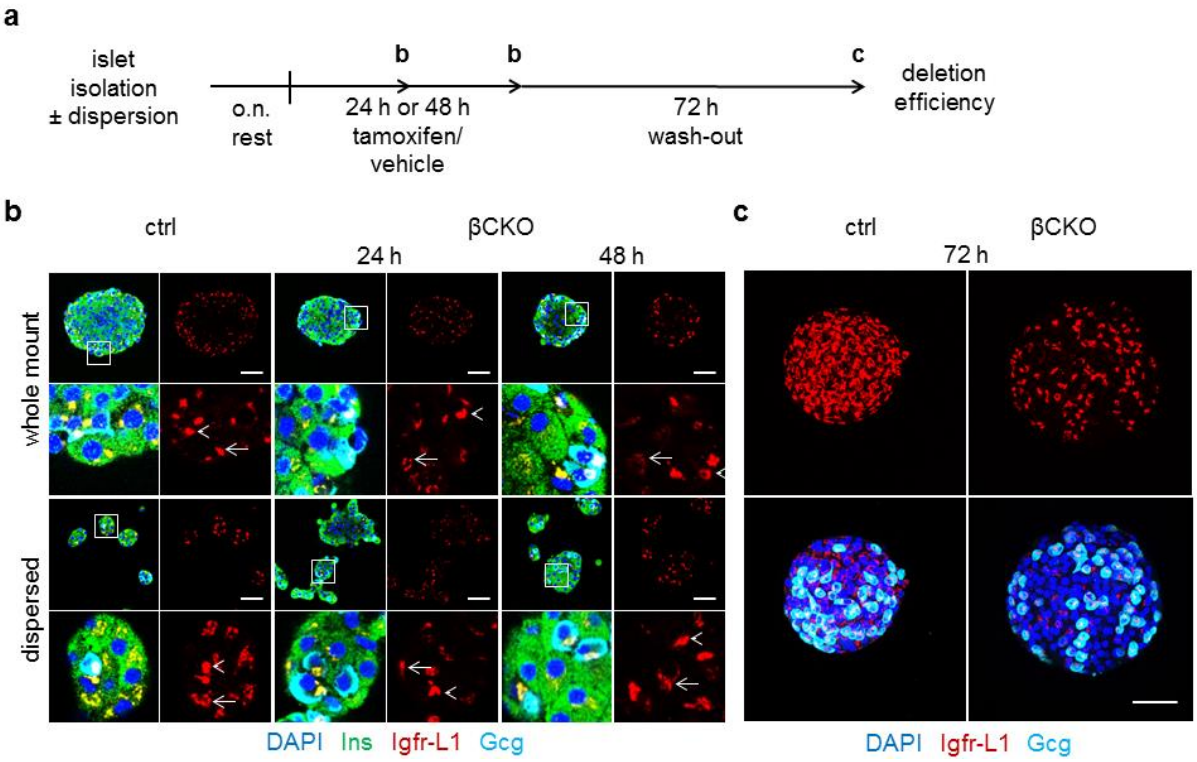

Figure 4.1.4.1 Deletion efficiency in *ex vivo* induced βCKO islets

a, Experimental design for the analysis of the deletion efficiency in βCKO islets after *ex vivo* induction.

b, Representative LSM images of the expression of Igfr-L1 (red) in whole mount and dispersed islets after 24 h and 48 h of tamoxifen treatment compared to ctrl together with insulin (green, arrow) and glucagon (cyan, arrowhead). Scale bar, 50 µm.

c, Representative LSM images of the expression of Igfr-L1 (red) in whole mount islets (max. projection) after 48 h of tamoxifen treatment and additional 72 h wash-out together with glucagon (cyan). Scale bar, 50 µm.

For the study of Insr/Igf1r signaling, βCKO islets were treated for 48 h with tamoxifen and ctrl islets with vehicle followed by a 72 h wash period to avoid any effects of tamoxifen itself (Figure 4.1.4.2a). Cells were starved for 2 h in HEPES-balanced salt solution (HBSS) and subsequently stimulated with 10 nM insulin for 5 min (Figure 4.1.4.2b-c). Igfr-L1 levels were significantly reduced whereas phosphorylation was significantly increased after normalization to both Insr and Igf1r. This suggests that Igfr-L1 might act as a negative regulator of Insr/Igf1r signaling in β-cells.

To see if the increased activity of Insr and Igf1r results in proliferation, which was increased in endocrine cells of Igfr-L1$^{-/-}$ at E16.5, islets were incubated for 24 h with 5'-Ethynyl-2'-deoxyuridine (EdU) after the wash period (Figure 4.1.4.3a). It was reported that the human growth hormone can be expressed within the islets due to the MIP-CreERT transgene, which could trigger proliferation (Oropeza et al., 2015). Thus, ctrl islets were treated with vehicle. On cryosections, proliferation was assessed by visualization of EdU incorporated into newly synthesized DNA and phospho-Histone H3 (p-HH3) indicating chromatin modification for transcription (Figure 4.1.4.3b). The proliferation in adult islets was generally very low and no measurable difference could be observed between βCKO and ctrl islets under the used conditions.

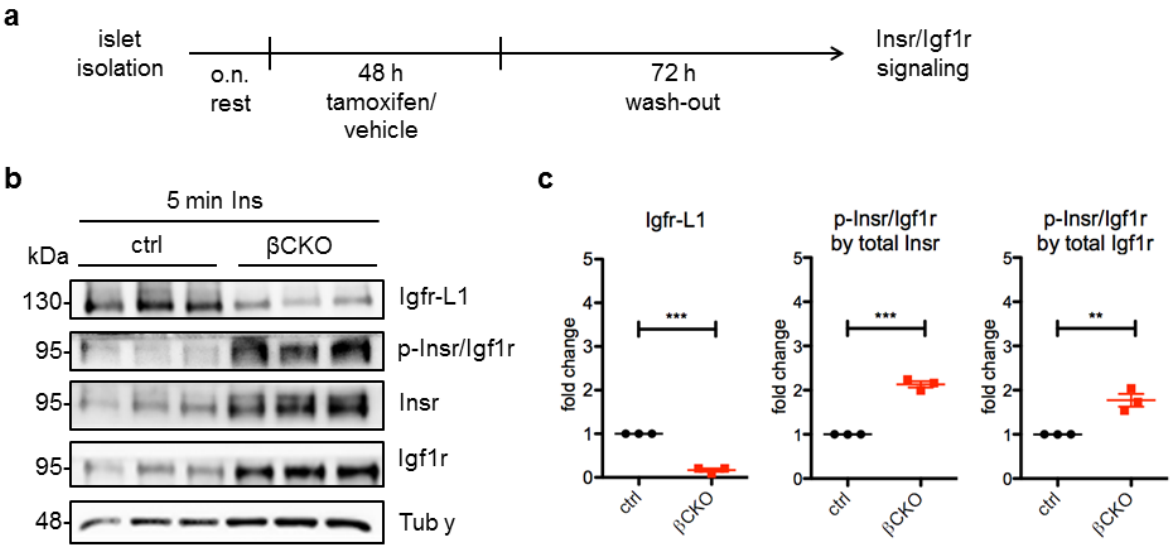

Figure 4.1.4.2 Insr/Igf1r signaling in βCKO islets

a, Experimental design for the analysis of Insr/Igf1r signaling in βCKO islets after *ex vivo* induction of MIP-CreERT with tamoxifen.

b-c, WB (b) and quantification (c) of Insr/Igf1r signaling in βCKO and ctrl islets upon stimulation with 10 nM insulin for 5 min after 2 h starvation.
***, Igfr-L1, $P<0.0001$; ***, p-Insr/Igf1r by total Insr, $P<0.0001$;
**, p-Insr/Igf1r by total Igf1r, $P=0.0061$; βCKO, n=3; ctrl, n=3 mice.

Error bars represent SEM and *, $P<0.05$; **, $P<0.01$; ***, $P<0.001$. *P*-values were analyzed using a two-tailed, unpaired student's t-test.

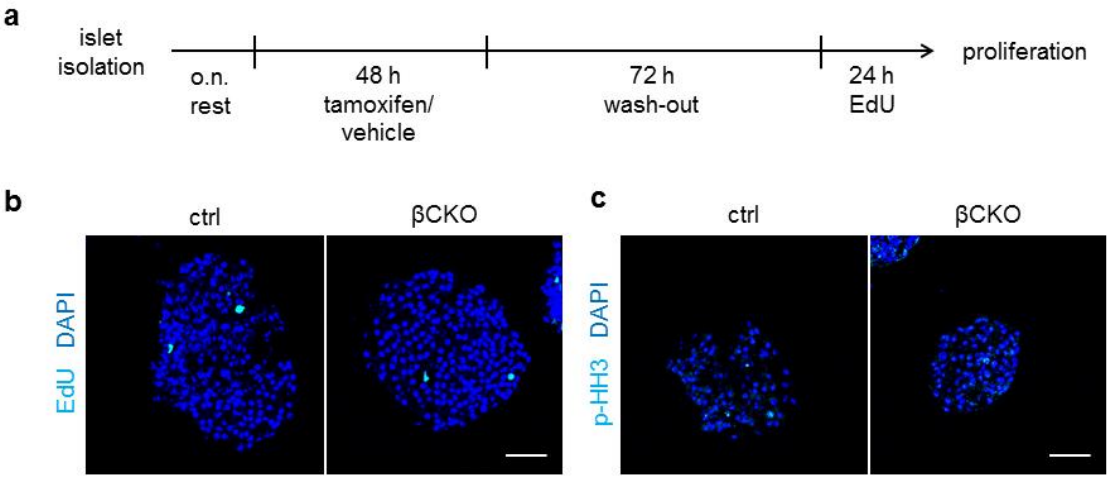

Figure 4.1.4.3 Proliferation in βCKO islets

a, Experimental design for the analysis of proliferation in βCKO islets after *ex vivo* induction.

b, Representative LSM images for the incorporation of EdU and expression of p-HH3 (cyan) in isolated islets of βCKO and ctrl animals. Scale bar, 50 µm.

4.1.5 Analysis of endocrine-specific Igfr-L1$^{-/-}$ (Ngn3-Cre)

Igfr-L1 was not only differentially expressed during secondary transition when the endocrine pancreas is formed but can also be found in all endocrine subtypes, i.e. α-, β-, δ- and PP-cells. To further investigate, how lack of Igfr-L1 in the entire islet of Langerhans is connected to the postnatal lethality and glucose homeostasis, endocrine-specific Igfr-L1$^{-/-}$ mice (CKO) were generated (Figure 4.1.5.1). Therefore, a constitutive Cre-recombinase driven by the promoter of neurogenin3 (Ngn3), the master regulator of the formation of all endocrine lineages (Gradwohl et al., 2000), was used.

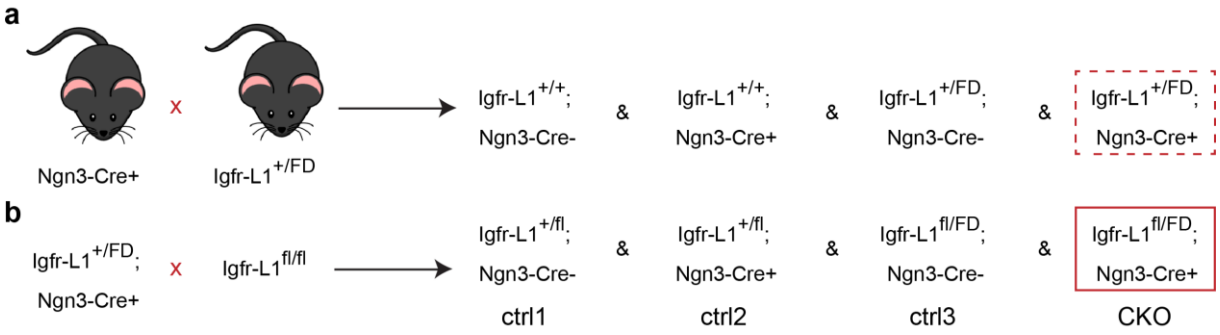

Figure 4.1.5.1 Generation of endocrine CKO and ctrl animals

a-b, Mating scheme for the generation of the parental line (a) as well as CKO and ctrl animals (b) for analysis.

Assessment of the Mendelian ratio at weaning age showed approximately the expected percentage for all four genotypes with 31 % ctrl1, 28 % ctrl2, 14 % ctrl3 and 27 % CKO (Figure 4.1.5.2a). Neonates that died postpartum were genotyped as well assuming CKO offspring to be lethal. However, apart from a very low percentage of ctrl2, there was no susceptibility to death of one specific genotype (Figure 4.1.5.2b). To conclude, Igfr-L1 endocrine CKO animals were viable and showed no developmental defects or obvious phenotype. Specific deletion of Igfr-L1 in the pancreatic endocrine compartment was confirmed by IHC, i.e. no protein could be detected in the islets of Langerhans (Figure 4.1.5.2c). Interestingly, islet composition seemed to be altered as an increased number of glucagon-positive cells was detected, which has to be confirmed by thorough quantification.

It was anticipated that the lack of Igfr-L1 within the glucose homeostasis regulating cells and the increase in α-cell area might result in a metabolic dysregulation. Hence, glucose tolerance after intraperitoneal glucose injection (2g/kg BW) together with body weight and fasting blood glucose levels was analyzed at 1 m, 3 m and 6 m in male and female mice.
In males, neither body weight nor 6 h fasting blood glucose levels (morning fast) at 1 m and 3 m or overnight fast at 6 m were significantly different in CKO and ctrl mice (Figure 4.1.5.3a-c and Figure 4.1.5.3d-f). There was only a tendency to lower 6 h fasting glucose levels in CKO compared to ctrl3 at 3 m. In a glucose tolerance test (GTT), no difference between CKO and ctrl animals was observed at 1 m or 6 m, whereas blood glucose levels of ctrl2 were significantly lower after 15 min compared to ctrl3 (Figure 4.1.5.3g-i). At 3 m, ctrl1 animals showed significantly higher glucose levels after 30 min.

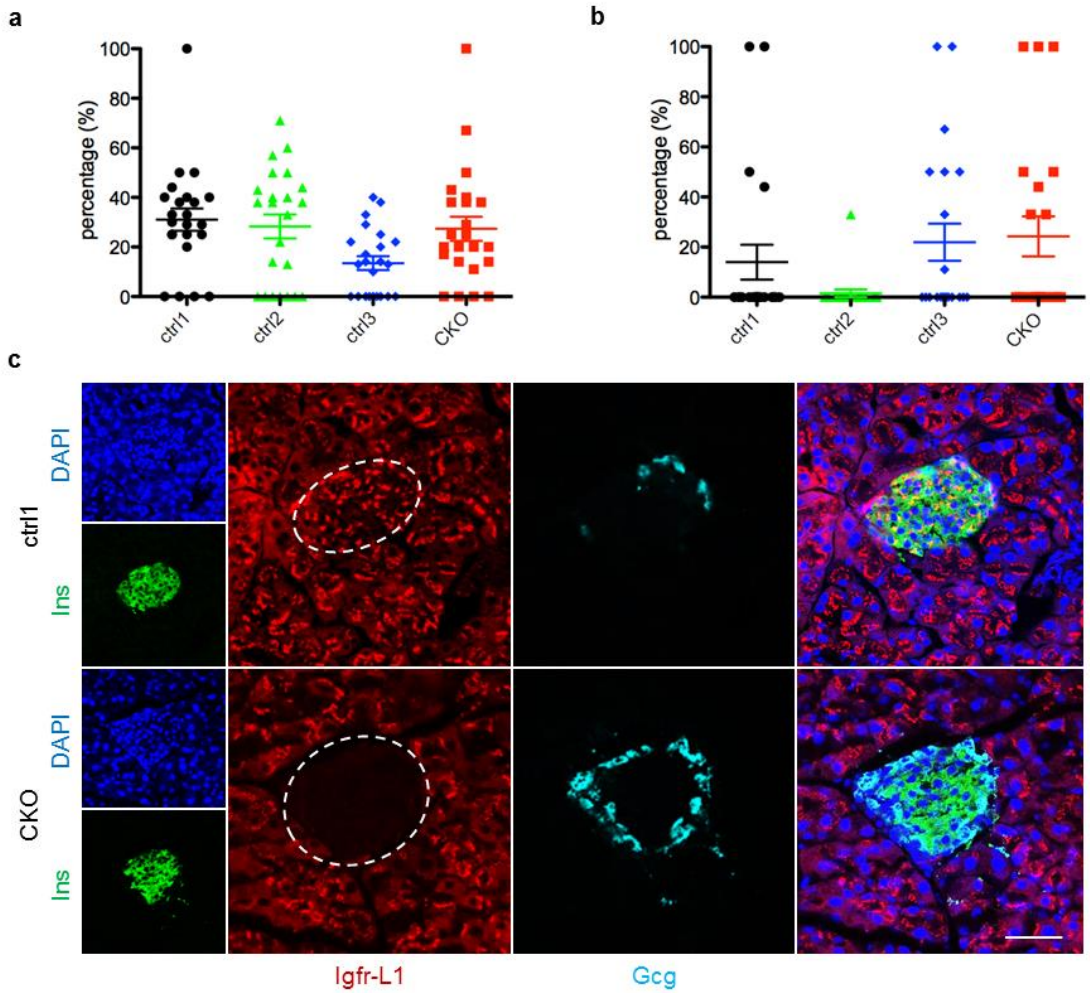

Figure 4.1.5.2 Mendelian ratio and confirmation of endocrine CKO

a-b, Mendelian ratio of weaned (a) and postnatally lethal (b) offspring during CKO generation. Weaned, n=23; lethal, n=21 litter.

c, Representative LSM images (max. projection) for the lack of expression of Igfr-L1 (red) in the islets of endocrine CKO and ctrl1 mice marked by insulin (green) and glucagon (cyan). Scale bar, 50 µm.

In females, body weight was not significantly different between CKO and ctrl groups, whereas at 3m, ctrl2 showed a tendency to lower body weight compared to ctrl1 and ctrl3. 6 h fasting blood glucose levels (morning fast) at 1 m and 3 m or overnight fast at 6 m were not significantly different. There was a tendency to lower blood glucose levels of ctrl2 compared to ctrl3 and CKO at 1m and ctrl3 compared to ctrl1 at 3m. In a GTT, lower blood glucose levels after 15 min were observed for ctrl2 compared to ctrl3 and CKO at 1 m and ctrl3 compared to CKO at 3m, whereas no difference was observed at 6 m.

In conclusion, endocrine CKO of Igfr-L1 in males and females did not result in postnatal death but in a potential increase in α-cell area, which had, however, no significant effect on body weight, fasting glucose levels or glucose tolerance.

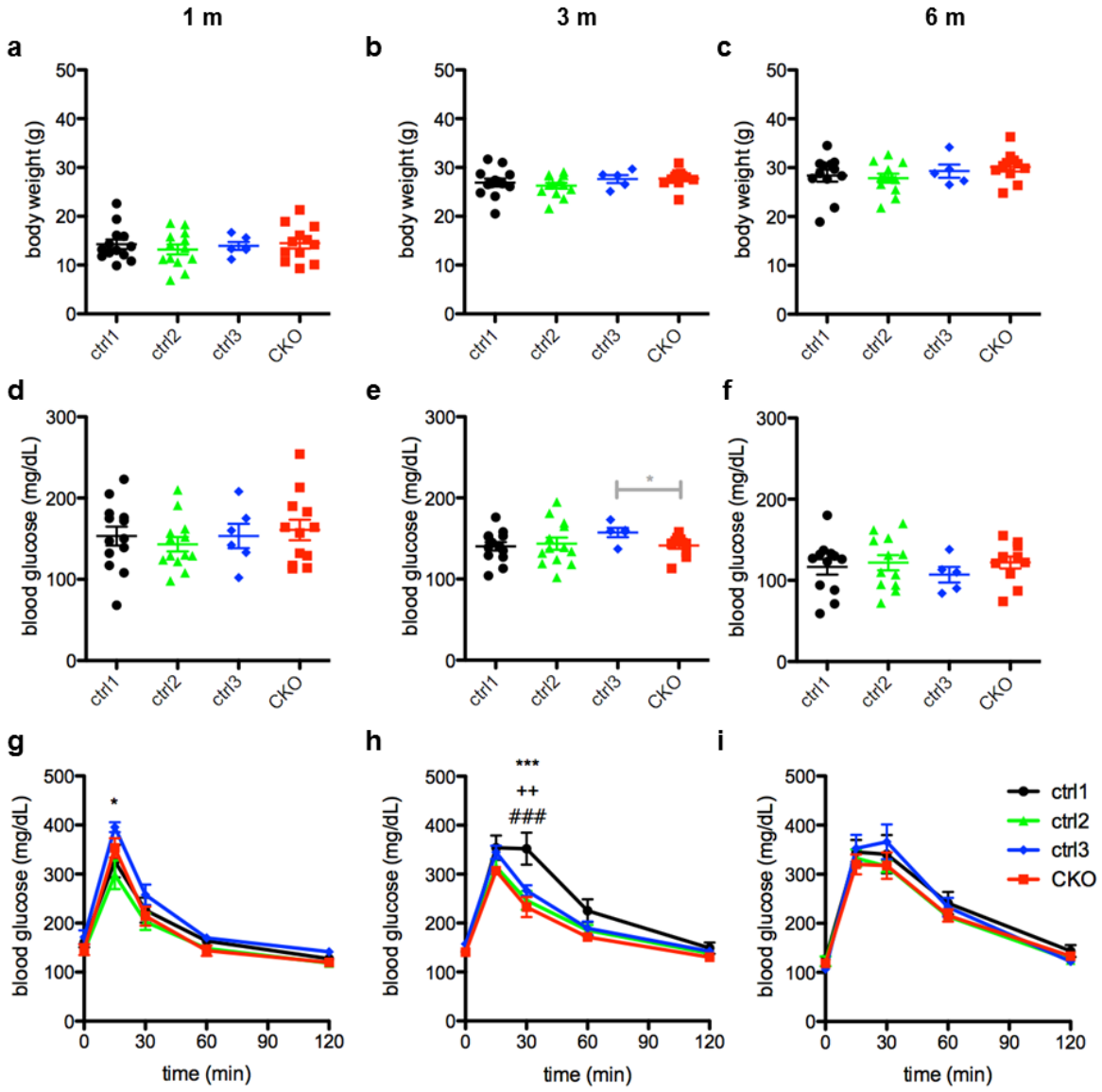

Figure 4.1.5.3 Glucose tolerance tests in male CKO and ctrl animals

a-c, Body weight of CKO and ctrl males at 1 m (a), 3 m (b) and 6 m (c).
- a, n.s., *P*=0.8055; ctrl1, n=13; ctrl2, n=13; ctrl3, n=6; CKO, n=12;
- b, n.s., *P*=0.3224; ctrl1, n=13; ctrl2, n=13; ctrl3, n=5; CKO, n=11;
- c, n.s., *P*=0.4283; ctrl1, n=12; ctrl2, n=12; ctrl3, n=5; CKO, n=11;

d-f, Fasting glucose levels of CKO and ctrl males at 1 m (d), 3 m (e) and 6 m (f).
- d, n.s., *P*=0.7323; ctrl1, n=13; ctrl2, n=13; ctrl3, n=6; CKO, n=12;
- e, n.s., *P*=0.4338; ctrl3 vs CKO, *, *P*=0.0331; ctrl1, n=13; ctrl2, n=13; ctrl3, n=5; CKO, n=11;
- f, n.s., *P*=0.7748; ctrl1, n=12; ctrl2, n=12; ctrl3, n=5; CKO, n=11;

g-i, Blood glucose levels in a GTT with CKO and ctrl males at 1 m (g), 3 m (h) and 6 m (i).
- g, n.s., *P*=0.2038; *, 15', ctrl2 vs ctrl3; ctrl1, n=12; ctrl2, n=13; ctrl3, n=4; CKO, n=8;
- h, *, *P*=0.0114; ***, 30', ctrl1 vs ctrl2; ++, 30', ctrl1 vs ctrl3; ###, 30', ctrl1 vs CKO; ctrl1, n=13; ctrl2, n=13; ctrl3, n=5; CKO, n=11;
- i, n.s., *P*=0.6373, ctrl1, n=9; ctrl2, n=11; ctrl3, n=5; CKO, n=9.

Error bars represent SEM and *, *P*<0.05; **, *P*<0.01; ***, *P*<0.001. a-f, *P*-values were analyzed using a 1way-ANOVA with Bonferroni post-test and a two-tailed, unpaired student's t-test for tendencies (grey); g-i, *P*-values were analyzed using a 2way-ANOVA with Bonferroni post-test.

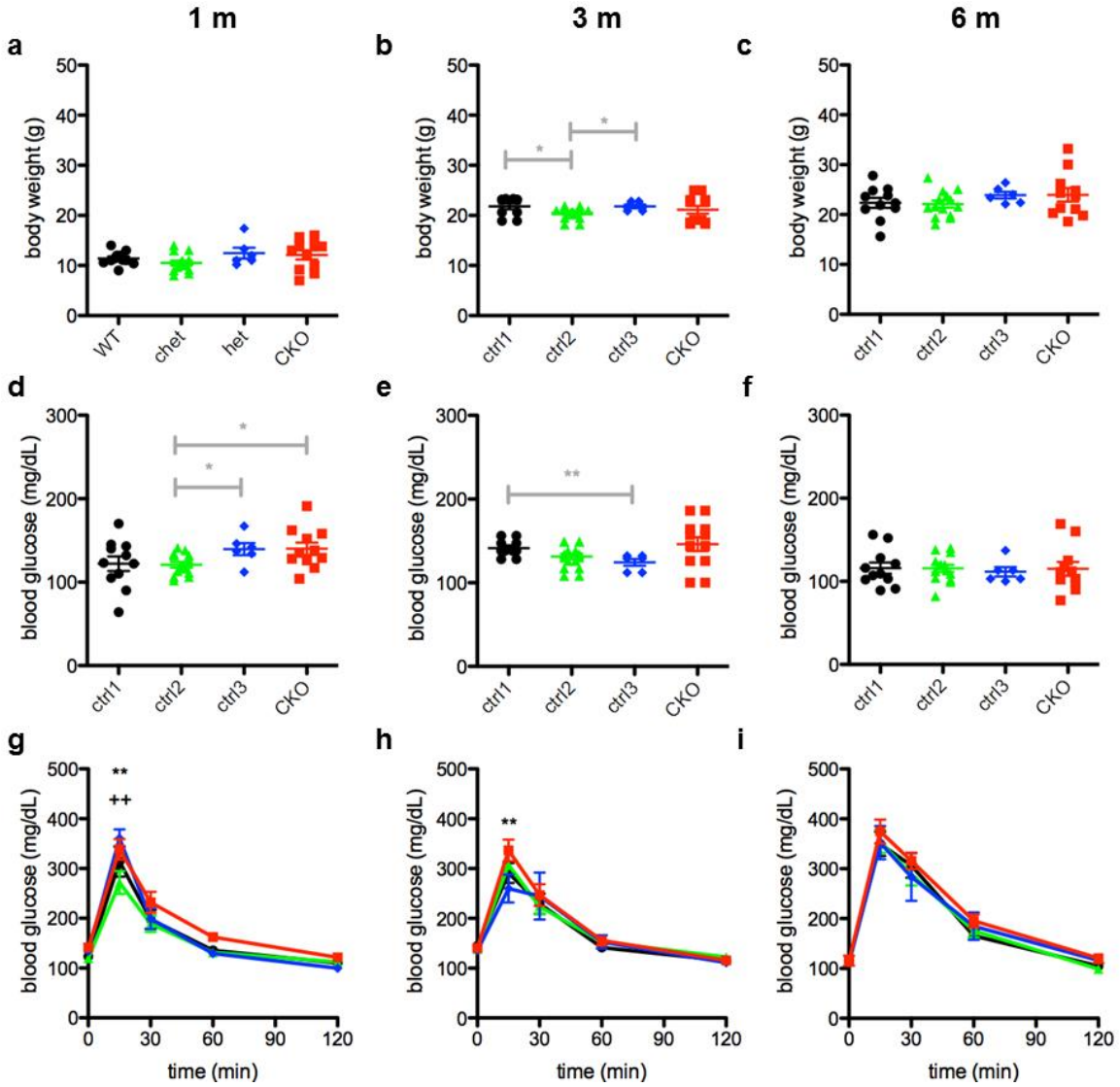

Figure 4.1.5.4 Glucose tolerance tests in female CKO and ctrl animals

a-c, Body weight of CKO and ctrl females at 1 m (a), 3 m (b) and 6 m (c).

a, n.s., *P*=0.2051; ctrl1, n=11; ctrl2, n=14; ctrl3, n=6; CKO, n=11;

b, n.s., *P*=0.2468; ctrl1 vs ctrl2, *, *P*=0.0315; ctrl2 vs ctrl3, *, *P*=0.0197; ctrl1, n=10; ctrl2, n=16; ctrl3, n=6; CKO, n=12;

c, n.s., *P*=0.4373; ctrl1, n=11; ctrl2, n=14; ctrl3, n=6; CKO, n=11;

d-f, Fasting glucose levels of CKO and ctrl females at 1 m (d), 3 m (e) and 6 m (f).

d, n.s., *P*=0.0816; ctrl2 vs ctrl3, *, *P*=0.0154; ctrl2 vs CKO, *, *P*=0.0180; ctrl1, n=11; ctrl2, n=14; ctrl3, n=6; CKO, n=11;

e, n.s., *P*=0.0615; ctrl1 vs ctrl3, **, *P*=0.0047; ctrl1, n=10; ctrl2, n=16; ctrl3, n=6; CKO, n=12;

f, n.s., *P*=0.9792; ctrl1, n=11; ctrl2, n=14; ctrl3, n=6; CKO, n=11;

g-i, Blood glucose levels in a GTT with CKO and ctrl females at 1 m (g), 3 m (h) and 6 m (i).

g, n.s., *P*=0.1196; **, 15', ctrl2 vs ctrl3; ++, 15', ctrl2 vs CKO; ctrl1, n=10; ctrl2, n=11; ctrl3, n=4; CKO; n=10;

h, n.s., *P*=0.6545; **, 15', ctrl3 vs CKO; ctrl1, n=10; ctrl2, n=16; ctrl3, n=6; CKO, n=12;

i, n.s., *P*=0.6905; ctrl1, n=9; ctrl2, n=10; ctrl3, n=5; CKO, n=9.

Error bars represent SEM and *, *P*<0.05; **, *P*<0.01; ***, *P*<0.001. a-f, *P*-values were analyzed using a 1way-ANOVA with Bonferroni post-test and a two-tailed, unpaired student's t-test for tendencies (grey); g-i, *P*-values were analyzed using a 2way-ANOVA with Bonferroni post-test.

4.2 Analysis of Igfr-L1 in diabetes mellitus

Full-body KO of Igfr-L1 resulted in postnatal death of newborn mice with signs of hypoglycemia and hyperinsulinemia. βCKO mice displayed improved glucose tolerance and increased Insr/Igf1r signaling in the islets of Langerhans. This suggested an important role of Igfr-L1 in β-cell biology and entailed the question if Igfr-L1 might be a target in diabetes therapy. Therefore, the expression and function of Igfr-L1 was analyzed in diabetic animals.

4.2.1 Differential expression of Igfr-L1

Transgenic labeling of proteins with fluorescent markers is a powerful tool to study their endogenous expression in a spatio-temporal manner in live cells. In our laboratory, the function of the crucial pancreatic transcription factors (TFs) Foxa2 and Pdx1 was studied by generating Foxa2-Venus-fusion (FVF (Burtscher et al., 2013)) and Pdx1-BFP-fusion (blue-fluorescent protein, PBF (Bastidas-Ponce, Roscioni, et al., 2017)) knock-in (KI) animals. Interestingly, neither FVF^{HOM} nor PBF^{HOM} single KI but double homozygous KI males $FVFPBF^{DHom}$ (FP) suffer from severe hyperglycemia at weaning age. Mechanistically, Foxa2 and Pdx1 cooperatively activate enhancers and promoters of β-cell-specific target genes, what is impaired in the FP model due to the bulky fluorescent proteins leading to MODY (Bastidas-Ponce, Roscioni, et al., 2017). Regarding islet biology, alterations in islet composition and architecture are observed due to a loss of β-cell identity and maturation mainly caused by reduced expression of Pdx1, which underlies a positive feedback regulation. To study these changes in respect of Igfr-L1, its expression was analyzed in this MODY model in comparison to C57Bl/6J (Bl6) at P14 and P25.

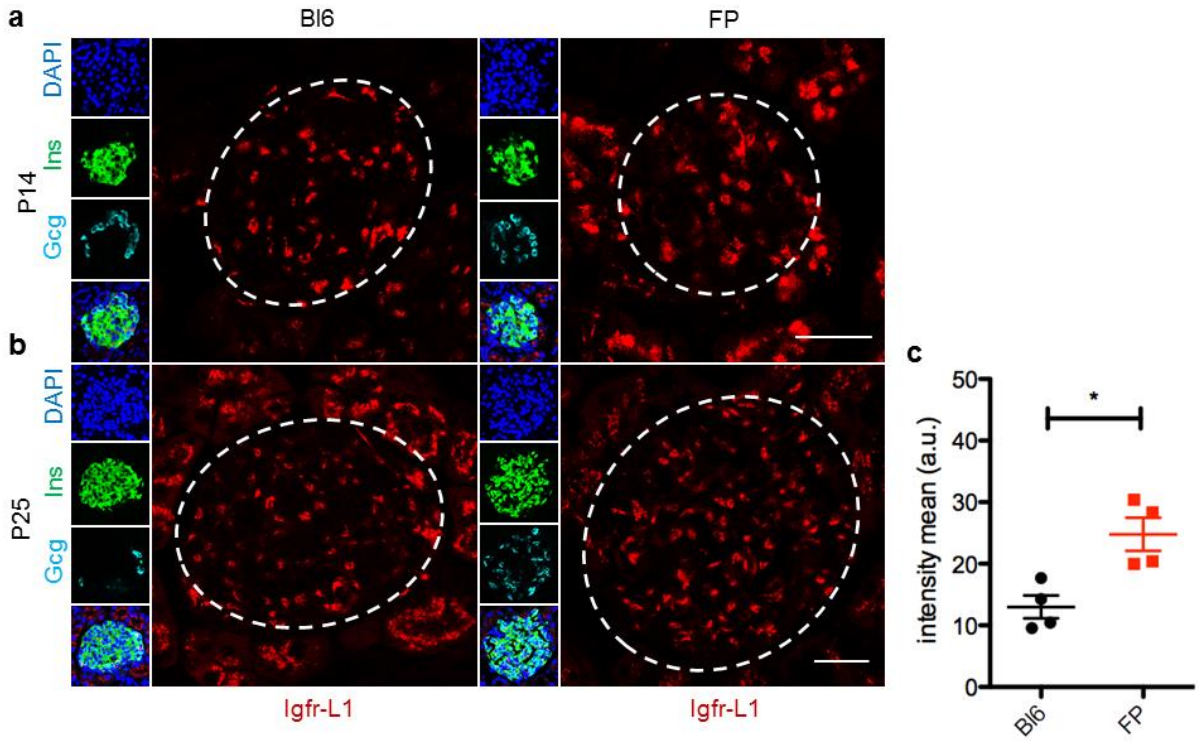

Figure 4.2.1.1 Pancreatic expression of Igfr-L1 in Bl6 and FP mice

a-b, Representative LSM images of the expression of Igfr-L1 (red) in islets marked by insulin (green) and glucagon (cyan) of male Bl6 and FP mice at P14 (a) and P25 (b). Scale bar, 25 µm.

c, Quantification of the expression of Igfr-L1 in the islets of Langerhans at P25 in b. *, *P*=0.0114; 5 islets of Bl6, n=4; FP, n=4 mice.

Error bars represent SEM and *, *P*<0.05; **, *P*<0.01; ***, *P*<0.001. *P*-values were analyzed using a two-tailed, unpaired student's t-test.

At P14, Igfr-L1 was expressed in the endocrine pancreas of FP and Bl6 animals at comparable levels when no physiological difference in terms of glucose levels was reported (Figure 4.2.1.1a). At P25, however, expression of Igfr-L1 was significantly upregulated in hyperglycemic FP animals compared to Bl6 (Figure 4.2.1.1b-c). The question if increased levels of Igfr-L1 are a potential cause or a consequence of β-cell failure remains open.

4.2.2 Analysis of FVFPBF^{DHom}; Igfr-L1$^{+/-}$ (ΔEx3)

To identify whether genetic reduction of Igfr-L1 expression is beneficial for β-cell function and systemic glucose regulation as observed in full-body and βCKO mice, FP x Igfr-L1 (ΔEx3) animals were generated (Figure 4.2.2.1a-b). For analysis, FP-het x FP-het intercrosses were set up, while some FP-hom animals survived until adulthood (data not shown).

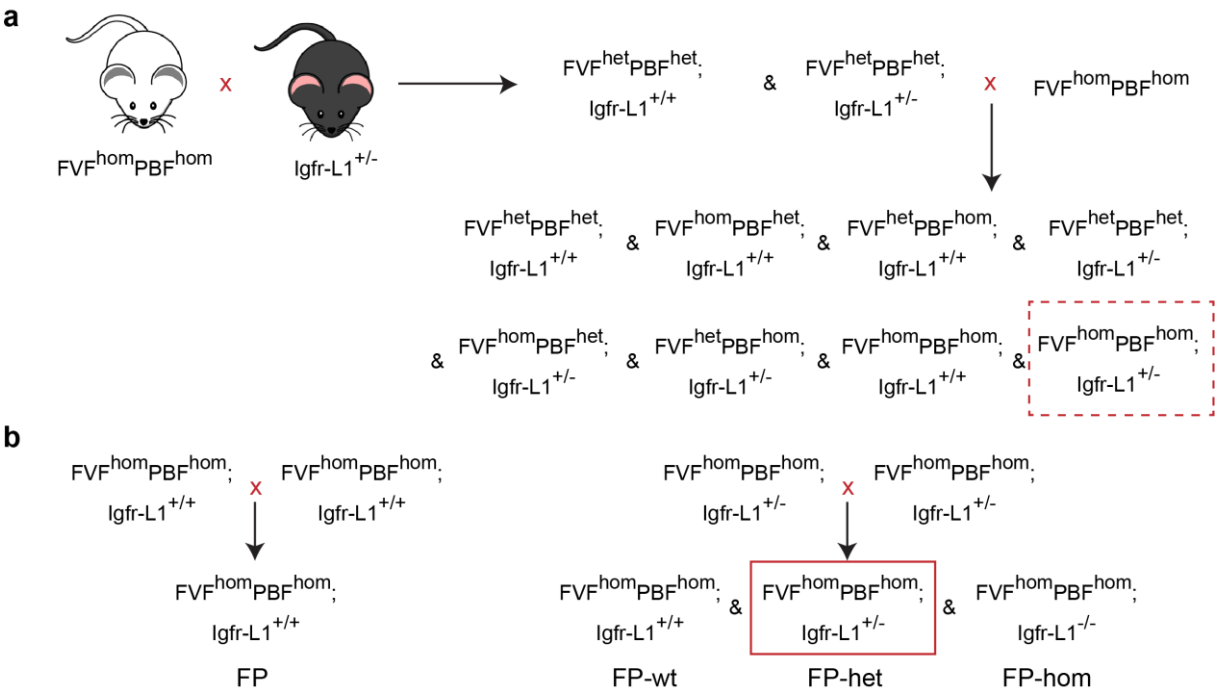

Figure 4.2.2.1 Generation of FP x Igfr-L1 animals

a, Sequential steps for the generation of FP-het animals either with the Igfr-L1 ΔEx3 or FD allele (see 4.1.1).

b, Generation of FP, FP-wt, FP-het and FP-hom animals for analysis.

Body weight and 6 h fasting blood glucose levels of male and female offspring were analyzed at two different stages, P14 and P25, of β-cell maturation as well as during the progression of hyperglycemia at 1.5 m. No differences were observed between FP-wt and FP-het animals at P14 (Figure 4.2.2.2a-d). At P25, body weight was not altered, while both male and female mice displayed elevated glucose levels (Figure 4.2.2.2e-h). Strikingly, blood glucose levels of FP-het males were significantly lower than the ones of FP-wt, which was not the case for females. At 1.5 m, neither blood glucose levels nor body weight were significantly different in males or females, while the variation in glucose levels was very high (Figure 4.2.2.2i-l). Thus, genetic reduction of Igfr-L1 levels in diabetic FP animals lowered blood glucose levels in males particularly at P25. Interestingly, females showed increased glucose levels at P25, which decreased until 1.5 m without effects of the Igfr-L1 allele.

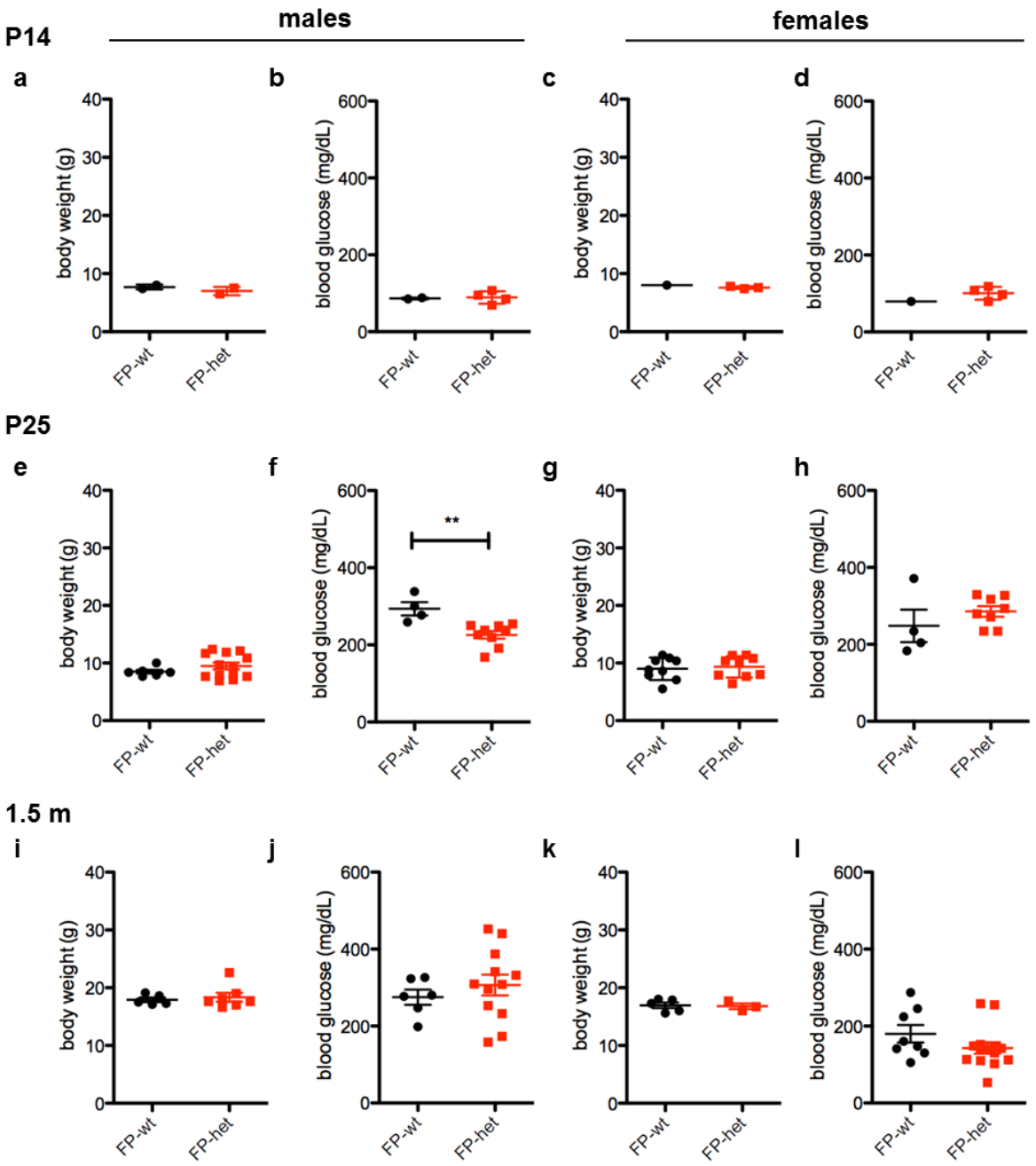

Figure 4.2.2.2 Body weight and glucose levels of Bl6 and FP x Igfr-L1 (ΔEx3)

a-b, Body weight (a) and 6 h fasting blood glucose levels (b) of males at P14.
a, n.s., *P*=0.3528; FP-wt, n=2; FP-het, n=2; b, n.s., *P*=0.8464; FP-wt, n=2; FP-het, n=4;
c-d, Body weight (c) and 6 h fasting blood glucose levels (d) of females at P14.
c, (FP-wt, n=1;) FP-het, n=3; d, (FP-wt, n=1;) FP-het, n=4;
e-f, Body weight (e) and 6 h fasting blood glucose levels (f) of males at P25.
e, n.s., *P*=0.2787, FP-wt, n=6; FP-het, n=13; f, **, *P*=0.0036; FP-wt, n=4; FP-het, n=9;
g-h, Body weight (g) and 6 h fasting blood glucose levels (h) of females at P25.
g, n.s., *P*=0.7058; FP-wt, n=9; FP-het, n=9; h, n.s., *P*=0.3023; FP-wt, n=4; FP-het, n=8;
i-j, Body weight (i) and 6 h fasting blood glucose levels (j) of males at 1.5 m.
i, n.s., *P*=0.6630; FP-wt, n=5; FP-het, n=7; j, n.s., *P*=0.4519; FP-wt, n=6; FP-het, n=12;
k-l, Body weight (k) and 6 h fasting blood glucose levels (l) of females at 1.5 m.
k, n.s., *P*=0.8379; FP-wt, n=5; FP-het, n=3; l, n.s., *P*=0.1670; FP-wt, n=8; FP-het, n=14.
Error bars represent SEM and *, *P*<0.05; **, *P*<0.01; ***, *P*<0.001. *P*-values were analyzed using a two-tailed, unpaired student's t-test.

To connect the reduced blood glucose levels to the alterations in β-cell biology observed in FP mice, maturation and functionality were analyzed by IHC in comparison to Bl6. Islet composition and architecture were not obviously changed (data not shown). Reduced levels of Igfr-L1 in FP-het compared to FP-wt animals were confirmed and correlated with weak expression of the β-cell maturation marker Urocortin 3 (Ucn3), which was undetectable in FP-wt but highly expressed in Bl6 (Figure 4.2.2.3a). Low levels of E-Cadherin (ECad) as marker for cell-cell adhesion were observed in both FP-wt and FP-het, whereas weak expression of the type 2 glucose transporter (Glut2) was only observed in FP-het mice, while both markers were highly expressed in Bl6 animals (Figure 4.2.2.3b).This suggests that glucose stimulated insulin secretion might be intact in some cells resulting in lower blood glucose levels.

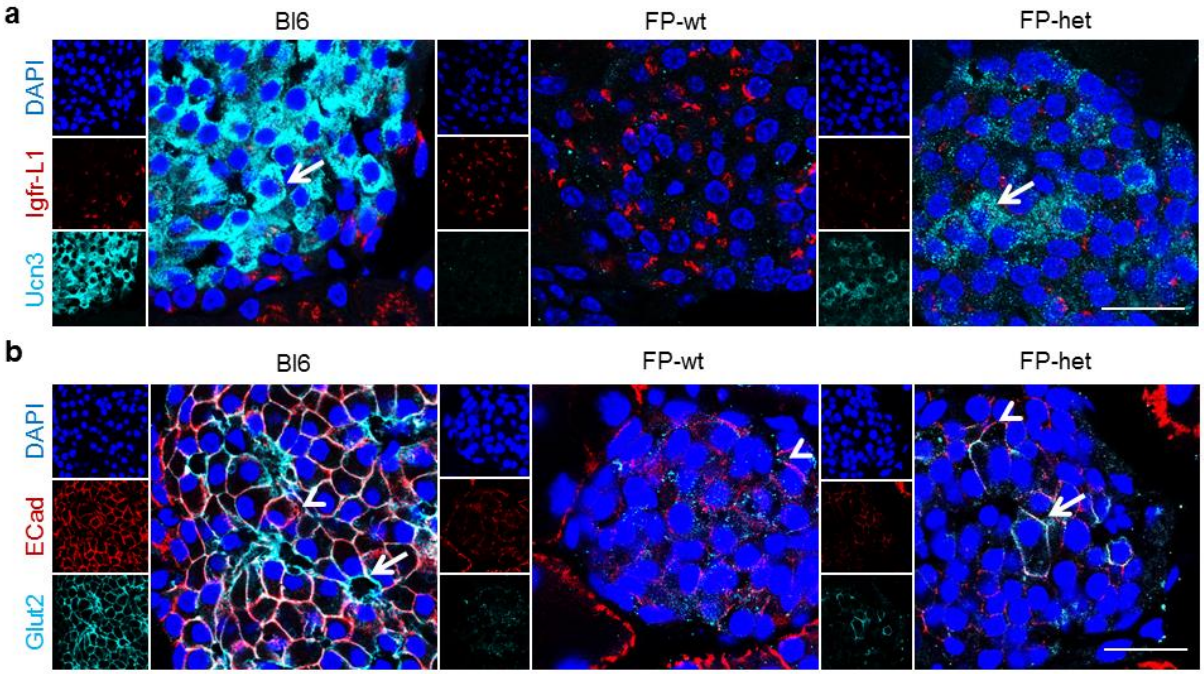

Figure 4.2.2.3 Maturation and functionality in islets of Bl6 and FP x Igfr-L1 (∆Ex3)

a, Representative LSM images of the expression of Igfr-L1 (red) and Ucn3 (cyan, arrows) in islets of male Bl6, FP-wt and FP-het at P25. Scale bar, 25 µm.

b, Representative LSM images of the expression of ECad (red, arrowheads) and Glut2 (cyan, arrows) in islets of male Bl6, FP-wt and FP-het at P25. Scale bar, 25 µm.

Albeit MODY females display only slightly increased blood glucose levels in adulthood, they develop gestational diabetes as islets were already damaged at P25. To identify a role of Igfr-L1 in glucose tolerance, an ipGTT was performed (1g/kg BW) in adult Bl6, FP-wt and FP-het females. Compared to Bl6, body weight was significantly lower in FP-wt and with a tendency in FP-het (Figure 4.2.2.4a). 6 h fasting blood glucose levels were still significantly increased without a difference in respect of the Igfr-L1 allele (Figure 4.2.2.4b). Upon glucose challenge, both FP-wt and FP-het showed a similar increase in blood glucose levels, which was significantly higher compared to Bl6 (Figure 4.2.2.4c-d). Glucose tolerance was highly impaired as shown by the area under the curve (AUC) and basal levels were not reached after 2 h showing that apart from being close to normoglycemia, β-cell function is still affected in MODY females.

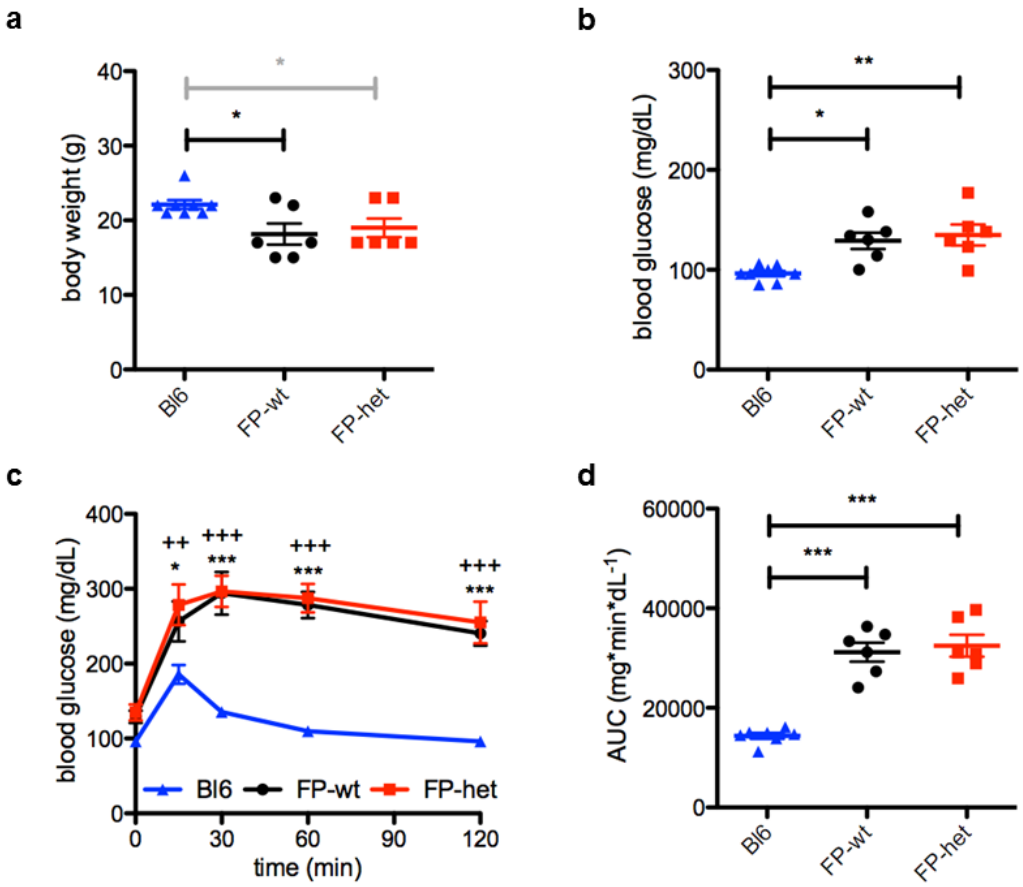

Figure 4.2.2.4 GTT in Bl6 and FP x Igfr-L1 (ΔEx3) females

a-b, Body weight (a) and 6 h fasting blood glucose levels (b) of Bl6, FP-wt and FP-het females at Ø3m.
a, *, *P*=0.0342; Bl6 vs FP-het, *, *P*=0.0305; Bl6, n=8; FP-wt, n=6; FP-het, n=6;
b, **, *P*=0.0020; Bl6, n=8; FP-wt, n=6; FP-het, n=6;

c-d, Blood glucose levels during an ipGTT (c) and quantification as AUC (d) in Bl6, FP-wt and FP-het females Ø3m.
c, ***, *P*<0.0001; Bl6 vs FP-wt, 15', *, 30' ***, 60', ***, 120', ***; Bl6 vs FP-het, 15', ++, 30', +++, 60', +++, 120', +++; Bl6, n=7; FP-wt, n=6; FP-het, n=6;
d, ***, *P*<0.0001; Bl6, n=7; FP-wt, n=6; FP-het, n=6.

Error bars represent SEM and *, *P*<0.05; **, *P*<0.01; ***, *P*<0.001. a,b,d, *P*-values were analyzed using a 1way-ANOVA with Bonferroni post-test and a two-tailed, unpaired student's t-test for tendencies (grey). c, *P*-values were analyzed using a 2way-ANOVA with Bonferroni post-test.

To summarize, Igfr-L1 is involved in blood glucose regulation in males during postnatal development of hyperglycemia in the FP model as a reduction in its expression could transiently lower blood glucose levels. In females, no difference could be observed between FP-wt and FP-het including a GTT. This sexual dimorphism is probably related to estrogen, which is known to be beneficial for β-cell health and might also regulate the expression of Igfr-L1 alias estrogen-induced gene 121 (EIG121) in β-cells.

4.2.3 Analysis of FVFPBF^{DHom}; Igfr-L1$^{+/-}$ (FD)

A high variation in the blood glucose levels of FP-het mice was observed during adulthood (data not shown) and a few FP-hom animals survived, which was assumed to be due to the ΔEx3 allele. In order to circumvent alternative splicing via the LacZ cassette observed in this allele, the FP x Igfr-L1 (FD) line was generated (see 4.1.1, Figure 4.2.2.1).

Matings of male x female FP-wt x FP-wt, FP-het x FP-wt, FP-wt x FP-het and FP-het x FP-het were set up to determine effects of the parental *Igfr-L1* allele on the physiology of the offspring. As animal numbers for FP-het x FP-wt and FP-wt x FP-het were too low, only data from FP-wt x FP-wt (FP) and FP-het x FP-het (FP-wt, FP-het, FP-hom) is presented in this work. Despite the *Igfr-L1* FD allele, FP-hom mice were viable, albeit the exact Mendelian ratio can only be determined with a higher animal number.

First, body weight and 6 h fasting blood glucose levels were determined at P25, 1.5 m, 3 m and 6 m of age to analyze the progression of hyperglycemia in comparison to Bl6 and FP. Here, FP and FP-wt animals were pooled (FP-wt).
At P25, FP-wt males had significantly higher body weight compared to Bl6 and FP-het (Figure 4.2.3.1a). 6 h fasting blood glucose levels were significantly increased in MODY animals compared to Bl6, whereas FP-het mice showed significantly lower blood glucose levels compared to FP-wt (Figure 4.2.3.1b). This confirms the result of FP x Igfr-L1 (ΔEx3). In females, body weight was not significantly different between Bl6, FP-wt, FP-het and FP-hom but there was a tendency to increased body weight in FP-het females compared to Bl6 (Figure 4.2.3.1c). 6 h fasting blood glucose levels were significantly increased in all MODY animals compared to Bl6 but not different in between FP-wt, FP-het and FP-hom (Figure 4.2.3.1d).
At 1.5 m, body weight was not significantly different in males but there was a tendency to lower body weight in FP-wt compared to Bl6 (Figure 4.2.3.1e). 6 h fasting blood glucose levels were significantly higher in MODY animals compared to Bl6 with a tendency of FP-het showing even higher blood glucose levels than FP-wt (Figure 4.2.3.1f). In females, body weight was not significantly different but there was a tendency to lower body weight in FP-hom compared to Bl6 (Figure 4.2.3.1g). Similarly, 6 h fasting blood glucose levels were not significantly different between the groups but FP-hom mice had a tendency to increased glucose levels compared to Bl6 (Figure 4.2.3.1h).
At 3 m, body weight was significantly lower in FP-wt compared to Bl6 with no difference in between FP-wt and FP-het animals (Figure 4.2.3.1i). 6 h fasting blood glucose levels were still significantly higher in MODY animals compared to Bl6 and FP-het animals showed significantly increased blood glucose levels compared to FP-wt (Figure 4.2.3.1j). In females, body weight of FP-wt was significantly lower compared to Bl6 and FP-het (Figure 4.2.3.1k). FP-hom also showed a tendency to lower body weight compared to Bl6. 6 h fasting blood glucose levels were not significantly different between the groups, whereas FP-het had a tendency to increased blood glucose levels compared to Bl6 (Figure 4.2.3.1l). Thus, MODY females were quasi normoglycemic in adulthood.
At 6 m, body weight was not significantly different in males but there was a tendency to lower body weight in FP-wt compared to Bl6 (Figure 4.2.3.1m). 6 h fasting blood glucose levels were significantly lower in Bl6 compared to FP-wt mice with the same tendency compared to FP-het (Figure 4.2.3.1n). FP-wt and FP-het displayed similar blood glucose levels. In females, there was no significant difference in body weight or blood glucose levels (Figure 4.2.3.1o-p).

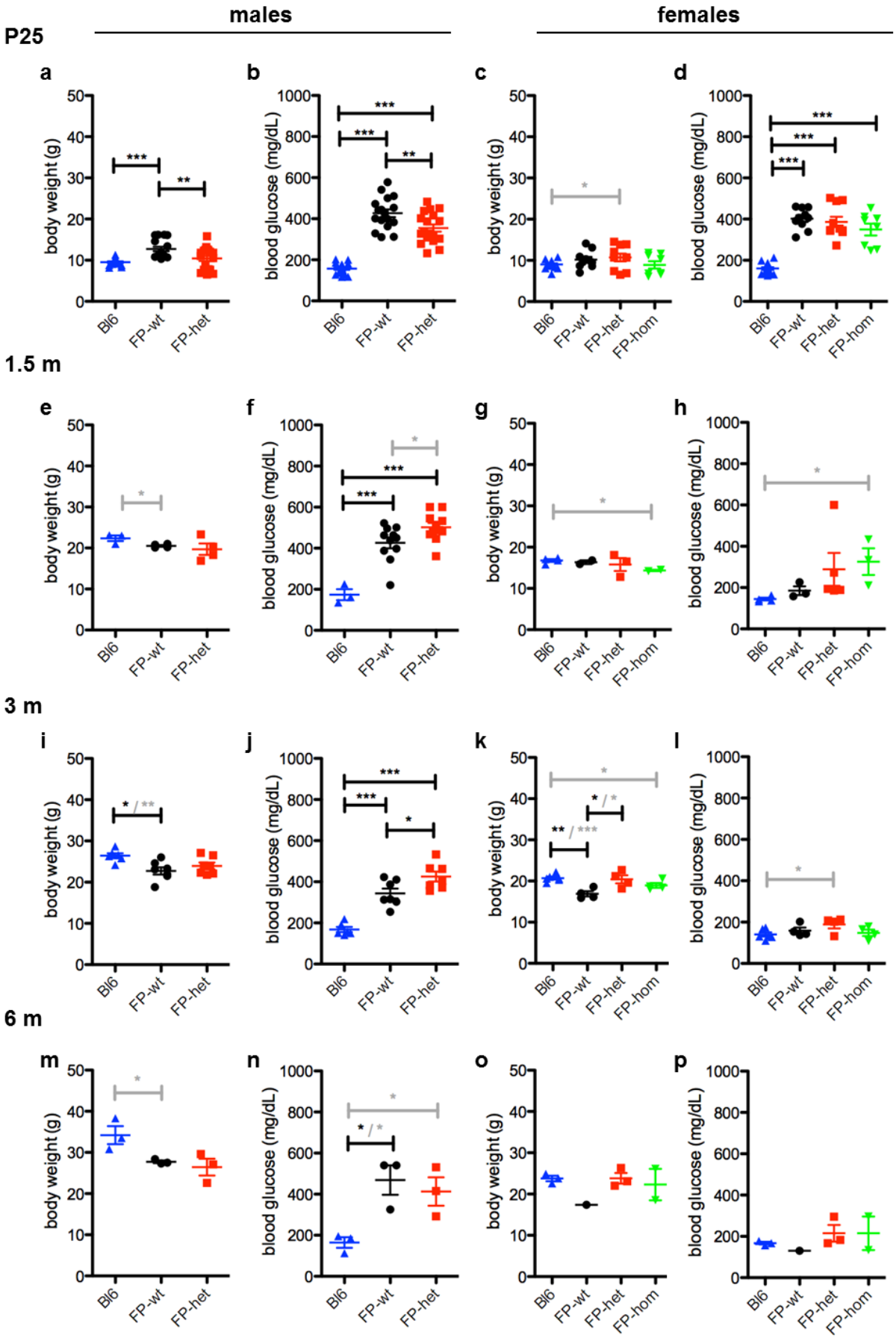
males
females
P25
1.5 m
3 m
6 m
a
b
c
d
e
f
g
h
i
j
k
l
m
n
o
p
body weight (g)
blood glucose (mg/dL)
Bl6
FP-wt
FP-het
FP-hom

Figure 4.2.3.1 Body weight and glucose levels of Bl6 and FP x Igfr-L1 (FD)

a-b, Body weight (a) and 6 h fasting blood glucose levels (b) of males at P25.
a, ***, *P*<0.0001; Bl6, n=17; FP-wt, n=17; FP-het, n=18;
b, ***, *P*<0.0001; Bl6, n=17; FP-wt, n=17; FP-het, n=18;
c-d, Body weight (c) and 6 h fasting blood glucose levels (d) of females at P25.
c, n.s., *P*=0.1522; Bl6 vs FP-het, *, *P*=0.0437;
Bl6, n=16; FP-wt, n=10; FP-het, n=10; FP-hom, n=8;
d, ***, *P*<0.0001; Bl6, n=16; FP-wt, n=10; FP-het, n=10; FP-hom, n=8;
e-f, Body weight (e) and 6 h fasting blood glucose levels (f) of males at 1.5 m.
e, n.s., *P*=0.2145; Bl6 vs FP-wt, *, *P*=0.0328; Bl6, n=3; FP-wt, n=4; FP-het, n=4;
f, ***, *P*<0.0001; FP-wt vs FP-het, *, *P*=0.0338; Bl6, n=3; FP-wt, n=12; FP-het, n=11;
g-h, Body weight (g) and 6 h fasting blood glucose levels (h) of females at 1.5 m.
g, n.s., *P*=0.3939; Bl6 vs FP-hom, *, *P*=0.0102;
Bl6, n=4; FP-wt, n=2; FP-het, n=3; FP-hom, n=2;
h, n.s., *P*=0.1921; FP-wt vs FP-hom, *, *P*=0.0209;
Bl6, n=4; FP-wt, n=3; FP-het, n=5; FP-hom, n=3;
i-j, Body weight (i) and 6 h fasting blood glucose levels (j) of males at 3 m.
i, n.s., *P*=0.0149; Bl6 vs FP-wt, **, *P*=0.0065; Bl6, n=6; FP-wt, n=7; FP-het, n=7;
j, ***, *P*<0.0001; Bl6, n=6; FP-wt, n=7; FP-het, n=7;
k-l, Body weight (k) and 6 h fasting blood glucose levels (l) of females at 3 m.
k, **, *P*=0.0026; Bl6 vs FP-wt, ***, *P*=0.0004; Bl6 vs FP-hom, *, *P*=0.0247;
FP-wt vs FP-het, *, *P*=0.0223; Bl6, n=6; FP-wt, n=4; FP-het, n=4; FP-hom, n=4;
l, n.s., *P*=0.1364; Bl6 vs FP-het, *, *P*=0.0392;
Bl6, n=6; FP-wt, n=4; FP-het, n=4; FP-hom, n=4;
m-n, Body weight (m) and 6 h fasting blood glucose levels (n) of males at 6 m.
m, *, *P*=0.0411; Bl6 vs FP-wt, *, *P*=0.0435; Bl6, n=3; FP-wt, n=3; FP-het, n=3;
n, *, *P*=0.0237; Bl6 vs FP-wt, *, *P*=0.0163; Bl6 vs FP-het, *, *P*=0.0280;
Bl6, n=3; FP-wt, n=3; FP-het, n=3;
o-p, Body weight (o) and 6 h fasting blood glucose levels (p) of females at 6 m.
o, n.s., *P*=0.8258; Bl6, n=3; (FP-wt, n=1;) FP-het, n=3; FP-hom, n=2;
p, n.s., *P*=0.6547; Bl6, n=3; (FP-wt, n=1;) FP-het, n=3; FP-hom, n=2.

Error bars represent SEM and *, *P*<0.05; **, *P*<0.01; ***, *P*<0.001; *P*-values were analyzed using a 1way-ANOVA with Bonferroni post-test and a two-tailed, unpaired student's t-test for tendencies (grey).

To summarize, Igfr-L1 was involved in systemic blood glucose homeostasis in MODY males but not females. At P25, reduced levels of Igfr-L1 led to lower blood glucose levels. During progression to adulthood, however, higher blood glucose levels were observed at 1.5 m and 3 m without a difference at 6 m, again hinting to a transient improvement of β-cell health.

To further analyze the responsiveness to insulin in MODY animals, an insulin tolerance test (ITT) was performed at P25. Hyperglycemic animals showed a drop of glucose levels by approximately half of the basal levels after 20 min. In males, FP-het mice had significantly lower basal blood glucose levels resulting in a significantly lower AUC (Figure 4.2.3.2a-b). However, normalization to basal values revealed that there was no difference in glucose clearance in response to insulin (Figure 4.2.3.2c). In females, basal glucose levels were comparable in all groups and no difference in insulin tolerance was observed between FP-wt and FP-het animals (Figure 4.2.3.2d-e). Strikingly, FP-hom females showed a drastic drop in blood glucose levels already after 10 min resulting in a significantly lower AUC (Figure 4.2.3.2d-e). Normalization further revealed higher blood glucose levels in FP-het compared to FP-wt and FP-hom after 5 min and compared to FP-hom after 20 min. Thus, reduced

expression of Igfr-L1 does barely affect response to insulin, whereas a complete lack of it enhances glucose clearance.

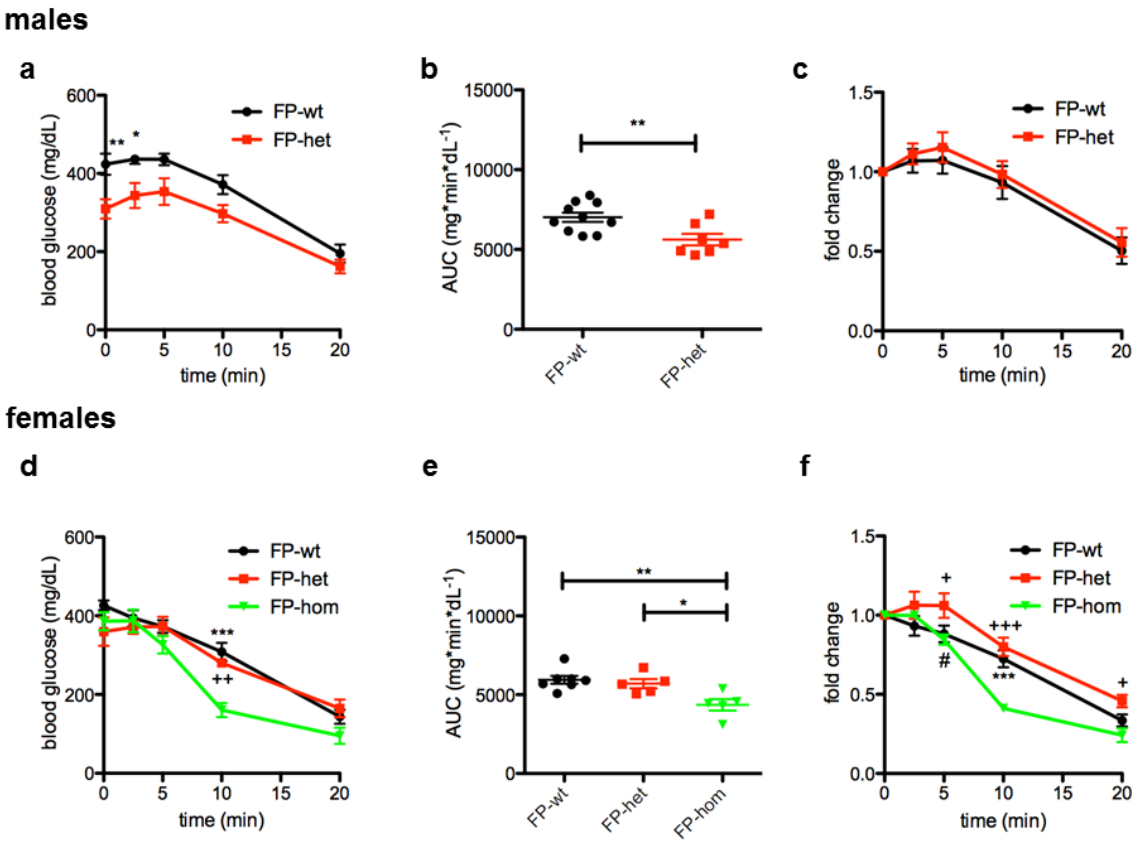

Figure 4.2.3.2 Insulin tolerance test in FP x Igfr-L1 (FD)

Absolute (a,d) and normalized (c,f) blood glucose levels with quantification of the AUC (b,e) during an ITT in FP-wt and FP-het males (upper panel) and FP-wt, FP-het and FP-hom females (lower panel) at P25 .

a, ***, *P*=0.0008; FP-wt, n=10; FP-het, n=7;

b, **, *P*=0.0083; FP-wt, n=10; FP-het, n=7;

c, n.s., *P*=0.6227; FP-wt, n=10; FP-het, n=7;

d, *, *P*=0.0468; FP-wt vs FP-hom, 10', ***; FP-het vs FP-hom, 10', ++; FP-wt, n=7; FP-het, n=5; FP-hom, n=5;

e, **, *P*=0.0049; FP-wt, n=7; FP-het, n=5; FP-hom, n=5;

f, **, *P*=0.0038; FP-wt vs FP-het, 5', #; FP-wt vs FP-hom, 10', ***; FP-het vs FP-hom, 5', +; 10', +++; 20', +; FP-wt, n=7; FP-het, n=5; FP-hom, n=5.

Error bars represent SEM and *, *P*<0.05; **, *P*<0.01; ***, *P*<0.001. a,c,d,f, *P*-values were analyzed using a 2way-ANOVA with Bonferroni post-test. b, *P*-values were analyzed using a two-tailed, unpaired student's t-test. e, *P*-values were analyzed using a 1way-ANOVA with Bonferroni post-test.

Apart from enhanced insulin action to trigger glucose uptake, higher amounts of insulin could be found in the circulation resulting in increased glucose uptake. To test this hypothesis, both insulin and C-peptide levels were measured in serum at P25 and 1.5 m.

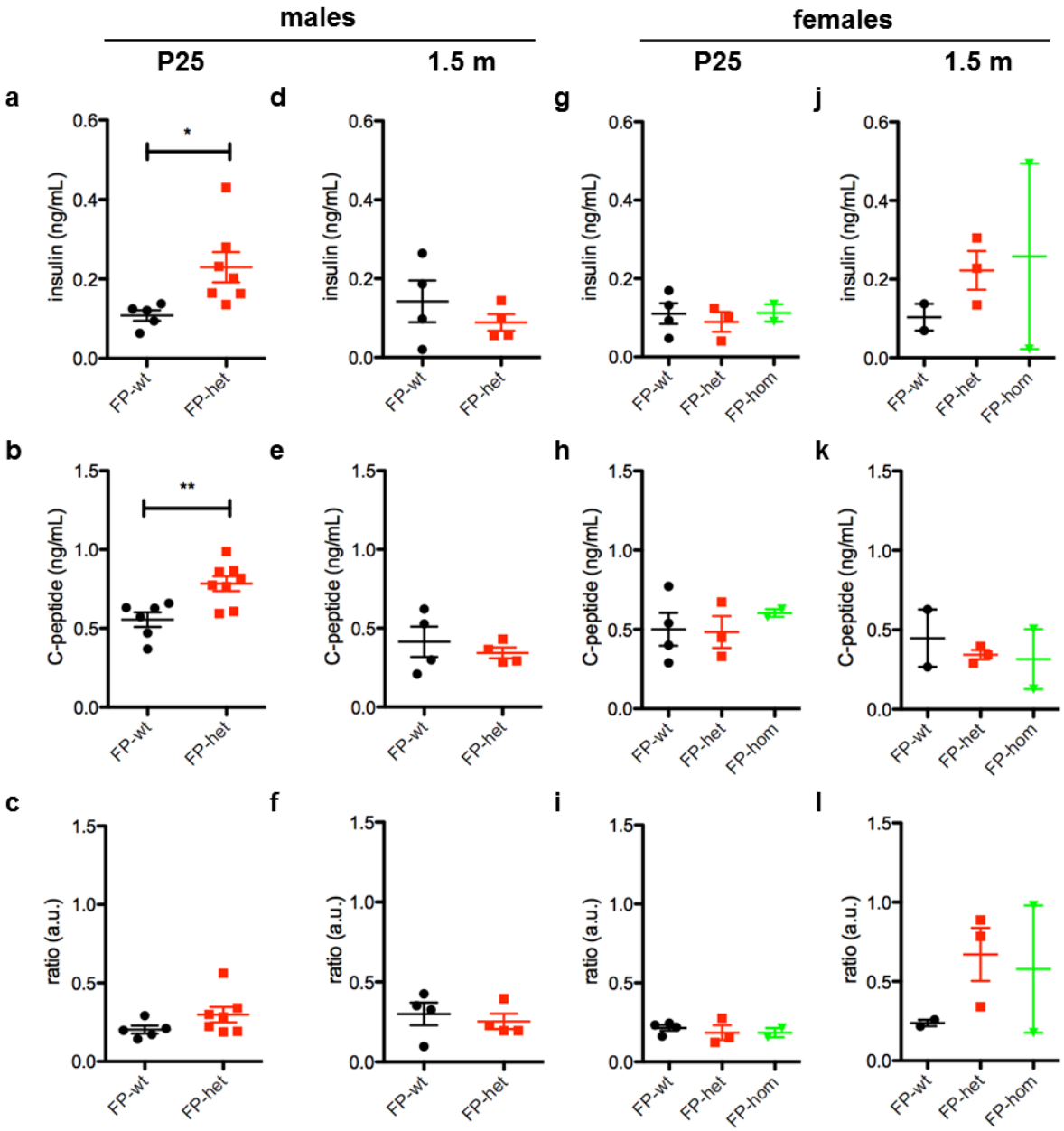

Figure 4.2.3.3 Insulin and C-peptide levels of FP x Igfr-L1 (FD)

Insulin (a,d,g,j) and C-peptide (b,e,h,k) levels and their ratio (c,f,i,l) in males and females at P25 and 1.5 m.

a-c, Serum insulin (a) and C-peptide (b) levels and their ratio (c) of males at P25.
a, *, *P*=0.0270; FP-wt, n=5; FP-het, n=7; b,**, *P*=0.0053; FP-wt, n=6; FP-het, n=8;
c, n.s., *P*=0.1571; FP-wt, n=5; FP-het, n=7;

d-f, Serum insulin (d) and C-peptide (e) levels and their ratio (f) of males at 1.5 m.
d, n.s., *P*=0.3866; e, n.s., *P*=0.5115; f, n.s., *P*=0.6065; FP-wt, n=4; FP-het, n=4;

g-i, Serum insulin (g) and C-peptide (h) levels and their ratio (i) of females at P25.
g, n.s., *P*=0.8125; h, n.s., *P*=0.7477; i, n.s., *P*=0.7359;
FP-wt, n=4; FP-het, n=3; FP-hom, n=2;

j-l, Serum insulin (j) and C-peptide (k) levels and their ratio (l) of females at 1.5 m.
j, n.s., *P*=0.6816; k, n.s., *P*=0.7688; l, n.s., *P*=0.4599;
FP-wt, n=2; FP-het, n=3; FP-hom, n=2.

Error bars represent SEM and *, *P*<0.05; **, *P*<0.01; ***, *P*<0.001. Males, *P*-values were analyzed using a two-tailed, unpaired student's t-test. Females, *P*-values were analyzed using a 1way-ANOVA with Bonferroni post-test.

In males, insulin as well as C-peptide levels were significantly increased in FP-het compared to FP-wt at P25, whereas the insulin/C-peptide ratio was not different (Figure 4.2.3.3a-c). At 1.5 m, the difference was gone correlating with similar blood glucose levels. In females, apart from the high variation, no difference in insulin and C-peptide levels or their ratio was observed at P25 or 1.5 m, which coincides with the blood glucose levels (Figure 4.2.3.3g-l).

To further analyze the onset of diabetes, offspring was analyzed during postnatal development, i.e. body weight and blood glucose levels were measured at P14, P18 and P25.
In males, body weight was significantly different at P14 originating from lower body weight of FP-het compared to Bl6 and FP (Figure 4.2.3.4a). 6 h fasting blood glucose levels of FP males were significantly higher compared to Bl6, FP-wt and FP-het (Figure 4.2.3.4b). At P18, body weight was comparable between the groups, while 6 h fasting glucose levels were significantly lower in Bl6 than in FP, FP-wt, FP-het and FP-hom (Figure 4.2.3.4c-d). At P25, body weight was significantly different in males originating from higher body weight of Bl6 compared to FP-wt, FP-het and FP-hom (Figure 4.2.3.4e). Random-fed blood glucose levels were significantly different due to increased blood glucose levels in MODY males compared to Bl6, while no difference was observed in respect of the Igfr-L1 alleles (Figure 4.2.3.4f). Thus, the increase in glucose levels of FP mice occurs at P14 and in FP-wt, FP-het and FP-hom at P18, which is potentially connected to the metabolism of the mother.
In females, body weight was not significantly different at P14 (Figure 4.2.3.4g). There was a tendency to increased body weight in FP females compared to FP-het and FP-hom as well as Bl6 to FP-het. 6 h fasting blood glucose levels were also not significantly different between the groups but there was a tendency to increased blood glucose levels in FP compared to Bl6 similar to males (Figure 4.2.3.4h). At P18, body weight was also not significantly different in between the groups, while there was a tendency to lower body weight in FP compared to Bl6 and FP-hom compared to FP-wt (Figure 4.2.3.4i). 6 h fasting blood glucose levels were not significantly different between all groups, however, MODY females had a tendency to increased blood glucose levels compared to Bl6 (Figure 4.2.3.4j). At P25, body weight was again not significantly different but there was a tendency to higher body weight of Bl6 compared to FP, FP-het and FP-hom (Figure 4.2.3.4k). Random-fed glucose levels were significantly different due to lower blood glucose levels in Bl6 compared to MODY females (Figure 4.2.3.4l). Additionally, there was a tendency to higher blood glucose levels in FP-het compared to FP-hom. Hence, the same observations were made for females as for males, i.e. onset of hyperglycemia occurred in FP mice at P14 and in FP-wt, FP-het and FP-hom at P18, while severe hyperglycemia in MODY females was observed at P25.

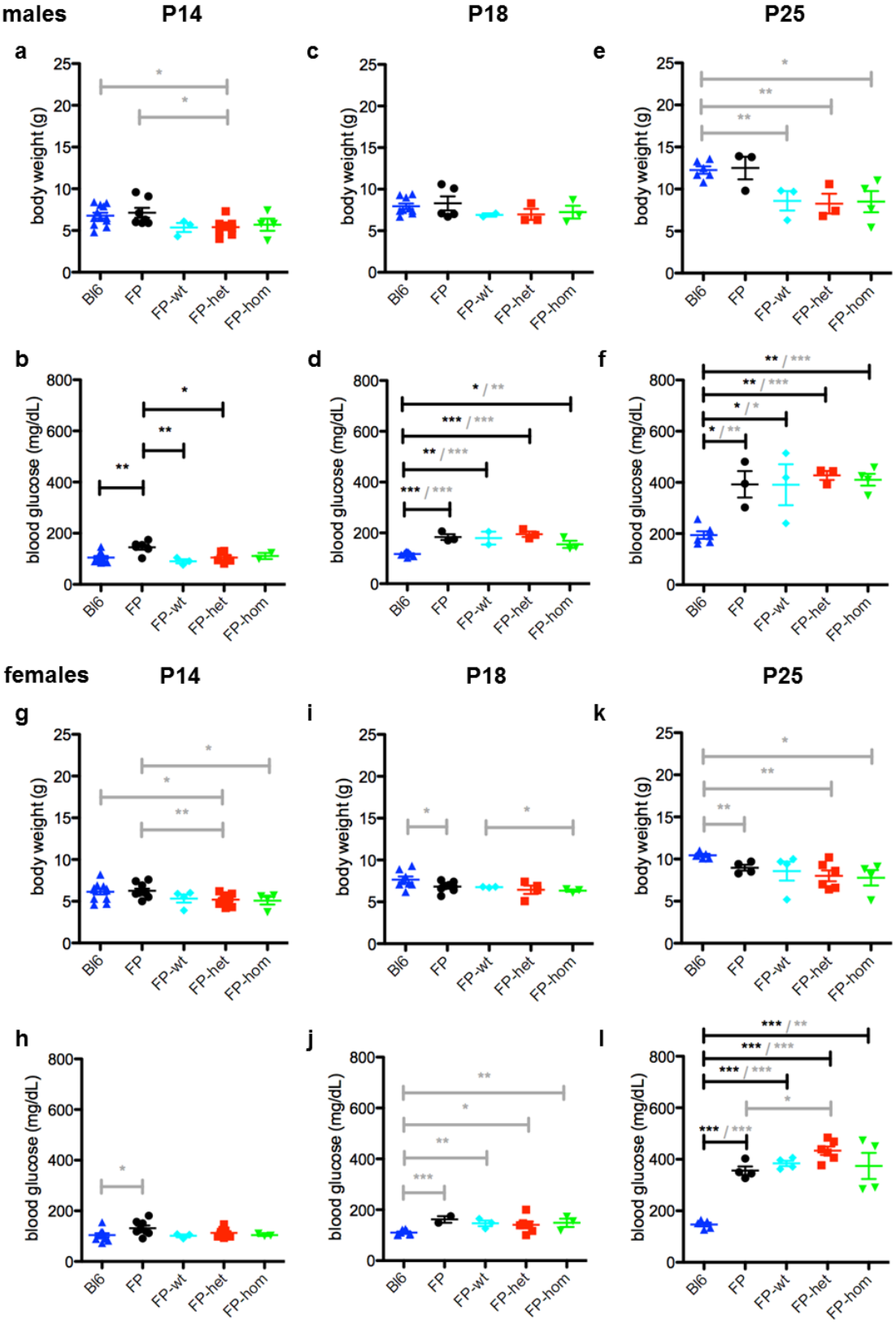
males
P14
P18
P25
a
b
c
d
e
f
females
g
h
i
j
k
l
body weight (g)
blood glucose (mg/dL)
Bl6
FP
FP-wt
FP-het
FP-hom

Figure 4.2.3.4 Postnatal body weight and glucose levels of Bl6 and FP x Igfr-L1 (FD)

a-b, Body weight (a) and 6 h fasting blood glucose levels (b) of males at P14.
a, *, *P*=0.0403; Bl6 vs FP-het, *, *P*=0.0141; FP vs FP-het, *, *P*=0.0233;
Bl6, n=12; FP, n=7; FP-wt, n=3; FP-het, n=8; FP-hom, n=4;
b, **, *P*=0.0029; Bl6, n=12; FP, n=6; FP-wt, n=3; FP-het, n=6; FP-hom, n=2.
c-d, Body weight (c) and 6 h fasting blood glucose levels (d) of males at P18.
c, n.s., *P*=0.5011; Bl6, n=9; FP, n=5; FP-wt, n=2; FP-het, n=3; FP-hom, n=3;
d, ***, *P*<0.0001; Bl6 vs FP, ***, *P*<0.0001; Bl6 vs FP-wt, ***, *P*=0.0003;
Bl6 vs FP-het, ***, *P*<0.0001; Bl6 vs FP-hom, **, *P*=0.0014;
Bl6, n=9; FP, n=3; FP-wt, n=2; FP-het, n=3; FP-hom, n=3.
e-f, Body weight (e) and random-fed blood glucose levels (f) of males at P25.
e, *, *P*=0.0116; Bl6 vs FP-wt, **, *P*=0.0075; Bl6 vs FP-het, **, *P*=0.0052;
Bl6 vs FP-hom, *, *P*=0.0104;
Bl6, n=6; FP, n=3; FP-wt, n=3; FP-het, n=3; FP-hom, n=4;
f, ***, *P*=0.0007; Bl6 vs FP, **, *P*=0.0017; Bl6 vs FP-wt, *, *P*=0.0105;
Bl6 vs FP-het, ***, *P*<0.0001; Bl6 vs FP-hom, ***, *P*<0.0001;
Bl6, n=6; FP, n=3; FP-wt, n=3; FP-het, n=3; FP-hom, n=4;
g-h, Body weight (g) and 6 h fasting blood glucose levels (h) of females at P14.
g, *, *P*=0.0239; Bl6 vs FP-het, *, *P*=0.0221; FP vs FP-het, **, *P*=0.0042;
FP vs FP-hom, *, *P*=0.0369;
Bl6, n=11; FP, n=10; FP-wt, n=4; FP-het, n=11; FP-hom, n=4;
h, n.s., *P*=0.0976; Bl6 vs FP, *, *P*=0.0378;
Bl6, n=10; FP, n=8; FP-wt, n=3; FP-het, n=8; FP-hom, n=3;
i-j, Body weight (i) and 6 h fasting blood glucose levels (j) of females at P18.
i, *, *P*=0.0444; Bl6 vs FP, *, *P*=0.0375; FP-wt vs FP-hom, *, *P*=0.0255;
Bl6, n=8; FP, n=10; FP-wt, n=3; FP-het, n=4; FP-hom, n=3;
j, *, *P*=0.0316; Bl6 vs FP, ***, *P*=0.0004; Bl6 vs FP-wt, **, *P*=0.0021;
Bl6 vs FP-het, *, *P*=0.0332; Bl6 vs FP-hom, **, *P*=0.0059;
Bl6, n=8; FP, n=2; FP-wt, n=3; FP-het, n=6; FP-hom, n=3;
k-l, Body weight (k) and random-fed blood glucose levels (l) of females at P25.
k, n.s., *P*=0.0839; Bl6 vs FP, **, *P*=0.0044; Bl6 vs FP-het, **, *P*=0.0088;
Bl6 vs FP-hom, *, *P*=0.0146;
Bl6, n=5; FP, n=4; FP-wt, n=4; FP-het, n=6; FP-hom, n=4;
l, ***, *P*<0.0001; Bl6 vs FP, ***, *P*<0.0001; Bl6 vs FP-wt, ***, *P*<0.0001;
Bl6 vs FP-het, ***, *P*<0.0001; Bl6 vs FP-hom, **, *P*=0.0015;
FP vs FP-het, *, *P*=0.0122;
Bl6, n=5; FP, n=4; FP-wt, n=4; FP-het, n=6; FP-hom, n=4.
Error bars represent SEM and *, *P*<0.05; **, *P*<0.01; ***, *P*<0.001. *P*-values were analyzed using a 1way-ANOVA with Bonferroni post-test and a two-tailed, unpaired student's t-test for tendencies (grey).

Furthermore, gestational diabetes was investigated in MODY females compared to Bl6. Blood glucose levels of seven months old dams were determined in their second pregnancy. Before gestation, blood glucose levels were not significantly different in MODY females compared to Bl6 (Figure 4.2.3.5a). During early gestation, FP-het females suffered from severe hyperglycemia and blood glucose levels were significantly higher compared to Bl6 and FP-wt (Figure 4.2.3.5b). The same observation was made during lactation, while also FP-wt animals showed significantly increased blood glucose levels compared to Bl6 (Figure 4.2.3.5c). After weaning, FP-het females had difficulties to recover from hyperglycemia as blood glucose levels were still significantly higher compared to Bl6 and with a tendency to FP-wt (Figure 4.2.3.5d). In conclusion, lack of one allele of *Igfr-L1* is unfavorable during

pregnancy hinting to dysregulation in gestational hormones. For better temporal resolution, additional stages would need to be analyzed.

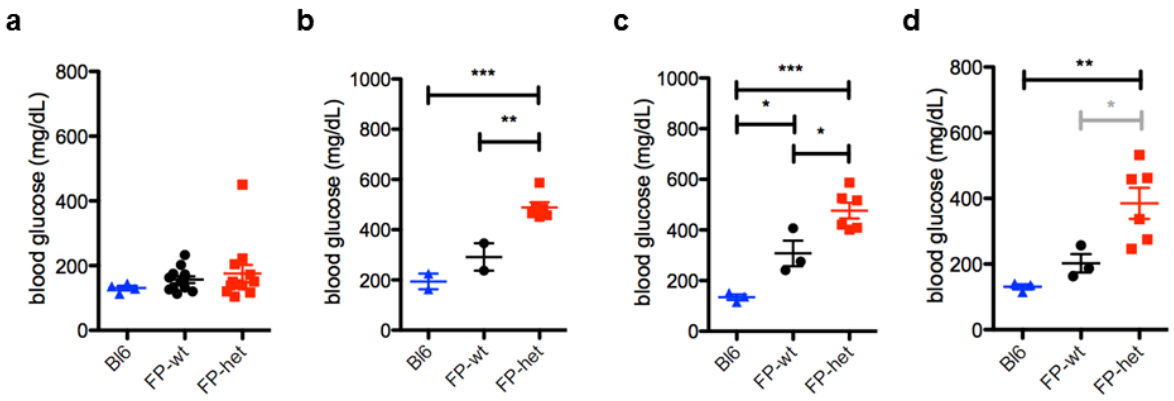

Figure 4.2.3.5 Gestational diabetes of FP x Igfr-L1 (FD)

a-d, Random-fed blood glucose levels before gestation (a), at gestation day 11.5 (b), at lactation days 8-10 (c) and after weaning (d) of Bl6, FP-wt and FP-het females.
a, n.s., *P*=0.4860; Bl6, n=4; FP-wt, n=12; FP-het, n=12;
b, ***, *P*=0.0005; Bl6, n=2; FP-wt, n=2; FP-het, n=6;
c, ***, *P*=0.0003; Bl6, n=3; FP-wt, n=3; FP-het, n=6;
d, **, *P*=0.0061; FP-wt vs FP-het, *, *P*=0.0376; Bl6, n=3; FP-wt, n=3; FP-het, n=6.
Error bars represent SEM and *, *P*<0.05; **, *P*<0.01; ***, *P*<0.001. *P*-values were analyzed using a 1way-ANOVA with Bonferroni post-test and a two-tailed, unpaired student's t-test for tendencies (grey).

4.2.4 Analysis of endocrine-specific FVFPBF^{DHom}; Igfr-L1$^{-/-}$

A complete deletion of Igfr-L1 specifically within the endocrine compartment was analyzed in the FP MODY model as FP-hom mice were assumed to die postnatally. A similar or even stronger regulation of blood glucose levels seen in male FP-het mice was expected. In parallel to the endocrine CKO in Bl6, the diabetic endocrine CKO was generated (see 4.1.5, Figure 4.2.4.1).

Specific deletion of Igfr-L1 within all endocrine cells was confirmed by IHC at P25 (Figure 4.2.4.2). Interestingly, visualization of glucagon hinted again to an increased α-cell number as already observed in endocrine CKO animals in Bl6 but thorough quantification is needed. In FP animals, intra-islet cell adhesion is lost and islets are expanded, whereas in endocrine diabetic CKO animals, islets appear more compact, which has to be confirmed in IHC.

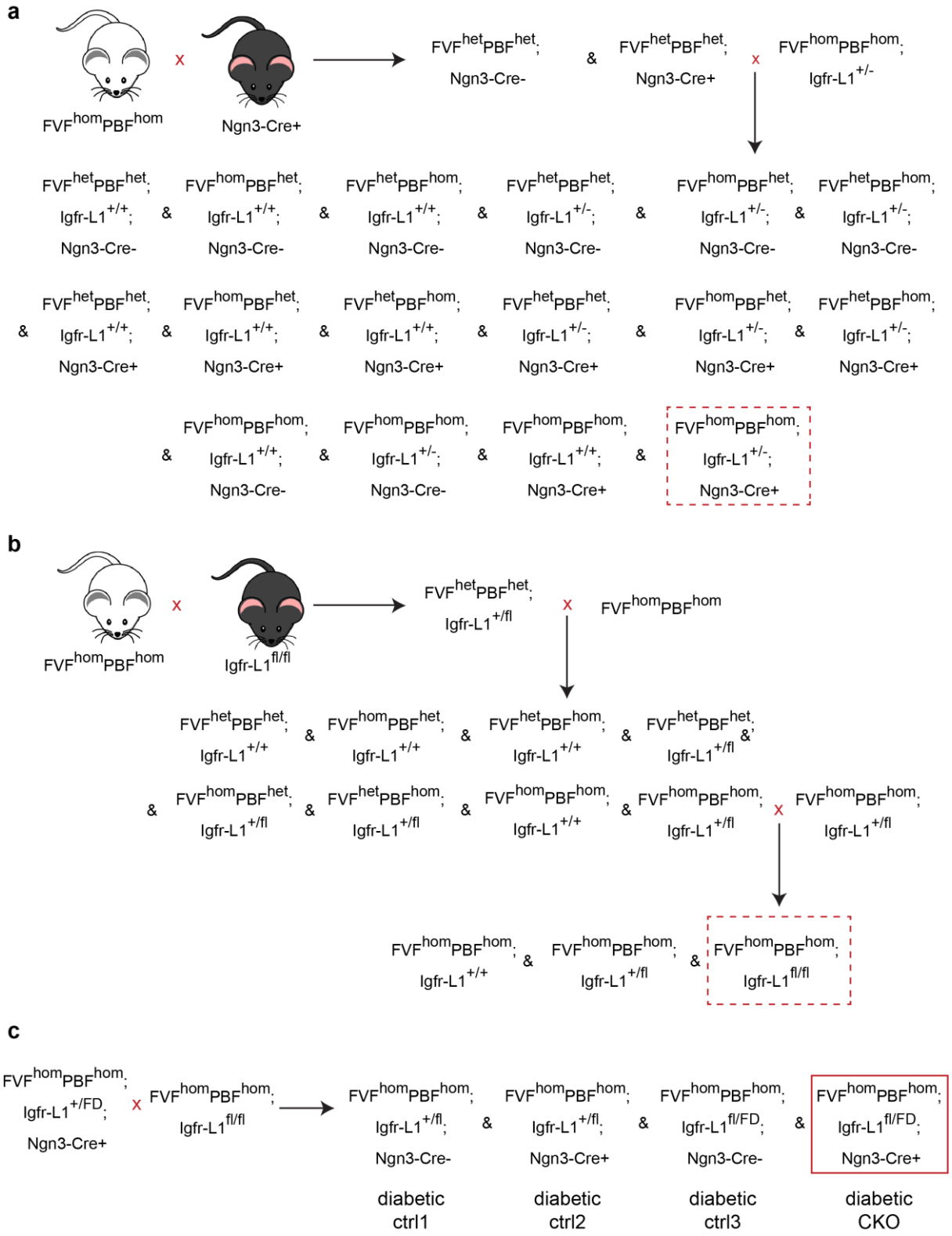

Figure 4.2.4.1 Generation of diabetic endocrine CKO and ctrl animals

Mating scheme for the generation of endocrine CKO and ctrl animals in the MODY line. a, Parental line 1; b, parental line 2; c, Intercrosses of parental lines 1 and 2 to obtain CKO and ctrl animals for analysis.

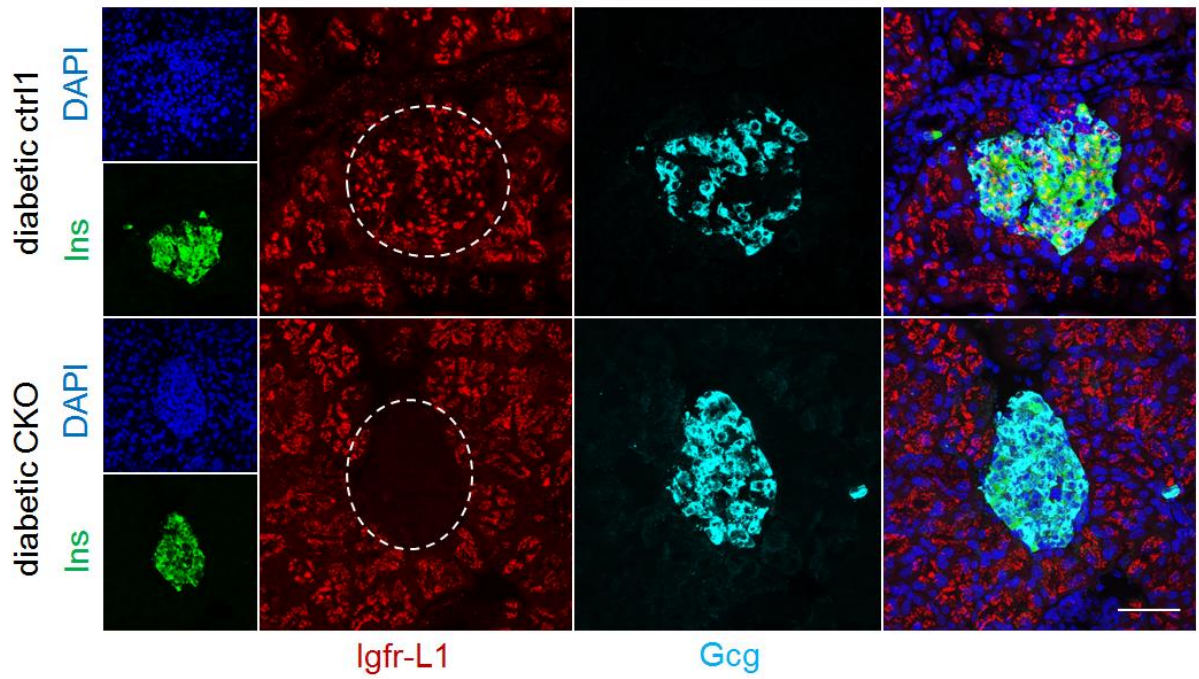

Figure 4.2.4.2 Confirmation of endocrine CKO in MODY animals

Representative LSM images (max. projection) for the lack of expression of Igfr-L1 (red) in the islets of diabetic endocrine CKO and diabetic ctrl 1 males marked by insulin (green) and glucagon (cyan) at P25. Scale bar, 50µm.

So far, body weight and 6 h fasting blood glucose levels of only two litters could be analyzed at P25, which were not significantly different in males or in females (Figure 4.2.4.3a-d). There was a tendency to lower body weight of diabetic endocrine CKO males compared to diabetic ctrl1. However, animal numbers have to be increased for proper analysis of all four genotypes.

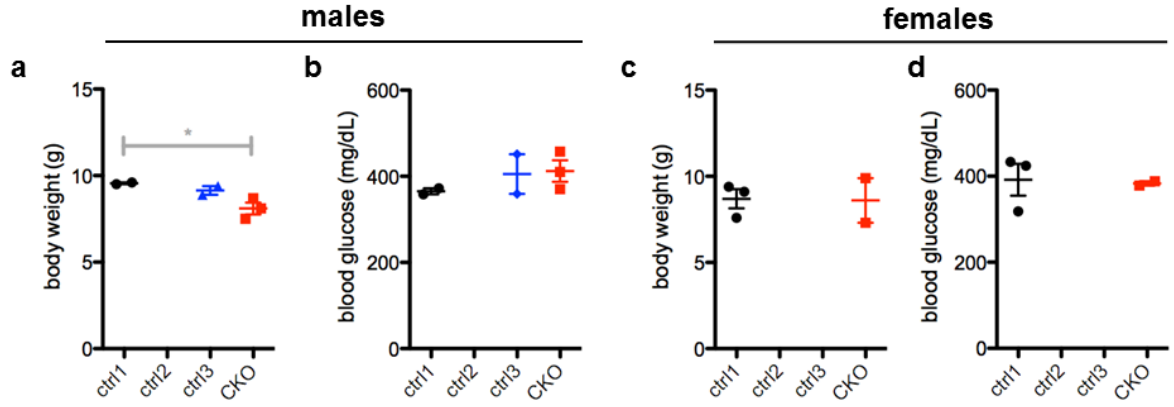

Figure 4.2.4.3 Body weight and blood glucose levels of diabetic endocrine CKO mice

a-b, Body weight (a) and 6 h fasting blood glucose levels (b) of males at P25.
a, n.s., *P*=0.0531; ctrl1 vs CKO, *, *P*=0.0482; b, n.s., *P*=0.5449;
ctrl1, n=2; ctrl3, n=2; CKO, n=3;
c-d, Body weight (c) and 6 h fasting blood glucose levels (d) of females at P25.
c, n.s., *P*=0.9392; d, n.s., *P*=0.8677; ctrl1, n=3; CKO, n=2.
Error bars represent SEM and *, *P*<0.05; **, *P*<0.01; ***, *P*<0.001. Males, *P*-values were analyzed using a 1way-ANOVA with Bonferroni post-test and a two-tailed, unpaired student's t-test for tendencies (grey). Females, *P*-values were analyzed using a two-tailed, unpaired student's t-test.

4.3 Interaction partners of Igfr-L1

Cellular and molecular functions of proteins are often defined by their interaction with other proteins. As part of the Ins/Igf system, Insr and Igf1r initiate the interaction of various downstream signaling proteins that specifically translate their phosphorylation into metabolic control or proliferation. To find potential interaction partners that give a hint about the signaling pathway or subcellular functions of Igf-L1 and might explain the *in vivo* phenotypes, a protein-protein interaction screen was performed in the murine β-cell line Min6 by analyzing co-immunoprecipitated proteins by High Performance Liquid Chromatography-Mass Spectrometry (HPLC-MS) in collaboration with Dr. Karsten Boldt.

4.3.1 Immunoprecipitation of Igfr-L1

In immunoprecipitations, the protein of interest is immobilized on beads via a specific antibody and can thus be affinity purified from the cell lysate. First, antibodies had to be tested to effectively and specifically pull down Igfr-L1. Therefore, antibodies from three different species against different domains of IGFR-L1 were used in several concentrations or dilutions (Table 4.3.1.1). Supernatants (SN) after immunoprecipitation, i.e. lysates with unbound proteins were analyzed as control. Igfr-L1$^{-/-}$ lysate, immunoglobulins or rabbit pre-immunization serum served as negative control. Depending on the intensity of immunoprecipitated Igfr-L1, detection of Igfr-L1 in the whole cell lysate (Input, In) or SN was not always visible.

Table 4.3.1.1 Anti-IGFR-L1 antibodies tested in immunoprecipitation
Antigen, ID number, subclass and host of different anti-IGFR-L1 antibodies.

antigen	ID/clone	subclass	host
cytoplasmic tail	36D7	2b	mouse
	14F1	2a	rat
	16F6	2a	rat
	animal 1, 2, 3	polyclonal	rabbit
extracellular domain – B	9C2	2c	rat
	10D9	2c	rat
	18B2	2c	rat
extracellular domain – A	31G11	2b	mouse
	32H8	2b	mouse
whole extracellular domain	1374	polyclonal	rabbit
	1692	polyclonal	rabbit

The three rabbit antibodies against the cytoplasmic tail, pulled down the monomer of Igfr-L1 at 130 kDa in a concentration-dependent manner, which coincided with the SN (Figure 4.3.1.1a). Similarly, dimers or tetramers at above 250 kDa were immunoprecipitated, whereas a higher antibody dilution resulted in a higher monomer to dimer ratio. Mouse antibody 36D7 against the cytoplasmic tail was also able to immunoprecipitate both the monomer and the dimer above 250 kDa, whereas rat antibody 14F1 only pulled down the monomer (Figure 4.3.1.1b). For both, 1 µg of antibody per 100 µg cell lysate was sufficient to pull down Igfr-L1 completely. Rat anit-cytoplasmic-IGFR-L1 16F6 was also able to pull down Igfr-L1 monomers in a concentration-dependent manner (Figure 4.3.1.1c). From the antibodies against different parts of the extracellular domain of IGFR-L1, none of the three rat antibodies B9C2, B10D9 or B18B2 was able to pull down Igfr-L1 (Figure 4.3.1.1c). Only

the two mouse antibodies A31G11 and A32H8 showed a strong band at around 110 kDa, which is the calculated size for Igfr-L1 without glycosylation (Figure 4.3.1.1c). A32H8 additionally pulled the monomer at 130 kDa. The two rabbit polyclonal antibodies against the extracellular domain 1374 and 1692 were also capable of precipitating Igfr-L1 and could be used in very high dilutions (Figure 4.3.1.1d). After longer exposure, the dimer could be detected as well, what was independent of the antibody concentration. To highlight, the majority of anti-IGFR-L1-antibodies generated effectively pulled down Igfr-L1 either as monomer, dimer or both which could depend on the epitopes they recognize. Even though aggregation in Laemmli buffer during boiling cannot be excluded, dimerization of IGFR-L1 in a concentration-dependent, ligand-independent manner was already observed by Dr. Ünal Coskun during purification of the recombinant protein (Figure 4.3.1.1e).

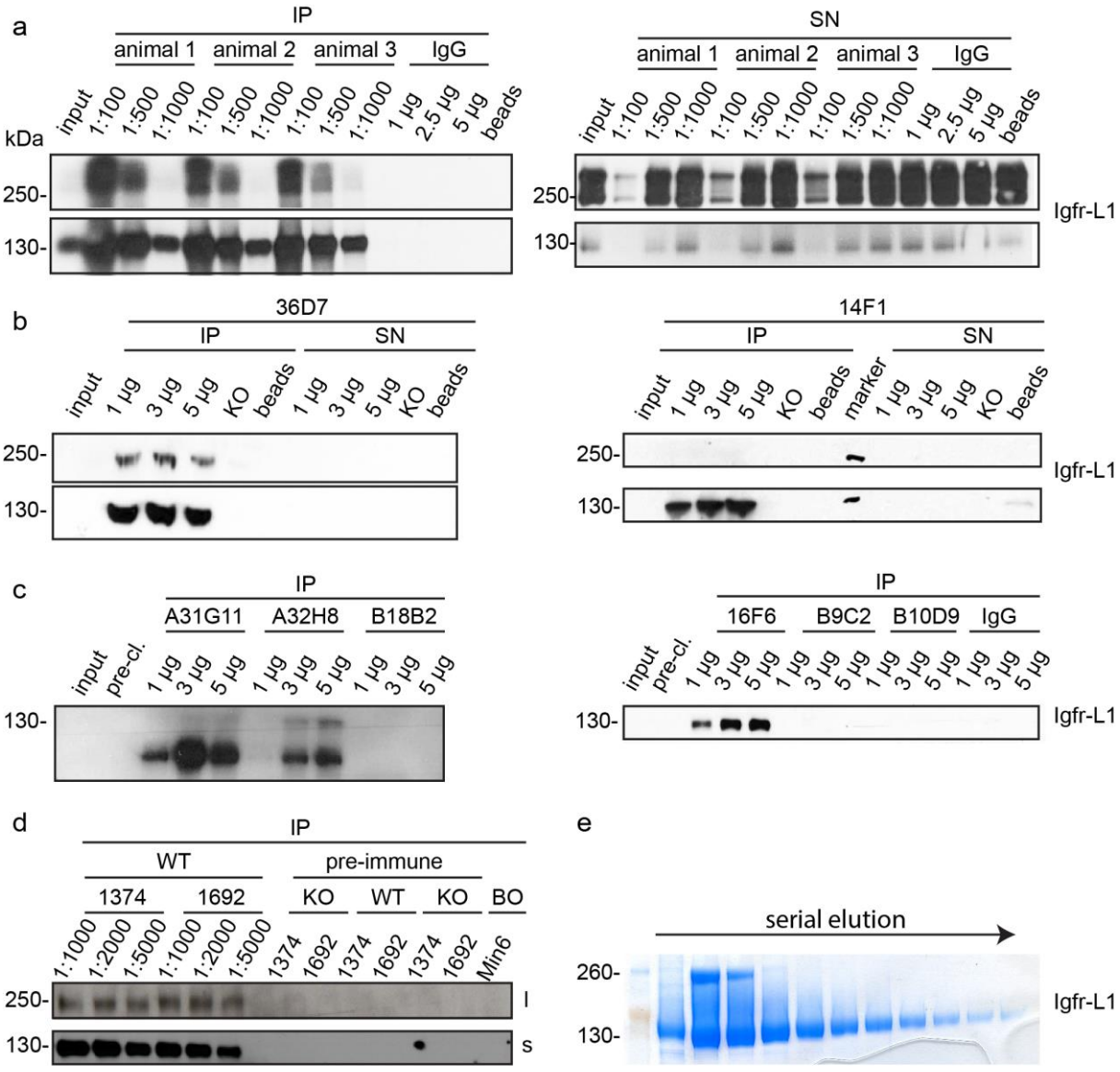

Figure 4.3.1.1 Immunoprecipitation of Igfr-L1

a-d, Detection of Igfr-L1 monomers (130 kDa) and dimers (260 kDa) after immunoprecipitation performed with various antibodies from different species and different domains of IGFR-L1 with several dilutions/concentrations (see Table 4.3.1.1). IP, immunoprecipitation; SN, supernatant; BO, beads only; s/l, short/long exposure.

e, Detection of IGFR-L1 monomers (130 kDa) and dimers (260 kDa) after serial elution during affinity purification stained with Coomassie (Dr. Ünal Coskun).

To optimize the conditions for co-IPs, different factors like incubation time, washing and elution conditions had to be considered. Furthermore, crosslinking of antibodies to avoid excessive presence of their light and heavy chains during MS analysis was tested. For sufficient removal of unspecific proteins from the tube, sepharose G beads were transferred to spin columns containing a membrane and washed before acidic elution, which was confirmed to be complete. Additionally, lysis buffers with different detergents were tested to preserve interactions on one hand but to also avoid false-positive interaction partners on the other hand (data not shown). Regarding the pull-down efficiency and co-IP of Ap2 (see 4.3.3) and Grp78 (Kang et al., 2015) as well as detergent costs, the buffer containing the detergent Brij®O10 was chosen for performing the HPLC-MS analysis.

4.3.2 Identification of interaction partners (HPLC-MS)

For the identification of potential interaction partners of Igfr-L1, co-immunoprecipitations (co-IP) were performed and the eluates analyzed by HPLC-MS. In a trial experiment, Igfr-L1 was precipitated with the crosslinked mouse anti-cytoplasmic-IGFR-L1 36D7 to find potential ligands and with the polyclonal rabbit anti-ectodomain-IGFR-L1 1374 to identify potential interactions with downstream signaling proteins, which was indistinguishable in the end. Igfr-L1$^{-/-}$ Min6 cells served as negative control and for the calculation of the ratio peptide count in Igfr-L1$^{+/+}$ to Igfr-L1$^{-/-}$. Finally, Igfr-L1$^{+/+}$ and Igfr-L1$^{-/-}$ Min6 cells were lysed under different metabolic conditions that might favor a subset of interaction partners, i.e. under growth conditions or after starvation in HBSS for 15 min (Figure 4.3.2.1a).

In general, proteins involved in RNA processing, protein synthesis and degradation, cellular proliferation and metabolism were co-immunoprecipitated. With the anti-cytoplasmic-IGFR-L1 antibody, 20 and 33 significantly enriched proteins were identified under growth conditions and after starvation, respectively, with nine being shared. With the anti-extracellular-Igfr-L1 antibody, 47 and 43 significantly enriched proteins were found under growth conditions and after starvation, respectively, with 13 being shared. Co-immunoprecipitated proteins (robust outliers) are shown in supplementary Table 10.1.1.1, Table 10.1.1.2, Table 10.1.1.3 and Table 10.1.1.4.
Interestingly, the most abundant interaction partner under both metabolic conditions was the Igfr-L1 paralogue KIAA1324-like which we renamed Igfr-L2 accordingly (see 4.4). In accordance to the bioinformatic analysis and experimental data, potential interaction of Igfr-L1 with components of (Insr/Igf1r-) endocytosis such as clathrin light chain A and Ap2-complex subunit α-2, as well as the E3 ubiquitin-protein ligase Nedd4, E3 ubiquitin-protein ligase Ubr4, signal transducing adapter molecule 1 and glucose-induced degradation protein 8 homolog were found. Intracellular trafficking of Igfr-L1 was associated with proteins like Ap-3 complex subunit sigma-1, vesicle-trafficking protein SEC22b, transmembrane emp24 domain-containing protein 9, receptor-type tyrosine-protein phosphatase-like N and vesicular integral-membrane protein VIP36. As expected from the subcellular localization within the ER-Golgi compartments, potential interaction of Igfr-L1 with endoplasmic reticulum-Golgi intermediate compartment protein 1, calnexin, surfeit locus protein 4 and translocon-associated protein subunit α were identified. Several subunits of 14-3-3 proteins were also detected by co-IP.

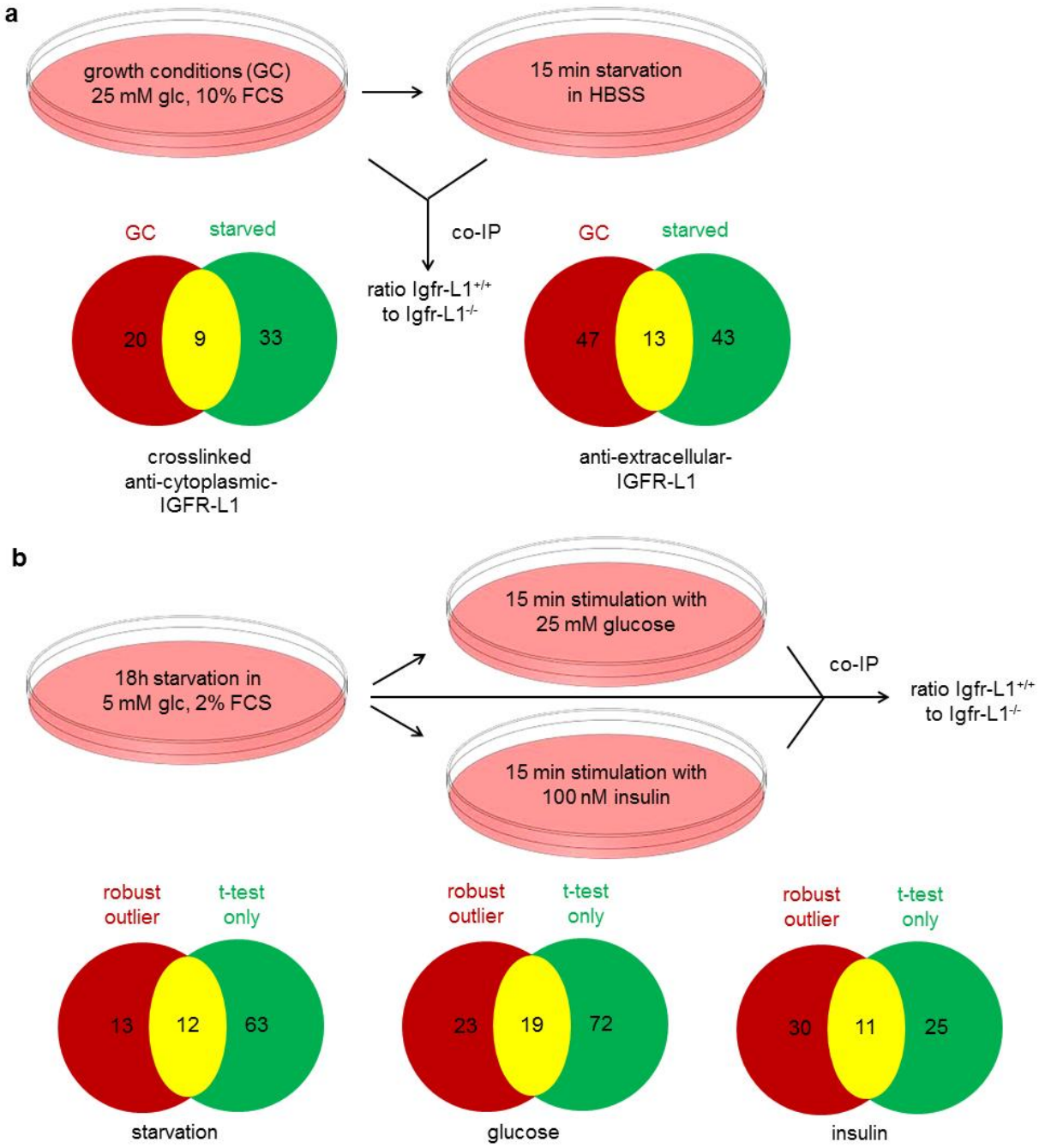

Figure 4.3.2.1 Overview of the co-IP analysis by MS

a, Experimental set-up and summary of the trial experiment.
b, Experimental set-up and summary of the final experiment.

Transcriptional regulation of insulin downstream signaling in Min6 cells after overnight (18h) starvation in low glucose (5 mM) and 2% fetal calf serum (FCS) and subsequent stimulation either with high glucose (25 mM) or insulin (100 nM) for 15 min was reported (Ohsugi et al., 2004). Thus, cells were starved accordingly in order to dissect differences between glucose-induced insulin secretion and direct insulin action on potential interactions of Igfr-L1 (Figure 4.3.2.1b). Results of the final experiment with 5 replicates and immunoprecipitation with the rabbit polyclonal anti-extracellular-IGFR-L1 are shown in supplementary Table 10.1.2.1, Table 10.1.2.2 and Table 10.1.2.3.

Immunoprecipitation of Igfr-L1 was successful, however, the ratio between wildtype and Igf-L1$^{-/-}$ Min6 cells was relatively low under the different metabolic conditions compared to the trial experiment. This could be due to adaptation of the cells and a not drastic enough change in the metabolic state. Eventually, 12 co-immunoprecipitated proteins were identified as robust outliers and significantly different between wildtype and Igf-L1$^{-/-}$ Min6 cells in a student's t-test, 19 proteins for the subsequent stimulation with 25 mM glucose and 11 for the stimulation with 100 nM insulin after starvation.
Again, the most abundant interaction partner was the paralogue Igfr-L2. After stimulation with both high glucose and insulin, different subunits of ATPases (V-type proton ATPase catalytic subunit A, sodium/potassium-transporting ATPase subunit α-1/-2, sarcoplasmic/ endoplasmic reticulum calcium ATPase 3, transitional endoplasmic reticulum ATPase) and the mitochondrial ATP synthase subunit α were found as potential interaction partners of Igfr-L1 suggesting an involvement in GSIS and energy homeostasis.

Exocytosis of Igfr-L1

Three- to seven-fold decreased levels of precipitated Igfr-L1 during growth conditions and glucose or insulin stimulation compared to starvation entailed the question if Igfr-L1 might be secreted (Table 4.3.2.1). In coherence, IGFR-L1 was detected in exosomes of human saliva (Gonzalez-Begne et al., 2009), which can also be isolated from islets.

Table 4.3.2.1 Amount of immunoprecipitated Igfr-L1 during MS

Counts of Igfr-L1 detected in the eluate after immunoprecipitation with different antibodies under different metabolic conditions and indication of approximate ratios.

antibody	growth conditions		15' starvation
anti-intracellular IGFR-L1	457	x 7 →	3188
anti-extracellular IGFR-L1	477	x 4 →	1985

	18 h starvation		glucose stimulation	insulin stimulation
anti-extracellular IGFR-L1	7437	: 3 →	2745	2593

4.3.3 Interaction of Igfr-L1 with Ap2, Insr and Igf1r (co-IP)

Potential interaction partners were further analyzed by co-immunoprecipitation followed by WB analysis. An Ap2-binding motif involved in CME was identified in the cytoplasmic tail of Igfr-L1. Hence, Igfr-L1 and Ap2 were co-immunoprecipitated (Figure 4.3.3.1a). The potential interaction was confirmed *vice versa* in independent experiments.
Even though Insr and Igf1r were not found in the co-IP followed by HPLC-MS analysis, a potential either direct or indirect interaction with Igfr-L1 was hypothesized due to the domain structure similarities. Insr or Igf1r were immunoprecipitated under growth conditions and Igfr-L1 detected in the eluate (Figure 4.3.3.1b). Because expression of Igfr-L1 and its interactions were metabolically regulated the co-immunoprecipitation with Insr was performed under starvation and subsequent glucose or insulin stimulation (Figure 4.3.3.1c). Interestingly, more Igfr-L1 could be co-immunoprecipitated together with Insr upon insulin stimulation hinting to a ligand-induced interaction. Due to the elution of primary antibodies resulting in high background, immunoprecipitated Insr and Igf1r could not be detected nicely.

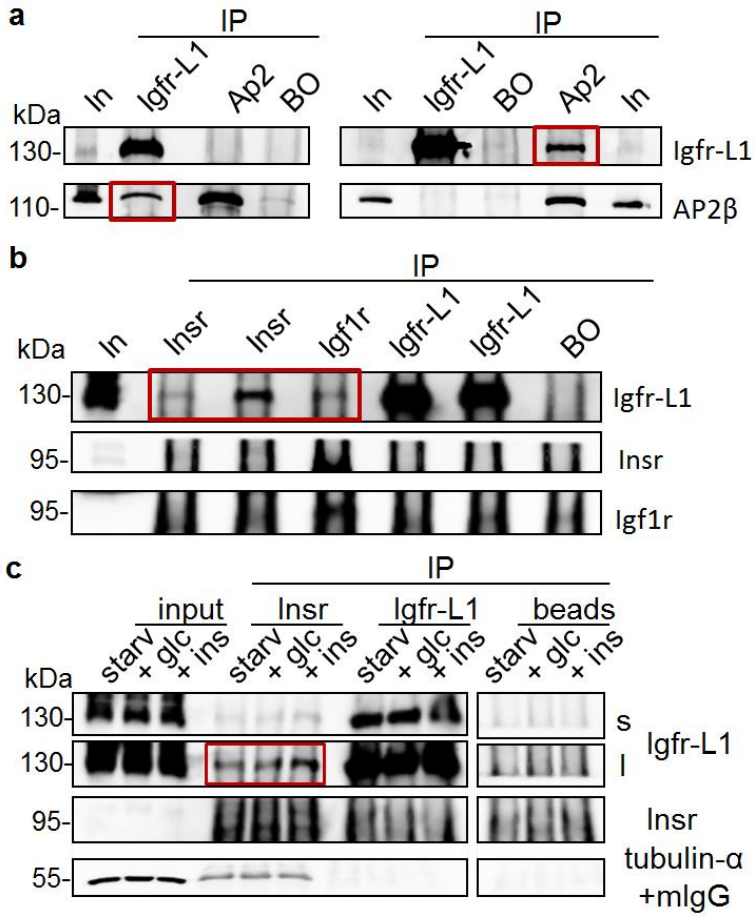

Figure 4.3.3.1 Co-immunoprecipitation of Igfr-L1

a, Co-immunoprecipitation of Igfr-L1 and Ap2 *vice versa.*
b, Co-immunoprecipitation of Igfr-L1 together with Insr and Igf1r.
c, Co-immunoprecipitation of Igfr-L1 together with Insr under different metabolic conditions. Starv, 1 h HBSS; +glc, 25 mM glucose after 1h HBSS;
+ ins, 100 nM insulin after 1 h HBSS.

4.3.4 Interaction of IGFR-L1 with INSR, IGF1R and INS (PLA)

Protein-protein interactions can be direct or indirect including the presence of other proteins e.g. in a complex. In the Sigma™ proximity ligation assay (PLA), proximity of two proteins is detected, which gives a hint on their potential interaction in combination with the subcellular localization. As shown by co-IP, Igfr-L1 potentially interacts with Insr and Igf1r in Min6. Also in EndoC, proximity of IGFR-L1 to INSR, IGF1R and the activated form as well as to INS was detected (Figure 4.3.4.1). Apart from the typical ER-Golgi pattern, potential interactions might also occur at the PM, which requires a different technique such as total internal reflection fluorescence for analysis. Trial affinity purification experiments with recombinant proteins and biotinylated insulin further suggested that insulin might bind directly to IGFR-L1 (data not shown).

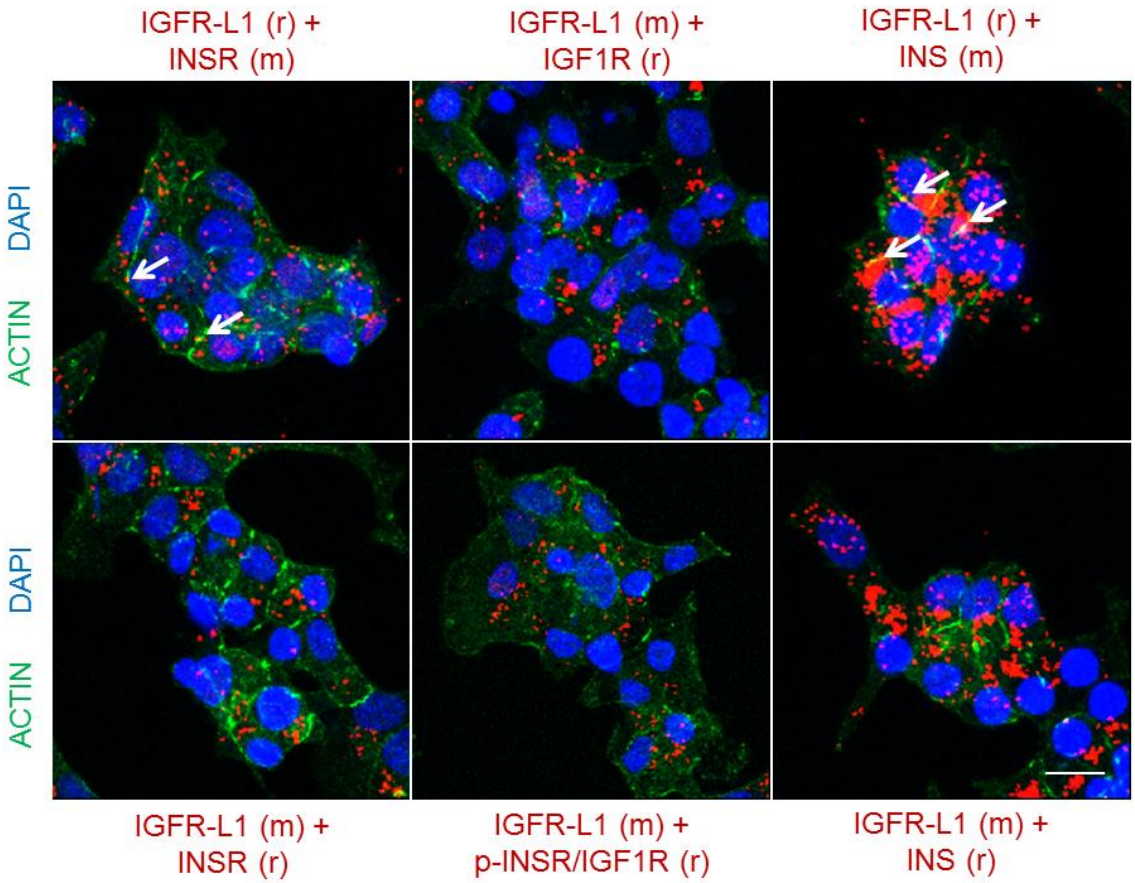

Figure 4.3.4.1 Proximity ligation assay in EndoC

LSM images (max. projection) of the detection of potential interactions between IGFR-L1 (mouse or rabbit) and INSR (mouse or rabbit), IGF1R (rabbit) or p-INSR/IGF1R (rabbit) as well as INS (mouse or rabbit) by PLA (red) together with ACTIN (green). Scale bar, 10 µm.

4.3.5 Endocytosis of Igfr-L1, Insr and Igf1r

Receptor-ligand interactions take place at the plasma membrane (PM). After initiation of signal transduction, the activated complex is internalized and either recycled back to the membrane or degraded in lysosomes. To specifically analyze the interaction of Igfr-L1 with Insr and Igfr1r at the PM, surface proteins were analyzed after biotinylation and affinity precipitation. Endocytosis was induced by transferring cells from growth conditions, under which internalization and recycling are in a steady state, to complete growth factor and glucose deprivation. Therefore, wildtype and Igfr-L1$^{-/-}$ Min6 cells were incubated in HBSS for up to 2 h (Figure 4.3.5.1a). In wildtype cells, Igfr-L1, Insr and Igf1r were internalized from the surface after 15 min and recycled back after 1 h. In Igfr-L1$^{-/-}$ cells, however, Insr and Igf1r accumulated at the PM with the greatest difference at 30 min, while after 1 h, Insr and Igf1r were less abundant at the PM. Hence, lack of Igfr-L1 interferes with the kinetics of Insr and Igf1r internalization and recycling.

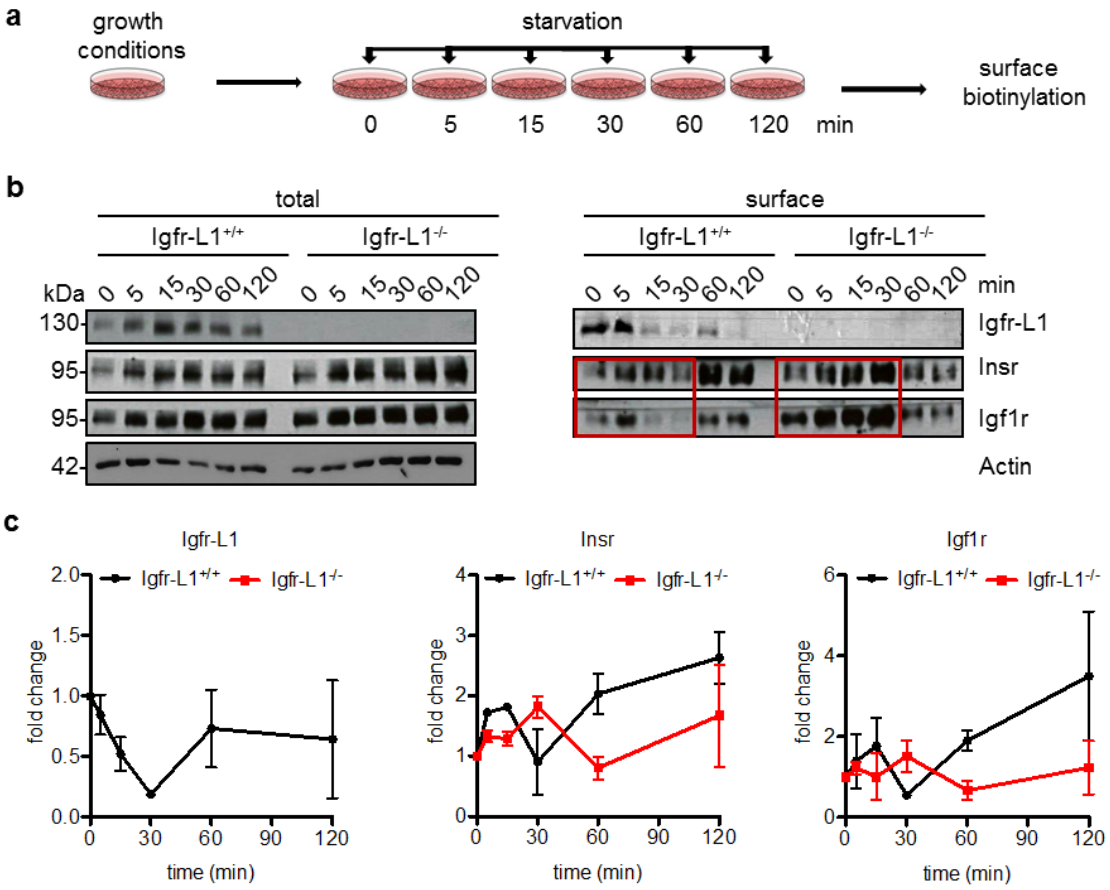

Figure 4.3.5.1 Insr/Igf1r endocytosis in wildtype and Igfr-L1$^{-/-}$ Min6

a, Experimental set-up for the starvation time course followed by surface biotinylation in wildtype and Igfr-L1$^{-/-}$ Min6.

b-c, Representative WB (b) and quantification (c) of total (left panel) and surface- (right panel) Insr, Igf1r and Igfr-L1 at different time points of starvation.
Insr, n.s., *P*=0.1487; Igf1r, n.s., *P*=0.2401; n=2.

Error bars represent SEM and *, *P*<0.05; **, *P*<0.01; ***, *P*<0.001. *P*-values were analyzed using a 2way-ANOVA with Bonferroni post-test.

4.4 Bioinformatic description of Igfr-L2

Co-IP with subsequent HPLC-MS analysis identified the paralogue Igfr-L2 as the most abundant potential interaction partner of Igfr-L1. Because of the domain structure similarities to Insr and Igf1r in respect of the growth factor receptor cysteine-rich domain (CRD) and the mannose-6-phosphate receptor (M6PR) binding domain found in the Igf2r, EIG121 was re-named Igf receptor-like in our laboratory. To investigate whether the same nomenclature is suitable for the paralogue EIG121-like (EIG121L), bioinformatic analyses with generally accessible databases were performed regarding gene and protein structure, expression and potential function.

4.4.1 The gene *9330182L06Rik*

Gene *9330182L06Rik* has been identified in the Riken project for sequencing the murine genome by use of cDNA microarrays (Bono, Kasukawa, Furuno, et al., 2002; Bono, Kasukawa, Hayashizaki, et al., 2002; Bono et al., 2003; Miki et al., 2001). The gene is located on the forward strand of chromosome 5 from base pair (bp) 9,266,118 to 9,481,825. It has 22 exons with two promoters, one upstream of and one around exon 1, as well as several promoter flanks and enhancers predicted throughout the sequence (Figure 4.4.1.1a). Via alternative splicing eight transcripts are predicted, of which only three are protein coding (Table 4.4.1.1, Figure 4.4.1.1b). The largest transcript *9330182L06Rik*-201 is transcribed from all 22 exons and has 4688 bp resulting in a protein with 1028 aa. Transcript *9330182L06Rik*-204 with 4115 bp has a slightly longer exon 21 but misses exon 22. The translated protein has 1014 aa. The shortest transcript *9330182L06Rik*-202 with only 3403 bp lacks exons 5 to 21 and the translated protein has only 236 aa. All predicted transcripts have the same start codon ATG in the beginning of exon 1 after a 5' untranslated region (UTR), which is slightly shorter in transcript -202. The stop codon of the longest (-201) and the shortest (-202) transcript is TGA in exon 22, whereas the 3' UTR of transcript -202 is much longer. Transcript -204 has its stop codon TAA in exon 21 followed by a 3' UTR.

Apart from the paralogue *5330417C22Rik/Igfr-L1*, 120 orthologues are predicted for gene *9330182L06Rik* in vertebrates. The ancestor gene was already found in *C. elegans* (Y73F8A.5) and duplicated three times so that the paralogues were formed (data not shown). Similarly, the paralogue has 22 exons and 3 protein coding transcripts. In coherence, Insr und Igf1r emerged as paralogous proteins in vertebrates with 22 exons too.

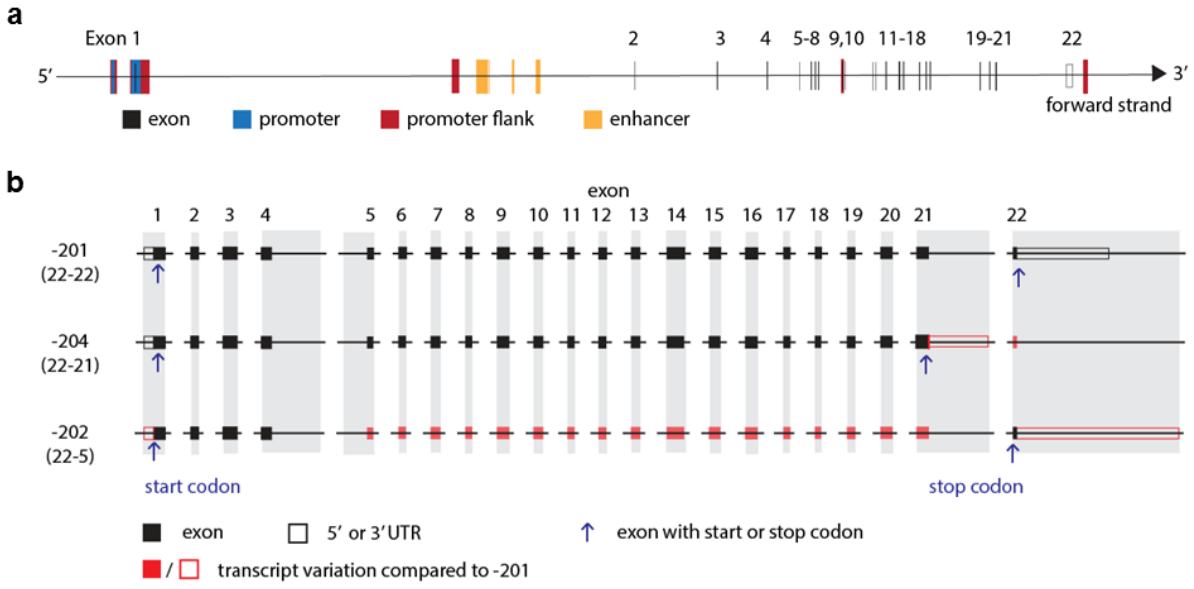

Figure 4.4.1.1 Gene *9330182L06Rik*

a, Schematic representation of the 22 exons (black lines), promoters (blue boxes), promoter flanks (red boxes) and enhancers (yellow boxes) predicted for gene locus *9330182L06Rik.* Modified from Ensembl (www.ensembl.org).

b, Schematic representation of total and protein coding exons (boxes) as well as 5' or 3' UTRs (frames) of the three protein coding transcripts with indications of start and stop codon. Transcript variations compared to *9330182L06Rik*-201 are highlighted in red, opacity indicates non-transcribed exons. Modified from Ensembl (www.ensembl.org).

Table 4.4.1.1 Transcripts of gene *9330182L06Rik*

Predicted protein coding transcripts with ID, number of protein coding exons as well as transcript and protein length. Modified from Ensembl (www.ensembl.org).

no.	name	Transcript ID	protein coding exons	transcript length (bp)	protein length (aa)
1	*9330182L06Rik* -201	ENSMUST 00000069538.13	22	4688	1028
2	*9330182L06Rik* -204	ENSMUST 00000134991.7	21	4115	1014
3	*9330182L06Rik* -202	ENSMUST 00000115348.8	5	3403	236

4.4.2 The protein Igfr-L2

Since its emerging in *C.elegans*, the protein Igfr-L2 has been, similar to Igfr-L1, highly conserved during evolution (www.ncbi.nlm.nih.gov/homologene/27396). Primary sequence identity between *M. musculus* and *R. norvegicus, P. troglodytes, M. mulatta, C. lupus* or *B. taurus* as well as *H. sapiens* is more than 90%.

To further describe the protein, amino acid sequences were obtained from the UniProt Knowledgebase (www.uniprot.org). For Igfr-L2, isoform 1 (Q3UZV7), the so-called canonical sequence, corresponds to transcript *9330182L06Rik*-201 from the Ensembl database and isoforms 2 and 6 to transcripts -204 and -202, respectively.
As shown by aa alignment, murine Igfr-L2 (Q3UZV7) and human IGFR-L2 (A8MWY0) are almost identical, while the few non-identical aa are often conserved in their properties (Figure 4.4.2.1a). Apart from that, the murine protein is one amino acid shorter due to the lack of Ser59. The transmembrane domain, cysteines for disulfide bond formation as well as sites for N-glycosylation and post-translational modifications are conserved.
Analogously, the paralogues Igfr-L1 and Igfr-L2 share an overall sequence identity of 52 % both in mouse and human. Primary sequence alignment of Igfr-L2 (Q3UZV7) with Igfr-L1 (A2AFS3) showed high similarity within the transmembrane (62 %) and the cysteine-rich domain, in which all six cysteine residues enabling disulfide bonds are conserved (Figure 4.4.2.1b). Of the three predicted N-glycosylation sites, two are almost in the same position. The cytoplasmic tails are 62 % identical and even 84 % including aa with highly similar properties, whereas the signal peptides show great differences.

a

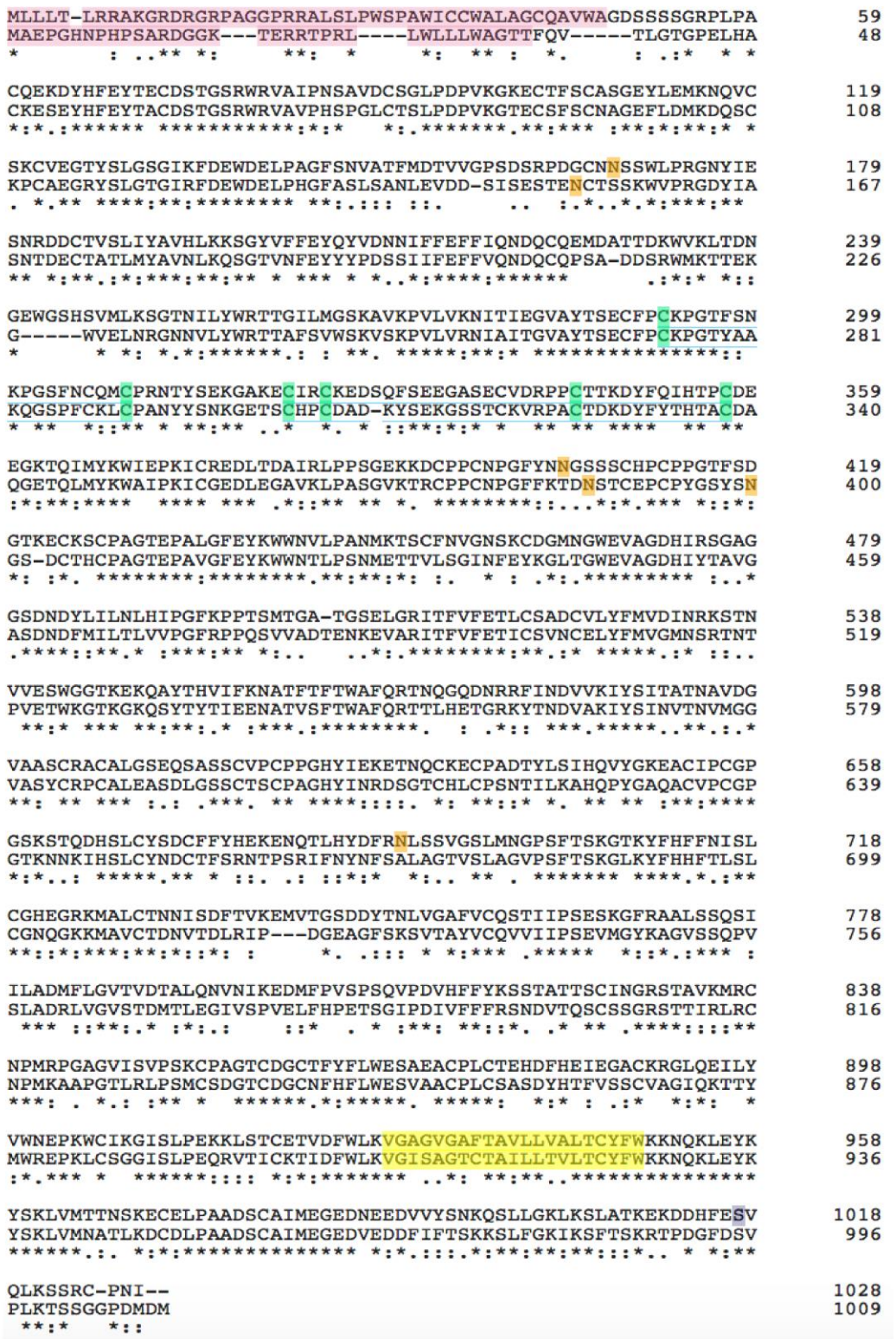
MLLLT-LRRAKGRDRGRPAGGPRRALSLPWSPAWICCWALAGCQAVWAGDSSSSGRPLPA 59
MAEPGHNPHPSARDGGK---TERRTPRL----LWLLLWAGTTFQV-----TLGTGPELHA 48
CQEKDYHFEYTECDSTGSRWRVAIPNSAVDCSGLPDPVKGKECTFSCASGEYLEMKNQVC 119
CKESEYHFEYTACDSTGSRWRVAVPHSPGLCTSLPDPVKGTECSFSCNAGEFLDMKDQSC 108
SKCVEGTYSLGSGIKFDEWDELPAGFSNVATFMDTVVGPSDSRPDGCNNSSWLPRGNYIE 179
KPCAEGRYSLGTGIRFDEWDELPHGFASLSANLEVDD-SISESTENCTSSKWVPRGDYIA 167
SNRDDCTVSLIYAVHLKKSGYVFFEYQYVDNNIFFEFFIQNDQCQEMDATTDKWVKLTDN 239
SNTDECTATLMYAVNLKQSGTVNFEYYYPDSSIIFEFFVQNDQCQPSA-DDSRWMKTTEK 226
GEWGSHSVMLKSGTNILYWRTTGILMGSKAVKPVLVKNITIEGVAYTSECFPCKPGTFSN 299
G-----WVELNRGNNVLYWRTTAFSVWSKVSKPVLVRNIAITGVAYTSECFPCKPGTYAA 281
KPGSFNCQMCPRNTYSEKGAKECIRCKEDSQFSEEGASECVDRPPCTTKDYFQIHTPCDE 359
KQGSPFCKLCPANYYSNKGETSCHPCDAD-KYSEKGSSTCKVRPACTDKDYFYTHTACDA 340
EGKTQIMYKWIEPKICREDLTDAIRLPPSGEKKDCPPCNPGFYNNGSSSCHPCPPGTFSD 419
QGETQLMYKWAIPKICGEDLEGAVKLPASGVKTRCPPCNPGFFKTDNSTCEPCPYGSYSN 400
GTKECKSCPAGTEPALGFEYKWWNVLPANMKTSCFNVGNSKCDGMNGWEVAGDHIRSGAG 479
GS-DCTHCPAGTEPAVGFEYKWWNTLPSNMETTVLSGINFEYKGLTGWEVAGDHIYTAVG 459
GSDNDYLILNLHIPGFKPPTSMTGA-TGSELGRITFVFETLCSADCVLYFMVDINRKSTN 538
ASDNDFMILTLVVPGFRPPQSVVADTENKEVARITFVFETICSVNCELYFMVGMNSRTNT 519
VVESWGGTKEKQAYTHVIFKNATFTFTWAFQRTNQGQDNRRFINDVVKIYSITATNAVDG 598
PVETWKGTKGKQSYTYTIEENATVSFTWAFQRTTLHETGRKYTNDVAKIYSINVTNVMGG 579
VAASCRACALGSEQSASSCVPCPPGHYIEKETNQCKECPADTYLSIHQVYGKEACIPCGP 658
VASYCRPCALEASDLGSSCTSCPAGHYINRDSGTCHLCPSNTILKAHQPYGAQACVPCGP 639
GSKSTQDHSLCYSDCFFYHEKENQTLHYDFRNLSSVGSLMNGPSFTSKGTKYFHFFNISL 718
GTKNNKIHSLCYNDCTFSRNTPSRIFNYNFSALAGTVSLAGVPSFTSKGLKYFHHFTLSL 699
CGHEGRKMALCTNNISDFTVKEMVTGSDDYTNLVGAFVCQSTIIPSESKGFRAALSSQSI 778
CGNQGKKMAVCTDNVTDLRIP---DGEAGFSKSVTAYVCQVVIIPSEVMGYKAGVSSQPV 756
ILADMFLGVTVDTALQNVNIKEDMFPVSPSQVPDVHFFYKSSTATTSCINGRSTAVKMRC 838
SLADRLVGVSTDMTLEGIVSPVELFHPETSGIPDIVFFFRSNDVTQSCSSGRSTTIRLRC 816
NPMRPGAGVISVPSKCPAGTCDGCTFYFLWESAEACPLCTEHDFHEIEGACKRGLQEILY 898
NPMKAAPGTLRLPSMCSDGTCDGCNFHFLWESVAACPLCSASDYHTFVSSCVAGIQKTTY 876
VWNEPKWCIKGISLPEKKLSTCETVDFWLKVGAGVGAFTAVLLVALTCYFWKKNQKLEYK 958
MWREPKLCSGGISLPEQRVTICKTIDFWLKVGISAGTCTAILLTVLTCYFWKKNQKLEYK 936
YSKLVMTTNSKECELPAADSCAIMEGEDNEEDVVYSNKQSLLGKLKSLATKEKDDHFESV 1018
YSKLVMNATLKDCDLPAADSCAIMEGEDVEDDFIFTSKKSLFGKIKSFTSKRTPDGFDSV 996
QLKSSRC-PNI-- 1028
PLKTSSGGPDMDM 1009

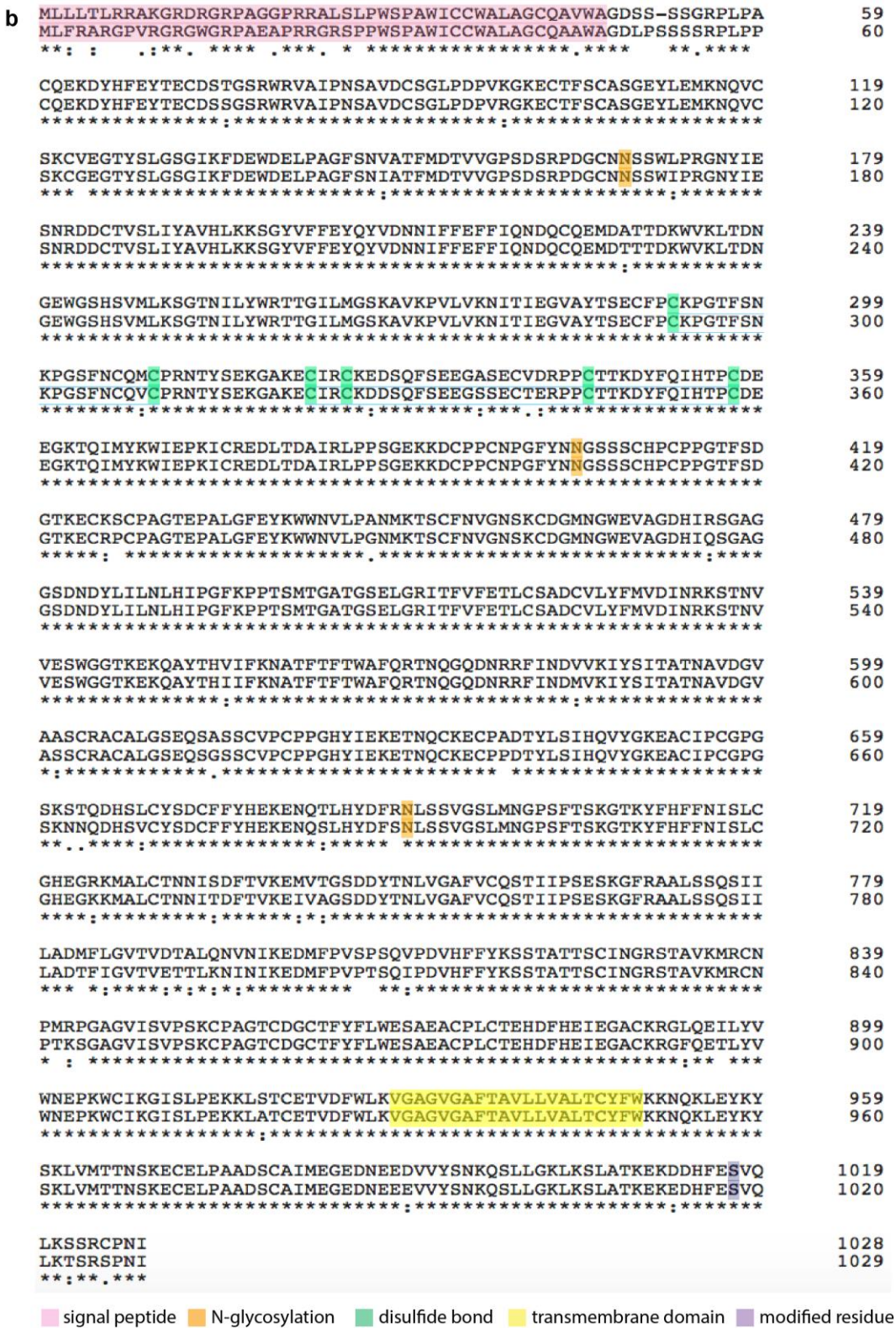

Figure 4.4.2.1 Amino acid alignment of Igfr-L2 with IGFR-L2 and Igfr-L1

a-b, Primary sequence alignment of Igfr-L2 (upper line) and IGFR-L2 (a, lower line) or Igfr-L1 (b, lower line) with indications of signal peptide (pink) and transmembrane domain (yellow) as well as sites for N-glycosylation (orange), disulfide bond formation (green) and post-translational modifications (purple). "*" indicates single, fully conserved positions, ":" indicates conservation between groups of strongly and "." weakly similar properties (score > or < 0.5 in the Gonnet PAM 250 Matrix respectively of Clustal Omega). Modified from UniProt (www.uniprot.org).

In more detail, a helical transmembrane domain of 21 aa (VGAGVGAFTAVLLVALTCYFW) separates the short intracellular (78 aa) from the extracellular part of Igfr-L2 (Figure 4.4.2.2a). The ectodomain contains a signal peptide, a cysteine rich domain with three disulfide bonds (Cys292-Cys309, Cys322-Cys345, Cys325-Cys357) and three potential N-glycosylation sites (Asn169, Asn404, Asn690). The cytoplasmic tail is 99 % evolutionary conserved and has a potentially phosphorylated serine residue (Ser1017). As a single-pass type I membrane protein, the N-terminus of Igfr-L2 is extracellular, while the C-terminus stays intracellular after removal of the signal peptide. Only proteins destined to the secretory pathway carry a signal peptide for translocation before its cleavage by signal peptidases. Thus, Igfr-L2 resides in the membrane of cellular organelles such as the ER-Golgi or endosomes as well as in the plasma membrane or might even be secreted to the extracellular space. The calculated protein size of Igfr-L2 is 113.66 kDa with an isoelectric point of pH=5.56 (www.isoelectric.org), whereas glycosylation might alter those parameters.

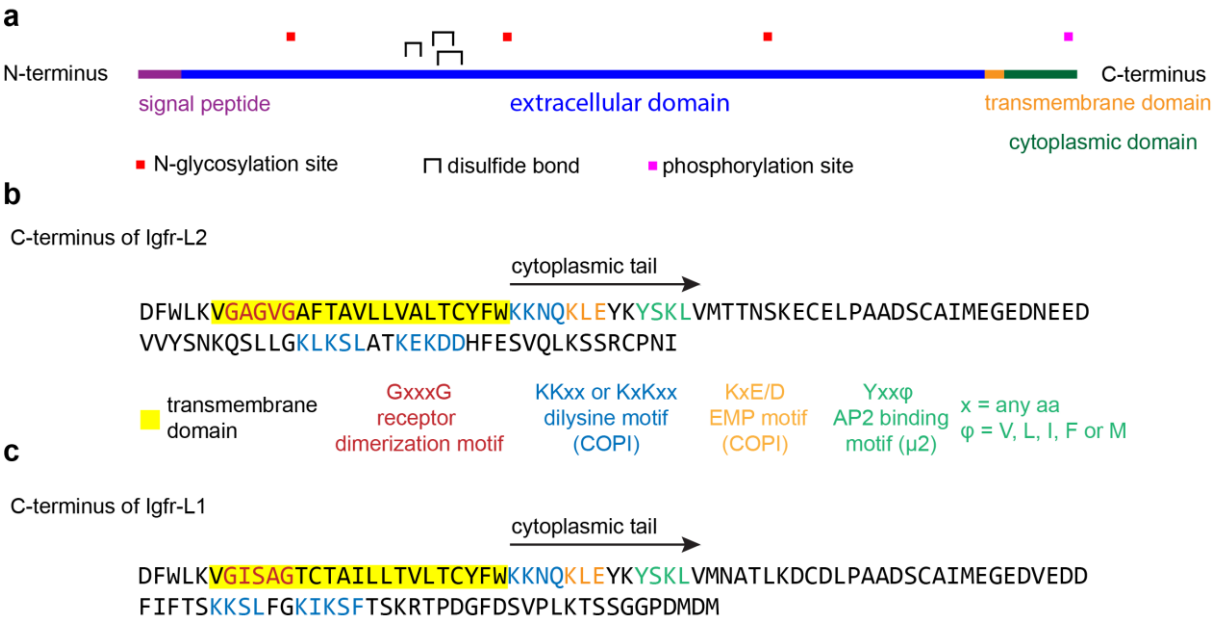

Figure 4.4.2.2 Topological domains and C-terminal functional motifs of Igfr-L2

a, Schematic representation of the topological domains (extracellular, transmembrane and cytoplasmic) of Igfr-L2 with indications of N-glycosylation and phosphorylation sites (red and pink boxes) or disulfide bonds (brackets). Modified from UniProt (www.uniprot.org).

b-c, Primary sequence of the carboxyl-terminus of Igfr-L2 (b) in comparison to Igfr-L1 (c) with indication of potential functional motifs. Modified from UniProt (www.uniprot.org).

Regarding potential functional properties of Igfr-L2, different motifs were identified in the carboxyl terminus (Figure 4.4.2.2b). The GxxxG motif (GAGVG) within the transmembrane domain could be important for homo- and heterodimerization as described for human epidermal growth factor receptor (EGFR) isoforms. KKxx or KxKxx dilysine motifs (KKNQ, KLKSL, KEKDD) are recognized by subunits of the coatamer complexes I (COPI) resulting in retrieval from the Golgi to ER in COPI-coated vesicles. In line with this, an adjacent KxE/D (KLE) motif involved in retrograde transport of endomembrane protein 12 (EMP12) in *A. thaliana* was found, which is conserved in eukaryotic EMPs. The motif Yxxφ (YSKL) is recognized by the μ2 subunit of the heterotetrameric (α2, β2, μ2, σ2) adaptor protein 2 (Ap2) involved in clathrin-mediated endocytosis (CME) of RTKs. All six motifs are conserved (D→E in KEKED) in the human protein. Unlike Insr and Igf1r but similar to the Igf2 scavenger receptor, Igfr-L2 does not have a tyrosine kinase domain.

In comparison to Igfr-L1, the same functional motifs are predicted in the C-terminus (Figure 4.4.2.2c). The Ap2 interaction (YSKL) and KLE motif for retrograde transport are identical, while Igfr-L1 has two KKxx motifs and one KxKxx (KKNQ, KKSL and KIKSF), Igfr-L2 has one of the KKxx (KKNQ) but two KxKxx motifs (KLKSL and KEKDD). The sequence of the dimerization motif GxxxG of Igfr-L1 (GISAG) is also different from Igfr-L2 (GAGVG). These small differences could lead to fine tuning of the paralogue and Insr or Igf1r interactions.

Regarding the extracellular domain, three domains homologous to tyrosine-protein kinase ephrin type A/B receptor-like (EphA/B, SM01411) and four to the growth factor receptor CRD superfamily (SSF57184 and SSF50911/M6PR domain) are predicted (Figure 4.4.2.3). EphA/B receptors are transmembrane proteins with a cytoplasmic catalytic domain that transfers a phosphate group from ATP to protein tyrosine residues. The growth factor receptor CRD can be found in the Insr and Igf1r as well as Igf binding proteins but also in other RTKs such as ErbB3. The M6PR domain is present in both the cation dependent-M6PR and the cation independent-M6PR/Igf2r, whereas only the latter can be found on the cell surface where it also serves as a scavenger receptor for Igf2 (domain 11).

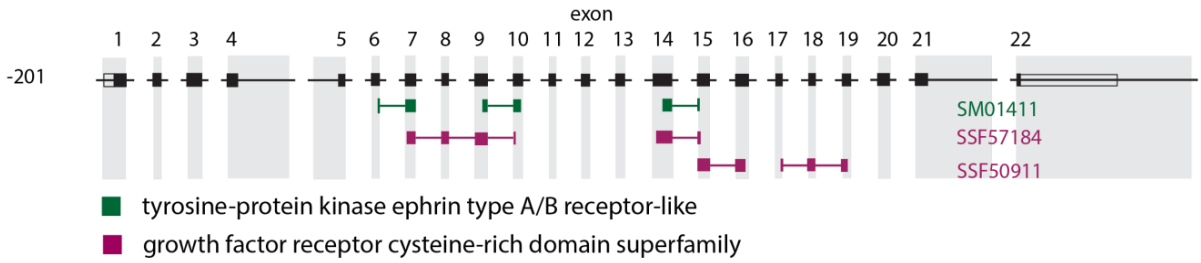

Figure 4.4.2.3 Predicted domains of Igfr-L2

Schematic representation of domain homology prediction to EphA/B receptor (green) and to growth factor receptor CRD including M6PR (purple) in the extracellular domain of Igfr-L2. Modified from Ensembl (www.ensembl.org).

HHpred (www.toolkit.tuebingen.mpg.de) is a database for homology detection and structure prediction in between distantly related proteins by HMM-HMM comparison in *H. sapiens* and other species. Again, very high probability (> 90 %) for domain conservation of CI-M6PR and EPHA receptor but also of the tumor necrosis factor/tumor necrosis factor receptor superfamily is predicted (data not shown). Homology to domains of the EGFR superfamily and to INSR and IGF1R are also identified. Predicted domains of IGFR-L2 are highly similar to the ones for IGFR-L1 apart from differences in probability. However, especially similarities to Laminin are specific to IGFR-L1, whereas for IGFR-L2, rather homology to enzymes of lipid and saccharide metabolism is found.

To summarize, Igfr-L2 is an evolutionary highly conserved single-pass type I transmembrane protein and thus present at the cell surface and the membrane of different subcellular organelles. Apart from being a monomer, homo- and heterodimerization with its paralogue or other growth factor receptors could be accomplished via the receptor dimerization motif within the transmembrane helix. In its short cytoplasmic tail, binding motifs for COPI hint to trafficking within the ER-Golgi compartments, whereas endocytosis of Igfr-L2 from the PM is probably mediated by CME via Ap2 found in clathrin-coated vesicles. Post-translational modifications such as N-glycosylation, phosphorylation or ubiquitinylation may be important for the protein's function. Ultimately, the protein translated from gene *9330182L06Rik* has a extracellular CRD found in the Insr and the Igf1r as well as a M6PR binding domain found in the Igf2r. Analogous to Igfr-L1, EIG121L was re-named **Igf receptor-like 2 (Igfr-L2)**.

4.4.3 mRNA and protein expression of Igfr-L2 and IGFR-L2

To draw first conclusions on the physiological function of Igfr-L2, a search for mRNA expression was performed using the EMBL-EBI expression atlas (www.ebi.ac.uk). According to results of the RIKEN Fantom5 project, highest mRNA expression in transcripts per million (TPM) is detected within the central nervous system (Ø 50 TPM), especially in the pituitary gland, of adult mice (Figure 4.4.4.1a). Median expression levels are found in lung and adrenal gland (Ø 12 TPM), whereas in the gastrointestinal tract, sex-related tissues and other organs only low expression has been identified (< 5 TPM).
In human, both in the RIKEN Fantom5 and the genotype-tissue expression project, only low mRNA levels of IGFR-L2 have been found (< 15 PTM) for all analyzed samples (Figure 4.4.4.1b). Lung, pituitary gland, cerebellum, breast and subcutaneous adipose tissue show the highest expression values. In contrast, Igfr-L1 is highly expressed in almost all tissues especially in endocrine and exocrine cell types.

However, low mRNA levels do not conclusively result in low protein expression. According to proteomics DB (www.proteomicsdb.org), high levels of IGFR-L2 are found in colon and heart, medium ones in retina and brain including prefrontal and cerebral cortex and low ones in lung and placenta (Figure 4.4.4.1c). In the human protein atlas (www.proteinatlas.org), only data from cell lines is available, where IGFR-L2 is highly expressed in human lung tumor cells (SCLC-21H) and chronic myeloid leukemia cells (K-562) and localizes in the ER. Additionally, medium expression is found in cells derived from brain and female as well as male reproductive systems and renal/urinary cells.
Furthermore, analysis of whole tissue mRNA or protein does not reveal information regarding cell type-specific expression, which can be analyzed by IHC.

4.4.4 Association of IGFR-L2 with physiological traits and diseases

To further identify a role of IGFR-L2 in human physiology and disease, an association with single nucleotide polymorphisms (SNPs) within gene *KIAA1324L* was investigated using the Type 2 Diabetes Knowledge Portal (www.type2diabetesgenetics.org). Various genome-wide association studies (GWAS) or sequence analyses from different countries are available. The database suggests common variants, high impact variants and strongest associations of SNPs, whereas suggestive evidence for an association of a common variant with a phenotype is assumed for *P*-values<0.0005. The majority of SNPs is located in the intron between exon 1 and exon 2.
Regarding height, 4 common variants and 2 strongest associations are found in the Giant UK Biobank GWAS and 1 high-impact variant in the 13K exome sequence analysis which also identified 2 high impact variants associated with the body mass index (BMI) and 2 with waist circumference (Figure 4.4.4.2a). For the latter also a common variant is described in the GIANT GWAS: active men, Europeans.
In respect of T2DM, 8 common (70KforT2D GWAS) and 2 high impact variants (BioMe AMP T2D GWAS) as well as 9 strongest associations (ExTexT2D exome chip analysis) are reported (Figure 4.4.4.2b). Adjustment to the BMI results in 8 strongest associations (ExTexT2D exome chip analysis) and 1 common variant (AGEN GWAS). However, the chip analyses do not show significant *P*-values. Furthermore, 7 strongest associations are found for all diabetic kidney diseases (The Diabetic Kidney Diseases GWAS: subjects with T1D or T2D) and 9 by comparing end-stage renal disease ESRD vs no ESRD and 6 for ESRD vs ctrl (Figure 4.4.4.2c).

Thus, IGFR-L2 might be important in respect of growth and development of obesity (Yusuf et al., 2017). SNPs in the *IGFR-L2* gene were especially associated with T2DM in general and diabetic kidney disease including ESRD.
In contrast, SNPs in the *IGFR-L1* gene showed strong evidence for an association with low- and high-density lipoprotein cholesterol as well as BMI, height and coronary artery disease. Thus, the paralogue might be rather important for metabolism.

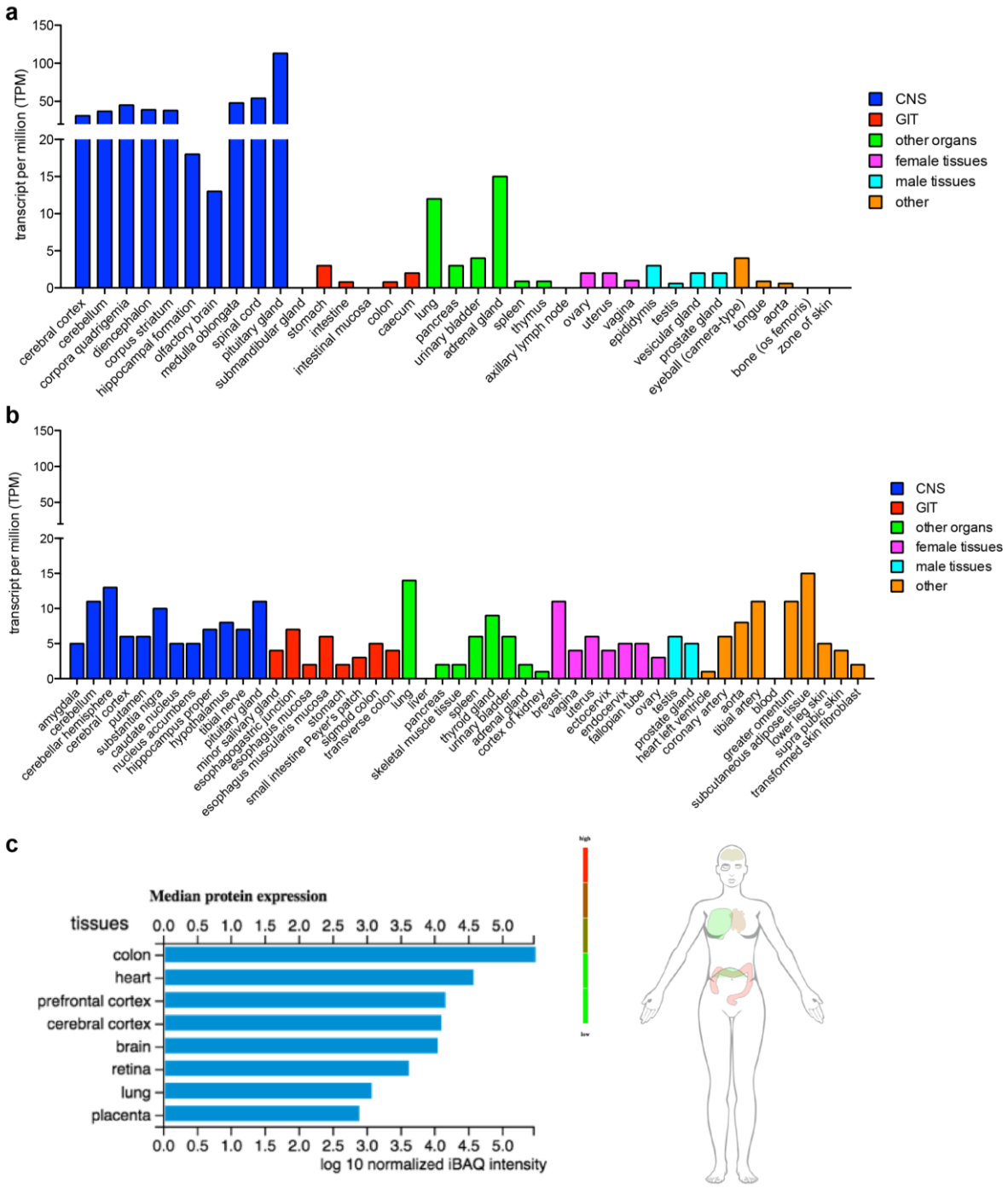

Figure 4.4.4.1 mRNA and protein expression of murine Igfr-L2 and human IGFR-L2

a-b, mRNA expression of murine Igfr-L2 (a) and human IGFR-L2 (b) in different tissues; RIKEN Fantom5 project, modified from EMBL-EBI expression atlas (www.ebi.ac.uk).

c, Protein expression of IGFR-L2 in human tissues (www.proteomicsdb.org).

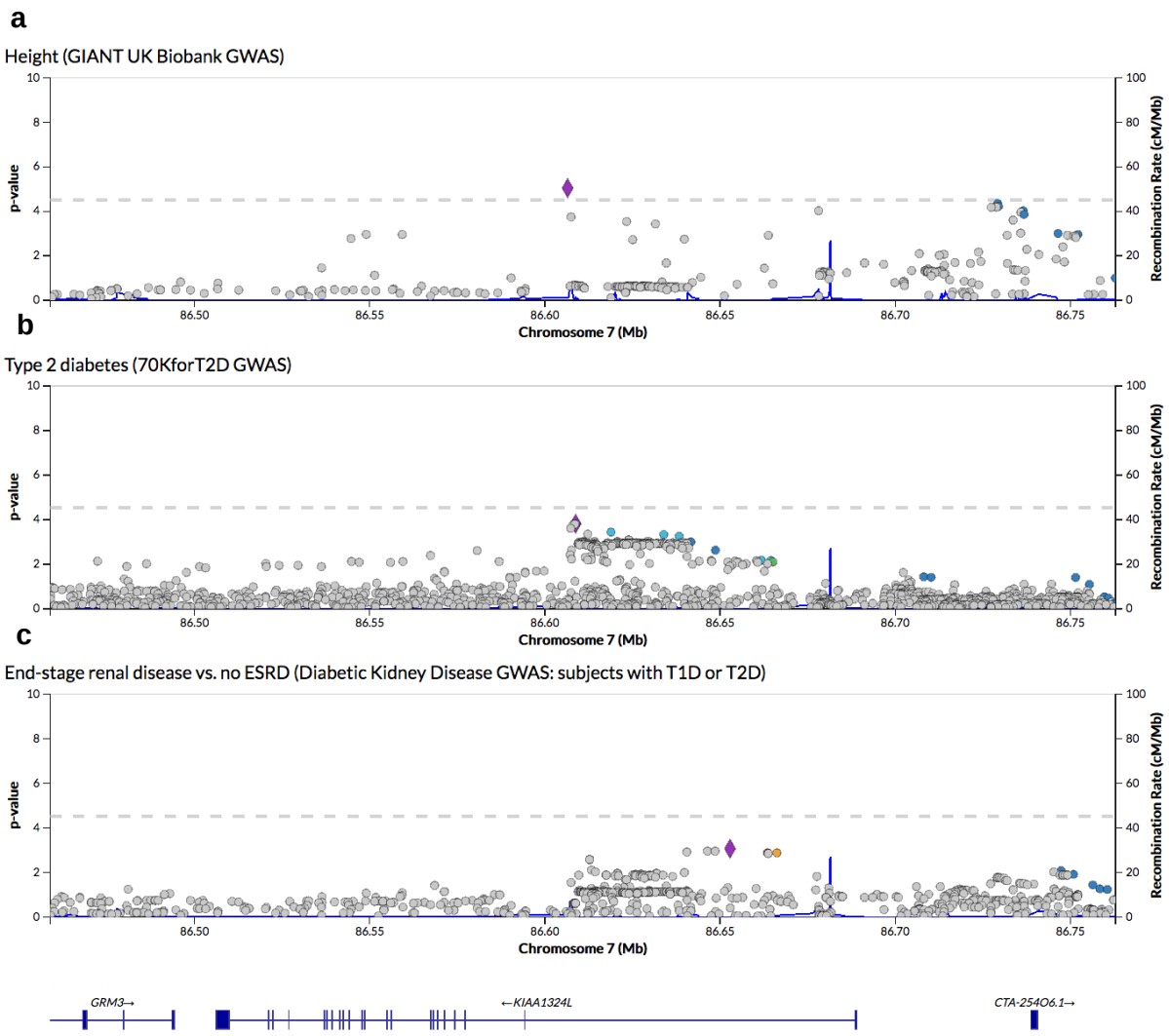

Figure 4.4.4.2 Association of SNPs in *IGFR-L2* with height, T2DM and ESRD

a-c, *P*-values for the association of SNPs in gene *KIAA1324L* with height (a), T2DM (b) and ESRD (c). (www.type2diabetesgenetics.org)

4.5 Igfr-L2 *in vitro* and *in vivo*

As bioinformatic analyses revealed only little information on the expression pattern of Igfr-L2 in *M. musculus*, antibodies were generated first to localize Igfr-L2 in different organs as well as subcellularly within the cells. This information could give hints onto the function of Igfr-L2 apart from the potential involvement in the Ins/Igf system due to the domain structure similarities to Insr, Igf1r and Igf2r. In addition, expression of Igfr-L2 was analyzed in comparison to its paralogue Igfr-L1.

4.5.1 Antibodies against IGFR-L2

Specific antibodies for protein visualization are a very useful and valuable tool. Therefore, antibodies against human IGFR-L2 were generated by Dr. Regina Feederle (monoclonal antibody core facility of the Helmholtz Zentrum, München) and in cooperation with Dr. Ünal Coskun and Dr. Michal Grzybek (Paul Langerhans Institute, TU Dresden). Protein recognition and specificity was confirmed in wildtype and Igfr-L2$^{-/-}$ Min6 cells (see 4.7.1) in immunocytochemistry (ICC). MCF7 or EndoC cells were used as human samples. On overview of all tested antibodies is given in Table 4.5.1.1.

Anti-cytoplasmic domain

First, mouse and rat monoclonal antibodies against the cytoplasmic tail of IGFR-L2 were generated by immunization with a peptide of 17 aa (ATKEKEDHFESVQLKTS). This primary sequence was 88 % identical to the murine one with only two different amino acids. Sequence identity to the paralogue IGFR-L1 was 53 %.
Of the 18 antibodies generated in mouse, only three were unable to detect Igfr-L2. As expected, none of the antibodies gave a signal in Igfr-L2$^{-/-}$ Min6 cells, however, human IGFR-L2 could not be detected in MCF7 (Figure 4.5.1.1a). Of the 35 antibodies produced in rat, a signal was only detected for two but again not for the human protein (Figure 4.5.1.1b). In IHC, mouse antibodies were not useful because the secondary antibodies gave a strong background, also in a sandwich with a subclass-specific secondary antibody. Rat antibodies did also not recognize Igfr-L2 on murine pancreas sections (data not shown).

Anti-extracellular domain

Second, rat monoclonal and rabbit polyclonal antibodies against the extracellular domain were generated by immunization with the recombinant ectodomain of IGFR-L2 purified in its native confirmation from HEK293T cells.
Of the 32 antibodies produced in rat, 19 recognized Igfr-L2 and IGFR-L2 (Figure 4.5.1.1c). Even though the human protein sequence was used for immunization, four antibodies were specific to the murine protein. Three antibodies showed cross-reactivity to Igfr-L1 due to the high conservation of the paralogues, i.e. the antibodies recognize the same epitope (Figure 4.5.1.1c). After the final bleed, both polyclonal rabbit antibodies detected Igfr-L2 and even stronger Igfr-L1 due to their high similarity (data not shown). Unfortunately, monoclonal antibody generation was not available for rabbit antibodies.

Table 4.5.1.1 Overview of antibodies against IGFR-L2

a-f, ID and predicted IgG subclass of 18 mouse anti-cytoplasmic-IGFR-L2 (a), 35 rat anti-cytoplasmic-IGFR-L2 (b), 32 rat anti-ectodomain-IGFR-L2 (c), 2 polyclonal rabbit anti-ectodomain-IGFR-L2, 67 rat anti-membranous-IGFR-L2 (e) and 6 mouse anti-membranous-IGFR-L2 (f).

a ID	IgG	ID	IgG	ID	IgG	ID	IgG	ID	IgG
25B12	2b	27A11	2a	27E8	2a	28E3	2a	31G7	2a
25F1	2b	27B2	2b	28A5	2a	28G11	2a	32C6	2b
26A11	2b	27B3	2b	28C10	2b	29G3	2b	32C6	2b
26B12	2a	27B4	G3	28D9	2b	31E9	2a		

b ID	IgG	ID	IgG	ID	IgG	ID	IgG	ID	IgG
1C10	2b	7F3	2c	12G7	G1	17E10	G1/2a	20B7	G1
1F6	G1	8A5	G1/2a	12H6	2a	17F12	G1	20E7	G1
1H7	2c	8F6	2c	13H2	G1/2a	18A4	G1	20F7	G1
2D7	2c	9C5	G1	15A8	2c	18A10	G1/2a/2c	23A5	2b
3B9	2b	11B11	G1	15E9	2a	18C8	G1	23E2	G1/2c
7B3	2c	11G4	G1	16F4	2a	18D11	2c	24B2	G1
7B8	G1	12D12	G1	17E5	G1/2c	19D6	G1	24C2	G1

c ID	IgG	ID	IgG	ID	IgG	ID	IgG	ID	IgG
1F4	G1	9D9	G1+2a	19G1	G1	3A9	2a	12G8	2a
1G6	2a	10A11	2a	20G6	2a	4D2	2a	18C9	2a
5H6	2a	11A6	2a	20H4	2a	9A2	2a	18F3	G1
6A4	2b	12D6	G1	21E6	2a	10B4	G1	20A10	G1
6C10	G1	15F8	G1	22B6	2c	10C9	G1	20E11	2a
7B11	2a	17E7	2a	23H1	2a	12C11	2a		
7D1	2a	18E3	2c			12D11	G1		

d ID	IgG
E43578	-
E43670	-

f ID	IgG	ID	IgG	ID	IgG
26C7	2a	26E6	2a	28H8	2a
26E5	2b	27F2	2b	31D4	2a

e ID	IgG	ID	IgG	ID	IgG	ID	IgG	ID	IgG
1D12	2c	14E5	2c	4H11	2c	9E12	2c	16H11	2c
2F3	2c	14E8	2c	5B9	2c	9G9	2c	17F4	2c
3B4	2a	18D5	2c	5D7	2c	9H10	2a	17H9	2c
3C8	G1	19E5	2a	5D9	2c	10A9	2c	18B10	2c
3H5	2c	19F9	2c	5D12	2b	10D10	2a	18C9	2c
5H11	2c			7B8	2c	11D10	2c	18G7	2c
6B1	2c			7D12	2a	11F7	2c	19D12	2c
6E8	2c			8D5	2c	12A11	2c	19G7	2c
6 h10	2c	1B11	2c	8D7	2c	13A12	2c	20B11	2c
7D7	2c	1F12	2c	8D12	2c	13E12	2c	20F7	2c
7D10	2c	3A7	2c	8G11	2c	13H6	2c	20G8	2a
7E11	2a	4C7	2c	9C11	2c	15A12	2c	21C11	2c
13E2	2c	4D4	2c	9E2	2c	15D9	2c	22A10	2a
13H8	2c	4F12	2c	9E10	2c	16B11	2c	22B12	2a

Anti-membranous extracellular domain

Third, rat and mouse monoclonal antibodies against the membranous ectodomain of IGFR-L2 were produced, which results in antibodies recognizing the functional conformation including glycosylation and interaction with membrane components.
Of the 67 rat and 6 mouse antibodies, a signal was only detected for one of the rat and four of the mouse, which were all specific to murine Igfr-L2 despite immunization with the human protein. This could imply that Igfr-L2 embedded in a membrane was not recognized as an antigen by the murine or rat immune system.
Interestingly, the two mouse antibodies 26C7 and 27F2 showed a distinct pattern of Igfr-L2 expression in Min6 as not all cells were stained equally seen for antibody 28H8 (Figure 4.5.1.1d). The antibodies might be specific to an epitope, which is only present in a subset of cells, e.g. Igfr-L2 single-positive Min6 cells. To exclude differences in glycosylation patterns between mouse and human, these antibodies were not only tested in MCF7 as immortalized human cell line but also on human pancreas sections as primary tissue. Nevertheless, all of the antibodies still specifically recognized murine Igfr-L2.

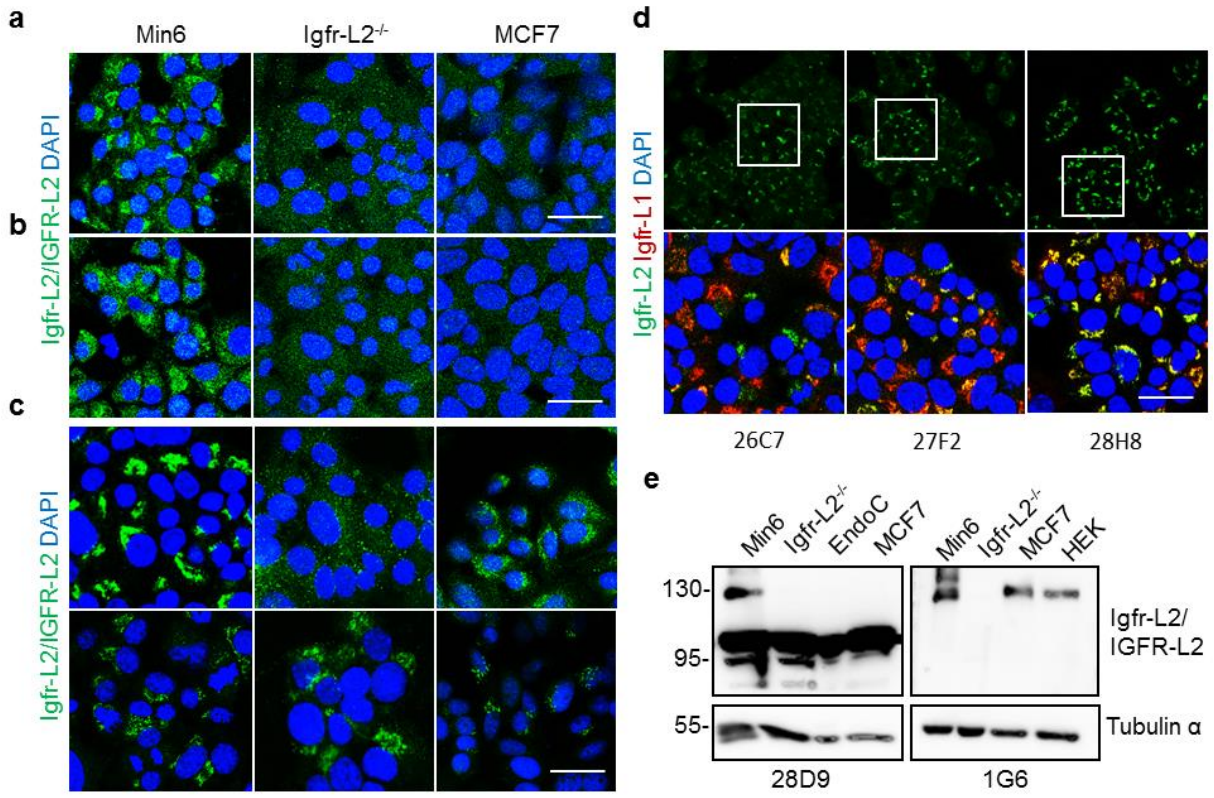

Figure 4.5.1.1 Validation of anti-IGFR-L2 antibodies

a-b, Detection of Igfr/IGFR-L2 (green) with mouse (a, 27E8) and rat (b, 7F3) anti-cytoplasmic-IGFR-L2 in wildtype and Igfr-L2$^{-/-}$ Min6 cells and MCF7. Scale bar, 25 µm.

c, Detection of Igfr/IGFR-L2 (green) with rat anti-ectodomain-IGFR-L2 in wildtype and Igfr-L2$^{-/-}$ Min6 cells and MCF7. Upper panel, 9D9 recognizing mouse Igfr-L2 and human IGFR-L2; lower panel, 5H6 recognizing mouse Igfr-L2 and human IGFR-L2 with cross-reactivity to Igfr-L1. Scale bar, 25 µm.

d, Detection of Igfr-L2 (green) and Igfr-L1 (red) in wildtype Min6 cells with 3 different mouse anti-membranous-IGFR-L2. 26C7, 27F2, distinct expression pattern. Scale bar, 25 µm.

e, Western Blot for the detection of Igfr-L2 and IGFR-L2 in lysates of wildtype and Igfr-L2$^{-/-}$ Min6, EndoC, MCF7 or HEK cells with a mouse anti-cytoplasmic-IGFR-L2 (28D9) and a rat anti-ectodomain-IGFR-L2 (1G6).

Western Blot

In WB, lysate of Igfr-L2$^{-/-}$ revealed that the denatured protein runs at 130 kDa instead of 110 kDa, which is the predicted size calculated from the primary sequence (Figure 4.5.1.1e). The same pattern was observed for Igfr-L1 and is due to post-translational modifications e.g. glycosylation. Mouse anti-cytoplasmic-IGFR-L2 showed a very strong unspecific band at 110 kDa, which could still be detected in Igfr-L2$^{-/-}$ and in human samples where the antibody was unable to detect IGFR-L2 in ICC. Antibodies generated against the membranous ectodomain in their native conformation were not tested in WB as their lysis and denaturation might destroy the epitopes that can be a combination of protein and membrane.

Furthermore, three commercial rabbit anti-IGFR-L2 antibodies (PA5-24451/60738/67405) were obtained and validated in respect of their expression pattern and on Igfr-L2$^{-/-}$ samples. Unfortunately, all antibodies gave a strong unspecific cytoplasmic staining, while in WB, also only unspecific bands could be detected (data not shown).

To sum up, mouse antibodies against the cytoplasmic tail of IGFR-L2 strongly recognized the murine protein and could be used for ICC and WB. Lots of rat antibodies against the ectodomain of IGFR-L2 recognized the murine and human protein in ICC, IHC and WB. Thus, subcellular localization and expression of Igfr-L2 could be further analyzed *in vitro* and *in vivo*.

4.5.2 Subcellular localization of Igfr-L2 and IGFR-L2

Validation of the antibodies revealed a strong expression of Igfr-L2 in the perinuclear region *in vitro*. To further define this subcellular localization, co-stainings with markers for different organelles and compartments were performed in wildtype and Igfr-L1$^{-/-}$ Min6 cells under growth conditions (Figure 4.5.2.1a-b). Igfr-L2 localized mainly in the ER-Golgi (Ergic, GM130, Golgb1, TGN46) but could also be detected in COP vesicles (CM1), early and late endosomes (Eea1, Rab7) and lysosomes (Lamp2) with no obvious difference in Igfr-L1$^{-/-}$.
By using rat anti-ectodomain-IGFR-L2 antibodies, expression of IGFR-L2 could also be confirmed in the human β-cell line EndoC (Figure 4.5.2.1c). Both IGFR-L2 and IGFR-L1 were present in the same subcellular compartments and co-localized mainly in the ER-Golgi (ERGIC, GOLGB1, TGN46) and not as much in endosomes (EEA1, RAB7). This suggests that Igfr-L2 is trafficking inside the cells between the PM, ER-Golgi and endosomal lysosomal compartments similar to Igf2r.

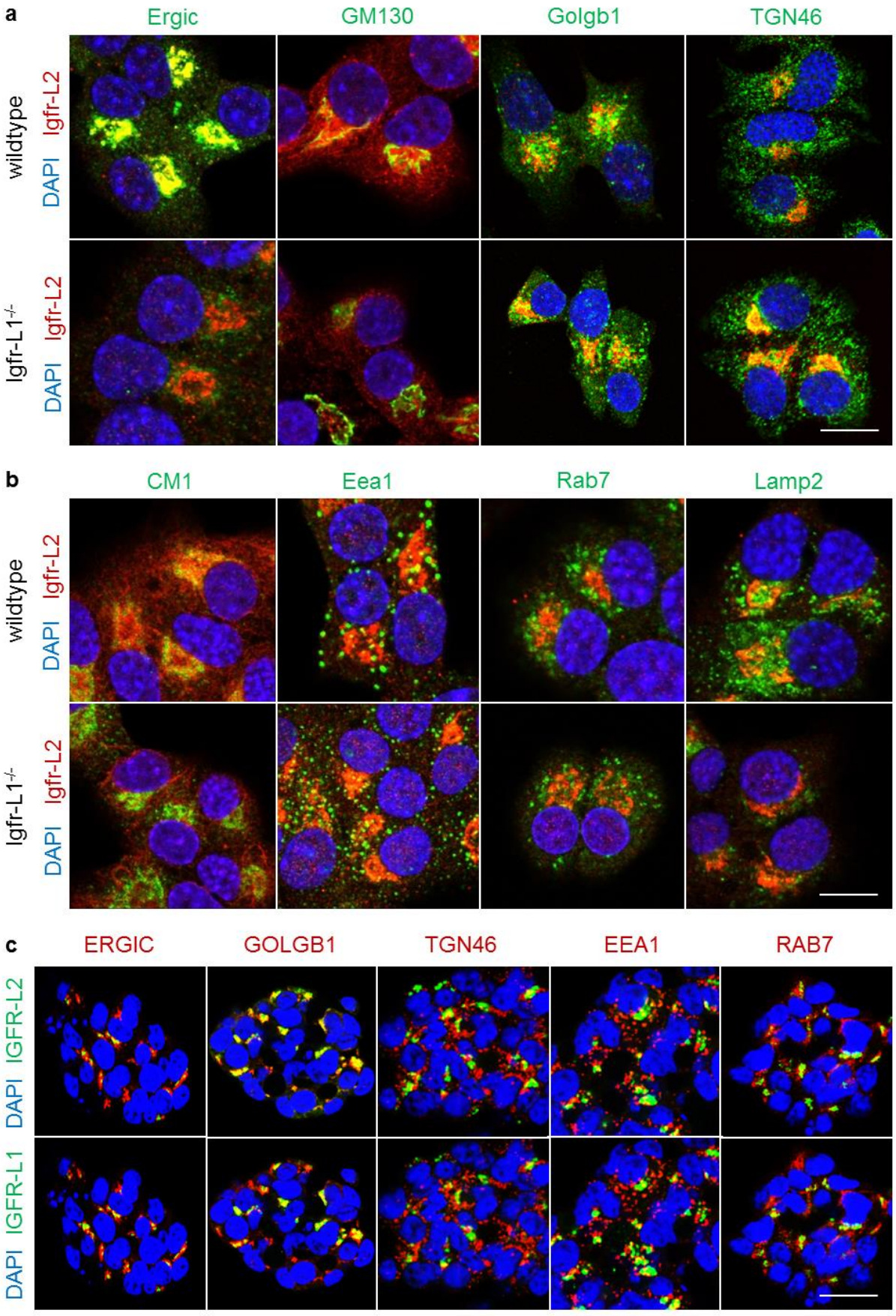
a
Ergic
GM130
Golgb1
TGN46
wildtype
Igfr-L2
DAPI
Igfr-L1-/-
Igfr-L2
DAPI
b
CM1
Eea1
Rab7
Lamp2
wildtype
Igfr-L2
DAPI
Igfr-L1-/-
Igfr-L2
DAPI
c
ERGIC
GOLGB1
TGN46
EEA1
RAB7
IGFR-L2
DAPI
IGFR-L1
DAPI

Figure 4.5.2.1 Subcellular localization of Igfr-L2 and IGFR-L2

a-b, LSM images for the co-localization of Igfr-L2 (red) with subcellular markers for ER-Golgi (a, green) and endosomal-lysosomal trafficking (b, green) compartments in wildtype and Igfr-L1$^{-/-}$ Min6 cells (upper and lower panel, respectively). Scale bar, 10 µm.

c, LSM images for the co-localization of IGFR-L2 and IGFR-L1 (green, upper and lower panel, respectively) with ER-Golgi and endosomal markers (red) in EndoC. Scale bar, 25 µm.

4.5.3 Expression of Igfr-L2 and IGFR-L2 *in vivo*

As little is known about the expression of Igfr-L2 in *M. musculus*, an initial real time polymerase chain reaction (RT-PCR) was performed by Dr. Silvia Schirge. *Igfr-L2* mRNA was strongly detected in pituitary, ovaries and brain similar to the database information (Figure 4.5.3.1a). For protein expression, different organs were isolated from Igfr-L2$^{+/+}$ and Igfr-L2$^{-/-}$ ΔEx6 animals (see 4.6.1) and analyzed by WB. High expression of Igfr-L2 (130 kDa) could be found in the brain and lung but also in the stomach and duodenum of hypomorphic animals (Figure 4.5.3.1b). Additionally, Igfr-L1 was found to be highly expressed in lung, pancreas, stomach and duodenum as well as in the brain, with no alterations due to a lack of Igfr-L2 apart from the lung and the pancreas (Figure 4.5.3.1c).
It was anticipated that Igfr-L2 is expressed in β-cells *in vivo* as it was identified in immortalized β-cells *in vitro.* No band for Igfr-L2 was detected in pancreas lysate, whereas the islets of Langerhans only make up a minor portion of the whole organ. Indeed, Igfr-L2 and also Igfr-L1 were detected in isolated islets at different ages (Figure 4.5.3.1d).

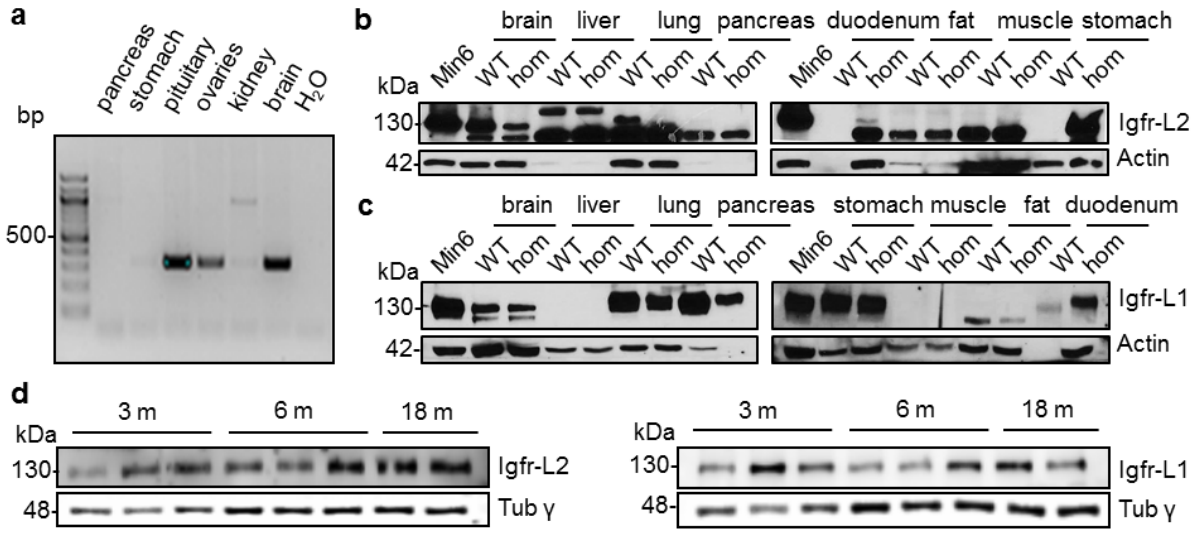

Figure 4.5.3.1 Expression of Igfr-L2 in different organs

a, RT-PCR for the expression of *Igfr-L2* in different organs (Dr. Silvia Schirge).

b-c, Detection of Igfr-L2 (b) and Igfr-L1 (c) in lysates of different organs of Igfr-L2$^{+/+}$ and Igfr-L2$^{-/-}$ ΔEx6 animals. Wildtype Min6 served as control.

d, Detection of Igfr-L2 (left panel) and Igfr-L1 (right panel) in isolated islets at different ages.

To further investigate the expression of Igfr-L2 in islets, validated antibodies were used on murine and human pancreas sections or isolated islets. Igfr-L2 was expressed specifically in all endocrine cells in the embryonic and adult pancreas, whereas Igfr-L1 could also be found in exocrine cells (Figure 4.5.3.2a). In adult, Igfr-L2 was found in mature β-cells marked by urocortin3 (Ucn3) but also in non-β-cells. In human, IGFR-L2 was also weakly detected in endocrine cells of isolated islets and pancreata of healthy donors, whereas IGFR-L1 was

strongly expressed (Figure 4.5.3.2b-c). Interestingly, IGFR-L2 was found in cells outside of the islets of Langerhans hinting to a potential different function in the human pancreas despite the high evolutionary conservation. The identity of those cells has to be investigated.
Additionally, expression of Igfr-L2 was analyzed in the pituitary where mRNA levels were found to be high. Again, Igfr-L2 was broadly expressed but could strongly and almost exclusively be detected in the anterior pituitary, i.e. endocrine cells, similar to the pancreas (Figure 4.5.3.2d). To identify a physiological function of Igfr-L2, its expression in a specific subtype of endocrine cells was analyzed by hormone co-staining. Co-expression was detected for growth hormone (Gh) and adrenal corticotropic hormone (ACTH), while analysis by fluorescence-activated cell sorting (FACS) would provide single cell resolution.

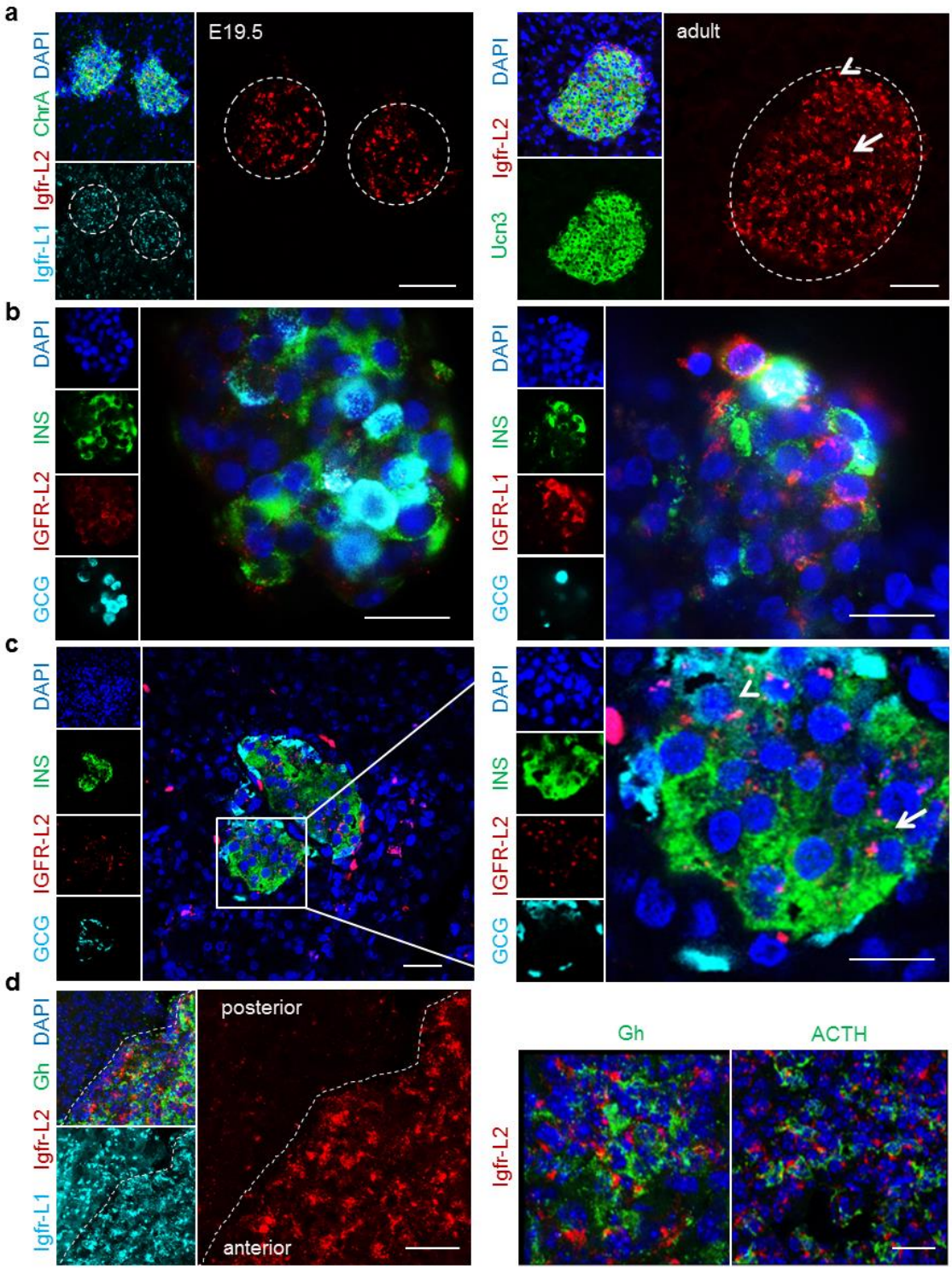

Figure 4.5.3.2 Expression of Igfr-L2 in pituitary and pancreas

a, Representative LSM images of the expression of Igfr-L2 (red) in the embryonic (E19.5) and adult endocrine pancreas marked by ChrA or Ucn3 (green), respectively. Left, expression of Igfr-L1 (cyan) in endocrine and exocrine cells; right, arrow, β-cell; arrowhead, non-β-cell; Scale bar, 50 µm.

b-c, Representative LSM images of the expression of IGFR-L2 or IGFR-L1 (red) in human endocrine cells of isolated islets (b) and pancreata (c) marked by INS (green, arrow) and GCG (cyan, arrowhead). Scale bar, 25 µm.

d, Representative LSM images of the expression of Igfr-L2 (red) in the anterior pituitary together with Gh and ACTH (green). Left, expression of Igfr-L1 (cyan) in the anterior and posterior pituitary. Scale bar, 50 µm.

4.5.4 Heterogeneous expression of the paralogues

Interestingly, co-stainings of Igfr-L2 with its paralogue Igfr-L1 revealed a heterogeneous expression pattern *in vitro* and *in vivo* (Figure 4.5.4.1a-b). Both proteins are co-expressed in the majority of cells with a general variation in expression levels but a minor portion with mostly only one or the other can be found. This suggests a different function of the paralogues in β-cells and other endocrine subtypes and needs to be further investigated e.g. in respect of proliferation or maturation markers or functionality.

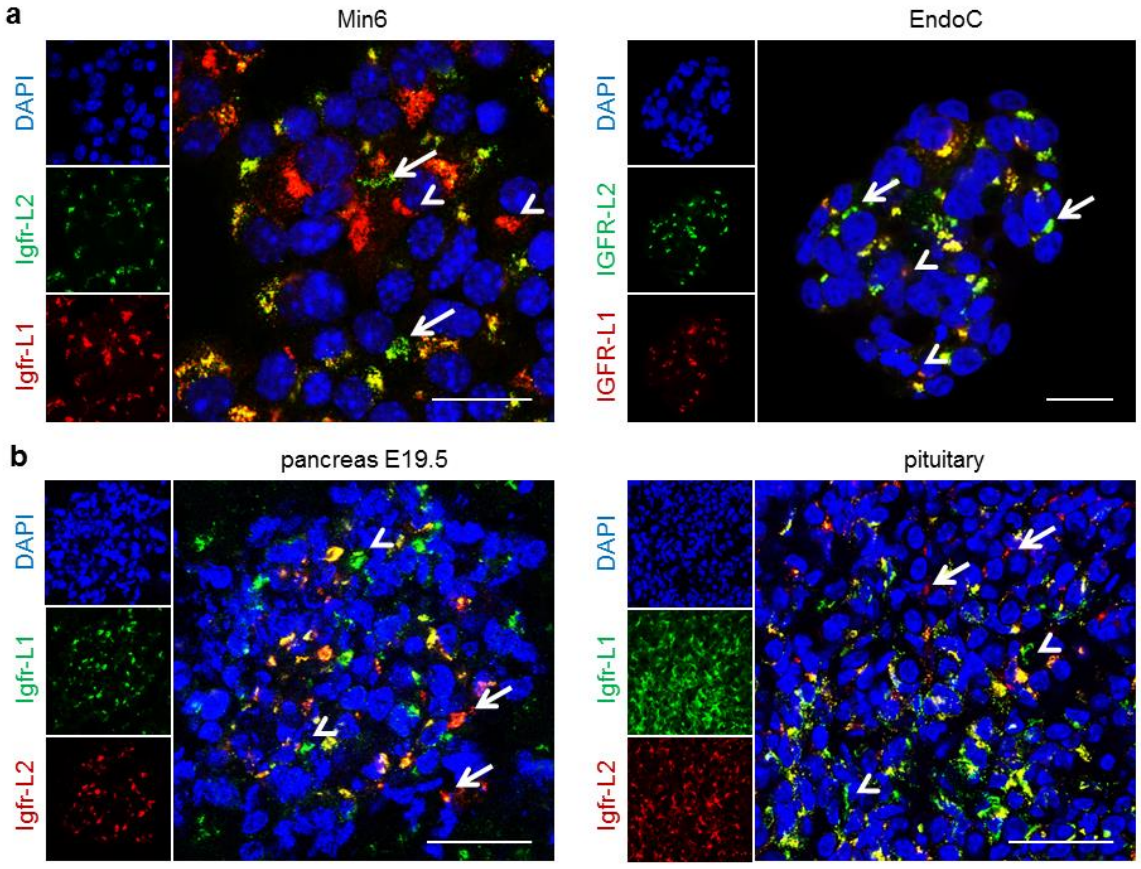

Figure 4.5.4.1 Heterogeneous expression of Igfr/IGFR-L2 and Igfr/IGFR-L1

a, Representative LSM images of the expression of Igfr/IGFR-L2 (green) and Igfr/IGFR-L1 (red) in β-cell lines. Scale bar, 25 µm.

b, Representative LSM images of the expression of Igfr-L2 (red) and Igfr-L1 (green) in the islets of Langerhans at E19.5 and in the pituitary. Scale bar, 50 µm.

Arrows hint to Igfr-L2 and arrowheads to Igfr-L1 single-positive cells.

Furthermore, absolute expression of Igfr-L1 and Igfr-L2 as well as Insr was determined by using recombinant proteins as standard (data not shown). Igfr-L1 was highest expressed in Min6, i.e. approximately twice as high as Igfr-L2 and 4 times as high as Insr. This suggests an important role of the paralogues in β-cells.

4.5.5 Heterodimerization of the paralogues

In cells that express both Igfr-L1 and Igfr-L2, heterodimerization was observed. Immunoprecipitation of Igfr-L1 and analysis of the eluates by HPLC-MS revealed a strong interaction with the paralogue Igfr-L2, which was dependent on the metabolic state of the cells (see 4.3.2, Table 4.5.5.1). Under growth conditions, the ratio of detected Igfr-L1 to Igfr-L2 was approximately 1:2-1:4 and decreased under starvation conditions to 1:10–1:40. Similarly, glucose and insulin stimulation resulted in an increase of the ratio Igfr-L1 to Igfr-L2 from 1:40 during starvation to 1:12-1:10. In summary, Igfr-L1 rather interacts with Igfr-L2 in metabolically active cells.

Table 4.5.5.1 Heterodimerization of Igfr-L1 and Igfr-L2 (HPLC-MS)

Indication of changes in approximate ratios (arrows) between co-immunoprecipitated Igfr-L1 and Igfr-L2 under starvation and stimulation.

antibody		growth conditions	15’ starvation
anti-intracellular IGFR-L1	Igfr-L1	457 → 1:2	3188 → 1:10
	Igfr-L2	237	387
anti-extracellular IGFR-L1	Igfr-L1	477 → 1:4	1985 → 1:40
	Igfr-L2	127	54

		18 h starvation	glucose stimulation	insulin stimulation
anti-extracellular IGFR-L1	Igfr-L1	7437 → 1:40	2745 → 1:10	2593 → 1:12
	Igfr-L2	192	287	206

In order to validate the strong interaction between Igfr-L1 and Igfr-L2, co-IPs were performed *vice versa* under growth conditions (Figure 4.5.5.1a). Antibodies were used in three different dilutions and the non-immunoprecipitated supernatant (SN) was analyzed as well, while Igfr-L1$^{-/-}$ Min6 cells served as control for antibody specificity. Both Igfr-L1 and Igr-L2 were detected when only one or the other was immunoprecipitated confirming their potential direct interaction. Also during *in vitro* KO generation (see 4.7.1), potential homo- and heterodimerization was observed. Monomers ran at 130 kDa and dimers above 250 kDa. Both homo- and heterodimers could be detected in wildtype cells, homodimers of Igfr-L1 in Igfr-L2$^{-/-}$ and of Igfr-L1 in Igfr-L2$^{-/-}$ Min6 cells and none in the Igfr-L1$^{-/-}$+L2$^{-/-}$ double KO (Figure 4.5.5.1b). Using the PLA, potential heterodimers of Igfr-L1 and Igfr-L2 were also visualized inside the cells (Figure 4.5.5.1c)

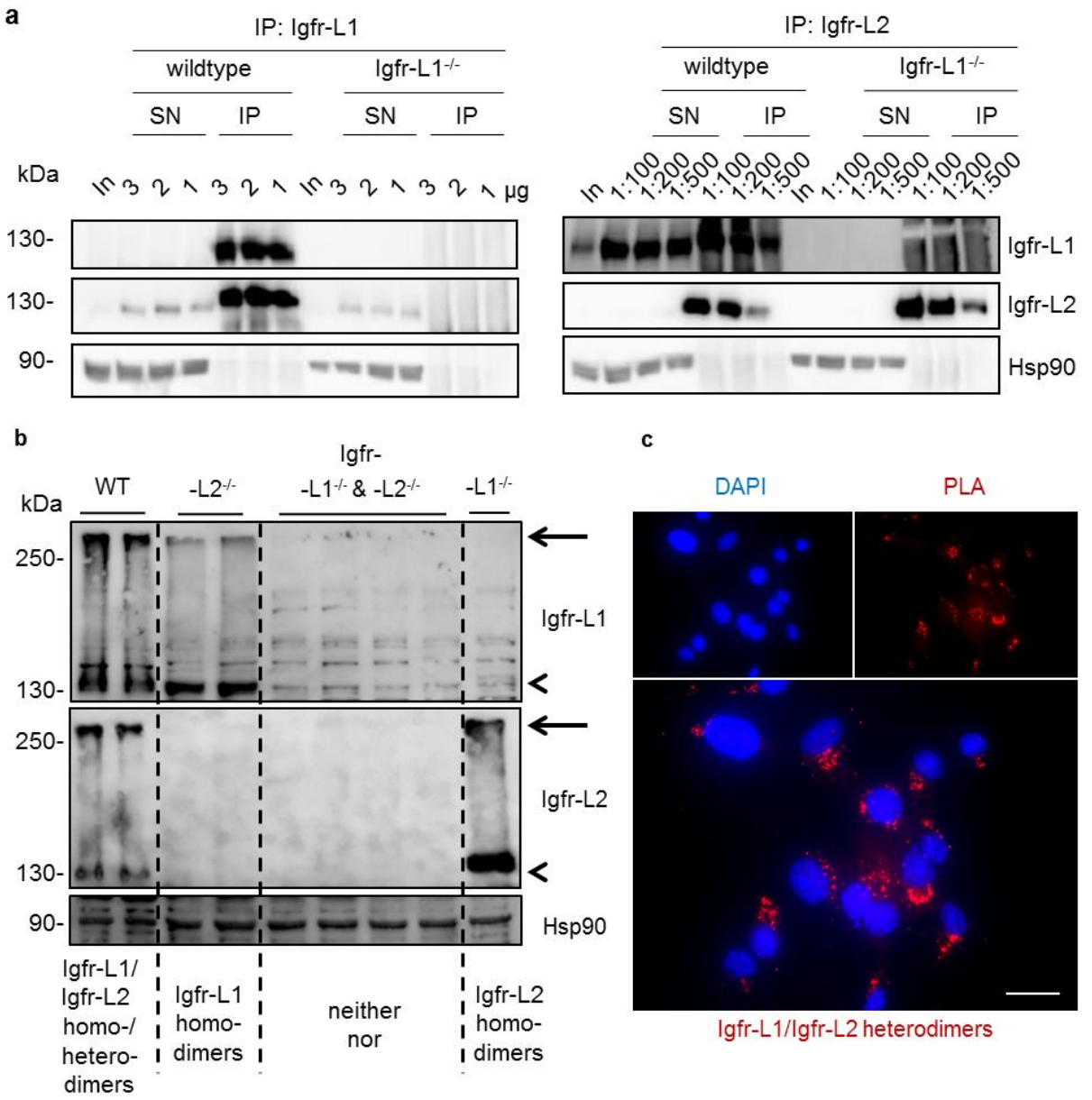

Figure 4.5.5.1 Heterodimerization of Igfr-L1 and Igfr-L2

a, Detection of Igfr-L1 and Igfr-L2 after co-IP with different concentrations of antibodies either against Igfr-L1 (left panel) or Igfr-L2 (right panel) in wildtype and Igfr-L1$^{-/-}$ Min6 cells.

b, Detection of Igfr-L1 and Igfr-L2 in wildtype, Igfr-L1$^{-/-}$, Igfr-L2$^{-/-}$ and Igfr-L1$^{-/-}$+L2$^{-/-}$ Min6 cells. Monomers run at 130 kDa (arrowheads), homo- or heterodimers at above 250 kDa (arrows).

c, Detection of potential Igfr-L1/Igfr-L2 heterodimers (red) by PLA. Scale bar, 25 µm.

In conclusion, Igfr-L2 is a novel endocrine marker as it can be specifically found in the islets of Langerhans and the anterior pituitary where it is mostly expressed in the ER-Golgi region. Thus, Igfr-L2 could function in systemic hormonal regulation via the HPG axis as its mRNA was also detected in ovaries.

The heterodimerization with its paralogue Igfr-L1 has to be defined in double KO cells and animals in respect of synergistic or compensatory effects. Heterogeneous expression could hint to a different cellular function of both proteins and needs to be investigated on the single cell level. Thus, Igfr-L1 and Igfr-L2 are not only similar to Insr and Igf1r regarding gene and protein structure but also functionally by forming homo- and heterodimers.

4.6 Analysis of Igfr-L2$^{-/-}$ *in vivo*

Expression analysis with the generated antibodies showed that Igfr-L2 is a novel endocrine marker and suggested a role in systemic hormonal regulation. So far, Igfr-L2 has neither been described in mouse nor in human. In *X. laevis,* lack of Igfr-L2 led to developmental defects via regulation of BMP signaling. In order to shed light on its biological function *in vivo*, full-body KO mice were generated.

4.6.1 Targeting strategy for Igfr-L2$^{-/-}$

Analogously to Igfr-L1, the Cre-loxP recombination system was used to generate KO animals together with Dr. Silvia Schirge. Therefore, mice heterozygous for the *9330182L06Rik* gene trap allele were obtained from EUCOMM (Figure 4.6.1.1, for explanation of the different alleles see 4.1.1).

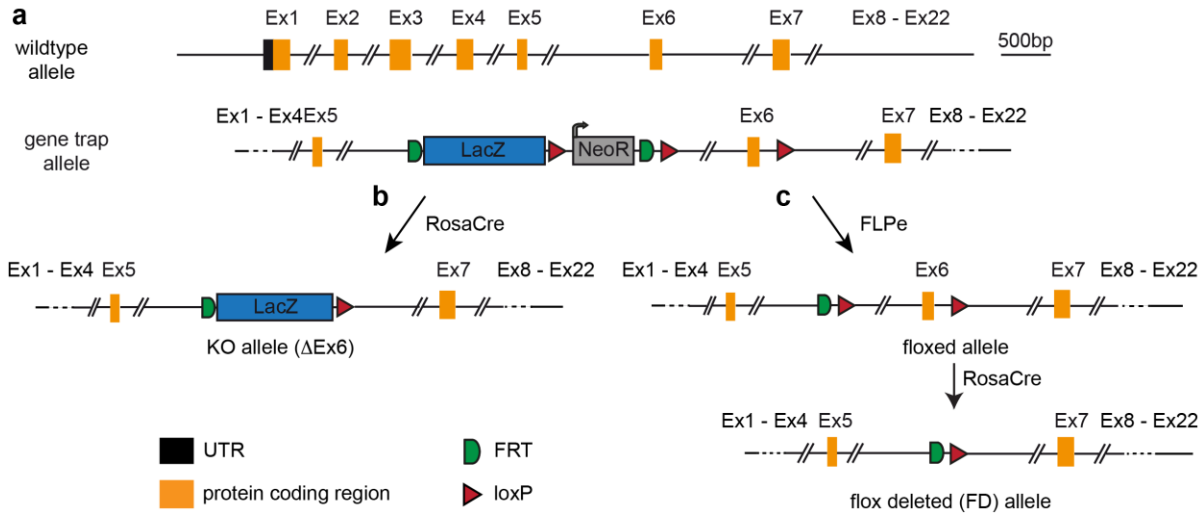

Figure 4.6.1.1 Targeting of gene *9330182L06Rik* to obtain Igfr-L2$^{-/-}$ animals

Schematic representation of the three alleles used for generation of Igfr-L2$^{-/-}$, i.e. gene trap (a), ΔEx6 (b) or flox-deleted (c).

a, Gene trap allele with the LacZ reporter and NeoR cassette as well as loxP and FRT sites for potential recombination in comparison to the wildtype allele.

b, KO allele (ΔEx6) with the LacZ reporter and NeoR cassette after recombination of loxP sites in the gene trap allele with Rosa-Cre.

c, flox-deleted (FD) allele after recombination of loxP sites in the floxed allele with Rosa-Cre recombinase. The floxed allele was obtained by excision of the LacZ reporter and NeoR cassette by recombination of FRT sites in the gene trap allele with FLPe.

Because the gene trap allele did not result in a null mutant, ΔEx6 animals were generated (Figure 4.6.1.1a-b). Analysis of brain lysate of Igfr-L2$^{+/+}$ and Igfr-L2$^{-/-(\Delta Ex6)}$ animals together with Min6 revealed hypomorphic expression with reduced levels of Igfr-L2 probably due to alternative splicing via the LacZ cassette (Figure 4.6.1.2a). Thus, animals with the FD allele were generated and lack of Igfr-L2 was confirmed by WB (Figure 4.6.1.2b) and IHC (Figure 4.6.2.2).

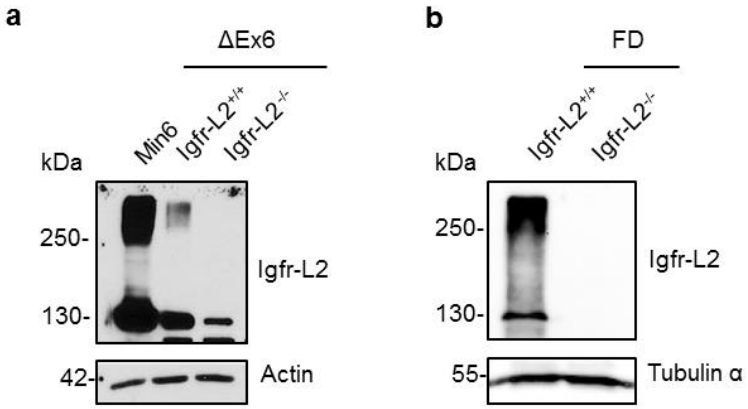

Figure 4.6.1.2 Confirmation of Igfr-L2$^{-/-}$

a, ΔEx6; Detection of Igfr-L2 in Min6 and brain lysate of Igfr-L2$^{+/+}$ and Igfr-L2$^{-/-}$ (ΔEx6) animals.

b, FD; Detection of Igfr-L2 in pituitary lysate of Igfr-L2$^{+/+}$ and Igfr-L2$^{-/-}$ (FD) animals.

4.6.2 Biological function of Igfr-L2

In order to generate animals for analysis, matings of Igfr-L2$^{+/+}$ (wt) or Igfr-L2$^{-/-}$ (hom) were set up to avoid Igfr-L2$^{+/-}$ (het) offspring. As a first observation, Igfr-L2$^{-/-}$ mice were viable and healthy. Compared to Igfr-L1$^{-/-}$, lack of Igfr-L2 was not lethal or affecting development as described for *X. laevis*. Nevertheless, crossing of female x male hom x hom compared to wt x wt, het x het, het x hom, hom x het, Bl6 x het and Bl6 x hom resulted in a significantly smaller litter size, i.e. Ø 7 versus 4 neonates (Figure 4.6.2.1a). Additionally, around 25 % of the offspring was missing at weaning age, whereas the frequency of pregnancies was unchanged (Figure 4.6.2.1b-d).

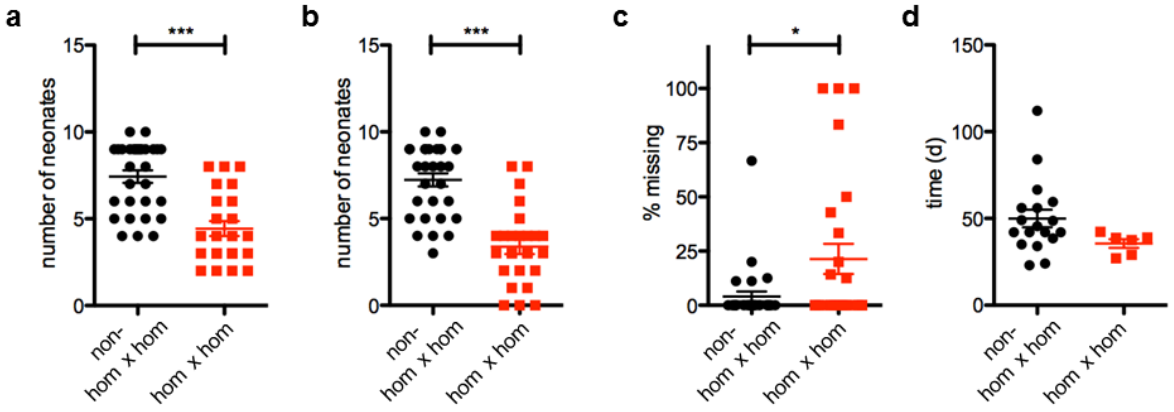

Figure 4.6.2.1 Postnatal lethality of Igfr-L2$^{-/-}$ offspring

a-c, Number of neonates obtained from non-hom x hom and hom x hom intercrosses at birth (a) and at weaning (b) with calculation of missing animals (c).
a, ***, P<0.0001, non-hom x hom, n=30; hom x hom, n=23;
b, ***, P<0.0001, non-hom x hom, n=30; hom x hom, n=26;
c, *, P=0.0152, non-hom x hom, n=30; hom x hom, n=26.

d, Number of pregnancies per mating duration.
n.s., P=0.1223, non-hom x hom, n=18; hom x hom, n=6.

Error bars represent SEM and *, P<0.05; **, P<0.01; ***, P<0.001. P-values were calculated using a two-tailed, unpaired student's t-test.

In conclusion, fertility of Igfr-L2$^{-/-}$ animals was not impaired but expression of Igfr-L2 appeared to be crucial in both parents to ensure embryonic development and postnatal survival of offspring hinting to a dysregulation in the HPG axis.

To identify effects of Igfr-L2 loss in endocrine cells, where it is specifically expressed, the anterior pituitary and islets of Langerhans were looked at in IHC confirming Igfr-L2$^{-/-}$ (Figure 4.6.2.2). No obvious morphological changes or alterations in hormone expression were observed. In the pituitary, Gh and ACTH were similarly expressed, while absolute amounts would need to be quantified by WB or enzyme-linked immunosorbent assay (ELISA) (Figure 4.6.2.2a). Within islets, composition in respect of α- and β-cells was not obviously changed (Figure 4.6.2.2b) and maturation was accomplished (data not shown).

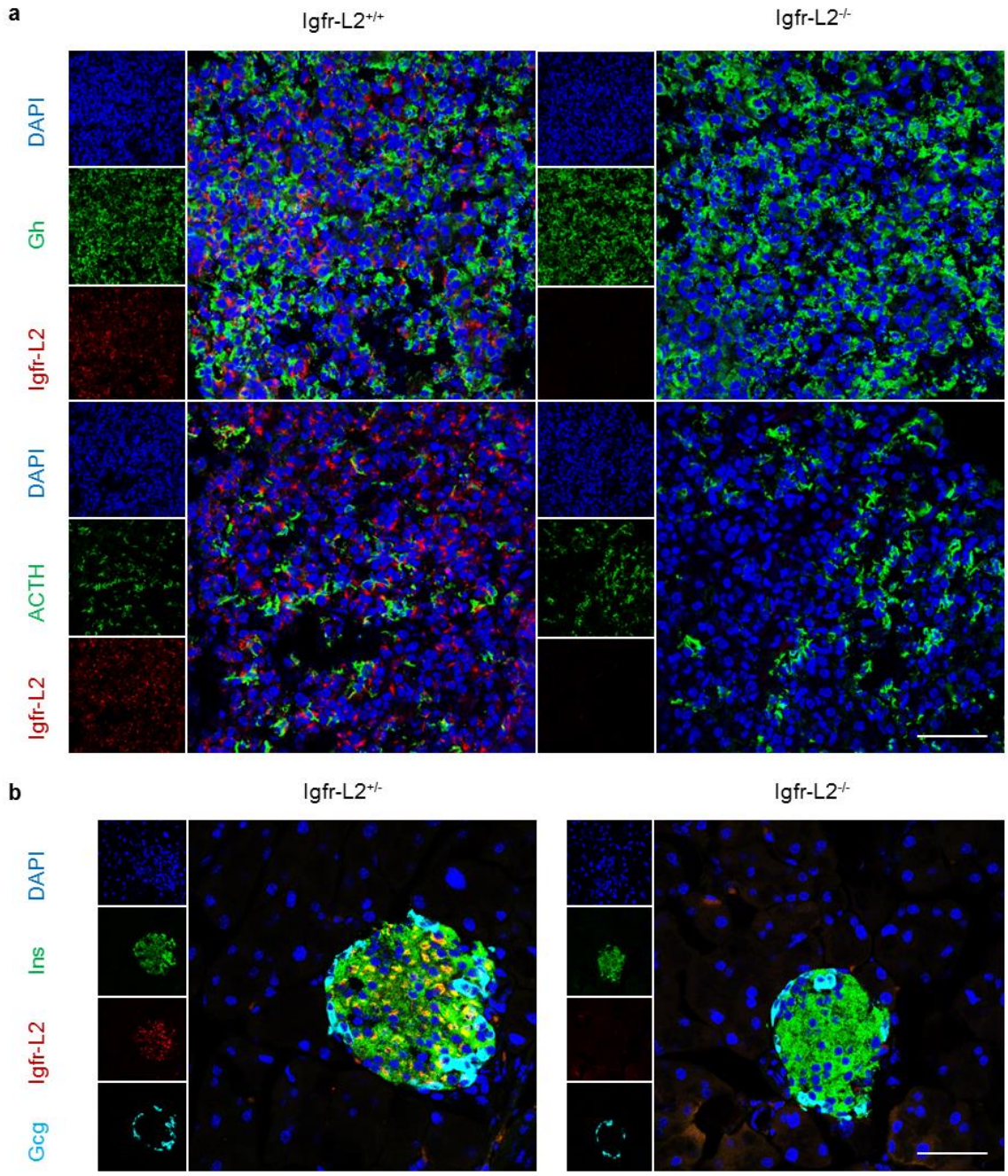

Figure 4.6.2.2 Analysis of Igfr-L2$^{-/-}$ in endocrine cells

a, Representative LSM images of the detection of Igfr-L2 (red) in the anterior pituitary of Igfr-L2$^{+/+}$ and Igfr-L2$^{-/-}$ animals together with Gh (upper panel, green) and ACTH (lower panel, green). Scale bar, 50 µm.

b, Representative LSM images of the detection of Igfr-L2 (red) in pancreatic islets of Igfr-L2$^{+/-}$ and Igfr-L2$^{-/-}$ animals together with insulin (green) and glucagon (cyan). Scale bar, 50 µm.

In order to identify any functional differences in the endocrine pancreas due to deletion of Igfr-L2, the response to an intraperitoneal glucose administration (2 g/kg BW) was analyzed in 8 m old Igfr-L2$^{+/+}$ and Igfr-L2$^{-/-}$ animals. After a 6 h morning fast, body weight and basal glucose levels were not significantly different in males or females (Figure 4.6.2.3a-d). Also upon glucose challenge, Igfr-L2$^{-/-}$ mice did not differ from Igfr-L2$^{+/+}$ (Figure 4.6.2.3e-f) hinting to compensation by Igfr-L1.

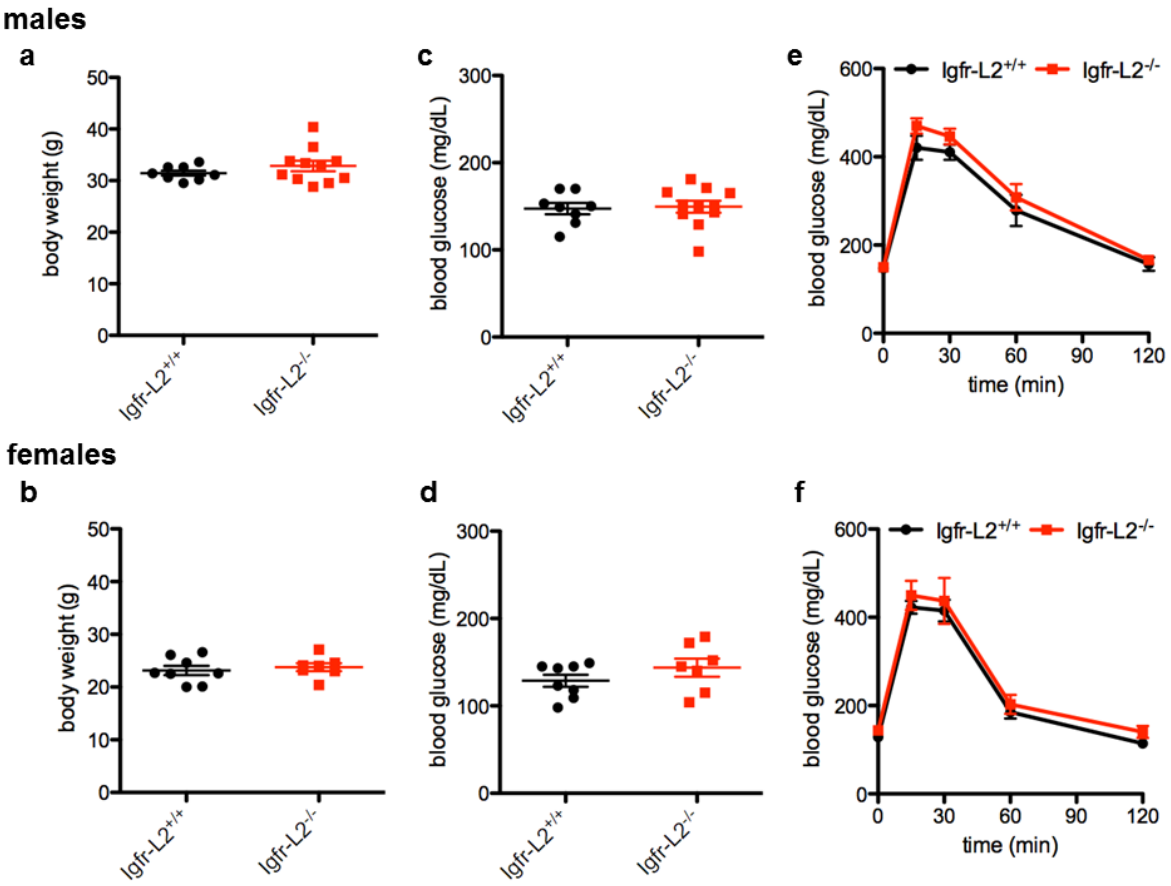

Figure 4.6.2.3 GTT with Igfr-L2$^{-/-}$ animals at 8m

a-b, Body weight of males (a) and females (b).
- a, n.s., *P*=0.2926; Igfr-L2$^{+/+}$, n=8; Igfr-L2$^{-/-}$, n=11;
- b, n.s., *P*=0.6060; Igfr-L2$^{+/+}$, n=8; Igfr-L2$^{-/-}$, n=7.

c-d, 6h fasting blood glucose levels of males (c) and females (d).
- c, n.s., *P*=0.8276; Igfr-L2$^{+/+}$, n=8; Igfr-L2$^{-/-}$, n=11;
- d, n.s., *P*=0.2354; Igfr-L2$^{+/+}$, n=8; Igfr-L2$^{-/-}$, n=7.

e-f, Blood glucose levels during an ipGTT in males (e) and females (f).
- e, n.s., *P*=0.2615; Igfr-L2$^{+/+}$, n=8; Igfr-L2$^{-/-}$, n=11;
- f, n.s., *P*=0.3372; Igfr-L2$^{+/+}$, n=8; Igfr-L2$^{-/-}$, n=7.

Error bars represent SEM and *, *P*<0.05; **, *P*<0.01; ***, *P*<0.001. a-d, *P*-values were calculated using a two-tailed, unpaired student's t-test. e-f, *P*-values were analyzed using a 2way-ANOVA with Bonferroni post-test.

4.7 Igfr-L2$^{-/-}$ and Igfr-L1$^{-/-}$; Igfr-L2$^{-/-}$ *in vitro*

In vivo analysis showed that Igfr-L2 is a novel endocrine marker, whereas its deletion had no effect on glucose tolerance. In order to shed light on the molecular function of Igfr-L2 specifically in β-cells, Igfr-L2$^{-/-}$ Min6 cells were generated *in vitro*. To further delineate whether the interaction of the paralogues Igfr-L1 and Igfr-L2 is synergistic or antagonistic, also Igfr-L1$^{-/-}$+L2$^{-/-}$ double KO Min6 cells were generated.

4.7.1 CRISPR/Cas9-mediated Igfr-L2$^{-/-}$ in Min6

For the specific targeting of genes, a bacterial technique for the defense against viruses was adopted and developed (F. A. Ran et al., 2013). Clustered regularly interspaced short palindromic repeats (CRISPR) with a promotor adjacent motive sequence were used to target the exonuclease CRISPR-associated protein 9 (Cas9) to a selective gene sequence by a single guide RNA (sgRNA) in order to introduce a double strand break. Non-homologous end joining or homology directed repair result in indels (insertions and deletions), which ideally lead to a frameshift and a premature stop of translation or the synthesis of a non-functional protein. In order to increase the probability of efficient gene targeting, small sequences can also be cut out of the genome by using several sgRNAs.
Therefore, two sgRNAs flanking the start codon (ATG) of *Igfr-L2* were chosen according to http://crispr.mit.edu depending on their quality score and location on the forward or reverse strand (Table 4.7.1.1, Figure 4.7.1.1). CACC and GGG were added in front of the forward and CAAA after the reverse sgRNA sequence to increase the efficiency of Cas9.

Table 4.7.1.1 sgRNAs for the generation of Igfr-L2$^{-/-}$ Min6

Quality score, direction and sequence of the four sgRNAs used to target the start codon of *Igfr-L2.*

guide	quality score	strand	sequence
#1	94	forward	GGATCGGGGGCGACCGGCCG
#2	94	reverse	GCACTGAATGGACTCCGGCG
#7	91	forward	CGTGACGGGAGCTCGGGCGC
#8	91	reverse	CCCTGCCTTTCGCCCGCCGC

Figure 4.7.1.1 sgRNAs for the generation of Igfr-L2$^{-/-}$ Min6

Location of the four sgRNAs (#1, #2, #7, #8) used to target the start codon of *Igfr-L2.*

In the first strategy, which was already used by Dr. Amir Morshedi to generate Igfr-L1$^{-/-}$ Min6, each sgRNA was cloned into a single expression vector. Thus, four sgRNA combinations, i.e. #1 & #2, #1 & #7, #7 & #8, #2 & #8, were transfected together with a Cas9-Venus plasmid into wildtype or Igfr-L1$^{-/-}$ Min6 cells and flow sorted after 48 h. Lack of protein expression in expanded colonies was confirmed by ICC and WB, while combinations of sgRNA #7 & #8 and #2 & #8 showed the highest KO efficiency (Figure 4.7.1.2 and Figure 4.7.3.1). From four different targeting rounds, four Igfr-L2$^{-/-}$ single and six Igfr-L1$^{-/-}$+L2$^{-/-}$ double KO clones were obtained.

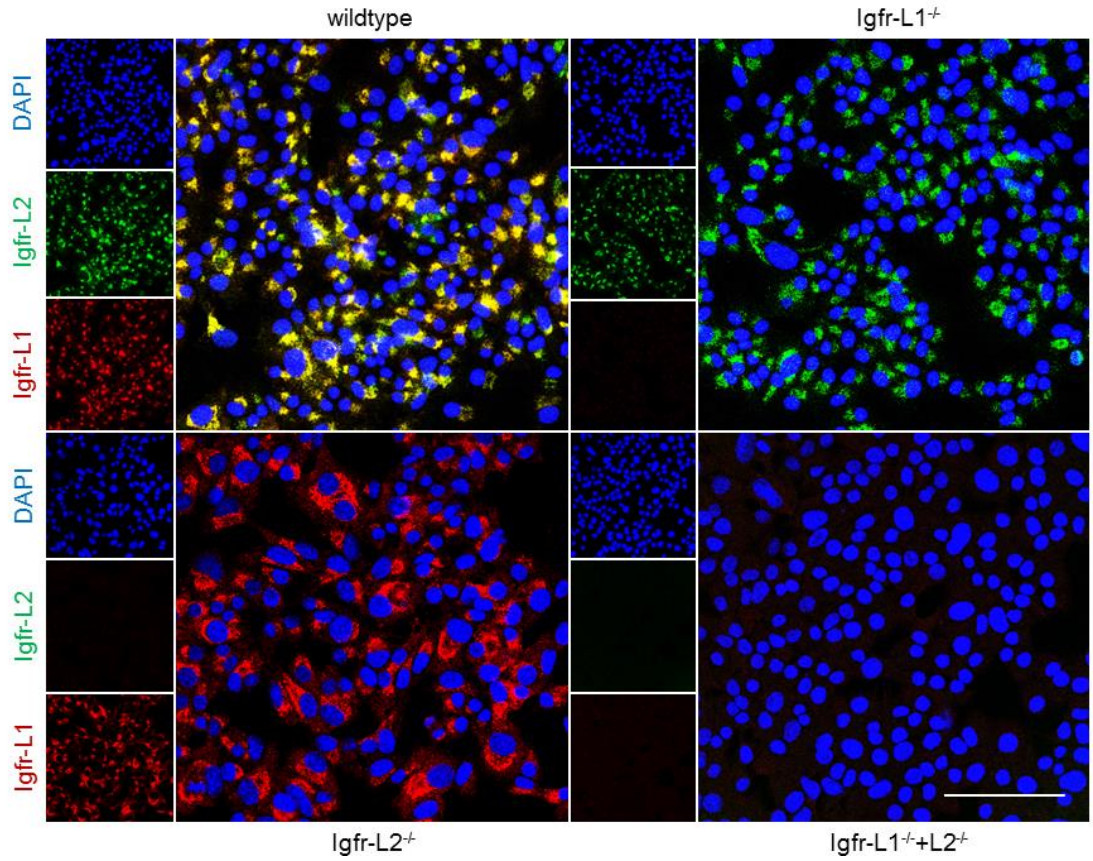

Figure 4.7.1.2 Confirmation of Igfr-L2$^{-/-}$ and Igfr-L1$^{-/-}$+L2$^{-/-}$ in Min6

Detection of Igfr-L1 (red) and Igfr-L2 (green) in wildtype, Igfr-L1$^{-/-}$, Igfr-L2$^{-/-}$ and Igfr-L1$^{-/-}$+L2$^{-/-}$ Min6. Scale bar, 50 µm.

Due to the high passage number of Min6 M9, especially after single cell expansion, and their reported impaired glucose-induced insulin secretion, Min6 K8 with low passage number and higher glucose-responsiveness were obtained (Iwasaki et al., 2010). For the generation of new single and double KO lines in the same process, a different strategy was pursued to increase the targeting efficiency. Therefore, both sgRNAs were cloned into the same vector also encoding for fluorescently-labeled Cas9, i.e. Venus for Igfr-L1 and red fluorescent protein (RFP) for Igfr-L2 (Figure 4.7.1.3). Plasmids were generously provided by Dr. Ralf Kühn (Yumlu et al., 2017). In order to avoid clonal variances, KO were separated from WT cells in bulk by FACS after labeling with anti-ectodomain-IGFR-L1-488 antibodies. However, cells were not viable after the procedure. Thus, cell lines obtained by use of the first targeting strategy were characterized.

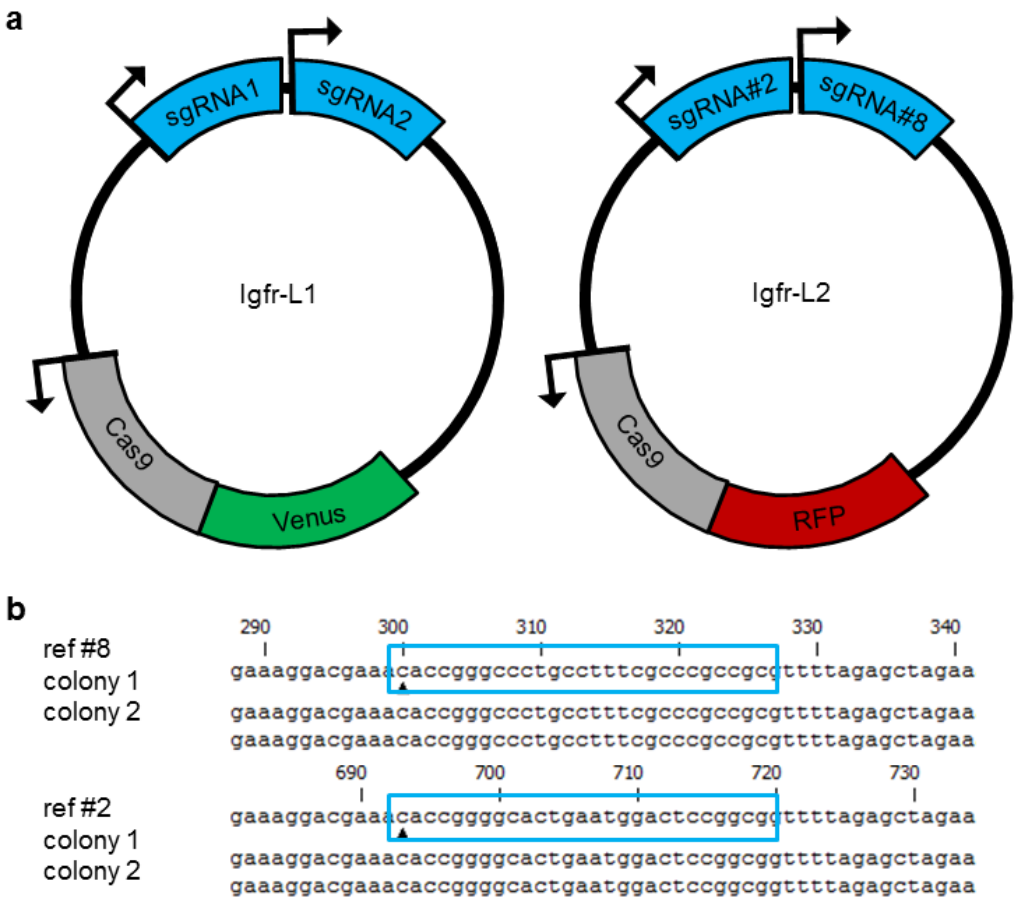

Figure 4.7.1.3 Targeting strategy *in vitro* with combined vectors

a, Combined expression vectors containing the Cas9 with a fluorescent reporter and two sgRNAs. Igfr-L1, Venus; Igfr-L2, RFP.

b, Confirmation of sgRNA sequences (#2, #8) cloned into the Cas9-RFP expression vector via Gibson cloning for targeting the start codon of Igfr-L2.

4.7.2 Proliferation of Igfr-L2$^{-/-}$ Min6

During maintenance of the different targeted Min6 lines, a lower cell count and sudden cell death was observed in Igfr-L2$^{-/-}$ cells. Thus, cellular proliferation was assessed by calculating the rate constant of exponential cell growth obtained from the number of seeded and harvested cells after a certain period of culture. Igfr-L2$^{-/-}$ cells had a significantly lower growth rate than wildtype, Igfr-L1$^{-/-}$ and Igfr-L1$^{-/-}$+L2$^{-/-}$ Min6 cells (Figure 4.7.2.1a). Analysis of DNA synthesis by EdU incorporation for 2 h, however, revealed no significant difference in *de novo* DNA synthesis hinting to augmented apoptosis in Igfr-L2$^{-/-}$ cells, which could result in the lower cell number during culture (Figure 4.7.2.1b-c). Cell cycle analysis by FACS was performed after propium iodide staining. Less cells were found in the growth phases G_0/G_1- and G_2/M-phase, while an increased number of apoptotic cells was detected in Igfr-L2$^{-/-}$ compared to wildtype Min6 cells (Figure 4.7.2.1d). In consequence, an Annexin V staining as indicator of apoptosis could be performed.

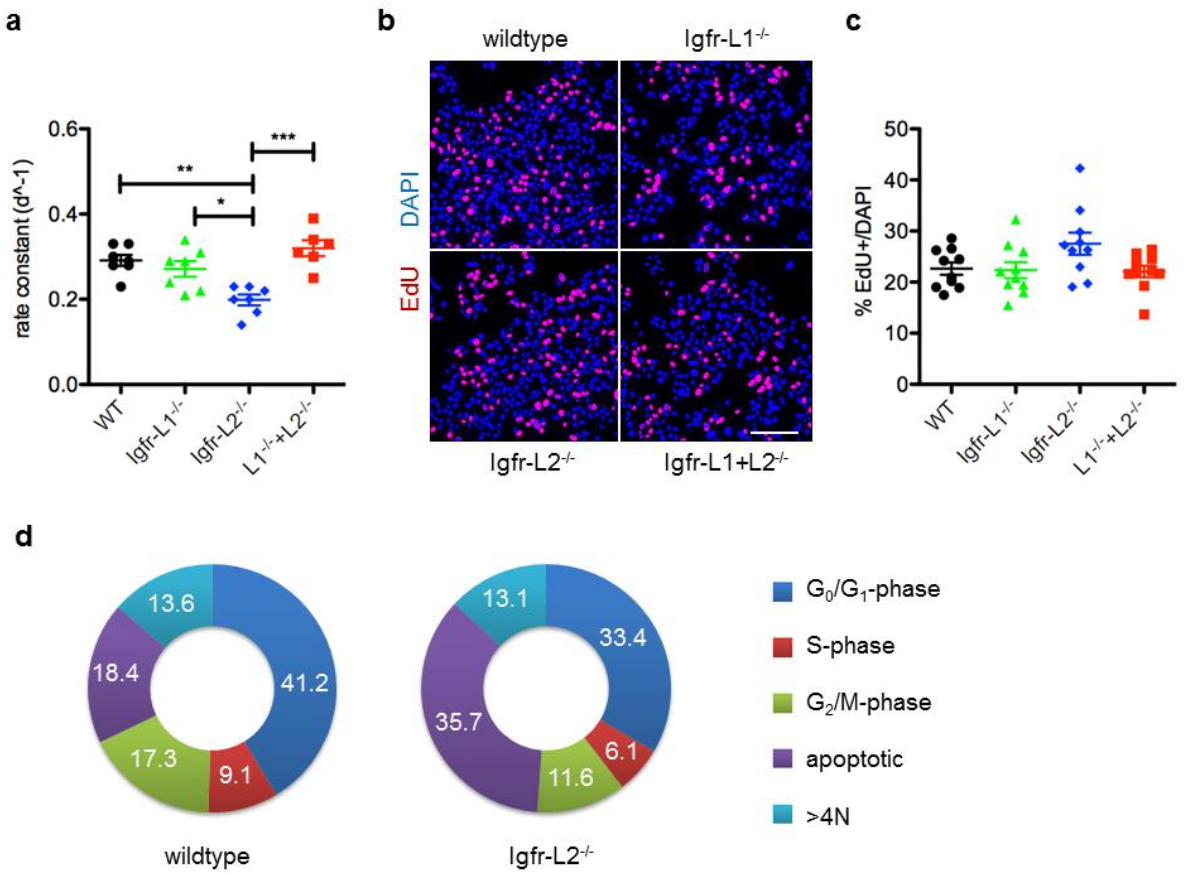

Figure 4.7.2.1 Proliferation in Igfr-L2$^{-/-}$ Min6

a, Proliferation assessed as rate constant calculated from passaging of wildtype, Igfr-L1$^{-/-}$, Igfr-L2$^{-/-}$ and Igfr-L1$^{-/-}$+L2$^{-/-}$ Min6.
***, *P*=0.0001; wildtype, n=7; Igfr-L1$^{-/-}$, n=7; Igfr-L2$^{-/-}$, n=7; Igfr-L1$^{-/-}$+L2$^{-/-}$, n=6 passages.

b-c, Representative LSM images (b) and quantification (c) of a 2 h EdU incorporation in wildtype, Igfr-L1$^{-/-}$, Igfr-L2$^{-/-}$ and Igfr-L1$^{-/-}$+L2$^{-/-}$ Min6. Scale bar, 100 µm.
n.s., *P*=0.0585; wildtype, n=3465; Igfr-L1$^{-/-}$, n=2315; Igfr-L2$^{-/-}$, n=2027; Igfr-L1$^{-/-}$+L2$^{-/-}$, n=2697 cells.

d, Cell cycle analysis with propium iodide in wildtype and Igfr-L2$^{-/-}$ Min6.

Error bars represent SEM and *, *P*<0.05; **, *P*<0.01; ***, *P*<0.001. *P*-values were calculated using a 1way-ANOVA with Bonferroni post-test.

4.7.3 Insr/Igf1r signaling in Igfr-L2$^{-/-}$ Min6

To investigate whether this pro-apoptotic anti-proliferative phenotype is connected to the Ins/Igf system which regulates both metabolism and proliferation, Insr/Igf1r signaling was analyzed in all Igfr-L2$^{-/-}$ and Igfr-L1$^{-/-}$+L2$^{-/-}$ in comparison to the parental wildtype line (Figure 4.7.3.1a).

On the one hand, Insr levels were highly upregulated in Igfr-L2$^{-/-}$ cells and significantly different to Igfr-L1$^{-/-}$+L2$^{-/-}$ Min6 cells (Figure 4.7.3.1b). On the other hand, Igf1r levels were strongly decreased in Igfr-L2$^{-/-}$, while total Igf1r levels of Igfr-L1$^{-/-}$+L2$^{-/-}$ Min6 showed a high variation (Figure 4.7.3.1c). In Igfr-L2$^{-/-}$ and most of the Igfr-L1$^{-/-}$+L2$^{-/-}$ cells, Insr/Igf1r phosphorylation was lower compared to wildtype and coincided with total Insr or Igf1r levels, respectively (Figure 4.7.3.1d-f). Whereas total levels of the downstream signaling mediator AMP-activated protein kinase (AMPK) were slightly decreased, its phosphorylation was highly increased in Igfr-L2$^{-/-}$ and significantly different from Igfr-L1$^{-/-}$+L2$^{-/-}$ cells, especially after

normalization to total levels (Figure 4.7.3.1g-i). Interestingly, Igfr-L1 levels were increased in Igfr-L2$^{-/-}$ cells. For comparison with Igfr-L1$^{-/-}$, all available clones need to be analyzed.

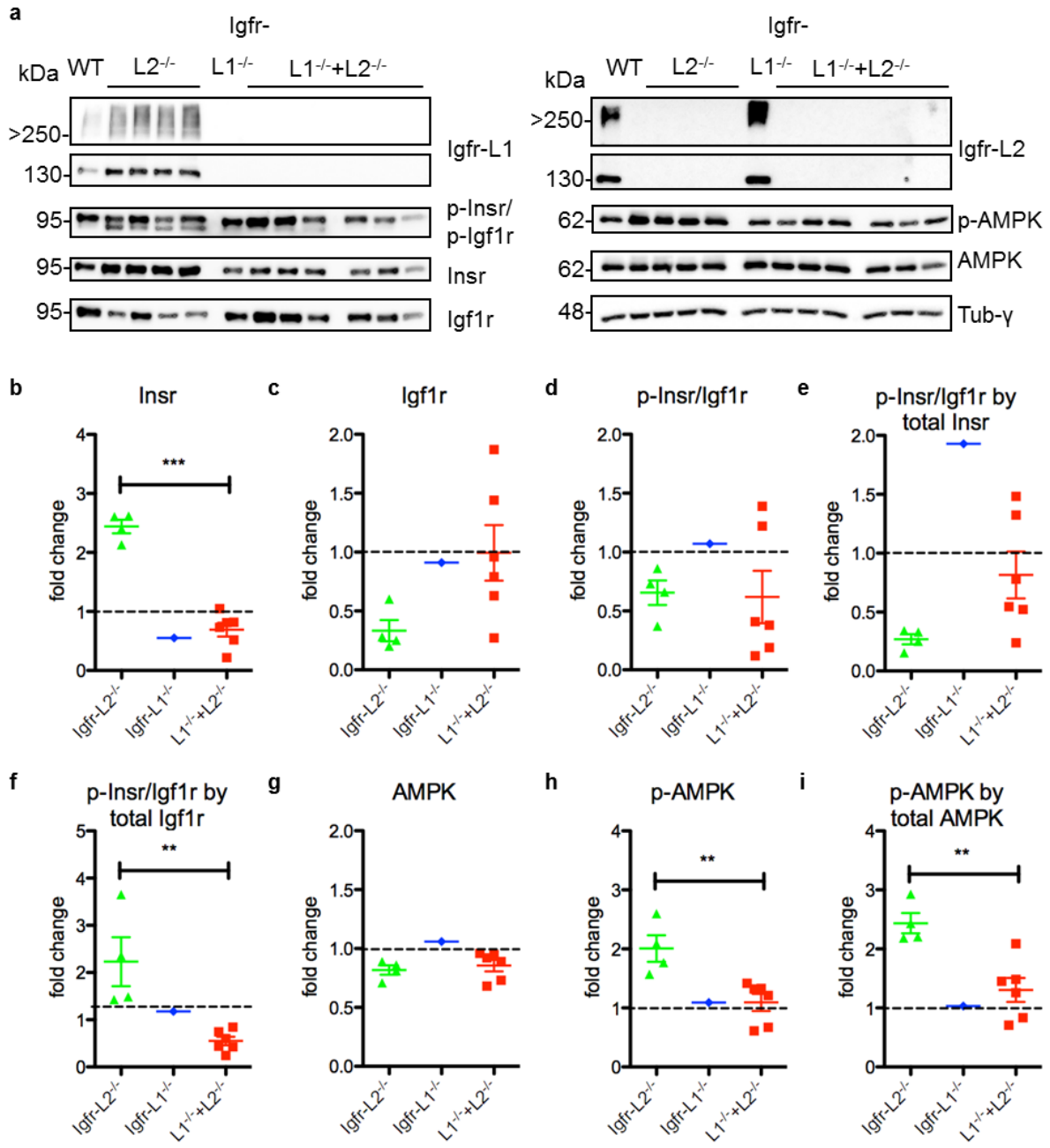

Figure 4.7.3.1 Insr/Igf1r signaling in Igfr-L2$^{-/-}$ and Igfr-L1$^{-/-}$+L2$^{-/-}$ clones

a-i, Western Blot (a) and quantification (b-i) of Insr/Igf1r signaling in Igfr-L2$^{-/-}$ and Igfr-L1$^{-/-}$+L2$^{-/-}$ Min6 normalized to wildtype and showing one Igfr-L1$^{-/-}$ Min6 clone.
b, ***, *P*<0.0001; c, n.s., *P*=0.0609; d, n.s., *P*=0.9026; e, n.s., *P*=0.0622; f, **, *P*=0.0043; g, n.s., *P*=0.5997; h, **, *P*=0.0071; i, **, *P*=0.0045;
Igfr-L2$^{-/-}$; n=4; (Igfr-L1$^{-/-}$, n=1;) Igfr-L1$^{-/-}$+L2$^{-/-}$; n=6 clones.
Error bars represent SEM and *, *P*<0.05; **, *P*<0.01; ***, *P*<0.001. *P*-values were calculated using a two-tailed, unpaired student's t-test.

4.8 Igfr-L1$^{-/-}$; Igfr-L2$^{-/-}$ double KO *in vivo*

4.8.1 Generation and preliminary analysis

In vitro experiments showed that Igfr-L1 and Igfr-L2 strongly interacted depending on the metabolic state of the cells and that Insr/Igf1r signaling was decreased correlating with Igf1r levels in Igfr-L1$^{-/-}$+L2$^{-/-}$ Min6. Additionally, a heterogeneous expression of Igfr-L1 and Igfr-L2 was observed both *in vitro* and *in vivo* suggesting a specific function in different subtypes of cells. In order to understand the physiological role of their interaction *in vivo* and to identify a synergistic or antagonistic function of these two receptors, double KO mice were started to be generated (Figure 4.8.1.1). The aim of this mouse line is to analyze adult Igfr-L1$^{+/-}$; Igfr-L2$^{-/-}$ (het-hom) in comparison to Igfr-L1$^{+/+}$; Igfr-L2$^{-/-}$ (wt-hom) on the metabolic level as well as probably postnatally lethal Igfr-L1$^{-/-}$; Igfr-L2$^{-/-}$ (hom-hom) animals to identify any potential developmental defects.

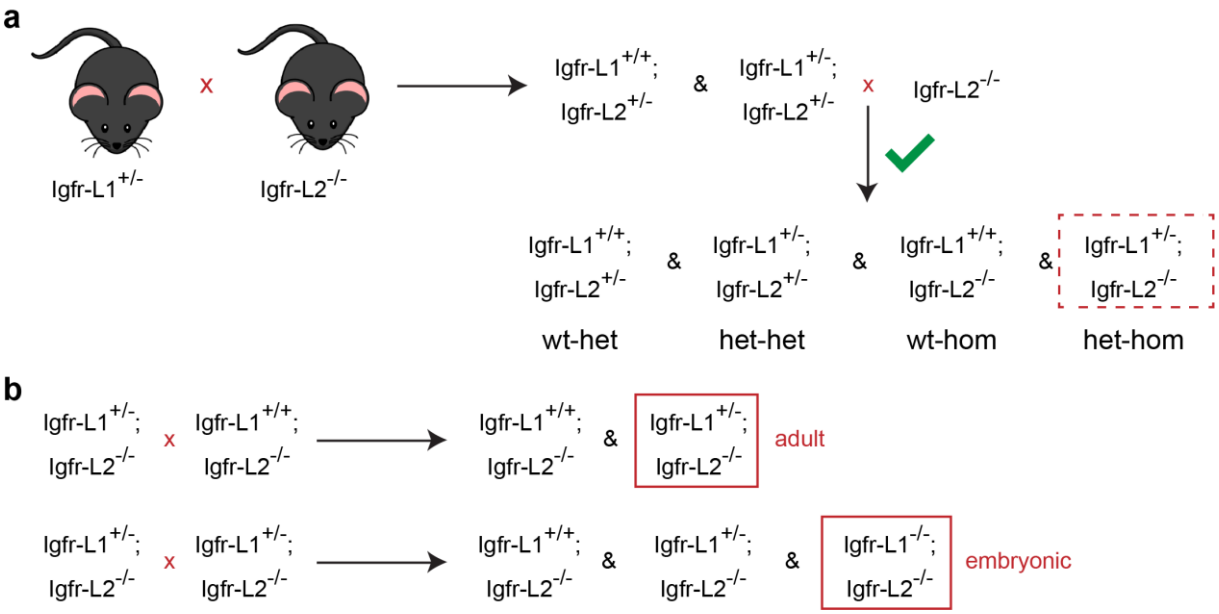

Figure 4.8.1.1 Mating scheme for the generation of Igfr-L1 x Igfr-L2

a-b, Sequential steps for the generation of het-hom animals (a) and intended analysis of their offspring (b)

Adult Igfr-L1$^{+/-}$, Igfr-L2$^{+/-}$ (het-het) animals from the first intercross showed no obvious defects. Compared to C57Bl/6J (Bl6, Figure 4.2.3.1i-l), body weight was comparable in males, while 6 h fasting blood glucose levels were significantly decreased (Figure 4.8.1.2a-b). In females, body weight was significantly higher in het-het mice, while 6 h fasting blood glucose levels were similar to Bl6 (Figure 4.8.1.2c-d). Thus, null mutants for Igfr-L2 might have a stronger phenotype.

Offspring obtained from het-het x wt-hom intercrosses had no obvious phenotype (Figure 4.8.1.2e-g), while not every genotype was available and only three het-hom females were generated. At 1.5 m, no differences were apparent apart from a tendency to lower 6 h fasting blood glucose levels in het-hom compared to wt-het females. Hence, complete lack of Igfr-L2 in combination with only one allele for Igfr-L1 could be involved in blood glucose homeostasis, while animal numbers have to be increased and analysis has to be performed at different ages.

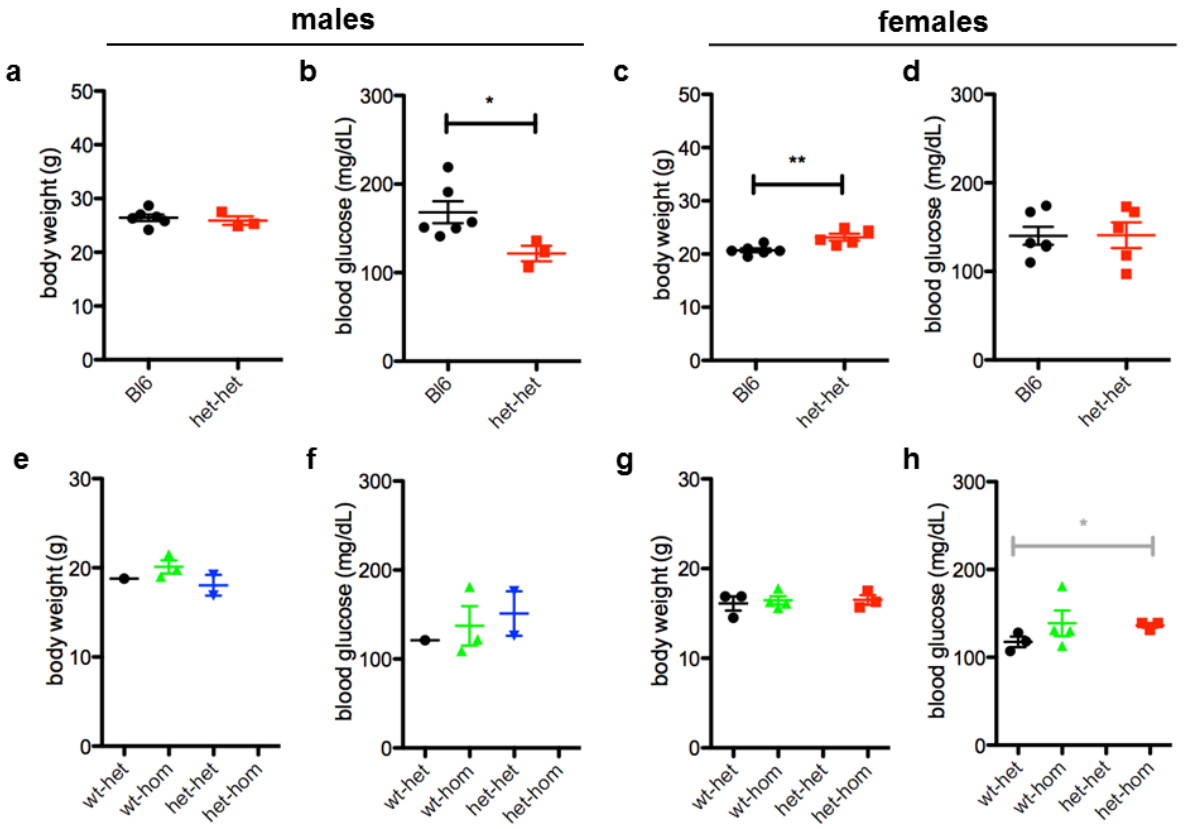

Figure 4.8.1.2 Body weight and glucose levels of Igfr-L1 x Igfr-L2

a-b, Body weight (a) and 6 h fasting glucose levels (b) of Bl6 and het-het males at 3-4 m.
a, n.s., *P*=0.6201; b, *, *P*=0.0441; Bl6, n=6; het-het, n=3;

c-d, Body weight (c) and 6 h fasting glucose levels (d) of Bl6 and het-het females at 3-4 m.
c, **, *P*=0.0067; d, n.s., *P*=0.9715; Bl6, n=5; het-het, n=5;

e-f, Body weight (e) and 6 h fasting glucose levels (f) of wt-het, wt-hom and het-het males at 1.5 m.
e, n.s., *P*=0.2078; f, n.s., *P*=0.7157; (wt-het, n=1;) wt-hom, n=3; het-het, n=2;

g-h, Body weight (g) and 6 h fasting glucose levels (h) of wt-het, wt-hom and het-hom females at 1.5 m.
g, n.s., *P*=0.8841; h, n.s., *P*=0.3994; wt-het vs het-hom, *, *P*=0.0479;
wt-het, n=3; wt-hom, n=4; het-hom, n=3.

Error bars represent SEM and *, *P*<0.05; **, *P*<0.01; ***, *P*<0.001. a-f, *P*-values were calculated using a two-tailed, unpaired student's t-test. g-h, *P*-values were analyzed using a 1way-ANOVA with Bonferroni post-test and a two-tailed, unpaired student's t-test for tendencies (grey).

5. Discussion

In this thesis, Igfr-L1 and Igfr-L2 were characterized particularly in the endocrine pancreas as two novel components of the Ins/Igf system, a major regulator of cellular metabolism and proliferation. Thus, the discussion aims on positioning Igfr-L1 and Igfr-L2 especially in the context of published findings for Insr, Igf1r and Igf2r as well as their ligands insulin, Igf1 and Igf2, while also the function of other hormone receptors is discussed. Future experiments will be suggested to finalize the phenotypical analysis of the different models and identify potential implications in diabetes research.

5.1 Biological function of Igfr-L1

Bioinformatic analysis of gene *5330417C22Rik* revealed domain structure similarities to Insr and Igf1r regarding the growth factor receptor CRD and to Igf2r in the M6PR binding domain. Hence, the protein was re-named Igf receptor-like 1 (Igfr-L1) and it was reasoned that Igfr-L1 might have a function in the Ins/Igf system. *Igfr-L1* mRNA was found to be highly expressed in the endocrine lineage during secondary transition of pancreas development. Similarly, the Igfr-L1 protein was detected in all endocrine subtypes and also in exocrine cells in the embryonic and adult pancreas.

Full-body Igfr-L1$^{-/-}$

To understand the biological function of Igfr-L1 with a focus on the pancreas, full-body Igfr-L1$^{-/-}$ animals were generated. Neonates died a few hours postpartum without any developmental defects but with signs of respiratory distress and hypoglycemia due to hyperinsulinemia. Structural analysis of the pancreas, where insulin is produced, showed no gross morphological defects and all three pancreatic lineages were formed. Insulin secretion upon glucose stimulation was not altered in Igfr-L1$^{-/-}$ pancreata at E19.5. In our laboratory, β-cell mass was found to be augmented potentially due to increased endocrine proliferation at E16.5 and overactivated Insr/Igf1r signaling specifically in the pancreas. Thus, Igfr-L1 has a pivotal function in β-cell biology and regulation of systemic blood glucose homeostasis similar to Insr and Igf1r.

Both full-body Insr$^{-/-}$ and Igf1r$^{-/-}$ mice are not viable but display distinct phenotypes. Insr$^{+/-}$ mice show no phenotype or impairment in glucose tolerance (Joshi et al., 1996). Complete lack of Insr does not affect embryonic development resulting in the expected Mendelian ratio. However, offspring only survives up to 7 days postpartum and suffers from growth retardation and diabetic ketoacidosis accompanied by other metabolic abnormalities. Mice display hyperglycemia accompanied by hyperinsulinemia, diminished glycogen storage and increased plasma triglyceride levels. Despite the high similarity to Insr, Igf1r$^{-/-}$ mice die immediately at birth due to respiratory failure and display severe growth retardation (J. P. Liu et al., 1993). Genetic disruption of the ligands Igf1 and Igf2 is similarly connected to growth regulation. Igf1$^{-/-}$ neonates die within 6 h after birth, while some survive until adulthood without disturbances depending on the genetic background.

Interestingly, the phenotype of full-body Igfr-L1$^{-/-}$ appeared to be a mixture of the phenotypes described for the KO of ligands and receptors of the Ins/Igf system. Offspring died within hours after birth with respiratory distress observed in Igf1r$^{-/-}$, Igf1$^{-/-}$ and Igf2$^{-/-}$ as well as double mutants (Epaud et al., 2012). Nevertheless, Igfr-L1$^{-/-}$ animals did not show any developmental defects being similar to Insr$^{-/-}$. At E14.5, Igfr-L1 was particularly expressed in the pancreas where its deletion led to increased proliferation and Insr/Igf1r signaling. Physiologically, disturbances in glucose metabolism and insulin action were rather connected to Insr and also no phenotype was observed in Igfr-L1$^{+/-}$ animals. In conclusion, Igfr-L1 could

act as a hybrid combining functions of Insr-A and Igf1r during embryonic development by negatively regulating Insr/Igf1r signaling.

β-cell-specific Igfr-L1$^{-/-}$

To further study the function of Igfr-L1 in adult insulin-secreting cells, a tamoxifen-inducible β-cell-specific Igfr-L1$^{-/-}$ line was generated. Animals had no obvious phenotype but showed improved glucose tolerance 4 weeks post tamoxifen induction. Similarly to full-body Igfr-L1$^{-/-}$, β-cell mass was increased and Insr/Igf1r signaling enhanced in islets *in vivo*. In this thesis, β-cell-specific deletion of Igfr-L1 after *ex vivo* Cre recombinase induction by tamoxifen in isolated islets was confirmed. After stimulation with insulin, Insr/Igf1r signaling was similarly enhanced in βCKO compared to ctrl islets. After a 24 h EdU pulse, proliferation was not measurably altered. As β-cell proliferation is relatively low in adult mice, a 72 h pulse during tamoxifen treatment could be analyzed to potentially explain the *in vivo* phenotype.
In contrast, β-cell-specific deletion of Insr results in impaired glucose tolerance as β-cells fail to secrete insulin resulting in a diabetic phenotype (Kulkarni et al., 1999). Islet size and insulin content are only slightly decreased, while no differences in islet morphology or glucose transporter 2 (Glut2) levels are detected. Similarly, β-cell-specific Igf1r$^{-/-}$ mice are unable to secrete insulin depicted by impaired glucose tolerance (Kulkarni et al., 2002). Additionally, β-cell proliferation was modulated via Irs2 showing that Igf1r is essential for the function of adult differentiated β-cells (Withers et al., 1999). Strikingly, β-cell-specific Insr$^{-/-}$; Igf1r$^{-/-}$ double KO leads to overt diabetes with severe disturbances in β-cell biology (Ueki et al., 2006). Diminished expression of the transcription factor MafA and phosphorylation of the Insr/Igf1r downstream mediator Akt was accompanied by augmented apoptosis and reduction in β-cell mass. In conclusion, Insulin- and Igf1-mediated Insr/Igf1r activation in β-cells plays a pivotal role in their proliferation in order to sustain normoglycemia (Shirakawa, Fernandez, et al., 2017).
Regarding β-cell physiology, the role of Igfr-L1 within the Ins/Igf system seems to be contrary to that of Insr and Igf1r. Ablation of Insr/Igf1r signaling abrogates glucose-induced insulin secretion, whereas βCKO mice show increased Insr/Igf1r signaling in the islets accompanied by improved glucose tolerance. Even though Insr predominantly mediates compensatory β-cell proliferation (Goldfine & Kulkarni, 2012), the function of Igfr-L1 in β-cells appears to be rather correlated to Igf1r in respect of the β-cell-specific KO. In conclusion, Igfr-L1 acts as a negative modulator of Insr/Igf1r signaling in β-cells, which regulates their proliferation and ensures GSIS. Targeting Igfr-L1 in diabetes might be a novel therapeutic strategy to increase β-cell mass and counteract hyperglycemia.

Endocrine-specific Igfr-L1$^{-/-}$

Apart from its expression in pancreatic β-cells, Igfr-L1 can also be found in the other endocrine subtypes, i.e. α-, δ-, ε- and PP-cells. To identify whether the lack of Igfr-L1 specifically in the whole endocrine pancreas similarly results in postnatal lethality and modulation of glucose homeostasis, Ngn3-Cre-mediated endocrine-specific conditional KO (CKO) animals were generated. CKO and ctrl animals were born at the expected Mendelian ratio and survived until adulthood. Thus, lethality of full-body Igfr-L1$^{-/-}$ suggests a function of Igfr-L1 in other organs, which might be responsible for their decease. Igfr-L1 is broadly expressed throughout the body including brain and lung, which could explain the abnormal feeding behavior and respiratory distress. Beyond that, confirmation of specific loss of Igfr-L1 in the endocrine pancreas revealed a potential increase in α-cell number at 1.5 m, while the functionality of these α-cells has to be confirmed (C. S. Lee et al., 2005). To investigate that neonates do not suffer from hyperinsulinemia at birth as observed in the full-body KO, alterations in islet composition including δ-, ε- and PP-cells have to be analyzed already

during embryonic and postnatal development. This would further suggest a function of Igfr-L1 in endocrine differentiation, which was not affected by lack of Insr or Igf1r.

It was anticipated that the observed increase in glucagon-positive cells might affect glucose and energy homeostasis. However, neither body weight nor fasting blood glucose levels were significantly different in CKO compared to ctrl animals during progression to adulthood. Further challenge in a glucose tolerance test at 1, 3 or 6 m of age did also not reveal differences in glucose handling. Unfortunately, no studies on Insr or Igf1r deletion in all endocrine cells by use of Ngn3-Cre were reported in the literature so far. Therefore, intra-islet hormone crosstalk was considered. Deletion of Igfr-L1 as negative regulator of Insr/Igf1r signaling in β-cells potentially results in hyperinsulinemia as described for full-body and βCKO mice. Within the islets, paracrine insulin action inhibits glucagon release from α-cells, even under hypoglycemic conditions (Banarer, McGregor, & Cryer, 2002). Insr is highly expressed in α-cells where its stimulation suppresses glucagon release via opening of ATP-regulated K^+-channels (Franklin, Gromada, Gjinovci, Theander, & Wollheim, 2005; Gromada, Duttaroy, & Rorsman, 2009). α-cell-specific $Insr^{-/-}$ leads to hyperglucagonemia as well as hyperglycemia and mild glucose intolerance (Kawamori, Akiyama, Hu, Hambro, & Kulkarni, 2011; Kawamori et al., 2009). Additionally, glucagon secretion is enhanced upon L-Arginine stimulation and during a hyperinsulinemic-hypoglycemic clamp and animals display an increase in β-cell mass during aging. Hence, by negatively regulating Insr signaling in α-cells, systemic glucagon action might be reduced, which can be further studied by KO of the glucagon receptor (Gcgr) or glucagon. Systemic $Gcgr^{-/-}$ mice display hyperglucagonemia and postnatal α-cell hyperplasia, whereas blood glucose levels are decreased and glucose tolerance is improved without a change in insulin levels (Gelling et al., 2003). Body weight and food intake are not altered, while adipositas and leptin levels are reduced. Thus, glucagon signaling is essential for embryonic endocrine differentiation and glucose homeostasis in adult animals. Mice that lack glucagon as well as Glp1 and Glp2 display α-cell hyperplasia without differences in glucose homeostasis (Hayashi et al., 2009). In db/db mice, insulin stimulation triggers α-cell proliferation via the Insr/Irs2/Akt/Mtor pathway, whereas Gcgr blockage inhibits α-cell proliferation and leads to higher insulin content in islets (Z. Liu et al., 2011). In conclusion, Igfr-L1 endocrine CKO mice potentially display decreased glucagon levels due to increased insulin and reduced glucagon stimulation of α-cells. Insr-mediated proliferation further results in an augmented α-cell number that does not affect glucose homeostasis.
Apart from islet-specific effects, it should be considered that Ngn3 is expressed in the brain and gastrointestinal tract (Jenny et al., 2002; Schonhoff, Giel-Moloney, & Leiter, 2004; Song, Xu, Hu, Choi, & Tong, 2010). Thus, other systemic factors including the hypothalamic-pituitary-gonadal (HPG) axis could be involved in survival and normal glucose homeostasis of the Igfr-L1 endocrine-specific CKO. For example, glucagon-like peptides have beneficial effects on β-cell health and are secreted from intestinal L-cells, where Igfr-L1 is also expressed (Cornu et al., 2009; Hayashi et al., 2009; Mauvais-Jarvis et al., 2017; Tiano, Tate, Yang, DiMarchi, & Mauvais-Jarvis, 2015; Wideman et al., 2006). To summarize, Igfr-L1 is potentially involved in intra-islet crosstalk via modulation of Insr/Igf1r signaling in α- and β-cells regulating maintenance of systemic glucose homeostasis.

5.2 Biological function of Igfr-L1 in diabetes mellitus

Lack of Insr or Igf1r alone results in impaired glucose tolerance whereas ablation of both leads to overt diabetes (Kulkarni et al., 1999; Kulkarni et al., 2002; Ueki et al., 2006). As Igfr-L1 has been shown to regulate β-cell biology contrary to Insr and Igf1r, its function in diabetes was investigated. In the FVFPBF^{DHom} (FP) MODY model, expression of Igfr-L1 was found to be upregulated at P25 compared to Bl6, which was also preliminary observed in animals with diet-induced obesity and streptozotocin-treated mice. However, it is not clear whether the increase in expression is a result of or if overexpression contributes to hyperglycemia and β-cell dysfunction. To study this, FP animals heterozygous for Igfr-L1 were generated both with the ΔEx3 and the FD allele.
At P14, no difference in expression of Igfr-L1 was observed between FP and Bl6 animals and blood glucose levels of FP-het mice were similar to litter mates. Both male and female offspring suffered from hyperglycemia at weaning age. In males, however, genetic reduction of Igfr-L1 resulted in decreased fasting blood glucose levels in both lines at P25. Performance of an ITT showed that FP-het males had overall lower blood glucose levels, while glucose clearance was comparable to FP-wt. Serum insulin and C-peptide levels were significantly increased in FP-het albeit their ratio was not different from FP-wt. Regarding β-cell function, expression of the maturation marker Ucn3 and glucose transporter Glut2 was still massively decreased in FP-het compared to Bl6, while in FP-wt, no signal was detectable at all. β-cell-specific single and double KO of Insr and Igf1r was also accompanied by a reduction in Glut2 levels showing that Igfr-L1 counterregulates Insr/Igf1r signaling (Kulkarni et al., 1999; Kulkarni et al., 2002; Ueki et al., 2006). Lack of cell-cell contacts, which are observed in MODY mice, could further modulate Insr and Igf1r availability and signaling as seen in breast cancer cells (Nagle et al., 2018). In summary, heterozygosity of Igfr-L1 did not enhance insulin sensitivity or insulin secretion but rather hinted to an increased number of functional β-cells shown by maturation and intact GSIS resulting in lower blood glucose levels. Potential changes in β-cell proliferation and mass, which were augmented in full-body KO and βCKO mice, have to be investigated. As random-fed blood glucose levels were comparable, loss of negative feedback upon starvation is further suggested. In conclusion, Igfr-L1 negatively regulates Insr/Igf1r signaling, while lowering the gene dose by one allele during hyperglycemia might potentially circumvent insulin resistance and delay β-cell failure in MODY males.
During transition to adulthood, however, 6 h fasting blood glucose levels of FP-het males rose to that of FP-wt at 1.5 m, were even higher at 3 m but again comparable at 6 m of age. In line, insulin and C-peptide levels were not augmented at 1.5 m anymore. Impaired glucose tolerance and hyperinsulinemia of β-cell-specific Insr$^{-/-}$ were also age- and sex-dependent (Kulkarni et al., 1999). In addition, Igfr-L1 might be further connected to glucose homeostasis during sexual maturation as also the androgen receptor is known to regulate GSIS (Navarro et al., 2016). In line, a systemic regulation of blood glucose levels via the HPG axis, where Igfr-L1 is broadly expressed, cannot be excluded. Apart from that, Pdx1 expression is crucial for β-cell identity and function. The destabilization of the β-cell-specific TF network caused by the double knock-in of fluorescent tags might abrogate the initially observed improvement. Thus, lowering one copy of Igfr-L1 only transiently slows down diabetes progression as chronic genetic pressure cannot be stopped by therapy.

In females, initial hyperglycemia was reverted during transition to adulthood with no difference in between FP-wt and FP-het suggesting a role of estrogen in the sexual dimorphism of MODY animals. Nevertheless, β-cell damage resulted in a massively impaired glucose tolerance in MODY females and development of gestational diabetes. During their second pregnancy, FP-het females displayed higher blood glucose levels during early

gestation, lactation and post-weaning suggesting that Igfr-L1 is crucial for glucose homeostasis during gestation. Gender differences in metabolic physiology and pathophysiology are reported (Gannon, Kulkarni, Tse, & Mauvais-Jarvis, 2018; Mauvais-Jarvis, 2018), while estrogen (17β-estradiol) is a key regulator of glucose homeostasis in females (Hevener, Clegg, & Mauvais-Jarvis, 2015; Louet, LeMay, & Mauvais-Jarvis, 2004; Mauvais-Jarvis, Clegg, & Hevener, 2013). Postmenopausal insulin resistance and obesity are reverted by hormone replacement therapy, while expression of IGFR-L1 was found to be upregulated under these conditions (Deng et al., 2005). Different mouse models suggest a role of estrogen in lipid and glucose metabolism as well as in β-cell health (S. Liu & Mauvais-Jarvis, 2010; Macotela, Boucher, Tran, & Kahn, 2009; Tiano et al., 2011; Tiano & Mauvais-Jarvis, 2012). Upregulation of ERα due to hyperglycemia is independent of Insr (Kilic et al., 2014) and its activation in β-cells improves mitochondrial function and relieves ER-stress to counteract apoptosis and enhance insulin secretion (Z. Zhou et al., 2018). Targeted delivery of estrogen by Glp1 is studied in the treatment of diabetes and other metabolic disorders (Finan et al., 2012). Again, systemic effects in endocrinology and glucose metabolism due to an involvement of Igfr-L1 in the HPG axis including feedback mechanisms cannot be excluded. On the one hand, induction of Igfr-L1 by estrogen might be crucial for glucose homeostasis during pregnancy and has to be determined by IHC. On the other hand, genetic reduction of Igfr-L1 in endocrine cells of the HPG axis might dysregulate estrogen and other hormones resulting in impaired glucose handling.

The metabolic challenge of animals by MODY might be the reason for a phenotype in heterozygous animals, which has to be confirmed in other diabetes mouse models. Survival of homozygous mice could be due to a different background, which is a mixture of CD1 and C57Bl/6J and C57Bl/6N, as it is known that the inbred strain plays an important role in respect of phenotypes and susceptibility to diseases (Fisher-Wellman et al., 2016; Fontaine & Davis, 2016; Goren, Kulkarni, & Kahn, 2004). Apart from that, survival could originate from alterations during embryonic and postnatal development due to the double knock-in of fluorescent proteins to the transcription factors Foxa2 and Pdx1. Pdx1 haploinsufficiency impairs compensatory mechanisms under hyperinsulinemia (Kulkarni et al., 2004) implying that transcription of genes involved in β-cell physiology is differential in the FP model (Bastidas-Ponce, Roscioni, et al., 2017). Therefore, analysis of embryonic stages when the transcription factors are expressed could be performed to explain prevention of postnatal lethality. Interestingly, homozygous animals had no phenotype regarding blood glucose homeostasis but showed a strong response to insulin suggesting that lack of Igfr-L1 leads to higher glucose uptake or serves as a scavenger for insulin.
In summary, Igfr-L1 could serve as a novel target to delay the onset of diabetes and preserve β-cell function resulting in improved blood glucose homeostasis.

Diabetic endocrine-specific Igfr-L1$^{-/-}$

As FP-hom animals were assumed to die postnatally, the endocrine-specific Igfr-L1$^{-/-}$ in the MODY animals was generated in parallel to the one in Bl6 animals. Similarly, islet composition was shifted towards α-cells, which has to be quantified thoroughly, in addition to the already increased number of glucagon-positive cells in the MODY model. Regarding preliminary data on blood glucose levels at P25, no significant difference was observed in males or females. A counterregulation of glucagon has to be studied in a time-resolved manner and correlated with insulin levels. However, it is known that in diabetes paradoxically rather more glucagon is secreted due to lack of insulin inhibition (Dunning & Gerich, 2007) and α-cells become glucose-responsive (Rorsman, Salehi, Abdulkader, Braun, & MacDonald, 2008). Apart from that, Igfr-L1 levels in the FP-het animals are reduced in the whole body including the brain and other endocrine organs, which might further play a role in

systemic glucose homeostasis. Therefore, the endocrine-specific Igfr-L1$^{-/-}$ in the MODY animals might be useful to distinguish between islet-driven and systemic effects.

5.3 Molecular function of Igfr-L1 *in vitro*

In vivo analysis of Igfr-L1 in the full-body KO and βCKO revealed a pivotal function in β-cell biology by being a negative regulator of Insr/Igf1r signaling-mediated proliferation. To further study the molecular function of Igfr-L1, the immortalized murine and human β-cell lines Min6 and EndoC were studied. To identify interaction partners, co-IPs with subsequent HPLC-MS analysis were performed under different metabolic conditions, i.e. growth conditions and 15 min starvation were analyzed first. Immunostainings showed that Igfr-L1 mainly localizes perinuclear in the ER-Golgi region similar to the Igf2r of which 90 % are present in the prelysosomal/late endosomal compartment, while the other 10 % are distributed at the PM, in early endosomes and in the trans-Golgi network (Griffiths, Matteoni, Back, & Hoflack, 1990). As expected from its extracellular M6PR binding domain, Igfr-L1 is also trafficking inside the cells (Ghosh et al., 2003; Griffiths & Simons, 1986). Hence, possible interactions of Igfr-L1 with the Ap3 complex subunit sigma-1, which is involved in the transport of cargo from tubular endosomes to late endosomes (Park & Guo, 2014), Sec22b, which is a SNARE protein that interacts with COPII in the ER (Mancias & Goldberg, 2007), and lectins of the secretory pathway such as VIP36 (Fullekrug, Scheiffele, & Simons, 1999) and Ergic1, whereas mainly Ergic53 is described (Hauri, Kappeler, Andersson, & Appenzeller, 2000), were found. Igfr-L1 potentially interacts with the ER chaperone calnexin probably during its processing (Williams, 2006), which is also responsible for the folding of Insr and Igf1r (Bass et al., 1998). Expected internalization from the PM via CME due to the Ap2 binding motif in the cytoplasmic tail of Igfr-L1, similar to Insr (Carpentier, 1994), was suggested by potential interactions with the clathrin light chain and the Ap2-α2 subunit (Goh & Sorkin, 2013; Popova et al., 2013). Furthermore, the E3 ubiquitin-ligases Nedd4 and Ubr4 were identified, which are involved in Insr and Igf1r internalization (Goh & Sorkin, 2013; Vecchione et al., 2003). In conclusion, Igfr-L1 is internalized from the cell surface and routing inside the cells similar to Insr, Igf1r and Igf2r. Apart from that, different subunits of 14-3-3 proteins were detected, which trigger anti-apoptotic effects in β-cells via regulation of the Bad pathway downstream of Insr/Igf1r signaling (Lim, Piske, & Johnson, 2013). Thus, Igfr-L1 might be involved in β-cell survival.

Reduction of metabolic activity by overnight incubation in low glucose and less FCS with subsequent glucose or insulin stimulation mainly resulted in potential interactions with various ATPases. The sodium/potassium ATPase is involved in active transport of nutrients e.g. glucose, while its activity is modulated by insulin (Sweeney & Klip, 1998). V-Type ATPases modulate insulin secretion in β-cells (Sun-Wada et al., 2006), the sarcoplasmic/ endoplasmic reticulum calcium ATPase is involved in the regulatory feedback of insulin exocytosis (Borge et al., 2002) and the mitochondrial ATP synthase participates in GSIS due to ATP generation after glucose uptake (Wiederkehr & Wollheim, 2006). Hence, Igfr-L1 might be further involved in β-cell energy homeostasis or GSIS in terms of Ca^{2+}-signaling (Kruger et al., 2008).

The potential interaction of Igfr-L1 and Ap2 was additionally confirmed by co-IP followed by WB analysis suggesting that Igfr-L1 is internalized from the PM via CME. Apart from that, Igfr-L1 was found in the eluates of both immunoprecipitated Insr and Igf1r hinting to their potential interaction. Whether this interaction occurs extracellularly where the ligands or intracellularly where the downstream signaling proteins bind has to be further defined. Dimerization of Igfr-L1 (and Igfr-L2) with RTKs could also potentially occur via the GxxxG dimerization motif in their transmembrane domain, which has been described for EGFR (Teese & Langosch, 2015). Interestingly, the potential interaction of Igfr-L1 with Insr was

increased after insulin stimulation suggesting a ligand-induced mechanism. Using the PLA technology, potential interaction of IGFR-L1 with INSR, IGF1R and their phosphorylated form was detected in the human β-cell line EndoC suggesting that our findings can be translated to human. Apart from the receptors, proximity was also seen for the ligand insulin and preliminary experiments with recombinant proteins and biotinylated insulin hinted to a potential direct interaction. Thus, Igfr-L1 could act as a scavenger for insulin, which could further explain hyperinsulinemia in the full-body KO and improved glucose uptake in FP-hom mice upon insulin administration. Furthermore, the likely interaction with Insr and Igf1r was analyzed in respect of their endocytosis after a switch from growth conditions to starvation showing that Igfr-L1 is present at the cell surface. Whereas Igfr-L1, Insr and Igf1r were internalized within 30 min from and recycled back after 1 h to the PM in wildtype Min6, Insr and Igf1r accumulated at the surface in Igfr-L1$^{-/-}$ cells. Thus, lack of Igfr-L1 disturbs the trafficking dynamics showing that Igfr-L1 facilitates ligand-induced internalization of Insr and Igf1r.
To sum up, as a novel component of the Ins/Igf system, Igfr-L1 potentially interacts with Insr and Igf1r and ensures their internalization and abrogation of signal transduction. Endocytosis is likely mediated by clathrin including the adaptor protein Ap2. This gives one mechanistic explanation for the hyperphosphorylation observed *in vivo*. Modulation of Igfr-L1 e.g. by antibodies or drugs to retain Insr and Igf1r at the PM for prolonged signal transduction could improve β-cell function during insulin resistance.

5.4 Biological and molecular function of Igfr-L2

Igfr-L2 was identified as the most abundant interaction partner of Igfr-L1 by HPLC-MS. Bioinformatic analyses showed that the paralogues share around 50 % sequence identity. Similar to Igfr-L1, Igfr-L2 has the same predicted domain structure similarities to Insr and Igf1r in the CRD and to Igf2r in the M6PR binding domain. It was therefore anticipated that Igfr-L2 is similarly involved in the regulation of glucose homeostasis and proliferation in respect of the Ins/Igf system. In *X. laevis,* almost complete knock-down of Igfr-L2 leads to developmental defects at birth because of suppression of the BMP signaling pathway showing that Igfr-L2 is able to modulate RTKs (T. Araki et al., 2011).
Interestingly, after generation of several specific monoclonal antibodies, Igfr-L2 was identified as a novel endocrine cell marker, as its expression was specific to the anterior pituitary and the islets of Langerhans. Apart from that, Igfr-L2 was found in the ovaries and prostate suggesting a function in the hypothalamic-pituitary-gonadal (HPG) axis, which regulates systemic growth, metabolism and reproduction in cooperation with the Ins/Igf system (F. Ma et al., 2011; Shirakawa, De Jesus, et al., 2017). To shed light on the biological function of Igfr-L2 in those systems and especially in the endocrine pancreas, full-body KO animals were generated. Unlike Igfr-L1$^{-/-}$, Igfr-L2$^{-/-}$ animals were viable and did not show any developmental defects as described for *X. laevis* suggesting that compensatory mechanisms exist.
Nevertheless, intercrosses of two Igfr-L2$^{-/-}$ animals resulted in a smaller litter size and loss of neonates until weaning. In conclusion, both parents are not infertile while Igfr-L2 might be involved in conception and proper embryonic development. It was found to be expressed in ovaries and prostate. Reproduction is controlled via the HPG axis and connected to energy homeostasis to ensure embryonic growth (Fernandez-Fernandez et al., 2006). In respect of the Ins/Igf system, insulin regulates reproduction via neural modulation of gonadotropin releasing hormone and luteinizing hormone secretion, while adult reproduction can already be programmed via insulin action during embryonic development (Sliwowska et al., 2014). KO of Insr in gonadotrophs in the pituitary was able to rescue diet-induced infertility in females (Brothers et al., 2010). Additionally, Insr/Igf1r signaling is involved in cell fate

decision in gonadal somatic progenitors (Pitetti et al., 2013) and ensures functionality of the placenta (Hiden et al., 2009), while its dysregulation during pregnancy is organ-specific in rat fetuses (White et al., 2015). Also, KO of Insr in neurons of the central nervous system did not only affect energy homeostasis but also ovarian follicle maturation and spermatogenesis due to alterations in luteinizing hormone (Bruning et al., 2000). Preliminary experiments hinted to increased total levels of Insr and Igf1r in the pituitary of Igfr-L2$^{-/-}$ mice. Thus, lack of Igfr-L2 might impair reproductive neuroendocrine function due to dysregulation of the Ins/Igf system involved in the HPG axis. Hence, the observed pre- and postnatal lethality has to be studied in more detail to identify the cause of death or survival and identify a function of Igfr-L2 during embryonic development.

In a GTT with 8 m old animals, Igfr-L2$^{-/-}$ animals did not show any alterations in glucose tolerance compared to wildtype controls, while in the islets of Langerhans, no difference in composition or maturation was observed. Preliminary experiments showed that stimulation of isolated islets with insulin resulted in lower phosphorylation of Insr/Igf1r in Igfr-L2$^{-/-}$. Due to their high similarity, Igfr-L1 might compensate for the loss of Igfr-L2, which will be further analyzed in the double KO.
That Igfr-L2 acts as a modulator of Insr/Igf1r signaling like Igfr-L1 is emphasized by data from the murine β-cell line Min6, in which Igfr-L2$^{-/-}$ resulted in downregulation of Igf1r accompanied by an upregulation of Insr and Igfr-L1. Cells displayed decreased proliferation and increased apoptosis, while phosphorylation of the energy sensor AMPK was enhanced (Gwinn et al., 2008; Jaafar et al., 2019; Shackelford & Shaw, 2009; Zhang, Zhou, & Li, 2009). Thus, Igfr-L2 could be important for β-cell survival as described in the β-cell-specific Insr/Igf1r double KO (Ueki et al., 2006) and be linked to β-cell fragility (Liston, Todd, & Lagou, 2017). To further study the antiapoptotic, mitogenic effects of Igfr-L2 observed in β-cells *in vitro*, compensatory β-cell proliferation should be investigated upon high fat diet feeding (Kleinert et al., 2018) or during gestation (Rieck & Kaestner, 2010) in adult Igfr-L2$^{-/-}$ mice.

5.5 The paralogues Igfr-L1 and Igfr-L2

Similar to Insr and Igf1r, the paralogues Igfr-L1 and Igfr-L2 have co-evolved from a common ancestral gene. They are highly similar and share domain structure similarities with Insr, Igf1r and Igf2r. Heterogeneous expression of Igfr-L1 and Igfr-L2 was found *in vitro* and *in vivo* in endocrine cells of the pancreas and the pituitary. This could hint to a different function of the two proteins similar to Insr and Igf1r albeit they share the same ligands and downstream-signaling components. It would be interesting to dissect this heterogeneity on a single cell level, as it might be connected to the heterogeneity observed in β-cells in terms of maturation, functionality, proliferation or aging (Avrahami, Klochendler, Dor, & Glaser, 2017; Bader et al., 2016; Bonner-Weir & Aguayo-Mazzucato, 2016; Katsuta et al., 2012; Roscioni et al., 2016; Tritschler, Theis, Lickert, & Bottcher, 2017; Wills et al., 2016).
Homo- and heterodimerization of Igfr-L1 and Igfr-L2 was confirmed by co-IP and PLA, while HPLC-MS analysis revealed a dependence on the metabolic state of the cells. During starvation less while during growth conditions and glucose or insulin stimulation more heterodimers were found. This suggests that Igfr-L1 and Igfr-L2 interact when Insr/Igf1r signal transduction is activated. Dimerization of Insr and Igf1r is also observed and modulates their ligand affinity and downstream signaling cascade. Interaction of Igfr-L1 with Insr and Igf1r was shown and is assumed for Igfr-L2. Hence, Igfr-L1 and Igfr-L2 could modulate each other as well as Insr and Igf1r achieving the necessary fine tuning for propagation of cellular outcomes of ligand stimulation, i.e. regulating the balance between growth and metabolism. Unlike Insr and Igf1r, Igfr-L1 and Igfr-L2 do not have a RTK domain suggesting that they could also serve as scavenger receptors similar to the Igf2r.

Physiologically, Igfr-L1 is broadly expressed throughout the whole body in various organs, while Igfr-L2 is specifically expressed in endocrine cells e.g. of the pituitary and the pancreas. A common but also distinct expression pattern is similarly observed for Insr and Igf1r in adult animals. Strikingly, single KO of both Insr and Igf1r in β-cells leads to impaired glucose tolerance, while the double KO develops diabetes at weaning age (Kulkarni et al., 1999; Kulkarni et al., 2002; Ueki et al., 2006). Hence, compensation of one or the other is most likely in the single KOs and could also be apparent for Igfr-L1 and Igfr-L2. In conclusion, mutual regulation of Igfr-L1 and Igfr-L2 could be studied in more detail in the single KOs in order to identify a synergistic or antagonistic function.
In addition, double KO animals were started to be generated, while so far neither Igfr-L1$^{+/-}$; Igfr-L2$^{+/-}$ nor Igfr-L1$^{+/-}$; Igfr-L2$^{-/-}$ showed a drastic regulation in glucose homeostasis. One aim is to analyze glucose tolerance in Igfr-L1$^{+/-}$; Igfr-L2$^{-/-}$ compared to Igfr-L1$^{+/+}$; Igfr-L2$^{-/-}$. Reduction of one copy of the Igfr-L1 allele in Igfr-L2$^{-/-}$ potentially leads to a difference in glucose tolerance. Ultimately, the double KO will be analyzed during embryonic development in respect of survival, endocrine function and glucose homeostasis.

Overall, Igfr-L1 and Igfr-L2 are two novel components of the Ins/Igf system, which is a major regulator of growth and metabolism. Thus, Igfr-L1 and Igfr-L2 might serve as novel targets in diabetes and/or cancer therapy. Detailed analysis of their molecular function and interaction dynamics will provide entry points for drug targeting.

6. Material and methods

6.1 Equipment

agarose gel chamber	Midi 450 (Neolab, Heidelberg)
balance	Scout™ Pro (OHAUS)
Biorep perfusion system	Biorep Technologies, Miami USA
cell counter	TC20TM automated cell counter (Bio-Rad, Heidelberg)
cell culture hood	BDK (Luft- und Reinraumtechnik GmbH, Sonnenbühl-Genkingen)
centrifuges	5417R, 5439C, 5804R (Eppendorf, Hamburg)
	microcentrifuge (Roth, Karlsruhe), Micro 220 (Hettich, Tuttlingen)
	Universal 320R (Hettich, Tuttlingen), 6767 (Corning)
cryostat	Ag Protect (Leica, Wetzlar)
developing machine	AGFA Curix 60 developing machine (AGFA HealthCare GmbH, Bonn)
FACS	FACS Aria III (Becton, Dickinson and Company, San Jose, USA) 405, 488, 555 and 633 nm laser; 75, 85 and 100 µm nozzle
film cassettes	hypercassette (Amersham, München)
freezer	-20°C Medline, premium no frost (Liebherr, Ochsenhausen)
	-80°C (Thermo Scientific, Waltham)
fridge	4°C comfort (Liebherr, Ochsenhausen)
gel documentation system	UVsolo TS Imaging System (Biometra, Göttingen)
glass ware	Schott-Duran (Schott, Mainz)
glucometer	Freestyle freedom lite (Abbot Diabetes Care Oxon, UK)
	ContourXT (Ascenia Diabetes Care Deutschland GmbH, Leverkusen
incubation systems/ovens	Thermomixer Comfort, Thermomixer 5436 (Eppendorf, Hamburg)
	oven (Thermo Scientific, Waltham)
incubator (cells)	BBD6220 (Thermo Scientific, Waltham)
	Inkubator C16 (Labotect, Rosdorf)
	KBF (Binder GmbH, Tuttlingen-Möhringen
	Shake'n'Stack (ThermoHybaid, Thermo Fisher Scientific Inc., Waltham)
magnetic rack	for immunoprecipitation (Bio-Rad, Feldkirchen)
microscopes	MS5, MZ75 (Leica Microsystems GmbH, Wetzlar)
	TCS SP5 and Cube (heating), Brick (CO2)(Leica Microsystems GmbH, Wetzlar)
	M80 and Dissection light (Leica, Wetzlar)
	LSM 800 AiryScan (Zeiss, Oberkochen)
microwave	700 W (Severin Elektrogeräte GmbH, Sundern)
N2 tank	Biostore systems (Cryo Anlagenbau GmbH, Wilnsdorf)
PCR machines	Personal Thermocycler, Professional Trio Thermocycler (Biometra, Göttingen)
	PXE0.2 Thermo Cycler (Thermo Fisher Scientific Inc., Waltham)
pH meter	Mettler Toledo (HANNA Instruments Deutschland GmbH, Kehl am Rhein)

photometer	NanoDrop 2000c (Thermo Fisher Scientific, Waltham)
	PHERAstar FS (BMG Labtech GmbH, Ortenberg)
	Varioskan LUX (Thermo Fisher Scientific, Vantaa, Finland)
pipetboy	Accu-JetR pro (Brand GmbH, Wertheim)
pipettes	2.5 µL Eppendorf, Hamburg)
	1000 µL, 200 µL, 20 µL (Gilson, Limburg-Offenheim)
plastic ware	(Vitlab GmbH, Großostheim)
polyacrylamide gel chamber	Mini Trans-Blot® Cell (Bio-Rad, Heidelberg)
power supply (gel chamber)	Power Source 300V (VWR International, Darmstadt)
roller/mixer	VSR 23 (VWR International, Darmstadt), Shaker DOS-10L (Neolab, Heidelberg), RMS (I), Rocker 247 (Everlast)
sonicator	Sonoplus HD2070 (Bandelin electronic GmbH & Co. KG, Berlin)
	Elmasonic, UW 2070 (Bandelin electronics, Berlin)
sterile hoods	MSC Advantage (Thermo Scientific, Waltham)
stirrer	D-6011 (Neolab, Heidelberg)
timer	Roth, Karlsruhe
tissue homogenizer	Ultra Turrax T25 (IKA)
ultrasonic bath	ultrasonic cleaner (VWR International, Darmstadt)
vortex	vortexer (VWR International, Darmstadt)
water bath	Memmert
	SWB25 (Thermo Fisher Scientific ins., Langenselbold)
water purification system	Millipore Q-POD, 0.22 µL filter (Merck Chemicals GmbH, Schwalbach)
Western blot semi-dry	Trans-Blot® SD, Semi-Dry Transfer Cell (Bio-Rad, Heidelberg)
WB imager	ChemStudio AS AnalytikJena

6.2 Consumables

15/50 mL Falcon tubes	Becton and Dickinson and Company, Franklin Lakes
6/10/15 cm dishes	Nunc (Thermo Fisher Scientific, Waltham)
96/48/24/12/6 well plates	Nunc (straight/conical) (Thermo Fisher Scientific, Waltham)
10 cm bacterial plates	BD Falcon™ (Becton and Dickinson and Company, Franklin Lakes)
8/16 well chambers	uncoated and coated 8-well imaging plate (Ibidi, Planegg)
1/2/5/10/25/50 mL plastic pipettes	Greiner Bio-One GmbH, Frickenhausen
adhesive covers	optical adhesive covers (Life Technologies, Frankfurt)
beads	Protein G Sepharose™ 4 Fast Flow (GE Healthcare, Penzberg)
	SureBeads™ Protein G magnetic beads (Bio-Rad, Feldkirchen)
blotting paper	whatman paper (GE Healthcare Buchler GmbH & Co. KG, München)
cell scrapers	Sarstedt, Nümbrecht
cell strainer	nylon cell strainer 70 µM (Falcon, Fisher Scientific, Waltham)
clamp (pancreas)	Bulldog SerrefinE - straight 35 mm (Fine Science Tools GmbH, Heidelberg
counting chambers	Bio-Rad
cryotubes	Sarstedt, Kleinstadt
cover slips	VWR International, Darmstadt

embedding moulds	Peel-A-WayR (Roth, Karlsruhe)
	Peel-A-Way embedding moulds, S-2 (Sigma Aldrich, Karlsruhe)
FACS tubes	5 mL polystyrene round bottom tube with cell strainer cap
	5 mL polystyrene round bottom tube (Falcon, Fisher Scientific, Waltham)
films	hyperfilm ECL (GE Healthcare Buchler GmbH & Co. KG, München)
	CEA, Rö. Blaufilm, RP new (Christiansen und Linhardt GmbH, München)
glass slides	Menzel Gläser superfrost plus (Thermo Scientific, Waltham)
microvettes	with clotting activator (Sarstedt, München)
needles	Sterican 27G 1/2 ", Sterican 30G 1/2 " (B.Braun, Puchheim)
nitrocellulose membrane	GE Healthcare Buchler GmbH & Co. KG, München
parafilm	Pechiney Plastic Packaging
PVDF membrane	Bio-Rad, München
scalpels	sterile (B.Braun, Tuttlingen)
syringes	Omnifix 3/30 mL; Omnican 50 mL (B. Braun Melsungen AG, Melsungen)
syringe filter	Millex-GP (Filter unit fast flow and low binding 0.22 µm)
pasteur pipettes, plastic	Roth, Karlsruhe
pasteur pipettes, glass	12/23 cm (LABOR-BRAND, Gießen; Hirschmann Laborgeräte GmbH & Co. KG, Eberstadt)
PCR tubes	Eppendorf, Hamburg
0.2/1.5/2 mL tubes	safe-lock reaction tubes (Eppendorf, Hamburg)

6.3 Chemicals

If not indicated otherwise, chemicals were obtained from Roth (Karlsruhe), Sigma-Aldrich (Hamburg) or Merck (Darmstadt).

A	acetic acid
	acrylamide/bis-acrylamide (Rotiphorese)
	agarose (Biozym Scientific)
	ammonium persulphate (APS)
B	Big Dye/Big Dye Buffer (Life Technologies 4337457 or Lager 500986)
	bovine serum albumin (BSA)
	Brij®010 (Sigma, Karlsruhe)
	bromophenol blue
C	calcium chloride
D	1,4-diazabocyclo[2.2.2]octan (DABCO)
	4', 6-diamidino-2-phenylindole (DAPI)
	developer G135 A/B (AGFA, Bonn)
	dimethyl sulfoxide (DMSO)
	dithiothreitol (DTT)
	dNTPs (Fermentas, St. Leon-Rot)
E	ethylene glycol-bis(β-aminoethyl ether)-N,N,N',N',-tetraacetic acid (EGTA)
	ethylenediaminetetraacetate (EDTA)
	5-Ethynyl-2'-deoxyuridine (EdU, Life Technologies, Frankfurt)
	ethanol
F	formaldehyde

G	glucose
	glutaraldehyde
	glycerol
	glycine
H	HEPES
	hydrochloric acid
I	isopropanol
M	magnesium chloride
	magnesium sulphate
	methanol
	milk powder
	mounting medium - Jung Tissue Freezing medium (Leica, Wetzlar)
N	nicotinamide adenine dinucleotide (NAD)
	nitrogen (l) (Linde AG, München)
	octylphenoxypolyethoxyethanol (Nonidet, NP-40)
O	Orange G
P	paraformaldehyde (PFA)
	polyethylene glycol (PEG)
	polyvinyl alcohol
	potassium chloride
	potassium dihydrogen phosphate
	potassium ferrocyanide
	potassium ferricyanide
R	rapid fixer G356 (AGFA)
	RNAse
S	sodium chloride
	sodium desoxycholate
	sodium dihydrogen phosphate
	sodium dodecyl sulphate
	sodium hydrogen carbonate
	disodium hydrogen phosphate
	sodium hydroxide
T	TEMED
	Tris(hydroxymethyl)aminomethane
	Triton X-100
	Tween-20
X	5-bromo-4-chloro-3-indolyl-β-D-galactopyranoside (X-Gal)

6.4 *In vivo* experiments

Animal experiments were performed at the central facilities at HMGU in accordance with the German animal welfare legislation and acknowledged guidelines of the Society of Laboratory Animals (GV-SOLAS) and of the Federation of Laboratory Animal Science Associations (FELASA). Post-mortem examination of organs was not subjected to regulatory authorization.

Mouse lines (for mating schemes, see results)

Rosa-Cre	(Grippo, Nowlin, Cassaday, & Sandgren, 2002)
FLPe	(Farley, Soriano, Steffen, & Dymecki, 2000)
Ngn3-Cre	(Desgraz & Herrera, 2009)
MIP-CreERT	(Tamarina et al., 2014)
FVFPBF^{DHom}: Foxa2-Venus-Fusion x Pdx-BFP-Fusion	(Bastidas-Ponce, Roscioni, et al., 2017)
Igfr-L1: C22Rik ΔEx3 and C22Rik floxed and C22Rik FD	5330417C22Rik$^{tm1a(EUCOMM)Hmgu}$ stem cells (H03) were aggregated with CD1 morula (Artus & Hadjantonakis, 2011)
Igfr-L2: L06Rik ΔEx6 and L06Rik FD	9330182L06Rik$^{tm1a(KOMP)Wtsi}$ mice were ordered from Jackson Laboratory
Ngn3-Cre x Igfr-L1 (FD)	Intercrosses between Ngn3-Cre and C22Rik FD
Ngn3-Cre x Igfr-L1 (FD) - CKO	Intercrosses between Ngn3-Cre x C22Rik FD and C22Rik floxed
FVFPBF^{DHom} x Igfr-L1 (ΔEx3)	Intercrosses between Foxa2-Venus-Fusion x Pdx-BFP-Fusion and C22Rik ΔEx3
FVFPBF^{DHom} x Igfr-L1 (FD)	Intercrosses between Foxa2-Venus-Fusion x Pdx-BFP-Fusion and C22Rik FD
FVFPBF^{DHom} x Igfr-L1 (floxed)	Intercrosses between Foxa2-Venus-Fusion x Pdx-BFP-Fusion and C22Rik floxed
Ngn3-Cre x FVFPBF^{DHom} x Igfr-L1 (FD)	Intercrosses between Foxa2-Venus-Fusion x Pdx-BFP-Fusion, C22Rik FD and Ngn-Cre3
Ngn3-Cre x FVFPBF^{DHom} x Igfr-L1 (FD) - CKO	Intercrosses between Foxa2-Venus-Fusion x Pdx-BFP-Fusion x C22Rik FD x Ngn-Cre3 and Foxa2-Venus-Fusion x Pdx-BFP-Fusion x C22Rik flox

Genotyping. Ear punches of weaned mice were digested in 500 µL tail lysis buffer (100 mM Tris pH 8.5, 200 mM NaCl, 5 mM EDTA, 0.2 % SDS) supplemented with proteinase K (100 µg/µL) at 55°C either for 2 h at 1400 rpm or overnight without agitation. DNA was precipitated by addition of 500 µL ice-cold isopropanol and pelleted at 14,000 rpm for 15 min at RT. The DNA pellet was washed with ice-cold 70 % ethanol, air-dried, dissolved in 100 µL nuclease-free water (NFW, Promega) and kept at 4°C. If not processed directly, biopsies were stored at -20°C.

DNA segments were amplified in a PCR: The mix contained DNA (1 µL), 10x Taq buffer without $(NH_4)_2SO_4$ and $MgCl_2$ (2 µL), 25 mM $MgCl_2$ (2 µL), 10 mM dNTP (1 µL), 10 µM primer (1 µL each) and 5 U/µL Taq DNA polymerase (0.3 µL) in a final volume of 20 µL. Gel electrophoresis was used to separate the amplified DNA segments by size. Therefore, 2 g agarose powder were dissolved in 100 mL Tris acetate-EDTA buffer (40 mM Tris, 1 mM glacial acetic acid, 1 mM EDTA) using a microwave. The solution was cooled down,

supplemented with 8 µL Midori Green Advance gel stain (NIPPON Genetics EUROPE GmbH, MG04) and poured into a gel tray equipped with 18x well combs. The samples were mixed with OrangeG (1:5) and loaded onto the polymerized gel which was placed into a gel chamber and covered with TAE buffer. After applying 100 V for 30-60 min, the separated bands were detected with UV-light in a gel documentation system.

Gene	Primers	PCR program	Size
Rosa-Cre	EP 0485 EP 0486	94°C 5min [94°C 30s / 58°C 40s / 72°C 90s] x 35 72°C 2min 16°C ∞	Rosa-Cre+: 450 bp
FLPe	EP 0176 EP 0177	94°C 5min [94°C 60s / 50°C 60s / 72°C 60s] x 36 72°C 10min 16°C ∞	FLPe+: 550 bp
Ngn3-Cre	EP 1842 EP 1843 EP 1844 EP 1845	94°C 3min [94°C 30s / 53°C 1min / 72°C 1min] x 35 72°C 10min 16°C ∞	Ngn3-Cre+: 430 bp ctrl: 180 bp
MIP-CreERT	EP 1486 EP 1487 EP 1433 EP 1436	94°C 5min [94°C 30s / 58°C 40s / 72°C 90s] x 35 72°C 2min 16°C ∞	MIP-CreERT+: 413 bp ctrl: 280 bp
Foxa2-Venus-Fusion	EP 0038 EP 0397 EP 0398	94°C 4min [94°C 30s / 56°C 60s / 72°C 60s] x 35 72°C 10min 16°C ∞	FVF: 506 bp WT: 207 bp
Pdx-BFP-Fusion	EP 1188 EP 1189 EP 1193	94°C 4min [94°C 30s / 56°C 60s / 72°C 60s] x 35 72°C 10min 16°C ∞	PBF: 421 bp WT: 211 bp
C22Rik ΔEx3/flox	EP 1584 EP 1585 EP 1586	95°C 3min [95°C 30s / 64°C 45s / 72°C 45s] x 1 [95°C 30s / 55°C 30s / 72°C 30s] x 35 72°C 5min 16°C ∞	ΔEx3: 341 bp WT: 239 bp flox**:** 431 bp
C22Rik FD/flox	EP 1270 EP 1425 EP 1583	95°C 3min [94°C 30s / 64°C 45s / 72°C 45s] x 9 [95°C 30s / 55°C 30s / 72°C 30s] x 35 72°C 5min 16°C ∞	FD: 285 bp WT**:** 395 bp flox: 431 bp
L06Rik ΔEx6	EP 1347 EP 1674 EP 1675	94°C 5min [94°C 30s / 57°C 30s / 72°C 45s] x 35 72°C 5min 16°C ∞	ΔEx6: 190 bp WT**:** 430 bp
L06Rik FD/ flox	EP 1752 EP 1683 EP 1682	94°C 5min [94°C 30s / 57°C 30s / 72°C 45s] x 35 72°C 5min 16°C ∞	FD: 295 bp WT: 431 bp flox: 404 bp

ID	T_m (°C)	sequence 5' → 3'
EP 038	60	CAAGATCCGCCACAACATCG
EP 0176	57	CTAATGTTGTGGGAAATTGGAGC
EP 0177	54	CTCGAGGATAACTTGTTTATTGC
EP 1188	72	TACTGCCTTCGGGCCTTAGCGTGTC
EP 1189	68	CGGCTATACCCAACTGGCTCTCG
EP 1193	67	CAGTCCGTGCTGAGCAAAGACC
EP 1270	63	CCAAGGCCAGCGATACAACC
EP 1374	59	GTCTGGATCCGGAATAACTTCG
EP 1425	59	GGAACTTCGTCGAGATAACTTCGTATAG
EP 1433	64	TTACAGCTGACCTGATGGAGTTG
EP 1436	64	CTGAGCCCTAGTCATTGCATACTG
EP 1486	70	CCTGGCGATCCCTGAACATGTCCT
EP 1487	65	TGGACTATAAAGCTGGTGGGCAT
EP 1583	59	GTGCACTCTGGGTAGTGTTC
EP 1584	62	GATGCCTGTCAGCCTTCATC
EP 1585	66	CACCTCCCCCTGAACCTGAAAC
EP 1586	63	GAGTGGGATGAGCTACCTCAC
EP 1674	58	TCAAGCCCGTGCTAGTAAAG
EP 1675	60	GCTCAGAAAGGCACAAGAGG
EP 1682	61	TCAAGCCCGTGCTAGTAAAG
EP 1683	62	GCTCAGAAAGGCACAAGAGG
EP 1752	62	AAGGCGCATAACGATACCAC
EP 1842	58	TCGATGCAACGAGTGATGAG
EP 1843	56	GCGATCGCTATTTTCCATGA
EP 1844	60	CGTGGAACTGTGAGCTTTGTG
EP 1845	63	AAGGATCACAGAGCTGAGGCTG
EP 397	57	CTACTACCAAGGAGTGTACTCC
EP 398	59	CTGTGGCCCATCTATTTAGGG
EP 485	65	ATGCCCAAGAAGAAGAGGAAGGT
EP 486	67	GAAATCAGTGCGTTCGAACGCTAGA

E19.5. Intercrosses of Igfr-L1$^{+/-}$ (ΔEx3) animals were set-up during the day and plug-checks were performed. At E19.5, embryos were obtained by Cesarian section, weighed and decapitated for dissection of the pancreas. Gross morphological images were acquired before fixation.

LacZ staining. Solution 1: 0.02 % NP-40, 5 mM EGTA, 2 mM $MgCl_2$, 1 % formaldehyde, 0.2 % glutaraldehyde in PBS; solution 2: 0.02 % NP-40, 2 mM $MgCl_2$, 5 mM $K_3[Fe(CN)_6]$, 5 mM $K_4[Fe(CN)_6]$ x 6 H_2O, 0.01 % sodium desoxycholate, 1 mg/mL X-Gal; Wash buffer: 0.02 % NP-40 in PBS.
Dissected pancreata (E19.5) were fixed in solution 1 for 1 h at room temperature (RT) under rotation, washed 3x and incubated for 2 h in solution 2. Samples were washed 3x and fixed in 4 % paraformaldehyde (PFA) for 1 h. After image acquisition, pancreata were embedded in paraffin.

Dynamic GSIS. Krebs-Ringer-buffer (KRB): 140 mM NaCl, 3.6 mM KCl, 0.5 mM NaH_2PO_4, 0.5 mM $MgSO_4$ x 7 H_2O, 1.5 mM $CaCl_2$, 10 mM HEPES, 2 mM $NaHCO_3$, 0.1 % BSA, pH 7.4.
Pancreata of Igfr-L1$^{+/+}$ and Igfr-L1$^{-/-}$ neonates were dissected at E19.5 and kept in KRB buffer in the incubator until perfusion. Dynamic GSIS was performed together with Dr. Ansarullah:

Columns were loaded with beads and pancreata embedded inside. The flow through was collected in 96 well plates every minute and stored at -20 °C until performance of the insulin ELISA (Mercodia) by Dr. Ansarullah.

Islet isolation. G-solution (500 mL): HBSS (Lonza Verviers, Belgium), 1 % P/S (Gibco, Invitrogen, Carlsbad, CA), 1 % BSA, sterile filtered (Sigma, Hamburg); gradient solution (10 mL): 5 mL G-solution, 30 µL 1 M HEPES (Life Technologies, Frankfurt), 970 µL DPBS (Lonza Verviers, Belgium), 2 mL Optiprep 60 % density gradient medium (D1556 – 250 mL; Sigma, Hamburg); collagenase P solution: 1 mg/mL collagenase P (Roche, Penzberg) in G-solution.
Before injection of collagenase P solution (3 mL) into the pancreatic duct, the ampulla was sealed with a clamp. The inflated pancreas was dissected, transferred into a Falcon tube with collagenase P solution (3 mL) and digested for 15 min in a 37 °C water bath with gentle inversion after 7.5 min. After adding G-solution (5 mL) to inactivate the enzyme, the digested pancreas was mechanically dissociated by pipetting up and down and centrifuged for 3 min at 1620 rpm at 4 °C. The supernatant was discarded and the pellet re-suspended in gradient solution (5.5 mL), slowly added on top of gradient solution (2.5 mL) in a Falcon tube and then overlaid with G-solution (6mL). After incubation for 10 min at RT, the three phases were carefully (acceleration 3, break 0) separated for 10 min at 1600 rpm at RT. By this, islets were enriched in the interphase of the upper and the middle phase, which was pipetted through a pre-wetted 70 µm cell strainer to retain the islets. Washed islets were transferred into culture medium and picked under a stereo microscope to remove any exocrine cells. Islets were cultured in RPMI 1640 + 10 % FCS and 1 % P/S overnight until analysis. For IHC, either whole mount, adherent after dissociation or cryosectioned islets were used. For WB, islets were washed with PBS and sonicated for further processing.

MIP-CreERT induction *ex vivo*. Isolated βCKO and ctrl islets were incubated with tamoxifen (1 µM in dimethyl sulfoxide (DMSO)) or vehicle. For IHC, whole or dispersed islets (5 min, TriplE) were fixed after 24 and 48 h or 48 h followed by a 72 h wash period. For Insr/Igf1r signaling, islets were induced for 48 h and kept another 72 h in medium to wash out tamoxifen. Islets were starved for 2 h in HBSS and stimulated with 10 nM insulin (Actrapid, NovoNordisk) for 5 min before WB. For proliferation analysis, islets were induced for 48 h followed by a 72 h wash period and 24 h incubation with EdU (10 µM in PBS) until fixation. EdU incorporation was visualized on cryosections by using a Click-iT-EdU imaging (Alexa Fluor® 647) kit (Thermo, C10340).

ipGTT. Glucose tolerance (GTT) was analyzed by injecting mice intraperitoneally with 1-2 g glucose/ kg BW after a 6 h morning or overnight fast. Blood glucose levels (mg/dL) were determined with a glucometer (FreeStyle, Abbot; ContourXT, Ascenia) before and 15, 30, 60 and 120 min after glucose administration.

ITT. Insulin tolerance (ITT) was analyzed by injecting 0.25 IU/g BW insulin (Actrapid, NovoNordisk) intraperitoneally after 6 h fasting. Blood glucose levels (mg/dL) were determined with a glucometer (ContourXT, Ascenia) before and 2.5, 5, 10 and 20 min after insulin administration.

Insulin and C-peptide. Blood was collected in microvettes coated with clotting activator. Serum was separated at 3600 rpm for 4 min at 4°C, kept on dry ice and stored at -80 °C. Insulin and C-peptide were measured according to the manufacturer's protocol (Ultra sensitive mouse insulin ELISA kit, CrystalChem, 90080; mouse C-peptide ELISA kit, CrystalChem, 90050).

6.5 *In vitro* experiments

Cell culture. Min6 wildtype (M9 and K8, S.Seino, Japan) and KO cells were cultured in DMEM (4.5 g/L glucose + L-glutamine + pyruvate) supplemented with 10 % FBS (FBS Good), 1 % P/S (10,000 U/mL) and 70 µM β-Mercaptoethanol. EndoC-βH1® (Univercell Biosolutions®, Inc.) were cultured according to the manufacturer's protocol in complete culture medium (OPTIβ1®) on 10 cm dishes (TPP) with coating matrix (βCOAT® in DMEM 4.5 g/L glucose + 1 % Penicillin/Streptomycin). MCF7 cells were cultured in DMEM (4.5 g/L glucose + L-glutamine + pyruvate) supplemented with 10 % FBS (FBS Good), 1 % P/S (10,000 U/mL) and 10 µM β-Estradiol.
For passaging, adherent Min6 and MCF7 or EndoC were washed with DPBS (-$CaCl_2$, -$MgCl_2$) and detached with 0.05 % trypsin-EDTA for 3 min at 37 °C. After enzyme inactivation with medium or neutralization buffer (20 % FCS in PBS, sterile filtered), cells were counted and pelleted at 1700 rpm for 3 min or 700 g for 5min. After resuspension in a suitable volume depending on the desired concentration, cells were seeded onto new culture dishes or plates. For cryopreservation, pelleted cells were re-suspended in FBS, mixed 1:1 with FBS containing 20 % DMSO and transferred to cryovials (2 mL). Cryovials were quickly frozen on dry ice, kept for one night at -80 °C and transferred to liquid nitrogen. For culturing, cryopreserved cells were thawed in a water bath (37 °C) and mixed with 8 mL of pre-warmed medium. After pelleting cells at 1700 rpm for 3 min or 700 g for 5 min to remove DMSO, cells were re-suspended in the volume according to the dish size. Medium was changed the next day to remove any dead cells.

CRISPR/Cas9-mediated KO. Two single guide RNAs (sgRNA) flanking the start codon ATG of *Igfr-L2* were chosen according to http://crispr.mit.edu and cloned into the expression vector (see 4.7.1).
For plasmid digestion, ca. 1 µg DNA (Pbs-U6-chimeric RNA, E234), 1 µL enzyme (BbsI) and 2 µL buffer (CutSmart) were incubated in a final volume of 20 µL for 1.5 h at 37 °C. Ligation with T4 DNA ligase of the linearized plasmid and the sgRNAs was performed for 1 h at 37 °C. The ligation products were separated in an agarose gel, the correct size was excised and purified by gel extraction according to the manufacturer's protocol.
For sequencing as quality control, the DNA was amplified with fluorescent dNTPs. Therefore, 2 µL Big Dye buffer, 0.5 µL Big Dye including the polymerase, the pbsU6-primer (EP 1512, 10 pM) and the DNA were incubated in a total volume of 5 µL for 1 min at 96°C and 35 cycles of [96°C 10s / 50°C 5s / 60°C 4min] until cooling to RT. For subsequent purification, the amplified DNA sequence was precipitated with a mixture of 50 µL EtOH, 0.5 µL 125 mM EDTA and 2 µL 3M NaAc during 15 min incubation at RT and pelleted at 11,000 rpm for 30 min at 4°C. After washing with 70 % EtOH, the pellet was air-dried and dissolved in 25 µL HPLC-H_2O. Samples were transferred into a 96-well plate and analyzed by the HMGU sequencing core facility.
For transformation of chemo-competent bacterial cells, E.coli Dh5α (100 µL) were thawed on ice for 10 min and plasmid DNA (2 µL) was added. After 7 min incubation on ice, cells were heat-shocked for 90 s at 42 °C and re-suspended in pre-warmed LB medium (1 mL). After 45 min incubation at 37 °C at 900 rpm, bacteria were pelleted for 3 min at 5000 rpm and re-suspended in LB medium (100 µL). One third was plated on ampicillin agar plates with glass spheroids and incubated overnight at 37 °C.
For plasmid preparation, bacterial colonies were picked with sterile pipette tips and inoculated in 3 mL LB-medium supplemented with ampicillin (1:1000) at 37 °C at 300 rpm overnight (mini preparation) or for 8 h (pre-culture) and overnight after transfer to 200 mL LB medium (maxi preparation). For mini preparations, 2 mL of the overnight culture were transferred to an Eppendorf tube and the bacteria pelleted at 8000 rpm for 2 min. The pellet

was lysed in 350 µL P1 by vortexing and incubated for 5 min after addition of 350 µL P2 and inversion. 350 µL P3 was added and the inverted solutions incubated first 10 min at 37 °C and then 10 min on ice. After centrifugation at 14,000 rpm for 10 min, 900 µL of the supernatant were transferred to a new Eppendorf tube and DNA precipitated by addition of 650 µL isopropanol. DNA was pelleted at 14,000 rpm for 15 min and washed with 750 µL 70 % EtOH. The pellet was air-dried and dissolved in 100 µL nuclease-free water and the concentration adjusted to approximately 1 µg/µL. For maxi preparation, the QIAGEN kit (12163) was used according to the manufacturer's protocol. Because of subsequent transfection of cells, the endotoxin-free kit was used.
For transfection, Lipofectamine 2000 (11668030, Thermo) was used according to the manufacturer's protocol. Shortly, OptiMem containing Lipofectamine and 5 µg plasmid DNA, i.e. the two sgRNA plasmids and Cas9-Venus E246, were added to the cells for 24 h. Transfection efficiency was determined after 48-72 h.
For FACS, cells were detached with 0.5 % trypsin/EDTA or 5 mM EDTA in PBS at 37 °C. After addition of medium, cells were pelleted at 1700 rpm for 3 min and resuspended in medium with only 2 % FCS. Cells were transferred to a FACS tube with a 70 µm filter to remove clusters and kept on ice. Cells were gated according to their forward (size) and sideward (granularity) scatter height as single cells. Sorted Cas9-Venus-positive cells were seeded in low density so that single colonies could be picked under a stereo microscope. Expanded cells were characterized as KO in ICC and WB.

Because of the low percentage of KO clones due to the transfection with three single plasmids and only the detection of the Cas9 plasmid by FACS, another targeting strategy was pursued. Clone Manager was used for sequence information as well as for planning and controlling the procedure. Plasmids for the new targeting strategy were generated as described previously (Yumlu et al., 2017). Shortly, plasmids E298 (Cas9-Venus) and E299 (Cas9-RFP) were digested with AscI and ligated with the sgRNAs. sgRNAs were amplified from the vector by using the following primers Igfr-L1-1 A_F + A_R and Igfr-L1-2 B_F + C_R, Igfr-L2-1 A_F (EP 1754) + A_R and Igfr-L2-2 B_F + C_R. The PCR was performed with Phusion: 35 µL NFW + 10 µL HF buffer + 1 µL dNTPs (10 mM) + 2.5 µL primer (10 µM each) + 1 µL DNA + 0.5 µL Phusion in a total volume of 50 µL. The PCR products were separated on a gel and a gel extraction performed. For Gibson assembly, 15 µL of a master mix containing isothermal buffer (5x: 25 % PEG 8000, 500 mM Tris-HCl pH 8.5, 50 mM $MgCl_2$, 50 mM dithiothreitol (DTT), 1 mM dNTPs, 5mM NAD, in H2O), T5 exonuclease, Phusion polymerase and Taq ligase in H_20 were added to ca. 100 ng linearized plasmid and 1 µL of each sgRNA PCR product and incubated for 2 h at 55 °C. A check-cut with SpeI was performed for quality control resulting in 6659 bp and 3861 bp for E298-Igfr-L1 or 5926 bp, 3069 bp, 2231 bp and 809 bp for E299-Igfr-L2. Sequencing was performed with primers EP1486, EP 0034 (only E298), EP 1558, EP 1512 or EP 1304.
In order to avoid clonal variances, cells were sorted in bulk. For the separation of homozygous from heterozygous or non-targeted cells, an anti-ectodomain-IGFR-L1 (19A6) labeled with Alexa Fluor® 488 was used. Transfection efficiency, which was lower for Min6 K8, as well as antibody concentration and incubation time were optimized. Finally, cells from a 6 well were incubated with 20 µg of antibody for 30 min at 37 °C, washed with PBS and trypsinized for 3 min at 37°C to cleave non-internalized and unspecifically bound antibodies. Unfortunately, sorted cells appeared dedifferentiated and were not proliferative anymore.

Starvation and stimulation. HEPES balanced salt solution (HBSS): 114 mM NaCl, 4.7 mM KCl, 1.2 mM KH_2PO_4, 1.16 mM $MgSO_4$, 20 mM HEPES, 2.5 mM $CaCl_2$, 25.5 mM $NaHCO_3$ (pH 7.2). Min6 under growth conditions were washed 5x with PBS and incubated for the

indicated durations in HBSS (starvation). Stimulation was performed after 1 h starvation with 25 mM glucose or 100 nM insulin in HBSS for 15 min.

(Co-) Immunoprecipitation. Sepharose or magnetic beads coated with protein G were incubated under rotation either with the primary antibody for 1 h at RT and overnight at 4 °C with protein lysate or overnight with protein lysate that was pre-incubated for 2 h with the primary antibody. Subsequently, beads were washed 3x with lysis buffer and precipitated proteins were eluted by boiling the samples in Laemmli-buffer + DTT (1:1) for 5 min at 96 °C.
The following primary antibodies were used: For anti-IGFR-L1 see Table 4.3.1.1; mouse anti-AP2β (1:100, BD, 610382); rabbit-anti IGFR-L1 (1 µg/ 100 µg protein, 1374); rat anti-IGFR-L1 (1 µg/ 100 µg protein, 16F6); mouse anti-INSRβ (1:100, CST, 8138); rabbit anti-INSRβ (1:100, CST, 3025); rabbit anti-IGF1Rβ (1:100, CST, 9750). For HPLC-MS analysis, co-IPs (see 4.3.2) were eluted with 100 mM glycine pH 3 and neutralized with Tris/glycine buffer, pH 8.0. Samples were further processed by Dr. Carsten Boldt, University of Tübingen.

Surface biotinylation. Wildtype and Igfr-L1$^{-/-}$ Min6 cells under growth conditions were washed 5x with PBS and starved for the indicated time points in HBSS. For surface-biotinylation, cells were washed 3x with ice-cold PBS (pH 8.0) and incubated with 2 mM EZ-Link™ Sulfo-N-Hydroxysulfosuccinimide-LC biotin reagent (21335, Thermo) in PBS (pH 8.0) for 10 min on ice. The biotin reagent was quenched by washing 3x with 100 mM glycine in PBS (pH 8.0). Cell lysates were split into input and affinity purification i.e. incubation with Pierce™ High Capacity NeutrAvidin™ Agarose (29202, Thermo) or magnetic Pierce™ Streptavidin magnetic beads (88816, Thermo) overnight at 4°C under rotation. After washing beads 3x with lysis buffer, biotinylated proteins were eluted with 4x Laemmli buffer + DTT (1:1) at 95 °C for 5 min for WB analysis.

Proximity ligation assay (PLA). The PLA was performed according to the manufacturer's protocol (Duolink® In Situ Detection Reagents Orange, Sigma, DUO92007-100RXN). Shortly, samples were prepared as for conventional ICC and processed with extensive washing with appropriate buffers between all steps. Mouse and rabbit primary antibodies were incubated overnight. PLA probes (DUO92001/92002/92004/92005, Sigma) were incubated for 1 h at 37 °C and ligation of oligonucleotides performed for 30 min at 37 °C. The rolling circle amplification was performed during incubation for 100 min at 37 °C. Nuclei were stained with DAPI and the cytoskeleton labeled with Phalloidin-Fluor® 488 for 2 h at RT. Cells were kept in Elvanol until microscopic analysis with the Leica SP5 confocal.
The following primary antibodies were used: rabbit-anti IGFR-L1 (1:1000, 1374); mouse anti-IGFR-L1 (1:500, 36D7); mouse anti-INSRβ (1:100, CST, 8138); rabbit anti-INSRβ (1:100, CST, 3025); rabbit anti-IGF1Rβ (1:100, CST, 9750); rabbit anti-INS (1:500, CST, 3014); mouse anti-INS (1:500, CST, 8138); mouse anti-IGFR-L2 (1:100, 28D9) and Phalloidin Alexa Fluor® 488 (1:100, Thermo, A12379).

Cell cycle analysis. For cell cycle analysis, harvested cells were fixed for 10 min at RT with 70 % EtOH (pre-cooled to -20 °C overnight) and pelleted at 1700 rpm for 3 min. After permeabilization for 15 min at RT in 0.25 % Triton-X100, 100 mM glycine, the pellet was re-suspended in 20 µg/mL propium iodide (Sigma, P-4170) in PBS supplemented with 10 µg/mL RNAse A and incubated for 30 min at RT in the dark. Cells were transferred to filter-cap FACS tubes and analyzed by FACS with the filter sets for PE Texas-Red and a linear intensity scale. Cells were gated according to their forward (size) and sideward (granularity) scatter height as single cells.

Proliferation (EdU). Cells were washed 3x with PBS and incubated for 4 h in a 1:500 and 1:1000 solution of 10 µM EdU in medium. After fixation, incorporated EdU was visualized according to the manufacturer's protocol (Click-iT EdU imaging kit, Alexa Fluor® 647, Thermo, C10340). LSM images were acquired and DAPI as well as EdU-positive cells quantified with IMARIS using the dot tool.

6.6 Immunostaining

Donkey blocking solution (DBS): 0.1 % Tween-20, 10 % FCS, 0.1 % BSA and 3 % donkey serum in PBS; Elvanol: 0.015 mM polyvinyl alcohol, 24 mM Tris pH 6.0, 2 g DABCO in 90 mL H_2O and 37.8 mL glycerol.

Immunocytochemistry (ICC). Cells seeded in ibidi chambers or glass bottom plates were rinsed with PBS, fixed in 4 % PFA for 10 min at RT, permeabilized in 0.1 % Triton-X100, 100 mM glycine in PBS for 15 min at RT and blocked for 60 min in DBS. Primary antibodies were diluted respectively in DBS and incubated overnight at 4 °C with agitation. After washing 3x with PBS-T for 10 min, cells were incubated with secondary fluorophore-labeled antibodies diluted 1:800 in DBS for 120 min at RT. After rinsing with PBS, nuclei were stained with DAPI diluted 1:500 in PBS-T for 20 min at RT. After washing 3x in PBS-T for 10 min, cells were embedded in Elvanol and stored at 4 °C until image acquisition.

Immunohistochemistry (IHC). Tissues or islets were washed with PBS and fixed in 4 % PFA overnight at 4 °C with agitation. Dehydration was performed by incubation in a sucrose gradient (10 % and 30 % in PBS) for 4 h each at 4 °C with agitation. Before embedding in OCT (optimal cutting temperature) medium, samples were incubated overnight in a mixture of 30 % sucrose and OCT (1:1). Cryomoulds were frozen on dry ice and stored at -80 °C. Slides with 3x 20 µm sections with a distance of 100 µm in between were cut at -20 °C with the Cryostat and stored at -20°C. After rehydration in PBS for 10 min, sections were permeabilized in 0.25 % Triton-X100, 100 mM glycine in PBS for 30 min at RT and blocked for 60 min in DBS. Primary antibodies were diluted respectively in DBS and incubated overnight at 4 °C and additionally 120 min at RT. After washing 3x in PBS-T for 10 min, cells were incubated with secondary fluorophore-labeled antibodies diluted 1:800 in DBS for 4 h at RT. After rinsing with PBS, nuclei were stained with DAPI diluted 1:500 in PBS-T for 30 min at RT. After washing 3x in PBS-T for 10 min, cells were mounted with Elvanol and Mendel's cover slips #1.5, dried overnight at RT and stored at 4 °C until image acquisition.
Human pancreas biopsies were provided by collaboration with and islet samples were obtained via the Islet Core Facility of the McDonald laboratory (Alberta, Canada).

Primary antibodies: rabbit-anti IGFR-L1 (1:1000, 1374); rat anti-IGFR-L1 (1:500, 16F6); mouse anti-IGFR-L1 (1:500, 36D7); mouse anti-IGFR-L2 (1:100, 28D9); rat anti-IGFR-L2 (1G6, 1:100). For IHC, rabbit-anti AMYα (1:300, abcam, ab21156); goat anti-CHRA (1:100, SCBZ, sc-1488); rabbit anti-ECAD (1:100, CST, 3195); guinea pig anti-GCG (1:3000, Takara Bio, M182); rabbit anti-GCG (1:1000, ENZO Life Sciences, NOBML-GA1181-0025); guinea pig anti-INS (1:50, Thermo, PA1-26938); guinea pig anti-INS (1:300, ABD Serotec, 5330-0104G); rabbit anti-INS (1:300, CST, 3014); rabbit anti-SOX9 (1:300, Millipore, AB5535); rabbit anti-ACTH (1:100, Abcam, ab74976); goat anti-GH (1:100; R&Dsystems, AF1067); rabbit anti-UCN3 (1:300; Phoenix Pharmaceuticals; H-019-29); rabbit anti-GLUT2 (1:100, Millipore, 07-1402); rabbit anti-pHH3 (1:300; Millipore; 06-570). For ICC, mouse anti-CM1 (1:300, Dr. Coskun, PLID); rabbit anti-EEA1 (1:300, CST, 2411); rabbit anti-Ergic53 (1:300, SCBT, sc-66880); rabbit anti-GOLGB1 (1:100, BioLegend, 924302); mouse anti-GM130

(1:300, BD, 610822); rat anti-LAMP2 (1:100; Abcam, ab13524); rabbit anti-RAB7 (1:100, CST, 9367); rabbit anti-TGN46 (1:100, Abcam, ab16059).
Secondary antibodies (1:800): donkey anti-goat Alexa Fluor® 488 (Invitrogen, A11055) or Alexa Fluor® 555 (Invitrogen, A21432); donkey anti-guinea pig Alexa Fluor® 488 (Dianova, 706-545-148) or Alexa Fluor® 555 (Invitrogen, A21435) or Alexa Fluor® 649 (Dianova, 706-495-148); donkey anti-mouse (Invitrogen, A21202) or Alexa Fluor® 555 (Invitrogen, A31570) or Alexa Fluor® 633 (Invitrogen, A21052); donkey anti-rabbit Alexa Fluor® 488 (Invitrogen, A21206) or Alexa Fluor® 555 (Invitrogen, A31572) or Alexa Fluor® 647 (Invitrogen, A31573); donkey anti-rat Alexa Fluor® 488 (Invitrogen, A21208) or Cy3 (Dianova, 712-165-153) or Alexa Fluor® 647 (Dianova, 712-605-150);

Laser scanning microscopy (LSM) images were acquired on a Leica SP5 or a Zeiss LSM 800 Airy Scan confocal microscope equipped with 405 nm, Argon, 561, 594 and 633 nm lasers and processed with the LAS AF or Zen blue software, respectively.
LSM images were quantified with IMARIS. For differential expression in diabetic animals, the insulin and glucagon channels were combined and a surface created, in which the mean intensity of the Igfr-L1 channel was determined.

Anti-IGFR-L2 antibodies. For antibody information see 4.5.1. Antibodies (SN, 1:10) were tested on wildtype and Igfr-L2$^{-/-}$ Min6 cells for specificity in ICC and WB in respect of their predicted IgG subclass. After binding of the primary antibody, cells were first incubated with the secondary subclass-specific unlabeled antibody diluted 1:5 in donkey blocking solution for 60 min at RT. Antibodies were provided by Dr. Regina Feederle, i.e. rat anti-mouse IgG 2a, 2b, 2c, G1, G2 and mouse anti-rat IgG 2a, 2b, 2c. After washing 3x in PBS-T for 10 min, a secondary fluorochrome-labeled antibody against the species of the first secondary antibody of the sandwich was used according to the standard protocol.

6.7 Western Blot

RIPA buffer: 50 mM Tris-HCl, 150 mM NaCl, 1 mM EDTA, 1 % NP-40, 0.1 % sodium dodecyl sulphate (SDS), 0.5 % sodium desoxycholate; HEPES-CHAPS buffer: 200 mM NaCl, 50 mM HEPES, 2 % CHAPS; BrijO10 buffer: 100 mM Tris-HCl, 150 mM NaCl, 1 % Triton-X100, 1 % Brij®010; 4x SDS loading buffer (Laemmli): 200 mM Tris-HCl, pH 6.8, 8 % SDS, 40 % glycerol, 0.4 % bromophenol blue; separating gel buffer (4x Tris-HCl/SDS buffer, 1.5 M Tris-HCl, 0.4 % SDS, pH 8.8); stacking gel buffer (4x Tris-HCl/SDS buffer, 500 mM Tris-HCl, 0.4 % SDS, pH 6.8); 10 % ammonium persulfate (APS) in H_2O; Tris-glycine running buffer: 25 mM Tris-HCl, 192 mM glycine, 0.1 % SDS; anode buffer I (API): 300 mM Tris-HCl, 10 % MeOH; anode buffer II (APII): 25 mM Tris-HCl, 10 % MeOH; cathode buffer (KP): 25 mM Tris-HCl, 40 mM glycine, 10 % MeOH; TBS-T: 10 mM Tris-HCl, 150 mM NaCl, 0.1 % Tween, pH 7.4.

Tissues or cells were rinsed with PBS and lysed on ice in lysis buffer supplemented with protease inhibitor cocktail (Sigma, P8340, 1:100), phosphatase inhibitor cocktail 2 (Sigma, P5726, 1:100) and 3 (Sigma, P0044, 1:100) and phenyl-methylsulfonic acid (PMSF, 1mM in EtOH, 1:1000). Cells were sheared with a cell scraper, whereas tissues were homogenized by sonication or in a tissuelyser. After centrifugation at 14,000 rpm for 15 min at 4 °C, the supernatant was collected and the protein concentration determined with the Pierce bicinchoninic acid (BCA) assay kit (23225, Thermo Scientific) according to the manufacturer's protocol. All samples were adjusted to the same concentration and boiled for 5 min at 95 °C after addition of 4x Laemmli buffer mixed 1:1 with 2 M dithiothreitol (DTT).

Denaturing sodium dodecylsulfate - polyacrylamide gel electrophoresis was performed to separate proteins of cell and tissue lysates by size according to the standard procedure. Loaded protein samples were separated in 6.5-10 % polyacrylamide gels for 1-2 h at 120 V together with pre-stained proteins (PageRuler, Life Technologies) and transferred to a polyvinylidendifluoride membrane by semi-dry transfer for 30 min at 0.22 A (25 V) per gel.
Membranes were blocked in 5 % milk in TBS-T for 60 min at RT before incubation of primary antibodies diluted in 5 % milk overnight at 4 °C on a rocker. After washing 3x 10 min in TBS-T, secondary horseradish peroxidase-labeled antibodies diluted 1:10,000 in 5 % milk were incubated for 1-2 h at RT on a rocker. After washing 3x 10 min in TBS-T, Western blots were developed in enhanced chemoluminescence solution (ECL, Bio-Rad, #1705061) for 3 min and covered with foil. In the dark room, X-ray films were exposed to the membranes from 1 s up to 20 min in a hypercassette and developed in a developer machine. In the Western Blot imager, emitted photons were captured by a camera and displayed as gray values.

Primary antibodies: mouse anti-AMPK α (1:1000, CST, 2532); rabbit anti-AMPK α-phospho (1:1000, CST, 2535); mouse anti-AP2β (1:500, BD, 610382); rabbit anti-HSP90 (1:10000, CST 4874); rabbit anti-IGF1Rβ (1:1000, CST, 9750); mouse anti-INSRβ (1:1000, CST, 8138); rabbit anti-INSRβ (1:1000, CST, 3025); rabbit anti-INSR/IGF1R-phospho (1:500, CST, 3024); mouse anti-TUB α (1:10000, Sigma, T6199); mouse anti-TUB γ (1:10000, Sigma, T5326); rat anti-IGFR-L1 16F6 (purified 1:1000); mouse anti-IGFR-L2 28D9 (SN, 1:10); rat-anti-IGFR-L2 1G6 (SN, 1:10); mouse anti-ACT (1:10000, BD, 612656)
Secondary antibodies (1:10,000): goat anti-mouse (Dianova 115-036-062 or DAB-087641); goat anti-rabbit (Dianova, 111-036-045 or DAB-087729); rabbit anti-rat (abcam, ab6734); goat anti-rat (Dianova, 112-035-175).
Quantification by densitometric analysis of unsaturated protein bands was performed with ImageJ. Protein abundance was normalized to that of a reference protein (loading control) such as Tubulin, Actin or HSP90. Phospho-protein abundance was additionally normalized to that of the total protein.

6.8 Statistics

Statistical analyses were performed with GraphPad Prism. Error bars represent SEM and *, $P<0.05$; **, $P<0.01$; ***, $P<0.001$. *P*-values were analyzed using a two-tailed, unpaired student's t-test or 1way-ANOVA with Bonferroni post-test for comparison of more than two groups or 2way-ANOVA with Bonferroni post-test in case of two parameters.

7. References

Abu-Gazala, S., Horwitz, E., Ben-Haroush Schyr, R., Bardugo, A., Israeli, H., Hija, A., . . . Ben-Zvi, D. (2018). Sleeve Gastrectomy Improves Glycemia Independent of Weight Loss by Restoring Hepatic Insulin Sensitivity. *Diabetes, 67*(6), 1079-1085. doi:10.2337/db17-1028

Aguayo-Mazzucato, C., & Bonner-Weir, S. (2018). Pancreatic beta Cell Regeneration as a Possible Therapy for Diabetes. *Cell Metab, 27*(1), 57-67. doi:10.1016/j.cmet.2017.08.007

Alberti, K. G., & Zimmet, P. Z. (1998). Definition, diagnosis and classification of diabetes mellitus and its complications. Part 1: diagnosis and classification of diabetes mellitus provisional report of a WHO consultation. *Diabet Med, 15*(7), 539-553. doi:10.1002/(SICI)1096-9136(199807)15:7<539::AID-DIA668>3.0.CO;2-S

American Diabetes, A. (2009). Diagnosis and classification of diabetes mellitus. *Diabetes Care, 32 Suppl 1*, S62-67. doi:10.2337/dc09-S062

Annunziata, M., Granata, R., & Ghigo, E. (2011). The IGF system. *Acta Diabetol, 48*(1), 1-9. doi:10.1007/s00592-010-0227-z

Araki, E., Lipes, M. A., Patti, M. E., Bruning, J. C., Haag, B., 3rd, Johnson, R. S., & Kahn, C. R. (1994). Alternative pathway of insulin signalling in mice with targeted disruption of the IRS-1 gene. *Nature, 372*(6502), 186-190. doi:10.1038/372186a0

Araki, T., Kusakabe, M., & Nishida, E. (2007). Expression of estrogen induced gene 121-like (EIG121L) during early Xenopus development. *Gene Expr Patterns, 7*(6), 666-671. doi:10.1016/j.modgep.2007.03.004

Araki, T., Kusakabe, M., & Nishida, E. (2011). A transmembrane protein EIG121L is required for epidermal differentiation during early embryonic development. *J Biol Chem, 286*(8), 6760-6768. doi:10.1074/jbc.M110.177907

Artus, J., & Hadjantonakis, A. K. (2011). Generation of chimeras by aggregation of embryonic stem cells with diploid or tetraploid mouse embryos. *Methods Mol Biol, 693*, 37-56. doi:10.1007/978-1-60761-974-1_3

Assmann, A., Ueki, K., Winnay, J. N., Kadowaki, T., & Kulkarni, R. N. (2009). Glucose effects on beta-cell growth and survival require activation of insulin receptors and insulin receptor substrate 2. *Mol Cell Biol, 29*(11), 3219-3228. doi:10.1128/mcb.01489-08

Avrahami, D., Klochendler, A., Dor, Y., & Glaser, B. (2017). Beta cell heterogeneity: an evolving concept. *Diabetologia, 60*(8), 1363-1369. doi:10.1007/s00125-017-4326-z

Bach, L. A., & Rechler, M. M. (1992). Insulin-like growth factors and diabetes. *Diabetes Metab Rev, 8*(3), 229-257. doi:10.1002/dmr.5610080304

Bader, E., Migliorini, A., Gegg, M., Moruzzi, N., Gerdes, J., Roscioni, S. S., . . . Lickert, H. (2016). Identification of proliferative and mature beta-cells in the islets of Langerhans. *Nature, 535*(7612), 430-434. doi:10.1038/nature18624

Baker, J., Liu, J. P., Robertson, E. J., & Efstratiadis, A. (1993). Role of insulin-like growth factors in embryonic and postnatal growth. *Cell, 75*(1), 73-82.

Bakhti, M., Bottcher, A., & Lickert, H. (2019). Modelling the endocrine pancreas in health and disease. *Nat Rev Endocrinol, 15*(3), 155-171. doi:10.1038/s41574-018-0132-z

Bakhti, M., & Lickert, H. (2019). Cell makeover for diabetes therapy. *Nat Metab, 1*, 312–313. doi:10.1038/s42255-019-0048-5

Banarer, S., McGregor, V. P., & Cryer, P. E. (2002). Intraislet hyperinsulinemia prevents the glucagon response to hypoglycemia despite an intact autonomic response. *Diabetes, 51*(4), 958-965. doi:10.2337/diabetes.51.4.958

Bass, J., Chiu, G., Argon, Y., & Steiner, D. F. (1998). Folding of insulin receptor monomers is facilitated by the molecular chaperones calnexin and calreticulin and impaired by rapid dimerization. *J Cell Biol, 141*(3), 637-646. doi:10.1083/jcb.141.3.637

Bastidas-Ponce, A., Roscioni, S. S., Burtscher, I., Bader, E., Sterr, M., Bakhti, M., & Lickert, H. (2017). Foxa2 and Pdx1 cooperatively regulate postnatal maturation of pancreatic beta-cells. *Mol Metab, 6*(6), 524-534. doi:10.1016/j.molmet.2017.03.007

Bastidas-Ponce, A., Scheibner, K., Lickert, H., & Bakhti, M. (2017). Cellular and molecular mechanisms coordinating pancreas development. *Development, 144*(16), 2873-2888. doi:10.1242/dev.140756

Bastidas-Ponce, A., Tritschler, S., Dony, L., Scheibner, K., Tarquis-Medina, M., Salinno, C., . . . Bakhti, M. (2019). Comprehensive single cell mRNA profiling reveals a detailed roadmap for pancreatic endocrinogenesis. *Development, 146*(12). doi:10.1242/dev.173849

Bauer, M., Aust, G., & Schumacher, U. (2004). Different transcriptional expression of KIAA1324 and its splicing variants in human carcinoma cell lines with different metastatic capacity. *Oncol Rep, 11*(3), 677-680.

Belfiore, A., Frasca, F., Pandini, G., Sciacca, L., & Vigneri, R. (2009). Insulin receptor isoforms and insulin receptor/insulin-like growth factor receptor hybrids in physiology and disease. *Endocr Rev, 30*(6), 586-623. doi:10.1210/er.2008-0047

Belfiore, A., & Malaguarnera, R. (2011). Insulin receptor and cancer. *Endocr Relat Cancer, 18*(4), R125-147. doi:10.1530/ERC-11-0074

Belfiore, A., Malaguarnera, R., Vella, V., Lawrence, M. C., Sciacca, L., Frasca, F., . . . Vigneri, R. (2017). Insulin Receptor Isoforms in Physiology and Disease: An Updated View. *Endocr Rev, 38*(5), 379-431. doi:10.1210/er.2017-00073

Bolton, K. A., Holliday, E. G., Attia, J., Bowden, N. A., Avery-Kiejda, K. A., & Scott, R. J. (2016). A novel polymorphic repeat in the upstream regulatory region of the estrogen-induced gene EIG121 is not associated with the risk of developing breast or endometrial cancer. *BMC Res Notes, 9*, 287. doi:10.1186/s13104-016-2086-3

Bonifacio, E., & Ziegler, A. G. (2010). Advances in the prediction and natural history of type 1 diabetes. *Endocrinol Metab Clin North Am, 39*(3), 513-525. doi:10.1016/j.ecl.2010.05.007

Bonner-Weir, S., & Aguayo-Mazzucato, C. (2016). Physiology: Pancreatic beta-cell heterogeneity revisited. *Nature, 535*(7612), 365-366. doi:10.1038/nature18907

Bono, H., Kasukawa, T., Furuno, M., Hayashizaki, Y., & Okazaki, Y. (2002). FANTOM DB: database of Functional Annotation of RIKEN Mouse cDNA Clones. *Nucleic Acids Res, 30*(1), 116-118. doi:10.1093/nar/30.1.116

Bono, H., Kasukawa, T., Hayashizaki, Y., & Okazaki, Y. (2002). READ: RIKEN Expression Array Database. *Nucleic Acids Res, 30*(1), 211-213. doi:10.1093/nar/30.1.211

Bono, H., Yagi, K., Kasukawa, T., Nikaido, I., Tominaga, N., Miki, R., . . . Members, G. S. L. (2003). Systematic expression profiling of the mouse transcriptome using RIKEN cDNA microarrays. *Genome Res, 13*(6B), 1318-1323. doi:10.1101/gr.1075103

Boothe, T., Lim, G. E., Cen, H., Skovso, S., Piske, M., Li, S. N., . . . Johnson, J. D. (2016). Inter-domain tagging implicates caveolin-1 in insulin receptor trafficking and Erk signaling bias in pancreatic beta-cells. *Mol Metab, 5*(5), 366-378. doi:10.1016/j.molmet.2016.01.009

Borge, P. D., Moibi, J., Greene, S. R., Trucco, M., Young, R. A., Gao, Z., & Wolf, B. A. (2002). Insulin receptor signaling and sarco/endoplasmic reticulum calcium ATPase in beta-cells. *Diabetes, 51 Suppl 3*, S427-433. doi:10.2337/diabetes.51.2007.s427

Braulke, T., & Bonifacino, J. S. (2009). Sorting of lysosomal proteins. *Biochim Biophys Acta, 1793*(4), 605-614. doi:10.1016/j.bbamcr.2008.10.016

Braun, M., Ramracheya, R., & Rorsman, P. (2012). Autocrine regulation of insulin secretion. *Diabetes Obes Metab, 14 Suppl 3*, 143-151. doi:10.1111/j.1463-1326.2012.01642.x

Briant, L., Salehi, A., Vergari, E., Zhang, Q., & Rorsman, P. (2016). Glucagon secretion from pancreatic alpha-cells. *Ups J Med Sci, 121*(2), 113-119. doi:10.3109/03009734.2016.1156789

Brissova, M., Fowler, M. J., Nicholson, W. E., Chu, A., Hirshberg, B., Harlan, D. M., & Powers, A. C. (2005). Assessment of human pancreatic islet architecture and composition by laser scanning confocal microscopy. *J Histochem Cytochem, 53*(9), 1087-1097. doi:10.1369/jhc.5C6684.2005

Brothers, K. J., Wu, S., DiVall, S. A., Messmer, M. R., Kahn, C. R., Miller, R. S., . . . Wolfe, A. (2010). Rescue of obesity-induced infertility in female mice due to a pituitary-specific knockout of the insulin receptor. *Cell Metab, 12*(3), 295-305. doi:10.1016/j.cmet.2010.06.010

Brown, J., Jones, E. Y., & Forbes, B. E. (2009). Interactions of IGF-II with the IGF2R/cation-independent mannose-6-phosphate receptor mechanism and biological outcomes. *Vitam Horm, 80*, 699-719. doi:10.1016/S0083-6729(08)00625-0

Bruning, J. C., Gautam, D., Burks, D. J., Gillette, J., Schubert, M., Orban, P. C., . . . Kahn, C. R. (2000). Role of brain insulin receptor in control of body weight and reproduction. *Science, 289*(5487), 2122-2125. doi:10.1126/science.289.5487.2122

Burtscher, I., Barkey, W., & Lickert, H. (2013). Foxa2-venus fusion reporter mouse line allows live-cell analysis of endoderm-derived organ formation. *Genesis, 51*(8), 596-604. doi:10.1002/dvg.22404

Cabail, M. Z., Li, S., Lemmon, E., Bowen, M. E., Hubbard, S. R., & Miller, W. T. (2015). The insulin and IGF1 receptor kinase domains are functional dimers in the activated state. *Nat Commun, 6*, 6406. doi:10.1038/ncomms7406

Cai, W., Sakaguchi, M., Kleinridders, A., Gonzalez-Del Pino, G., Dreyfuss, J. M., O'Neill, B. T., . . . Kahn, C. R. (2017). Domain-dependent effects of insulin and IGF-1 receptors on signalling and gene expression. *Nat Commun, 8*, 14892. doi:10.1038/ncomms14892

Carpentier, J. L. (1994). Insulin receptor internalization: molecular mechanisms and physiopathological implications. *Diabetologia, 37 Suppl 2*, S117-124.

Carpentier, J. L., Fehlmann, M., Van Obberghen, E., Gorden, P., & Orci, L. (1985). Insulin receptor internalization and recycling: mechanism and significance. *Biochimie, 67*(10-11), 1143-1145.

Cavelti-Weder, C., Li, W., Zumsteg, A., Stemann-Andersen, M., Zhang, Y., Yamada, T., . . . Zhou, Q. (2016). Hyperglycaemia attenuates in vivo reprogramming of pancreatic exocrine cells to beta cells in mice. *Diabetologia, 59*(3), 522-532. doi:10.1007/s00125-015-3838-7

Ceresa, B. P., Kao, A. W., Santeler, S. R., & Pessin, J. E. (1998). Inhibition of clathrin-mediated endocytosis selectively attenuates specific insulin receptor signal transduction pathways. *Mol Cell Biol, 18*(7), 3862-3870. doi:10.1128/mcb.18.7.3862

Chen, C., Cohrs, C. M., Stertmann, J., Bozsak, R., & Speier, S. (2017). Human beta cell mass and function in diabetes: Recent advances in knowledge and technologies to understand disease pathogenesis. *Mol Metab, 6*(9), 943-957. doi:10.1016/j.molmet.2017.06.019

Chen, H. S., Wu, T. E., Jap, T. S., Hsiao, L. C., Lee, S. H., & Lin, H. D. (2008). Beneficial effects of insulin on glycemic control and beta-cell function in newly diagnosed type 2 diabetes with severe hyperglycemia after short-term intensive insulin therapy. *Diabetes Care, 31*(10), 1927-1932. doi:10.2337/dc08-0075

Chen, J., Nagle, A. M., Wang, Y. F., Boone, D. N., & Lee, A. V. (2018). Controlled dimerization of insulin-like growth factor-1 and insulin receptors reveals shared and distinct activities of holo and hybrid receptors. *J Biol Chem, 293*(10), 3700-3709. doi:10.1074/jbc.M117.789503

Cheng, C. W., Villani, V., Buono, R., Wei, M., Kumar, S., Yilmaz, O. H., . . . Longo, V. D. (2017). Fasting-Mimicking Diet Promotes Ngn3-Driven beta-Cell Regeneration to Reverse Diabetes. *Cell, 168*(5), 775-788 e712. doi:10.1016/j.cell.2017.01.040

Chera, S., Baronnier, D., Ghila, L., Cigliola, V., Jensen, J. N., Gu, G., . . . Herrera, P. L. (2014). Diabetes recovery by age-dependent conversion of pancreatic delta-cells into insulin producers. *Nature, 514*(7523), 503-507. doi:10.1038/nature13633

Cheung, K. K., Luk, A. O., So, W. Y., Ma, R. C., Kong, A. P., Chow, F. C., & Chan, J. C. (2015). Testosterone level in men with type 2 diabetes mellitus and related metabolic effects: A review of current evidence. *J Diabetes Investig, 6*(2), 112-123. doi:10.1111/jdi.12288

Choi, E., Kikuchi, S., Gao, H., Brodzik, K., Nassour, I., Yopp, A., . . . Yu, H. (2019). Mitotic regulators and the SHP2-MAPK pathway promote IR endocytosis and feedback regulation of insulin signaling. *Nat Commun, 10*(1), 1473. doi:10.1038/s41467-019-09318-3

Clayton, P. E., Banerjee, I., Murray, P. G., & Renehan, A. G. (2011). Growth hormone, the insulin-like growth factor axis, insulin and cancer risk. *Nat Rev Endocrinol, 7*(1), 11-24. doi:10.1038/nrendo.2010.171

Cleaver, O., & Dor, Y. (2012). Vascular instruction of pancreas development. *Development, 139*(16), 2833-2843. doi:10.1242/dev.065953

Clemmensen, C., Muller, T. D., Finan, B., Tschop, M. H., & DiMarchi, R. (2016). Current and Emerging Treatment Options in Diabetes Care. *Handb Exp Pharmacol, 233*, 437-459. doi:10.1007/164_2015_7

Clemmensen, C., Muller, T. D., Woods, S. C., Berthoud, H. R., Seeley, R. J., & Tschop, M. H. (2017). Gut-Brain Cross-Talk in Metabolic Control. *Cell, 168*(5), 758-774. doi:10.1016/j.cell.2017.01.025

Collden, G., Tschop, M. H., & Muller, T. D. (2017). Therapeutic Potential of Targeting the Ghrelin Pathway. *Int J Mol Sci, 18*(4). doi:10.3390/ijms18040798

Cornu, M., Yang, J. Y., Jaccard, E., Poussin, C., Widmann, C., & Thorens, B. (2009). Glucagon-like peptide-1 protects beta-cells against apoptosis by increasing the activity of an IGF-2/IGF-1 receptor autocrine loop. *Diabetes, 58*(8), 1816-1825. doi:10.2337/db09-0063

De Vas, M., & Ferrer, J. (2016). Can Insulin Production Suppress beta Cell Growth? *Cell Metab, 23*(1), 4-5. doi:10.1016/j.cmet.2015.12.016

DeFronzo, R. A., Ferrannini, E., Groop, L., Henry, R. R., Herman, W. H., Holst, J. J., . . . Weiss, R. (2015). Type 2 diabetes mellitus. *Nat Rev Dis Primers, 1*, 15019. doi:10.1038/nrdp.2015.19

Deng, L., Broaddus, R. R., McCampbell, A., Shipley, G. L., Loose, D. S., Stancel, G. M., . . . Davies, P. J. (2005). Identification of a novel estrogen-regulated gene, EIG121, induced by hormone replacement therapy and differentially expressed in type I and type II endometrial cancer. *Clin Cancer Res, 11*(23), 8258-8264. doi:10.1158/1078-0432.CCR-05-1189

Deng, L., Feng, J., & Broaddus, R. R. (2010). The novel estrogen-induced gene EIG121 regulates autophagy and promotes cell survival under stress. *Cell Death Dis, 1*, e32. doi:10.1038/cddis.2010.9

Desgraz, R., & Herrera, P. L. (2009). Pancreatic neurogenin 3-expressing cells are unipotent islet precursors. *Development, 136*(21), 3567-3574. doi:10.1242/dev.039214

Dieters-Castator, D. Z., Rambau, P. F., Kelemen, L. E., Siegers, G. M., Lajoie, G. A., Postovit, L. M., & Kobel, M. (2019). Proteomics-Derived Biomarker Panel Improves Diagnostic Precision to Classify Endometrioid and High-grade Serous Ovarian Carcinoma. *Clin Cancer Res*. doi:10.1158/1078-0432.CCR-18-3818

Dorton, A. M. (2000). The pituitary gland: embryology, physiology, and pathophysiology. *Neonatal Netw, 19*(2), 9-17. doi:10.1891/0730-0832.19.2.9

Dunning, B. E., & Gerich, J. E. (2007). The role of alpha-cell dysregulation in fasting and postprandial hyperglycemia in type 2 diabetes and therapeutic implications. *Endocr Rev, 28*(3), 253-283. doi:10.1210/er.2006-0026

Edlund, H. (2002). Pancreatic organogenesis--developmental mechanisms and implications for therapy. *Nat Rev Genet, 3*(7), 524-532. doi:10.1038/nrg841

Epaud, R., Aubey, F., Xu, J., Chaker, Z., Clemessy, M., Dautin, A., . . . Holzenberger, M. (2012). Knockout of insulin-like growth factor-1 receptor impairs distal lung morphogenesis. *PLoS One, 7*(11), e48071. doi:10.1371/journal.pone.0048071

Estrella, J. S., Ma, L. T., Milton, D. R., Yao, J. C., Wang, H., Rashid, A., & Broaddus, R. R. (2014). Expression of estrogen-induced genes and estrogen receptor beta in pancreatic neuroendocrine tumors: implications for targeted therapy. *Pancreas, 43*(7), 996-1002. doi:10.1097/MPA.0000000000000203

Farley, F. W., Soriano, P., Steffen, L. S., & Dymecki, S. M. (2000). Widespread recombinase expression using FLPeR (flipper) mice. *Genesis, 28*(3-4), 106-110.

Fernandez-Fernandez, R., Martini, A. C., Navarro, V. M., Castellano, J. M., Dieguez, C., Aguilar, E., . . . Tena-Sempere, M. (2006). Novel signals for the integration of energy balance and reproduction. *Mol Cell Endocrinol, 254-255*, 127-132. doi:10.1016/j.mce.2006.04.026

Finan, B., Yang, B., Ottaway, N., Stemmer, K., Muller, T. D., Yi, C. X., . . . Tschop, M. H. (2012). Targeted estrogen delivery reverses the metabolic syndrome. *Nat Med, 18*(12), 1847-1856. doi:10.1038/nm.3009

Fisher-Wellman, K. H., Ryan, T. E., Smith, C. D., Gilliam, L. A., Lin, C. T., Reese, L. R., . . . Neufer, P. D. (2016). A Direct Comparison of Metabolic Responses to High-Fat Diet in C57BL/6J and C57BL/6NJ Mice. *Diabetes, 65*(11), 3249-3261. doi:10.2337/db16-0291

Fontaine, D. A., & Davis, D. B. (2016). Attention to Background Strain Is Essential for Metabolic Research: C57BL/6 and the International Knockout Mouse Consortium. *Diabetes, 65*(1), 25-33. doi:10.2337/db15-0982

Franklin, I., Gromada, J., Gjinovci, A., Theander, S., & Wollheim, C. B. (2005). Beta-cell secretory products activate alpha-cell ATP-dependent potassium channels to inhibit glucagon release. *Diabetes, 54*(6), 1808-1815. doi:10.2337/diabetes.54.6.1808

Frasca, F., Pandini, G., Scalia, P., Sciacca, L., Mineo, R., Costantino, A., . . . Vigneri, R. (1999). Insulin receptor isoform A, a newly recognized, high-affinity insulin-like growth factor II receptor in fetal and cancer cells. *Mol Cell Biol, 19*(5), 3278-3288. doi:10.1128/mcb.19.5.3278

Fridley, B. L., Dai, J., Raghavan, R., Li, Q., Winham, S. J., Hou, X., . . . Goode, E. L. (2018). Transcriptomic Characterization of Endometrioid, Clear Cell, and High-Grade Serous Epithelial Ovarian Carcinoma. *Cancer Epidemiol Biomarkers Prev, 27*(9), 1101-1109. doi:10.1158/1055-9965.EPI-17-0728

Fujimoto, K., Hanson, P. T., Tran, H., Ford, E. L., Han, Z., Johnson, J. D., . . . Polonsky, K. S. (2009). Autophagy regulates pancreatic beta cell death in response to Pdx1 deficiency and nutrient deprivation. *J Biol Chem, 284*(40), 27664-27673. doi:10.1074/jbc.M109.041616

Fullekrug, J., Scheiffele, P., & Simons, K. (1999). VIP36 localisation to the early secretory pathway. *J Cell Sci, 112 (Pt 17)*, 2813-2821.

Furuyama, K., Chera, S., van Gurp, L., Oropeza, D., Ghila, L., Damond, N., . . . Herrera, P. L. (2019). Diabetes relief in mice by glucose-sensing insulin-secreting human alpha-cells. *Nature, 567*(7746), 43-48. doi:10.1038/s41586-019-0942-8

Gahete, M. D., Cordoba-Chacon, J., Anadumaka, C. V., Lin, Q., Bruning, J. C., Kahn, C. R., . . . Kineman, R. D. (2011). Elevated GH/IGF-I, due to somatotrope-specific loss of both IGF-I and insulin receptors, alters glucose homeostasis and insulin sensitivity in a diet-dependent manner. *Endocrinology, 152*(12), 4825-4837. doi:10.1210/en.2011-1447

Gala-Lopez, B. L., Neiman, D., Kin, T., O'Gorman, D., Pepper, A. R., Malcolm, A. J., . . . Shapiro, A. M. J. (2018). Beta Cell Death by Cell-free DNA and Outcome After Clinical Islet Transplantation. *Transplantation, 102*(6), 978-985. doi:10.1097/tp.0000000000002083

Gannon, M., Kulkarni, R. N., Tse, H. M., & Mauvais-Jarvis, F. (2018). Sex differences underlying pancreatic islet biology and its dysfunction. *Mol Metab, 15*, 82-91. doi:10.1016/j.molmet.2018.05.017

Gao, N., Le Lay, J., Qin, W., Doliba, N., Schug, J., Fox, A. J., . . . Kaestner, K. H. (2010). Foxa1 and Foxa2 maintain the metabolic and secretory features of the mature beta-cell. *Mol Endocrinol, 24*(8), 1594-1604. doi:10.1210/me.2009-0513

Gao, N., LeLay, J., Vatamaniuk, M. Z., Rieck, S., Friedman, J. R., & Kaestner, K. H. (2008). Dynamic regulation of Pdx1 enhancers by Foxa1 and Foxa2 is essential for pancreas development. *Genes Dev, 22*(24), 3435-3448. doi:10.1101/gad.1752608

Gao, N., White, P., Doliba, N., Golson, M. L., Matschinsky, F. M., & Kaestner, K. H. (2007). Foxa2 controls vesicle docking and insulin secretion in mature Beta cells. *Cell Metab, 6*(4), 267-279. doi:10.1016/j.cmet.2007.08.015

Gelling, R. W., Du, X. Q., Dichmann, D. S., Romer, J., Huang, H., Cui, L., . . . Charron, M. J. (2003). Lower blood glucose, hyperglucagonemia, and pancreatic alpha cell hyperplasia in glucagon receptor knockout mice. *Proc Natl Acad Sci U S A, 100*(3), 1438-1443. doi:10.1073/pnas.0237106100

Ghosh, P., Dahms, N. M., & Kornfeld, S. (2003). Mannose 6-phosphate receptors: new twists in the tale. *Nat Rev Mol Cell Biol, 4*(3), 202-212. doi:10.1038/nrm1050

Goh, L. K., & Sorkin, A. (2013). Endocytosis of receptor tyrosine kinases. *Cold Spring Harb Perspect Biol, 5*(5), a017459. doi:10.1101/cshperspect.a017459

Goldfine, A. B., & Kulkarni, R. N. (2012). Modulation of beta-cell function: a translational journey from the bench to the bedside. *Diabetes Obes Metab, 14 Suppl 3*, 152-160. doi:10.1111/j.1463-1326.2012.01647.x

Gonzalez-Begne, M., Lu, B., Han, X., Hagen, F. K., Hand, A. R., Melvin, J. E., & Yates, J. R. (2009). Proteomic analysis of human parotid gland exosomes by multidimensional protein identification technology (MudPIT). *J Proteome Res, 8*(3), 1304-1314. doi:10.1021/pr800658c

Gorden, P., Arakaki, R., Collier, E., & Carpentier, J. L. (1989). Biosynthesis and regulation of the insulin receptor. *Yale J Biol Med, 62*(5), 521-531.

Goren, H. J., Kulkarni, R. N., & Kahn, C. R. (2004). Glucose homeostasis and tissue transcript content of insulin signaling intermediates in four inbred strains of mice: C57BL/6, C57BLKS/6, DBA/2, and 129X1. *Endocrinology, 145*(7), 3307-3323. doi:10.1210/en.2003-1400

Gradwohl, G., Dierich, A., LeMeur, M., & Guillemot, F. (2000). neurogenin3 is required for the development of the four endocrine cell lineages of the pancreas. *Proc Natl Acad Sci U S A, 97*(4), 1607-1611. doi:10.1073/pnas.97.4.1607

Grapin-Botton, A. (2005). Ductal cells of the pancreas. *Int J Biochem Cell Biol, 37*(3), 504-510. doi:10.1016/j.biocel.2004.07.010

Griffiths, G., Matteoni, R., Back, R., & Hoflack, B. (1990). Characterization of the cation-independent mannose 6-phosphate receptor-enriched prelysosomal compartment in NRK cells. *J Cell Sci, 95 (Pt 3)*, 441-461.

Griffiths, G., & Simons, K. (1986). The trans Golgi network: sorting at the exit site of the Golgi complex. *Science, 234*(4775), 438-443. doi:10.1126/science.2945253

Grippo, P. J., Nowlin, P. S., Cassaday, R. D., & Sandgren, E. P. (2002). Cell-specific transgene expression from a widely transcribed promoter using Cre/lox in mice. *Genesis, 32*(4), 277-286. doi:10.1002/gene.10080

Gromada, J., Duttaroy, A., & Rorsman, P. (2009). The insulin receptor talks to glucagon? *Cell Metab, 9*(4), 303-305. doi:10.1016/j.cmet.2009.03.008

Guo, L., Inada, A., Aguayo-Mazzucato, C., Hollister-Lock, J., Fujitani, Y., Weir, G. C., . . . Bonner-Weir, S. (2013). PDX1 in ducts is not required for postnatal formation of beta-cells but is necessary for their subsequent maturation. *Diabetes, 62*(10), 3459-3468. doi:10.2337/db12-1833

Gutmann, T., Kim, K. H., Grzybek, M., Walz, T., & Coskun, U. (2018). Visualization of ligand-induced transmembrane signaling in the full-length human insulin receptor. *J Cell Biol, 217*(5), 1643-1649. doi:10.1083/jcb.201711047

Gutmann, T., Schafer, I. B., Poojari, C., Brankatschk, B., Vattulainen, I., Strauss, M., & Coskun, U. (2020). Cryo-EM structure of the complete and ligand-saturated insulin receptor ectodomain. *J Cell Biol, 219*(1). doi:10.1083/jcb.201907210

Gwinn, D. M., Shackelford, D. B., Egan, D. F., Mihaylova, M. M., Mery, A., Vasquez, D. S., . . . Shaw, R. J. (2008). AMPK phosphorylation of raptor mediates a metabolic checkpoint. *Mol Cell, 30*(2), 214-226. doi:10.1016/j.molcel.2008.03.003

Habegger, K. M., Heppner, K. M., Geary, N., Bartness, T. J., DiMarchi, R., & Tschop, M. H. (2010). The metabolic actions of glucagon revisited. *Nat Rev Endocrinol, 6*(12), 689-697. doi:10.1038/nrendo.2010.187

Haeusler, R. A., McGraw, T. E., & Accili, D. (2018). Biochemical and cellular properties of insulin receptor signalling. *Nat Rev Mol Cell Biol, 19*(1), 31-44. doi:10.1038/nrm.2017.89

Hamer, I., Haft, C. R., Paccaud, J. P., Maeder, C., Taylor, S., & Carpentier, J. L. (1997). Dual role of a dileucine motif in insulin receptor endocytosis. *J Biol Chem, 272*(35), 21685-21691. doi:10.1074/jbc.272.35.21685

Harrison, L. B., Adams-Huet, B., Raskin, P., & Lingvay, I. (2012). beta-cell function preservation after 3.5 years of intensive diabetes therapy. *Diabetes Care, 35*(7), 1406-1412. doi:10.2337/dc11-2170

Hauge-Evans, A. C., King, A. J., Carmignac, D., Richardson, C. C., Robinson, I. C., Low, M. J., . . . Jones, P. M. (2009). Somatostatin secreted by islet delta-cells fulfills multiple roles as a paracrine regulator of islet function. *Diabetes, 58*(2), 403-411. doi:10.2337/db08-0792

Hauptman, N., Bostjancic, E., Zlajpah, M., Rankovic, B., & Zidar, N. (2018). Bioinformatics Analysis Reveals Most Prominent Gene Candidates to Distinguish Colorectal Adenoma from Adenocarcinoma. *Biomed Res Int, 2018*, 9416515. doi:10.1155/2018/9416515

Hauri, H. P., Kappeler, F., Andersson, H., & Appenzeller, C. (2000). ERGIC-53 and traffic in the secretory pathway. *J Cell Sci, 113 (Pt 4)*, 587-596.

Hayashi, Y., Yamamoto, M., Mizoguchi, H., Watanabe, C., Ito, R., Yamamoto, S., . . . Murata, Y. (2009). Mice deficient for glucagon gene-derived peptides display normoglycemia and hyperplasia of islet {alpha}-cells but not of intestinal L-cells. *Mol Endocrinol, 23*(12), 1990-1999. doi:10.1210/me.2009-0296

Heesom, K. J., Harbeck, M., Kahn, C. R., & Denton, R. M. (1997). Insulin action on metabolism. *Diabetologia, 40 Suppl 3*, B3-9. doi:10.1007/bf03168179

Heppner, K. M., Habegger, K. M., Day, J., Pfluger, P. T., Perez-Tilve, D., Ward, B., . . . Tschop, M. (2010). Glucagon regulation of energy metabolism. *Physiol Behav, 100*(5), 545-548. doi:10.1016/j.physbeh.2010.03.019

Heppner, K. M., Muller, T. D., Tong, J., & Tschop, M. H. (2012). Ghrelin in the control of energy, lipid, and glucose metabolism. *Methods Enzymol, 514*, 249-260. doi:10.1016/b978-0-12-381272-8.00015-5

Hevener, A. L., Clegg, D. J., & Mauvais-Jarvis, F. (2015). Impaired estrogen receptor action in the pathogenesis of the metabolic syndrome. *Mol Cell Endocrinol, 418 Pt 3*, 306-321. doi:10.1016/j.mce.2015.05.020

Hiden, U., Glitzner, E., Hartmann, M., & Desoye, G. (2009). Insulin and the IGF system in the human placenta of normal and diabetic pregnancies. *J Anat, 215*(1), 60-68. doi:10.1111/j.1469-7580.2008.01035.x

IDF. (2019). IDF Diabetes Atlas. 9th. Retrieved from http://www.diabetesatlas.org

Iwasaki, M., Minami, K., Shibasaki, T., Miki, T., Miyazaki, J., & Seino, S. (2010). Establishment of new clonal pancreatic beta-cell lines (MIN6-K) useful for study of incretin/cyclic adenosine monophosphate signaling. *J Diabetes Investig, 1*(4), 137-142. doi:10.1111/j.2040-1124.2010.00026.x

J. Giudice, L. S. B., F.F. Guaimas, A. Penas-Steinhardt, L. Giordano, E.A. Jares-Erjiman, F. C. Leskow. (2013). Insulin and insulin like growth factor II endocytosis and signaling via insulin receptor B. *Cell Communication & Signaling*.

Jaafar, R., Tran, S., Shah, A. N., Sun, G., Valdearcos, M., Marchetti, P., . . . Bhushan, A. (2019). mTORC1 to AMPK switching underlies beta-cell metabolic plasticity during maturation and diabetes. *J Clin Invest, 130*, 4124-4137. doi:10.1172/jci127021

Jaillard, S., Akloul, L., Beaumont, M., Hamdi-Roze, H., Dubourg, C., Odent, S., . . . Ravel, C. (2016). Array-CGH diagnosis in ovarian failure: identification of new molecular actors for ovarian physiology. *J Ovarian Res, 9*(1), 63. doi:10.1186/s13048-016-0272-5

Jenny, M., Uhl, C., Roche, C., Duluc, I., Guillermin, V., Guillemot, F., . . . Gradwohl, G. (2002). Neurogenin3 is differentially required for endocrine cell fate specification in the intestinal and gastric epithelium. *EMBO J, 21*(23), 6338-6347. doi:10.1093/emboj/cdf649

Jevdjovic, T., Bernays, R. L., & Eppler, E. (2007). Insulin-like growth factor-I mRNA and peptide in the human anterior pituitary. *J Neuroendocrinol, 19*(5), 335-341. doi:10.1111/j.1365-2826.2007.01539.x

Johnson, J. D., Ahmed, N. T., Luciani, D. S., Han, Z., Tran, H., Fujita, J., . . . Polonsky, K. S. (2003). Increased islet apoptosis in Pdx1+/- mice. *J Clin Invest, 111*(8), 1147-1160. doi:10.1172/jci16537

Johnson, J. D., & Alejandro, E. U. (2008). Control of pancreatic beta-cell fate by insulin signaling: The sweet spot hypothesis. *Cell Cycle, 7*(10), 1343-1347. doi:10.4161/cc.7.10.5865

Johnson, J. D., Bernal-Mizrachi, E., Alejandro, E. U., Han, Z., Kalynyak, T. B., Li, H., . . . Polonsky, K. S. (2006). Insulin protects islets from apoptosis via Pdx1 and specific changes in the human islet proteome. *Proc Natl Acad Sci U S A, 103*(51), 19575-19580. doi:10.1073/pnas.0604208103

Jonsson, J., Carlsson, L., Edlund, T., & Edlund, H. (1994). Insulin-promoter-factor 1 is required for pancreas development in mice. *Nature, 371*(6498), 606-609. doi:10.1038/371606a0

Joshi, R. L., Lamothe, B., Cordonnier, N., Mesbah, K., Monthioux, E., Jami, J., & Bucchini, D. (1996). Targeted disruption of the insulin receptor gene in the mouse results in neonatal lethality. *EMBO J, 15*(7), 1542-1547.

Kaestner, K. H. (2000). The hepatocyte nuclear factor 3 (HNF3 or FOXA) family in metabolism. *Trends Endocrinol Metab, 11*(7), 281-285. doi:10.1016/s1043-2760(00)00271-x

Kahn, C. R. (1995). Diabetes. Causes of insulin resistance. *Nature, 373*(6513), 384-385. doi:10.1038/373384a0

Kahn, C. R., Bruning, J. C., Michael, M. D., & Kulkarni, R. N. (2000). Knockout mice challenge our concepts of glucose homeostasis and the pathogenesis of diabetes mellitus. *J Pediatr Endocrinol Metab, 13 Suppl 6*, 1377-1384. doi:10.1515/jpem-2000-s611

Kahn, C. R., & Goldfine, A. B. (1993). Molecular determinants of insulin action. *J Diabetes Complications, 7*(2), 92-105. doi:10.1016/1056-8727(93)90034-v

Kaneto, H., & Matsuoka, T. A. (2015). Role of pancreatic transcription factors in maintenance of mature beta-cell function. *Int J Mol Sci, 16*(3), 6281-6297. doi:10.3390/ijms16036281

Kang, J. M., Park, S., Kim, S. J., Kim, H., Lee, B., Kim, J., . . . Kim, S. J. (2015). KIAA1324 Suppresses Gastric Cancer Progression by Inhibiting the Oncoprotein GRP78. *Cancer Res, 75*(15), 3087-3097. doi:10.1158/0008-5472.CAN-14-3751

Katsuta, H., Aguayo-Mazzucato, C., Katsuta, R., Akashi, T., Hollister-Lock, J., Sharma, A. J., . . . Weir, G. C. (2012). Subpopulations of GFP-marked mouse pancreatic beta-cells differ in size, granularity, and insulin secretion. *Endocrinology, 153*(11), 5180-5187. doi:10.1210/en.2012-1257

Kawamori, D., Akiyama, M., Hu, J., Hambro, B., & Kulkarni, R. N. (2011). Growth factor signalling in the regulation of alpha-cell fate. *Diabetes Obes Metab, 13 Suppl 1*, 21-30. doi:10.1111/j.1463-1326.2011.01442.x

Kawamori, D., Kurpad, A. J., Hu, J., Liew, C. W., Shih, J. L., Ford, E. L., . . . Kulkarni, R. N. (2009). Insulin signaling in alpha cells modulates glucagon secretion in vivo. *Cell Metab, 9*(4), 350-361. doi:10.1016/j.cmet.2009.02.007

Kawamori, D., Welters, H. J., & Kulkarni, R. N. (2010). Molecular pathways underlying the pathogenesis of pancreatic alpha-cell dysfunction. *Adv Exp Med Biol, 654*, 421-445. doi:10.1007/978-90-481-3271-3_18

Khan, A. H., & Pessin, J. E. (2002). Insulin regulation of glucose uptake: a complex interplay of intracellular signalling pathways. *Diabetologia, 45*(11), 1475-1483. doi:10.1007/s00125-002-0974-7

Khandekar, N., Berning, B. A., Sainsbury, A., & Lin, S. (2015). The role of pancreatic polypeptide in the regulation of energy homeostasis. *Mol Cell Endocrinol, 418 Pt 1*, 33-41. doi:10.1016/j.mce.2015.06.028

Kido, Y., Burks, D. J., Withers, D., Bruning, J. C., Kahn, C. R., White, M. F., & Accili, D. (2000). Tissue-specific insulin resistance in mice with mutations in the insulin receptor, IRS-1, and IRS-2. *J Clin Invest, 105*(2), 199-205. doi:10.1172/jci7917

Kilic, G., Alvarez-Mercado, A. I., Zarrouki, B., Opland, D., Liew, C. W., Alonso, L. C., . . . Mauvais-Jarvis, F. (2014). The islet estrogen receptor-alpha is induced by hyperglycemia and protects against oxidative stress-induced insulin-deficient diabetes. *PLoS One, 9*(2), e87941. doi:10.1371/journal.pone.0087941

Kleinert, M., Clemmensen, C., Hofmann, S. M., Moore, M. C., Renner, S., Woods, S. C., . . . Tschop, M. H. (2018). Animal models of obesity and diabetes mellitus. *Nat Rev Endocrinol, 14*(3), 140-162. doi:10.1038/nrendo.2017.161

Kornfeld, S. (1992). Structure and function of the mannose 6-phosphate/insulinlike growth factor II receptors. *Annu Rev Biochem, 61*, 307-330. doi:10.1146/annurev.bi.61.070192.001515

Kramer, C. K., Zinman, B., & Retnakaran, R. (2013). Short-term intensive insulin therapy in type 2 diabetes mellitus: a systematic review and meta-analysis. *Lancet Diabetes Endocrinol, 1*(1), 28-34. doi:10.1016/S2213-8587(13)70006-8

Kruger, M., Kratchmarova, I., Blagoev, B., Tseng, Y. H., Kahn, C. R., & Mann, M. (2008). Dissection of the insulin signaling pathway via quantitative phosphoproteomics. *Proc Natl Acad Sci U S A, 105*(7), 2451-2456. doi:10.1073/pnas.0711713105

Kulkarni, R. N. (2004). The islet beta-cell. *Int J Biochem Cell Biol, 36*(3), 365-371. doi:10.1016/j.biocel.2003.08.010

Kulkarni, R. N., Bruning, J. C., Winnay, J. N., Postic, C., Magnuson, M. A., & Kahn, C. R. (1999). Tissue-specific knockout of the insulin receptor in pancreatic beta cells creates an insulin secretory defect similar to that in type 2 diabetes. *Cell, 96*(3), 329-339. doi:10.1016/s0092-8674(00)80546-2

Kulkarni, R. N., Holzenberger, M., Shih, D. Q., Ozcan, U., Stoffel, M., Magnuson, M. A., & Kahn, C. R. (2002). beta-cell-specific deletion of the Igf1 receptor leads to hyperinsulinemia and glucose intolerance but does not alter beta-cell mass. *Nat Genet, 31*(1), 111-115. doi:10.1038/ng872

Kulkarni, R. N., Jhala, U. S., Winnay, J. N., Krajewski, S., Montminy, M., & Kahn, C. R. (2004). PDX-1 haploinsufficiency limits the compensatory islet hyperplasia that occurs in response to insulin resistance. *J Clin Invest, 114*(6), 828-836. doi:10.1172/jci21845

Kulkarni, R. N., & Kahn, C. R. (2004). Molecular biology. HNFs--linking the liver and pancreatic islets in diabetes. *Science, 303*(5662), 1311-1312. doi:10.1126/science.1095486

Kulkarni, R. N., & Okada, T. (2002). Tissue-specific targeting of the insulin receptor gene. *Endocrine, 19*(3), 257-266. doi:10.1385/endo:19:3:257

Kurlawala, Z., Dunaway, R., Shah, P. P., Gosney, J. A., Siskind, L. J., Ceresa, B. P., & Beverly, L. J. (2017). Regulation of insulin-like growth factor receptors by Ubiquilin1. *Biochem J, 474*(24), 4105-4118. doi:10.1042/bcj20170620

Lantz, K. A., Vatamaniuk, M. Z., Brestelli, J. E., Friedman, J. R., Matschinsky, F. M., & Kaestner, K. H. (2004). Foxa2 regulates multiple pathways of insulin secretion. *J Clin Invest, 114*(4), 512-520. doi:10.1172/JCI21149

Lau, M. M., Stewart, C. E., Liu, Z., Bhatt, H., Rotwein, P., & Stewart, C. L. (1994). Loss of the imprinted IGF2/cation-independent mannose 6-phosphate receptor results in fetal overgrowth and perinatal lethality. *Genes Dev, 8*(24), 2953-2963. doi:10.1101/gad.8.24.2953

Le Roith, D. (2003). The insulin-like growth factor system. *Exp Diabesity Res, 4*(4), 205-212. doi:10.1155/edr.2003.205

Lee, C. S., Sund, N. J., Behr, R., Herrera, P. L., & Kaestner, K. H. (2005). Foxa2 is required for the differentiation of pancreatic alpha-cells. *Dev Biol, 278*(2), 484-495. doi:10.1016/j.ydbio.2004.10.012

Lee, C. S., Sund, N. J., Vatamaniuk, M. Z., Matschinsky, F. M., Stoffers, D. A., & Kaestner, K. H. (2002). Foxa2 controls Pdx1 gene expression in pancreatic beta-cells in vivo. *Diabetes, 51*(8), 2546-2551. doi:10.2337/diabetes.51.8.2546

Lee, Y. H., Wang, M. Y., Yu, X. X., & Unger, R. H. (2016). Glucagon is the key factor in the development of diabetes. *Diabetologia, 59*(7), 1372-1375. doi:10.1007/s00125-016-3965-9

Leibiger, B., Leibiger, I. B., Moede, T., Kemper, S., Kulkarni, R. N., Kahn, C. R., . . . Berggren, P. O. (2001). Selective insulin signaling through A and B insulin receptors regulates transcription of insulin and glucokinase genes in pancreatic beta cells. *Mol Cell, 7*(3), 559-570. doi:10.1016/s1097-2765(01)00203-9

Leibiger, I. B., Leibiger, B., & Berggren, P. O. (2008). Insulin signaling in the pancreatic beta-cell. *Annu Rev Nutr, 28*, 233-251. doi:10.1146/annurev.nutr.28.061807.155530

Lemmon, M. A., & Schlessinger, J. (2010). Cell signaling by receptor tyrosine kinases. *Cell, 141*(7), 1117-1134. doi:10.1016/j.cell.2010.06.011

LeRoith, D., & Yakar, S. (2007). Mechanisms of disease: metabolic effects of growth hormone and insulin-like growth factor 1. *Nat Clin Pract Endocrinol Metab, 3*(3), 302-310. doi:10.1038/ncpendmet0427

Lim, G. E., Piske, M., & Johnson, J. D. (2013). 14-3-3 proteins are essential signalling hubs for beta cell survival. *Diabetologia, 56*(4), 825-837. doi:10.1007/s00125-012-2820-x

Liston, A., Todd, J. A., & Lagou, V. (2017). Beta-Cell Fragility As a Common Underlying Risk Factor in Type 1 and Type 2 Diabetes. *Trends Mol Med, 23*(2), 181-194. doi:10.1016/j.molmed.2016.12.005

Liu, J. P., Baker, J., Perkins, A. S., Robertson, E. J., & Efstratiadis, A. (1993). Mice carrying null mutations of the genes encoding insulin-like growth factor I (Igf-1) and type 1 IGF receptor (Igf1r). *Cell, 75*(1), 59-72.

Liu, S., & Mauvais-Jarvis, F. (2010). Minireview: Estrogenic protection of beta-cell failure in metabolic diseases. *Endocrinology, 151*(3), 859-864. doi:10.1210/en.2009-1107

Liu, S., Okada, T., Assmann, A., Soto, J., Liew, C. W., Bugger, H., . . . Kulkarni, R. N. (2009). Insulin signaling regulates mitochondrial function in pancreatic beta-cells. *PLoS One, 4*(11), e7983. doi:10.1371/journal.pone.0007983

Liu, Z., Kim, W., Chen, Z., Shin, Y. K., Carlson, O. D., Fiori, J. L., . . . Egan, J. M. (2011). Insulin and glucagon regulate pancreatic alpha-cell proliferation. *PLoS One, 6*(1), e16096. doi:10.1371/journal.pone.0016096

Lo, H. G., Jin, R. U., Sibbel, G., Liu, D., Karki, A., Joens, M. S., . . . Mills, J. C. (2017). A single transcription factor is sufficient to induce and maintain secretory cell architecture. *Genes Dev, 31*(2), 154-171. doi:10.1101/gad.285684.116

Louet, J. F., LeMay, C., & Mauvais-Jarvis, F. (2004). Antidiabetic actions of estrogen: insight from human and genetic mouse models. *Curr Atheroscler Rep, 6*(3), 180-185. doi:10.1007/s11883-004-0030-9

Ma, F., Wei, Z., Shi, C., Gan, Y., Lu, J., Frank, S. J., . . . Huang, Y. (2011). Signaling cross talk between growth hormone (GH) and insulin-like growth factor-I (IGF-I) in pancreatic islet beta-cells. *Mol Endocrinol, 25*(12), 2119-2133. doi:10.1210/me.2011-1052

Ma, X., Zhang, Y., Gromada, J., Sewing, S., Berggren, P. O., Buschard, K., . . . Eliasson, L. (2005). Glucagon stimulates exocytosis in mouse and rat pancreatic alpha-cells by binding to glucagon receptors. *Mol Endocrinol, 19*(1), 198-212. doi:10.1210/me.2004-0059

MacDonald, P. E., Joseph, J. W., & Rorsman, P. (2005). Glucose-sensing mechanisms in pancreatic beta-cells. *Philos Trans R Soc Lond B Biol Sci, 360*(1464), 2211-2225. doi:10.1098/rstb.2005.1762

Macotela, Y., Boucher, J., Tran, T. T., & Kahn, C. R. (2009). Sex and depot differences in adipocyte insulin sensitivity and glucose metabolism. *Diabetes, 58*(4), 803-812. doi:10.2337/db08-1054

Magenheim, J., Klein, A. M., Stanger, B. Z., Ashery-Padan, R., Sosa-Pineda, B., Gu, G., & Dor, Y. (2011). Ngn3(+) endocrine progenitor cells control the fate and morphogenesis of pancreatic ductal epithelium. *Dev Biol, 359*(1), 26-36. doi:10.1016/j.ydbio.2011.08.006

Magnuson, M. A., & Osipovich, A. B. (2013). Pancreas-specific Cre driver lines and considerations for their prudent use. *Cell Metab, 18*(1), 9-20. doi:10.1016/j.cmet.2013.06.011

Mancias, J. D., & Goldberg, J. (2007). The transport signal on Sec22 for packaging into COPII-coated vesicles is a conformational epitope. *Mol Cell, 26*(3), 403-414. doi:10.1016/j.molcel.2007.03.017

Matsuoka, T. A., Kawashima, S., Miyatsuka, T., Sasaki, S., Shimo, N., Katakami, N., . . . Shimomura, I. (2017). MafA Enables Pdx1 to Effectively Convert Pancreatic Islet Progenitors and Committed Islet alpha-Cells Into beta-Cells In Vivo. *Diabetes, 66*(5), 1293-1300. doi:10.2337/db16-0887

Mauvais-Jarvis, F. (2018). Gender differences in glucose homeostasis and diabetes. *Physiol Behav, 187*, 20-23. doi:10.1016/j.physbeh.2017.08.016

Mauvais-Jarvis, F., Clegg, D. J., & Hevener, A. L. (2013). The role of estrogens in control of energy balance and glucose homeostasis. *Endocr Rev, 34*(3), 309-338. doi:10.1210/er.2012-1055

Mauvais-Jarvis, F., & Kahn, C. R. (2000). Understanding the pathogenesis and treatment of insulin resistance and type 2 diabetes mellitus: what can we learn from transgenic and knockout mice? *Diabetes Metab, 26*(6), 433-448.

Mauvais-Jarvis, F., Le May, C., Tiano, J. P., Liu, S., Kilic-Berkmen, G., & Kim, J. H. (2017). The Role of Estrogens in Pancreatic Islet Physiopathology. *Adv Exp Med Biol, 1043*, 385-399. doi:10.1007/978-3-319-70178-3_18

Metzger, D., & Chambon, P. (2001). Site- and time-specific gene targeting in the mouse. *Methods, 24*(1), 71-80. doi:10.1006/meth.2001.1159

Miki, R., Kadota, K., Bono, H., Mizuno, Y., Tomaru, Y., Carninci, P., . . . Hayashizaki, Y. (2001). Delineating developmental and metabolic pathways in vivo by expression profiling using the RIKEN set of 18,816 full-length enriched mouse cDNA arrays. *Proc Natl Acad Sci U S A, 98*(5), 2199-2204. doi:10.1073/pnas.041605498

Muller, T. D., Finan, B., Clemmensen, C., DiMarchi, R. D., & Tschop, M. H. (2017). The New Biology and Pharmacology of Glucagon. *Physiol Rev, 97*(2), 721-766. doi:10.1152/physrev.00025.2016

Muller, T. D., Nogueiras, R., Andermann, M. L., Andrews, Z. B., Anker, S. D., Argente, J., . . . Tschop, M. H. (2015). Ghrelin. *Mol Metab, 4*(6), 437-460. doi:10.1016/j.molmet.2015.03.005

Nagle, A. M., Levine, K. M., Tasdemir, N., Scott, J. A., Burlbaugh, K., Kehm, J., . . . Lee, A. V. (2018). Loss of E-cadherin Enhances IGF1-IGF1R Pathway Activation and Sensitizes Breast Cancers to Anti-IGF1R/InsR Inhibitors. *Clin Cancer Res, 24*(20), 5165-5177. doi:10.1158/1078-0432.CCR-18-0279

Nakae, J., Kido, Y., & Accili, D. (2001). Distinct and overlapping functions of insulin and IGF-I receptors. *Endocr Rev, 22*(6), 818-835. doi:10.1210/edrv.22.6.0452

Navarro, G., Xu, W., Jacobson, D. A., Wicksteed, B., Allard, C., Zhang, G., . . . Mauvais-Jarvis, F. (2016). Extranuclear Actions of the Androgen Receptor Enhance Glucose-Stimulated Insulin Secretion in the Male. *Cell Metab, 23*(5), 837-851. doi:10.1016/j.cmet.2016.03.015

Ohsugi, M., Cras-Meneur, C., Zhou, Y., Warren, W., Bernal-Mizrachi, E., & Permutt, M. A. (2004). Glucose and insulin treatment of insulinoma cells results in transcriptional regulation of a common set of genes. *Diabetes, 53*(6), 1496-1508. doi:10.2337/diabetes.53.6.1496

Oropeza, D., Jouvet, N., Budry, L., Campbell, J. E., Bouyakdan, K., Lacombe, J., . . . Estall, J. L. (2015). Phenotypic Characterization of MIP-CreERT1Lphi Mice With Transgene-Driven Islet Expression of Human Growth Hormone. *Diabetes, 64*(11), 3798-3807. doi:10.2337/db15-0272

Otani, K., Kulkarni, R. N., Baldwin, A. C., Krutzfeldt, J., Ueki, K., Stoffel, M., . . . Polonsky, K. S. (2004). Reduced beta-cell mass and altered glucose sensing impair insulin-secretory function in betaIRKO mice. *Am J Physiol Endocrinol Metab, 286*(1), E41-49. doi:10.1152/ajpendo.00533.2001

Pan, F. C., & Wright, C. (2011). Pancreas organogenesis: from bud to plexus to gland. *Dev Dyn, 240*(3), 530-565. doi:10.1002/dvdy.22584

Park, S. Y., & Guo, X. (2014). Adaptor protein complexes and intracellular transport. *Biosci Rep, 34*(4). doi:10.1042/BSR20140069

Pelling, M., Anthwal, N., McNay, D., Gradwohl, G., Leiter, A. B., Guillemot, F., & Ang, S. L. (2011). Differential requirements for neurogenin 3 in the development of POMC and NPY neurons in the hypothalamus. *Dev Biol, 349*(2), 406-416. doi:10.1016/j.ydbio.2010.11.007

Pitetti, J. L., Calvel, P., Romero, Y., Conne, B., Truong, V., Papaioannou, M. D., . . . Nef, S. (2013). Insulin and IGF1 receptors are essential for XX and XY gonadal differentiation and adrenal development in mice. *PLoS Genet, 9*(1), e1003160. doi:10.1371/journal.pgen.1003160

Poher, A. L., Tschop, M. H., & Muller, T. D. (2018). Ghrelin regulation of glucose metabolism. *Peptides, 100*, 236-242. doi:10.1016/j.peptides.2017.12.015

Popova, N. V., Deyev, I. E., & Petrenko, A. G. (2013). Clathrin-mediated endocytosis and adaptor proteins. *Acta Naturae, 5*(3), 62-73.

Rabiee, A., Kruger, M., Ardenkjaer-Larsen, J., Kahn, C. R., & Emanuelli, B. (2018). Distinct signalling properties of insulin receptor substrate (IRS)-1 and IRS-2 in mediating insulin/IGF-1 action. *Cell Signal, 47*, 1-15. doi:10.1016/j.cellsig.2018.03.003

Ran, F. A., Hsu, P. D., Wright, J., Agarwala, V., Scott, D. A., & Zhang, F. (2013). Genome engineering using the CRISPR-Cas9 system. *Nat Protoc, 8*(11), 2281-2308. doi:10.1038/nprot.2013.143

Ran, X., Zhou, P., & Zhang, K. (2017). Autophagy plays an important role in stemness mediation and the novel dual function of EIG121 in both autophagy and stemness

regulation of endometrial carcinoma JEC cells. *Int J Oncol, 51*(2), 644-656. doi:10.3892/ijo.2017.4047

Rhodes, C. J., White, M. F., Leahy, J. L., & Kahn, S. E. (2013). Direct autocrine action of insulin on beta-cells: does it make physiological sense? *Diabetes, 62*(7), 2157-2163. doi:10.2337/db13-0246

Rieck, S., & Kaestner, K. H. (2010). Expansion of beta-cell mass in response to pregnancy. *Trends Endocrinol Metab, 21*(3), 151-158. doi:10.1016/j.tem.2009.11.001

Roder, P. V., Wu, B., Liu, Y., & Han, W. (2016). Pancreatic regulation of glucose homeostasis. *Exp Mol Med, 48*, e219. doi:10.1038/emm.2016.6

Romanelli, R. J., LeBeau, A. P., Fulmer, C. G., Lazzarino, D. A., Hochberg, A., & Wood, T. L. (2007). Insulin-like growth factor type-I receptor internalization and recycling mediate the sustained phosphorylation of Akt. *J Biol Chem, 282*(31), 22513-22524. doi:10.1074/jbc.M704309200

Rorsman, P. (1997). The pancreatic beta-cell as a fuel sensor: an electrophysiologist's viewpoint. *Diabetologia, 40*(5), 487-495. doi:10.1007/s001250050706

Rorsman, P., & Ashcroft, F. M. (2018). Pancreatic beta-Cell Electrical Activity and Insulin Secretion: Of Mice and Men. *Physiol Rev, 98*(1), 117-214. doi:10.1152/physrev.00008.2017

Rorsman, P., Eliasson, L., Renstrom, E., Gromada, J., Barg, S., & Gopel, S. (2000). The Cell Physiology of Biphasic Insulin Secretion. *News Physiol Sci, 15*, 72-77. doi:10.1152/physiologyonline.2000.15.2.72

Rorsman, P., & Huising, M. O. (2018). The somatostatin-secreting pancreatic delta-cell in health and disease. *Nat Rev Endocrinol, 14*(7), 404-414. doi:10.1038/s41574-018-0020-6

Rorsman, P., & Renstrom, E. (2003). Insulin granule dynamics in pancreatic beta cells. *Diabetologia, 46*(8), 1029-1045. doi:10.1007/s00125-003-1153-1

Rorsman, P., Salehi, S. A., Abdulkader, F., Braun, M., & MacDonald, P. E. (2008). K(ATP)-channels and glucose-regulated glucagon secretion. *Trends Endocrinol Metab, 19*(8), 277-284. doi:10.1016/j.tem.2008.07.003

Roscioni, S. S., Migliorini, A., Gegg, M., & Lickert, H. (2016). Impact of islet architecture on beta-cell heterogeneity, plasticity and function. *Nat Rev Endocrinol, 12*(12), 695-709. doi:10.1038/nrendo.2016.147

Roth, J., Qureshi, S., Whitford, I., Vranic, M., Kahn, C. R., Fantus, I. G., & Dirks, J. H. (2012). Insulin's discovery: new insights on its ninetieth birthday. *Diabetes Metab Res Rev, 28*(4), 293-304. doi:10.1002/dmrr.2300

Rui, L. (2014). Energy metabolism in the liver. *Compr Physiol, 4*(1), 177-197. doi:10.1002/cphy.c130024

Sachs, S., Bastidas-Ponce, A., Tritschler, S., Bakhti, M., Böttcher, A., Sánchez-Garrido, M., . . . Lickert, H. (2020). Targeted pharmacological therapy restores β-cell function for diabetes remission. *Nature Metabolism, in press*.

Saltiel, A. R., & Kahn, C. R. (2001). Insulin signalling and the regulation of glucose and lipid metabolism. *Nature, 414*(6865), 799-806. doi:10.1038/414799a

Samols, E., Bonner-Weir, S., & Weir, G. C. (1986). Intra-islet insulin-glucagon-somatostatin relationships. *Clin Endocrinol Metab, 15*(1), 33-58. doi:10.1016/s0300-595x(86)80041-x

Sarruf, D. A., Bonner-Weir, S., & Schwartz, M. W. (2012). New clues to bariatric surgery's benefits. *Nat Med, 18*(6), 860-861. doi:10.1038/nm.2801

Schlager, A., Khalaileh, A., Mintz, Y., Abu Gazala, M., Globerman, A., Ilani, N., . . . Zamir, G. (2011). A mouse model for sleeve gastrectomy: applications for diabetes research. *Microsurgery, 31*(1), 66-71. doi:10.1002/micr.20797

Schlumbrecht, M. P., Xie, S. S., Shipley, G. L., Urbauer, D. L., & Broaddus, R. R. (2011). Molecular clustering based on ERalpha and EIG121 predicts survival in high-grade serous carcinoma of the ovary/peritoneum. *Mod Pathol, 24*(3), 453-462. doi:10.1038/modpathol.2010.211

Schonhoff, S. E., Giel-Moloney, M., & Leiter, A. B. (2004). Neurogenin 3-expressing progenitor cells in the gastrointestinal tract differentiate into both endocrine and non-endocrine cell types. *Dev Biol, 270*(2), 443-454. doi:10.1016/j.ydbio.2004.03.013

Schwitzgebel, V. M., Scheel, D. W., Conners, J. R., Kalamaras, J., Lee, J. E., Anderson, D. J., . . . German, M. S. (2000). Expression of neurogenin3 reveals an islet cell precursor population in the pancreas. *Development, 127*(16), 3533-3542.

Shackelford, D. B., & Shaw, R. J. (2009). The LKB1-AMPK pathway: metabolism and growth control in tumour suppression. *Nat Rev Cancer, 9*(8), 563-575. doi:10.1038/nrc2676

Shirakawa, J., De Jesus, D. F., & Kulkarni, R. N. (2017). Exploring inter-organ crosstalk to uncover mechanisms that regulate beta-cell function and mass. *Eur J Clin Nutr, 71*(7), 896-903. doi:10.1038/ejcn.2017.13

Shirakawa, J., Fernandez, M., Takatani, T., El Ouaamari, A., Jungtrakoon, P., Okawa, E. R., . . . Kulkarni, R. N. (2017). Insulin Signaling Regulates the FoxM1/PLK1/CENP-A Pathway to Promote Adaptive Pancreatic beta Cell Proliferation. *Cell Metab, 25*(4), 868-882 e865. doi:10.1016/j.cmet.2017.02.004

Sliwowska, J. H., Fergani, C., Gawalek, M., Skowronska, B., Fichna, P., & Lehman, M. N. (2014). Insulin: its role in the central control of reproduction. *Physiol Behav, 133*, 197-206. doi:10.1016/j.physbeh.2014.05.021

Song, J., Xu, Y., Hu, X., Choi, B., & Tong, Q. (2010). Brain expression of Cre recombinase driven by pancreas-specific promoters. *Genesis, 48*(11), 628-634. doi:10.1002/dvg.20672

Spijker, H. S., Ravelli, R. B., Mommaas-Kienhuis, A. M., van Apeldoorn, A. A., Engelse, M. A., Zaldumbide, A., . . . de Koning, E. J. (2013). Conversion of mature human beta-cells into glucagon-producing alpha-cells. *Diabetes, 62*(7), 2471-2480. doi:10.2337/db12-1001

Sternberg, N., & Hamilton, D. (1981). Bacteriophage P1 site-specific recombination. I. Recombination between loxP sites. *J Mol Biol, 150*(4), 467-486. doi:10.1016/0022-2836(81)90375-2

Straub, S. G., & Sharp, G. W. (2002). Glucose-stimulated signaling pathways in biphasic insulin secretion. *Diabetes Metab Res Rev, 18*(6), 451-463. doi:10.1002/dmrr.329

Sun-Wada, G. H., Toyomura, T., Murata, Y., Yamamoto, A., Futai, M., & Wada, Y. (2006). The a3 isoform of V-ATPase regulates insulin secretion from pancreatic beta-cells. *J Cell Sci, 119*(Pt 21), 4531-4540. doi:10.1242/jcs.03234

Sund, N. J., Vatamaniuk, M. Z., Casey, M., Ang, S. L., Magnuson, M. A., Stoffers, D. A., . . . Kaestner, K. H. (2001). Tissue-specific deletion of Foxa2 in pancreatic beta cells results in hyperinsulinemic hypoglycemia. *Genes Dev, 15*(13), 1706-1715. doi:10.1101/gad.901601

Sweeney, G., & Klip, A. (1998). Regulation of the Na+/K+-ATPase by insulin: why and how? *Mol Cell Biochem, 182*(1-2), 121-133.

Swisa, A., Glaser, B., & Dor, Y. (2017). Metabolic Stress and Compromised Identity of Pancreatic Beta Cells. *Front Genet, 8*, 21. doi:10.3389/fgene.2017.00021

Szabat, M., Page, M. M., Panzhinskiy, E., Skovso, S., Mojibian, M., Fernandez-Tajes, J., . . . Johnson, J. D. (2016). Reduced Insulin Production Relieves Endoplasmic Reticulum Stress and Induces beta Cell Proliferation. *Cell Metab, 23*(1), 179-193. doi:10.1016/j.cmet.2015.10.016

Tamarina, N. A., Roe, M. W., & Philipson, L. (2014). Characterization of mice expressing Ins1 gene promoter driven CreERT recombinase for conditional gene deletion in pancreatic beta-cells. *Islets, 6*(1), e27685. doi:10.4161/isl.27685

Tamemoto, H., Kadowaki, T., Tobe, K., Yagi, T., Sakura, H., Hayakawa, T., . . . et al. (1994). Insulin resistance and growth retardation in mice lacking insulin receptor substrate-1. *Nature, 372*(6502), 182-186. doi:10.1038/372182a0

Taniguchi, C. M., Emanuelli, B., & Kahn, C. R. (2006). Critical nodes in signalling pathways: insights into insulin action. *Nat Rev Mol Cell Biol, 7*(2), 85-96. doi:10.1038/nrm1837

Teese, M. G., & Langosch, D. (2015). Role of GxxxG Motifs in Transmembrane Domain Interactions. *Biochemistry, 54*(33), 5125-5135. doi:10.1021/acs.biochem.5b00495

Thorel, F., Nepote, V., Avril, I., Kohno, K., Desgraz, R., Chera, S., & Herrera, P. L. (2010). Conversion of adult pancreatic alpha-cells to beta-cells after extreme beta-cell loss. *Nature, 464*(7292), 1149-1154. doi:10.1038/nature08894

Tiano, J. P., Delghingaro-Augusto, V., Le May, C., Liu, S., Kaw, M. K., Khuder, S. S., . . . Mauvais-Jarvis, F. (2011). Estrogen receptor activation reduces lipid synthesis in pancreatic islets and prevents beta cell failure in rodent models of type 2 diabetes. *J Clin Invest, 121*(8), 3331-3342. doi:10.1172/jci44564

Tiano, J. P., & Mauvais-Jarvis, F. (2012). Importance of oestrogen receptors to preserve functional beta-cell mass in diabetes. *Nat Rev Endocrinol, 8*(6), 342-351. doi:10.1038/nrendo.2011.242

Tiano, J. P., Tate, C. R., Yang, B. S., DiMarchi, R., & Mauvais-Jarvis, F. (2015). Effect of targeted estrogen delivery using glucagon-like peptide-1 on insulin secretion, insulin sensitivity and glucose homeostasis. *Sci Rep, 5*, 10211. doi:10.1038/srep10211

Tokarz, V. L., MacDonald, P. E., & Klip, A. (2018). The cell biology of systemic insulin function. *J Cell Biol, 217*(7), 2273-2289. doi:10.1083/jcb.201802095

Tong, J., Prigeon, R. L., Davis, H. W., Bidlingmaier, M., Kahn, S. E., Cummings, D. E., . . . D'Alessio, D. (2010). Ghrelin suppresses glucose-stimulated insulin secretion and deteriorates glucose tolerance in healthy humans. *Diabetes, 59*(9), 2145-2151. doi:10.2337/db10-0504

Trajkovic-Arsic, M., Kalideris, E., & Siveke, J. T. (2013). The role of insulin and IGF system in pancreatic cancer. *J Mol Endocrinol, 50*(3), R67-74. doi:10.1530/jme-12-0259

Tritschler, S., Theis, F. J., Lickert, H., & Bottcher, A. (2017). Systematic single-cell analysis provides new insights into heterogeneity and plasticity of the pancreas. *Mol Metab, 6*(9), 974-990. doi:10.1016/j.molmet.2017.06.021

Ueki, K., Okada, T., Hu, J., Liew, C. W., Assmann, A., Dahlgren, G. M., . . . Kulkarni, R. N. (2006). Total insulin and IGF-I resistance in pancreatic beta cells causes overt diabetes. *Nat Genet, 38*(5), 583-588. doi:10.1038/ng1787

Ullrich, S. (2013). *IGF-1 and Insulin Receptor Signalling in Insulin-Secreting Cells: From Function to Survival*: Springer, Dordrecht.

Van de Casteele, M., Leuckx, G., Baeyens, L., Cai, Y., Yuchi, Y., Coppens, V., . . . Heimberg, H. (2013). Neurogenin 3+ cells contribute to beta-cell neogenesis and proliferation in injured adult mouse pancreas. *Cell Death Dis, 4*, e523. doi:10.1038/cddis.2013.52

van der Lely, A. J., Tschop, M., Heiman, M. L., & Ghigo, E. (2004). Biological, physiological, pathophysiological, and pharmacological aspects of ghrelin. *Endocr Rev, 25*(3), 426-457. doi:10.1210/er.2002-0029

Vecchio, I., Tornali, C., Bragazzi, N. L., & Martini, M. (2018). The Discovery of Insulin: An Important Milestone in the History of Medicine. *Front Endocrinol (Lausanne), 9*, 613. doi:10.3389/fendo.2018.00613

Vecchione, A., Marchese, A., Henry, P., Rotin, D., & Morrione, A. (2003). The Grb10/Nedd4 Complex Regulates Ligand-Induced Ubiquitination and Stability of the Insulin-Like Growth Factor I Receptor. *Molecular and Cellular Biology, 23*(9), 3363-3372. doi:10.1128/mcb.23.9.3363-3372.2003

Walker, J. N., Ramracheya, R., Zhang, Q., Johnson, P. R., Braun, M., & Rorsman, P. (2011). Regulation of glucagon secretion by glucose: paracrine, intrinsic or both? *Diabetes Obes Metab, 13 Suppl 1*, 95-105. doi:10.1111/j.1463-1326.2011.01450.x

Wang, M., Li, J., Lim, G. E., & Johnson, J. D. (2013). Is dynamic autocrine insulin signaling possible? A mathematical model predicts picomolar concentrations of extracellular monomeric insulin within human pancreatic islets. *PLoS One, 8*(6), e64860. doi:10.1371/journal.pone.0064860

Wang, P., Fiaschi-Taesch, N. M., Vasavada, R. C., Scott, D. K., Garcia-Ocana, A., & Stewart, A. F. (2015). Diabetes mellitus--advances and challenges in human beta-cell proliferation. *Nat Rev Endocrinol, 11*(4), 201-212. doi:10.1038/nrendo.2015.9

Wang, Q., Chang, W., Yang, X., Cheng, Y., Zhao, X., Zhou, L., . . . Zhang, K. (2019). Levels of miR-31 and its target genes in dermal mesenchymal cells of patients with psoriasis. *Int J Dermatol, 58*(2), 198-204. doi:10.1111/ijd.14197

Wang, S., Jensen, J. N., Seymour, P. A., Hsu, W., Dor, Y., Sander, M., . . . Gu, G. (2009). Sustained Neurog3 expression in hormone-expressing islet cells is required for endocrine maturation and function. *Proc Natl Acad Sci U S A, 106*(24), 9715-9720. doi:10.1073/pnas.0904247106

Wang, S., Yan, J., Anderson, D. A., Xu, Y., Kanal, M. C., Cao, Z., . . . Gu, G. (2010). Neurog3 gene dosage regulates allocation of endocrine and exocrine cell fates in the developing mouse pancreas. *Dev Biol, 339*(1), 26-37. doi:10.1016/j.ydbio.2009.12.009

Wang, Y., Dorrell, C., Naugler, W. E., Heskett, M., Spellman, P., Li, B., . . . Grompe, M. (2018). Long-Term Correction of Diabetes in Mice by In Vivo Reprogramming of Pancreatic Ducts. *Mol Ther, 26*(5), 1327-1342. doi:10.1016/j.ymthe.2018.02.014

Wang, Z., York, N. W., Nichols, C. G., & Remedi, M. S. (2014). Pancreatic beta cell dedifferentiation in diabetes and redifferentiation following insulin therapy. *Cell Metab, 19*(5), 872-882. doi:10.1016/j.cmet.2014.03.010

Weir, G. C., & Bonner-Weir, S. (1985). Pancreatic somatostatin. *Adv Exp Med Biol, 188*, 403-423. doi:10.1007/978-1-4615-7886-4_22

Weir, G. C., & Bonner-Weir, S. (1990). Islets of Langerhans: the puzzle of intraislet interactions and their relevance to diabetes. *J Clin Invest, 85*(4), 983-987. doi:10.1172/jci114574

Weir, G. C., & Bonner-Weir, S. (1998). Islet transplantation as a treatment for diabetes. *J Am Optom Assoc, 69*(11), 727-732.

Weir, G. C., & Bonner-Weir, S. (2004). Five stages of evolving beta-cell dysfunction during progression to diabetes. *Diabetes, 53 Suppl 3*, S16-21. doi:10.2337/diabetes.53.suppl_3.s16

Weir, G. C., Bonner-Weir, S., & Leahy, J. L. (1990). Islet mass and function in diabetes and transplantation. *Diabetes, 39*(4), 401-405. doi:10.2337/diab.39.4.401

Weng, J., Li, Y., Xu, W., Shi, L., Zhang, Q., Zhu, D., . . . Cheng, H. (2008). Effect of intensive insulin therapy on beta-cell function and glycaemic control in patients with newly diagnosed type 2 diabetes: a multicentre randomised parallel-group trial. *Lancet, 371*(9626), 1753-1760. doi:10.1016/S0140-6736(08)60762-X

White, V., Jawerbaum, A., Mazzucco, M. B., Gauster, M., Desoye, G., & Hiden, U. (2015). Diabetes-associated changes in the fetal insulin/insulin-like growth factor system are organ specific in rats. *Pediatr Res, 77*(1-1), 48-55. doi:10.1038/pr.2014.139

Wideman, R. D., Yu, I. L., Webber, T. D., Verchere, C. B., Johnson, J. D., Cheung, A. T., & Kieffer, T. J. (2006). Improving function and survival of pancreatic islets by endogenous production of glucagon-like peptide 1 (GLP-1). *Proc Natl Acad Sci U S A, 103*(36), 13468-13473. doi:10.1073/pnas.0600655103

Wiederkehr, A., & Wollheim, C. B. (2006). Minireview: implication of mitochondria in insulin secretion and action. *Endocrinology, 147*(6), 2643-2649. doi:10.1210/en.2006-0057

Wiedmer, P., Nogueiras, R., Broglio, F., D'Alessio, D., & Tschop, M. H. (2007). Ghrelin, obesity and diabetes. *Nat Clin Pract Endocrinol Metab, 3*(10), 705-712. doi:10.1038/ncpendmet0625

Williams, D. B. (2006). Beyond lectins: the calnexin/calreticulin chaperone system of the endoplasmic reticulum. *J Cell Sci, 119*(Pt 4), 615-623. doi:10.1242/jcs.02856

Willmann, S. J., Mueller, N. S., Engert, S., Sterr, M., Burtscher, I., Raducanu, A., . . . Lickert, H. (2016). The global gene expression profile of the secondary transition during pancreatic development. *Mech Dev, 139*, 51-64. doi:10.1016/j.mod.2015.11.004

Wills, Q. F., Boothe, T., Asadi, A., Ao, Z., Warnock, G. L., Kieffer, T. J., & Johnson, J. D. (2016). Statistical approaches and software for clustering islet cell functional heterogeneity. *Islets, 8*(2), 48-56. doi:10.1080/19382014.2016.1150664

Withers, D. J., Burks, D. J., Towery, H. H., Altamuro, S. L., Flint, C. L., & White, M. F. (1999). Irs-2 coordinates Igf-1 receptor-mediated beta-cell development and peripheral insulin signalling. *Nat Genet, 23*(1), 32-40. doi:10.1038/12631

Yamada, T., Cavelti-Weder, C., Caballero, F., Lysy, P. A., Guo, L., Sharma, A., . . . Weir, G. C. (2015). Reprogramming Mouse Cells With a Pancreatic Duct Phenotype to Insulin-Producing beta-Like Cells. *Endocrinology, 156*(6), 2029-2038. doi:10.1210/en.2014-1987

Yang, Y. P., Thorel, F., Boyer, D. F., Herrera, P. L., & Wright, C. V. (2011). Context-specific alpha- to-beta-cell reprogramming by forced Pdx1 expression. *Genes Dev, 25*(16), 1680-1685. doi:10.1101/gad.16875711

Yumlu, S., Stumm, J., Bashir, S., Dreyer, A. K., Lisowski, P., Danner, E., & Kuhn, R. (2017). Gene editing and clonal isolation of human induced pluripotent stem cells using CRISPR/Cas9. *Methods, 121-122*, 29-44. doi:10.1016/j.ymeth.2017.05.009

Yusuf, N., Hidalgo, B., Irvin, M. R., Sha, J., Zhi, D., Tiwari, H. K., . . . Aslibekyan, S. W. (2017). An epigenome-wide association study of inflammatory response to fenofibrate in

the Genetics of Lipid Lowering Drugs and Diet Network. *Pharmacogenomics, 18*(14), 1333-1341. doi:10.2217/pgs-2017-0037

Zaret, K. S., & Carroll, J. S. (2011). Pioneer transcription factors: establishing competence for gene expression. *Genes Dev, 25*(21), 2227-2241. doi:10.1101/gad.176826.111

Zhang, B. B., Zhou, G., & Li, C. (2009). AMPK: An Emerging Drug Target for Diabetes and the Metabolic Syndrome. *Cell Metabolism, 9*(5), 407-416. doi:10.1016/j.cmet.2009.03.012

Zhou, Q., & Melton, D. A. (2018). Pancreas regeneration. *Nature, 557*(7705), 351-358. doi:10.1038/s41586-018-0088-0

Zhou, Z., Ribas, V., Rajbhandari, P., Drew, B. G., Moore, T. M., Fluitt, A. H., . . . Hevener, A. L. (2018). Estrogen receptor alpha protects pancreatic beta-cells from apoptosis by preserving mitochondrial function and suppressing endoplasmic reticulum stress. *J Biol Chem, 293*(13), 4735-4751. doi:10.1074/jbc.M117.805069

8. Acknowledgement

„Die Zeit bleibt stehen, ich geh kurz einen Schritt zurück,
und ich nehm‘ dich ein Stück mit, komm, folg mir auf meinem Weg.
Denn du musst sehen, was ich sah, du musst gehen, durch was ich ging,
um zu wissen, wer ich bin. Komm, folg mir auf meinem Weg…“
(KS, 2010)

Herewith, I would like to thank everyone who accompanied me in any sense on my way to obtain a PhD and make this success possible!

I am very happy for having had the chance to accomplish my PhD in the IDR under supervision of Heiko on this amazing, history-making project. I enjoyed very much presenting the receptor to the scientific community and contributing to the publication. Thank you, for all your support, trust and faith! Additionally, I thank the receptor group for making this project successful.

I would also like to give thanks to Donna, Elke and Mara as well as Ingo for the great organizational help and the lovely conversations. A special thanks goes to Kerstin, Gabi, Robert, Ines, Lisa, Zakiah, Anett, Jürgen, Julia and Jessy for nicely organizing the lab, providing input and helping me with my numerous requests. Thanks a lot to Michaela, Andrea, Franzi, Martina and Heike for taking care of my animals and creating a nice atmosphere in the mouse house. Thanks to everybody in IDR who contributed to my scientific and personal development and also for the fun, particularly in respect of the good old times in Garching!

I would further like to thank the collaboration partners who contributed to this work: Ünal, Michal, Regina and Andrew for the nicely working antibodies, Carsten for performing the HPLC-MS analysis as well as Julius and Matthias for introducing me to the PLA technique. In addition, I want to thank Anett for her input and support regarding mouse experiments. Thanks to Aimée for providing the FVFPBF^{DHom} and Ngn3-Cre animals and teaching me dissection of the pancreas as well as to Fataneh for the Igfr-L1 mice and to Silvi for sharing the Igfr-L2 animals and the great teamwork.

I am also incredibly thankful to Marc and his laboratory who paved my way for pursuing a PhD. You raised my interest in diabetes research and provided me the perfect training for a scientific career. Thanks a lot, Martin, for your technical support, which allowed me to be independent and work in any place at any time.

Aşkım, I thank you from my heart for accompanying me on this rocky road, for all your patience and love. I am grateful for all my good friends as well as for Bettina for strengthening me in my endeavors and making me happy.
Most of all, I want to express the deepest gratitude to my family for the love and support throughout my life. There are no words to explain how much I appreciate every single one of you.

9. Publications

Sachdeva, R., Fleming, T., Schumacher, D., Homberg, S., Stilz, K., Mohr, F., . . . Freichel, M. (2019). Methylglyoxal evokes acute Ca(2+) transients in distinct cell types and increases agonist-evoked Ca(2+) entry in endothelial cells via CRAC channels. *Cell Calcium, 78*, 66-75. doi:10.1016/j.ceca.2019.01.002

Manuscript in preparation for submission to Nature:
Homberg, S., Fathi Far, F., Gräfin von Hahn, F, Ansarullah, Jain, C., ... Lickert, H.
Igf receptor-like 1 desensitizes insulin and Igf1 receptor signaling in β-cells

10. Supplement

10.1 Co-IP with HPLC-MS analysis (see 4.3.2)

10.1.1 Trial experiment

Table 10.1.1.1 Significantly enriched proteins in co-IPs under growth conditions (36D7)

Protein and gene name of peptides identified in the eluate of immunoprecipitated Igfr-L1 by use of anti-cytoplasmic-IGFR-L1 and their enrichment indicated as ratio of wildtype to Igfr-L1$^{-/-}$ Min6. Italic writing indicates proteins found under both metabolic conditions.

protein	gene	ratio
UPF0577 protein KIAA1324	Kiaa1324	456
UPF0577 protein KIAA1324-like homolog		237
Protein-glutamine gamma-glutamyltransferase K	*Tgm1*	28,5
14-3-3 protein zeta/delta	*Ywhaz*	20,5
Proteasome subunit β type-3	Psmb3	14,2
Cofilin-1	*Cfl1*	12,2
60S ribosomal protein L24	Rpl24	9,73
Desmoglein-1-α;Desmoglein-1-β;Desmoglein-1-gamma	*Dsg1a;Dsg1b; Dsg1c*	8,00
60S ribosomal protein L28	*Rpl28*	7,80
28S ribosomal protein S27, mitochondrial	Mrps27	7,25
Signal recognition particle 14 kDa protein;Signal recognition particle 14 kDa protein, N-terminally processed	Srp14	7,15
Tubulin β-6 chain	Tubb6	5,91
T-complex protein 1 subunit gamma	Cct3	5,85
Endoplasmic reticulum-Golgi intermediate compartment protein 1	Ergic1	5,63
Histone H1.2	Hist1h1c	5,27
Protein SET	*Set*	5,25
Histone H2B type 1-P;Histone H2B type 1-K;Histone H2B type 1-C/E/G;Histone H2B type 2-B;Histone H2B type 1-H;Histone H2B type 1-B;Histone H2B type 1-M;Histone H2B type 1-F/J/L	*Hist1h2bp;Hist 1h2bk;Hist1h2 bc;Hist2h2bb; Hist1h2bh;Hist 1h2bb;Hist1h2 bm;Hist1h2bf*	5,15
Bleomycin hydrolase	Blmh	4,94
Eukaryotic translation initiation factor 4E	Eif4e	4,91
Calnexin	*Canx*	4,90
Constitutive coactivator of PPAR-gamma-like protein 1	FAM120A	4,83

Table 10.1.1.2 Significantly enriched proteins in co-IPs after 15' starvation (36D7)

Protein and gene name of peptides identified in the eluate of immunoprecipitated Igfr-L1 by use of anti-cytoplasmic-IGFR-L1 and their enrichment indicated as ratio of wildtype to Igfr-L1$^{-/-}$ Min6. Italic writing indicates proteins found under both metabolic conditions.

protein	gene	ratio
UPF0577 protein KIAA1324	Kiaa1324	3188
UPF0577 protein KIAA1324-like homolog		377
60S acidic ribosomal protein P1	Rplp1	39,6

60S ribosomal protein L28	*Rpl28*	26,6
40S ribosomal protein S28	Rps28	23,6
WAS protein family homolog 1	Wash1	19,8
Hepatoma-derived growth factor	Hdgf	19,5
Histone H1.0;Histone H1.0, N-terminally processed	H1f0	17,5
Histone H2B type 1-P;Histone H2B type 1-K;Histone H2B type 1-C/E/G;Histone H2B type 2-B;Histone H2B type 1-H;Histone H2B type 1-B;Histone H2B type 1-M;Histone H2B type 1-F/J/L	*Hist1h2bp/2bk/2bc/2bb/2bh/2bb/2bm/2bf*	17,5
U1 small nuclear ribonucleoprotein A	Snrpa	15,3
40S ribosomal protein S23	Rps23	13,1
Actin, α skeletal muscle;Actin, α cardiac muscle 1	Acta1;Actc1	12,0
Calnexin	*Canx*	11,2
14-3-3 protein gamma;14-3-3 protein gamma, N-terminally processed	Ywhag	11,0
40S ribosomal protein S6	Rps6	10,3
Triosephosphate isomerase	Tpi1	9,61
AP-2 complex subunit α-2	Ap2a2	9,20
14-3-3 protein zeta/delta	*Ywhaz*	9,07
Cofilin-1	*Cfl1*	8,37
Desmoglein-1-α;Desmoglein-1-β;Desmoglein-1-gamma	*Dsg1a;Dsg1b;Dsg1c*	8,21
Protein SET	*Set*	7,84
Peptidyl-prolyl cis-trans isomerase B	Ppib	7,80
40S ribosomal protein S15	Rps15	7,69
Y-box-binding protein 3	Ybx3	7,40
Protein disulfide-isomerase A3	Pdia3	7,27
14-3-3 protein theta	Ywhaq	6,38
60S ribosomal protein L23a	Rpl23a	6,35
40S ribosomal protein S10	Rps10	5,80
Oxysterol-binding protein 1	Osbp	5,64
Histone H1.4	Hist1h1e	5,63
Protein-glutamine gamma-glutamyltransferase K	*Tgm1*	5,44
40S ribosomal protein S7	Rps7	5,30
Calcium/calmodulin-dependent protein kinase type II subunit β;Calcium/calmodulin-dependent protein kinase type II subunit gamma	Camk2b;Camk2g	5,25
26S protease regulatory subunit 6B	Psmc4	4,93

Table 10.1.1.3 Significantly enriched proteins in co-IPs under growth conditions (1374)

Protein and gene name of peptides identified in the eluate of immunoprecipitated Igfr-L1 by use of anti-extracellular-IGFR-L1 and their enrichment indicated as ratio of wildtype to Igfr-L1$^{-/-}$ Min6. Italic writing indicates proteins found in both metabolic conditions.

protein	gene	ratio
UPF0577 protein KIAA1324	Kiaa1324	477
Kinesin-like protein KIF2C	*Kif2c*	291
UPF0577 protein KIAA1324-like homolog		127
Hepatoma-derived growth factor	Hdgf	28.6
60S ribosomal protein L17	*Rpl17*	14.0

60S ribosomal protein L21	Rpl21	13.4
60S ribosomal protein L22	Rpl22	13.1
Complement C4-B;Complement C4 β chain;Complement C4 α chain;C4a anaphylatoxin;Complement C4 gamma chain	C4b	12.9
60S ribosomal protein L38	Rpl38	12.5
Vesicle-trafficking protein SEC22b	Sec22b	12.4
Melanoma-associated antigen D1	*Maged1*	12.1
28S ribosomal protein S33, mitochondrial	*Mrps33*	11.0
YTH domain-containing family protein 3	*Ythdf3*	10.6
Histone H1.2	*Hist1h1c*	*10.2*
Transmembrane emp24 domain-containing protein 9	Tmed9	10.2
Surfeit locus protein 4	Surf4	10.2
40S ribosomal protein S26	*Rps26*	9.79
60S ribosomal protein L32	Rpl32	9.55
DNA-directed RNA polymerase II subunit RPB4	Polr2d	9.36
Phosphate carrier protein, mitochondrial	Slc25a3	9.15
60S ribosomal protein L28	*Rpl28*	8.69
Nuclease-sensitive element-binding protein 1	Ybx1	8.23
60S ribosomal protein L31	*Rpl31*	8.09
Receptor-type tyrosine-protein phosphatase-like N	*Ptprn*	7.42
60S ribosomal protein L8	*Rpl8*	7.40
Protein LSM12 homolog	Lsm12	7.23
28S ribosomal protein S6, mitochondrial	Mrps6	7.04
Y-box-binding protein 3	Ybx3	7.02
60S ribosomal protein L7	Rpl7	6.72
Proteasome subunit α type-4	Psma4	6.71
Transmembrane emp24 domain-containing protein 2	Tmed2	6.65
Eukaryotic translation initiation factor 4E	Eif4e	6.42
Signal transducing adapter molecule 1	Stam	6.33
60S ribosomal protein L36a	Rpl36a	6.29
26S protease regulatory subunit 7	Psmc2	6.03
Vesicular integral-membrane protein VIP36	Lman2	6.02
Calmodulin;Calmodulin-like protein 3	*Calm1;Calml 3*	5.87
Prothymosin α;Prothymosin α, N-terminally processed;Thymosin α	Ptma	5.84
Guanine nucleotide-binding protein G(I)/G(S)/G(T) subunit β-2/β-1/ β-4/β-3	Gnb2;Gnb1; Gnb4;Gnb3	5.77
Cystatin-B	Cstb	5.75
Protein argonaute-2;Protein argonaute-3	Ago2;Ago3	5.74
60S acidic ribosomal protein P2	Rplp2	5.67
Histone H1.1	Hist1h1a	5.62
Protein-glutamine gamma-glutamyltransferase K	Tgm1	5.62

Table 10.1.1.4 Significantly enriched proteins in co-IPs after 15' starvation (1374)

Protein and gene name of peptides identified in the eluate of immunoprecipitated Igfr-L1 by use of anti-extracellular-IGFR-L1 and their enrichment indicated as ratio of wildtype to Igfr-L1$^{-/-}$ Min6. Italic writing indicates proteins found under both metabolic conditions.

protein	gene	ratio
UPF0577 protein KIAA1324	Kiaa1324	1985
Kinesin-like protein KIF2C	*Kif2c*	554
UPF0577 protein KIAA1324-like homolog		54,4
E3 ubiquitin-protein ligase UBR4	Ubr4	34,1
Adenosylhomocysteinase	Ahcy	20,8
60S ribosomal protein L31	*Rpl31*	16,5
Receptor-type tyrosine-protein phosphatase-like N	*Ptprn*	14,2
Pyrroline-5-carboxylate reductase 3	Pycrl	14,1
Collagen α-1(XIV) chain	Col14a1	9,18
Eukaryotic translation initiation factor 5A-2;Eukaryotic translation initiation factor 5A-1	Eif5a2;Eif5a	8,24
Translocon-associated protein subunit α	Ssr1	7,86
40S ribosomal protein S26	*Rps26*	7,81
Histone H3.3;Histone H3.2;Histone H3.1;Histone H3.3C	H3f3a;Hist1h3b/3a;H3f3c	6,94
Clathrin light chain A	Clta	6,78
Importin subunit α-7	Kpna6	5,99
Protein SET	Set	5,84
V-type proton ATPase 116 kDa subunit a isoform 1	Atp6v0a1	5,79
Melanoma-associated antigen D1	*Maged1*	5,66
Calpain small subunit 1	Capns1	5,25
E3 ubiquitin-protein ligase NEDD4	Nedd4	5,11
60S ribosomal protein L5	Rpl5	4,74
DAZ-associated protein 1	Dazap1	4,56
Glucose-induced degradation protein 8 homolog	Gid8	4,44
AP-3 complex subunit sigma-1	Ap3s1	4,38
Translocon-associated protein subunit delta	Ssr4	4,35
28S ribosomal protein S33, mitochondrial	*Mrps33*	4,33
YTH domain-containing family protein 3	*Ythdf3*	4,00
Pyridoxal-dependent decarboxylase domain-containing protein 1	Pdxdc1	4,00
Dihydrolipoyllysine-residue succinyltransferase component of 2-oxoglutarate dehydrogenase complex, mitochondrial	Dlst	3,89
14-3-3 protein eta	Ywhah	3,85
Calmodulin;Calmodulin-like protein 3	*Calm1;Calm3*	3,82
60S ribosomal protein L29	Rpl29	3,58
ADP-ribosylation factor 4;ADP-ribosylation factor 5	Arf4;Arf5	3,42
28S ribosomal protein S35, mitochondrial	Mrps35	3,41
60S ribosomal protein L8	*Rpl8*	3,37
60S ribosomal protein L17	*Rpl17*	3,34
ATP synthase subunit gamma, mitochondrial	Atp5c1	3,33
Histone H2B type 1-P;Histone H2B type 1-K;Histone H2B type 1-C/E/G;Histone H2B type 2-B;Histone H2B type 1-H;Histone H2B type 1-B;Histone H2B type 1-M;Histone H2B type 1-F/J/L	Hist1h2bp/2bk/2bc/2bb/2bh/2bb/2bm/2bf	3,26

Nucleoside diphosphate kinase B and A	Nme2;Nme1	3,10
14-3-3 protein gamma;14-3-3 protein gamma, N-terminally processed	Ywhag	3,09
Microtubule-associated protein RP/EB family member 1	Mapre1	2,95
60S ribosomal protein L24	Rpl24	2,92
14-3-3 protein β/α;14-3-3 protein β/α, N-terminally processed	Ywhab	2,87
60S ribosomal protein L28	*Rpl28*	2,87
60S ribosomal protein L13a	Rpl13a	2,75
Histone H1.2	*Hist1h1c*	2,75
Carboxypeptidase E	Cpe	2,74
Proliferating cell nuclear antigen	Pcna	2,73

10.1.2 Final experiment

Table 10.1.2.1 Significantly different proteins in co-IPs after 18h starvation

Protein and gene name of peptides identified in the eluate of immunoprecipitated Igfr-L1 and their enrichment indicated as ratio of wildtype to Igfr-L1$^{-/-}$ Min6.

protein	gene	ratio
UPF0577 protein KIAA1324	Kiaa1324	7437
UPF0577 protein KIAA1324-like homolog		192
40S ribosomal protein S13	Rps13	4,01
Glycogen [starch] synthase, muscle	Gys1	3,70
Heterogeneous nuclear ribonucleoprotein A1;Heterogeneous nuclear ribonucleoprotein A1, N-terminally processed RNA	Hnrnpa1	2,75
D-3-phosphoglycerate dehydrogenase	Phgdh	2,52
Ras GTPase-activating protein-binding protein 1	G3bp1	2,16
T-complex protein 1 subunit β	Cct2	2,05
Ribose-phosphate pyrophosphokinase 1	Prps1	2,01
Heat shock protein HSP 90-α	Hsp90aa1	1,96
SWI/SNF-related matrix-associated actin-dependent regulator of chromatin subfamily D member 2	Smarcd2	1,86
CDKN2A-interacting protein	Cdkn2aip	1,86
Grancalcin	Gca	1,85

Table 10.1.2.2 Significantly different proteins in co-IPs after glucose stimulation

Protein and gene name of peptides identified in the eluate of immunoprecipitated Igfr-L1 and their enrichment indicated as ratio of wildtype to Igfr-L1$^{-/-}$ Min6.

protein	gene	ratio
UPF0577 protein KIAA1324	Kiaa1324	2745
UPF0577 protein KIAA1324-like homolog		288
V-type proton ATPase catalytic subunit A	Atp6v1a	16,1
Protein lin-7 homolog C;Protein lin-7 homolog A	Lin7c;Lin7a	7,30
Sodium/potassium-transporting ATPase subunit α-1;Sodium/potassium-transporting ATPase subunit α-2	Atp1a1;Atp1a2	3,94
mRNA cap guanine-N7 methyltransferase	Rnmt	3,47
Cathepsin Z	Ctsz	3,44
Sarcoplasmic/endoplasmic reticulum calcium ATPase 3	Atp2a3	2,46

60S ribosomal protein L15	Rpl15	2,01
ATP synthase subunit α, mitochondrial	Atp5a1	1,95
Eukaryotic translation initiation factor 3 subunit A	Eif3a	1,93
D-3-phosphoglycerate dehydrogenase	Phgdh	1,92
Nucleophosmin	Npm1	1,92
Gamma-interferon-inducible lysosomal thiol reductase	Ifi30	1,87
COP9 signalosome complex subunit 8	Cops8	1,86
Transitional endoplasmic reticulum ATPase	Vcp	1,80
Bifunctional methylenetetrahydrofolate dehydrogenase/ cyclohydrolase, mitochondrial; NAD-dependent methylenetetrahydrofolate dehydrogenase	Mthfd2	1,68
Isocitrate dehydrogenase [NAD] subunit α, mitochondrial	Idh3a	1,62
Band 4.1-like protein 3;Band 4.1-like protein 3, N-terminally processed	Epb41l3	1,59
Histone deacetylase 6	Hdac6	1,58

Table 10.1.2.3 Significantly different proteins in co-IPs after insulin stimulation

Protein and gene name of peptides identified in the eluate of immunoprecipitated Igfr-L1 and their enrichment indicated as ratio of Igfr-L1$^{+/+}$ to Igfr-L1$^{-/-}$ Min6.

protein	gene	ratio
UPF0577 protein KIAA1324	Kiaa1324	2593
UPF0577 protein KIAA1324-like homolog		206
Grancalcin	Gca	6,01
Sodium/potassium-transporting ATPase subunit α-1;Sodium/potassium-transporting ATPase subunit α-2	Atp1a1;Atp1a2	3,94
ATP synthase subunit β, mitochondrial	Atp5b	3,92
DNA-directed RNA polymerases I, II, and III subunit RPABC3	Polr2h	2,67
ATP synthase subunit α, mitochondrial	Atp5a1	2,47
Sarcoplasmic/endoplasmic reticulum calcium ATPase 3	Atp2a3	1,80
Integral membrane protein GPR180	Gpr180	1,61
B-cell receptor-associated protein 31	Bcap31	1,58
Triosephosphate isomerase	Tpi1	1,43
Histone H1.1	Hist1h1a	1,39